A Comparison of the Electrophysiological Properties of Sodium Channels in Cardiomyocytes of the Rat Pulmonary Vein and Atrium

Laura Hutchison

A thesis submitted in the fulfilment of the requirements for the degree of Doctor of Philosophy

April 2016

Strathclyde Institute of Pharmacy and Biomedical Science

University of Strathclyde

This thesis is the result of the author's original research. It has been composed by the author and has not been previously submitted for examination which has led to the award of a degree.

Signed:

Date:

Acknowledgements

First of all I would like to thank Edward Rowan for giving me this PhD opportunity as well as his advice, support and patience with me throughout my time at Strathclyde. I am also extremely grateful to Robert Drummond for all his help and support throughout my PhD, particularly during the writing up stage. I promise one day I will remember to putter the letters “t”, “h” and “e” together (haha). I am exceptionally appreciative of the time they both gave to me, particularly when I was learning the electrophysiology techniques as well as providing a friendly chat and encouragement at times when I was struggling to get things up and running. I am also thankful to the other students past and present in the lab, particularly Alasdair (thanks for putting up with me!), Molly, Craig and Sajjad, for helping to create a friendly environment to work in and for keeping me going during the bad days!

I am also appreciative of John Dempster for his help with setting up the sodium current protocols and for his endless advice regarding statistics. I would also like to thank Andrew Rankin for taking the time to listen to and discuss my results. I also want to extend my thanks to the many members of technical staff both in the lab and the BPU, as well as a number of lecturers for their assistance, advice and for providing a friendly face throughout my PhD. I am also grateful to Mark MacAskill and Junxi Wi for taking the time to pass on their knowledge of histology and immunohistochemistry. Many thanks should also be given to Susan Currie for the guidance on the set up of and for the use of her Langendorff apparatus. I also can’t forget to thank the cleaners for some great chats and for putting a smile on my face on the days of those early morning starts ☺.

I am lucky to have made a lot of great friends in SIPBS and I am thankful for all their support. I will miss the lunch time laughs, our Friday lunches, the theme nights out and putting Torrance back in her cage. I also have to say a massive thanks to my “Kirkie” friends, particularly Gayle and Kerry and the date night Friday regulars, for

the encouragement, laughs and generally keeping me sane throughout the PhD. I also want to thank Calum for being the most understanding person in the world, particularly throughout my write-up. To my mum (Big Marie!) and Avi, thank you so much for all the inspiration, for telling everyone in Scotland and Portugal how proud you are no matter what I do and for continuously reminding me that I have to think of life after my PhD (yes I did listen to your "so what job will you do when you finish" question haha). Lastly, to my sister, Leanne. I cannot stress how grateful I am for the endless support and reassurance you have given to me throughout my time at University. I would never have got this far without you, thank you so so so much for absolutely everything.

To my dad, I hope I have done you proud.

Communications

Hutchison, L., Rankin, A.C., Drummond, R.M., Rowan, E.G. The properties of sodium channels in rat left atrial and pulmonary vein cardiomyocytes. Physiological Society Main Meeting, 30th June – 2nd July 2014

Hutchison, L., Rankin, A.C., Drummond, R.M., Rowan, E.G. The properties of sodium channels in rat left atrial and pulmonary vein cardiomyocytes. Early Career Physiologists' Symposium (ECPS), 29th June 2014.

Hutchison, L., Rankin, A.C., Drummond, R.M., Rowan, E.G. Sodium channel properties in rat left atrial and pulmonary vein cardiomyocytes. Scottish Cardiovascular Forum, 22nd February 2014.

Hutchison, L., Rankin, A.C., Drummond, R.M., Rowan, E.G. The role of sodium channels present on the rat pulmonary vein in the generation of arrhythmogenic activity in atrial fibrillation. Scottish Cardiovascular Forum, 2nd February 2013.

Hutchison, L., Henry A. (joint authors), Rankin, A.C, Drummond, R.M., Rowan, E.G. Organisation of cardiomyocytes in the rat pulmonary vein. Physiological Society: Cardiac and Respiratory Physiology Meeting, 4-6th September 2012.

Table of Contents

List of Figures

List of Tables

Abbreviations

AF- Atrial fibrillation

APD – Action potential duration

APTES – (3-Aminopropyl)triethoxysaline

ATX-II - *Anemonia sulcata* toxin II

AV – atrioventricular

BIM - Bisindolylmaleimide

BPU - Biological Procedures Unit

Ca^{2+} - Calcium ion

CaMKII - Calcium/calmodulin-dependent protein kinase II

Ca_V – Voltage gated Ca^{2+} channel

CHO – Chinese hamster ovary

DAD – Delayed afterdepolarisation

dV/dt_{max} – Maximum upstroke velocity

EAD – Early afterdepolarisation

ERs – Electronic series resistance

ERP – Effective refractory period

G_{max} – Maximal peak Na^+ conductance

I_{CaL} - L-type calcium current

I_{CaT} - T-type calcium current

I_f - Funny current

I_{K1} - Inward rectifier potassium current

I_{KAChC} - Constitutive acetylcholine-dependent potassium current

I_{Kr} - Rapid activating delayed rectifier potassium current

I_{Ks} - Slow activating delayed rectifier potassium current

I_{max} – Maximum peak I_{Na}

I_{Na} – Sodium current

I_{NaL} – Late sodium current

IP_3R - Inositol 1,4,5-triphosphate receptor

I_{ti} – Transient inward current

I_{to} - Transient outward current

I-V – Current voltage relationship

K^+ - Potassium ion

$K_{D,R}$ – Dissociation constant of TTX-resistant sodium current

$K_{D,S}$ – Dissociation constant of TTX-sensitive sodium current

LA – Left atrium

LQTS – Long QT syndrome

MRI – Magnetic resonance imaging

MTSEA - (2-aminoethyl)methanethiosulfonate

Na^+ - Sodium ion

Na_v - Voltage gated sodium channels

NCX - Sodium/calcium exchanger

No stim – the absence of electrical stimulation

PAS - Periodic-acid Schiff

PBS – phosphate buffered saline

PKA – protein kinase A

PKC – protein kinase C

PV – Pulmonary vein

RAS- Renin-angiotensin system

R_s – Noncompensated series resistance

τ_f – Fast recovery time constant

τ_s – Slow recovery time constant

TsA201 – transformed human kidney cells

T-tubules – Transverse tubules

TTX – Tetrodotoxin

V_{dev} – Deviation from voltage command

$V_{½}$ – Voltage of half activation/inactivation

λ - Wavelength

Abstract

Atrial fibrillation is the most common cardiac arrhythmia, currently affecting up to one million people in the UK. Clinical studies have demonstrated that ectopic activity originating from the cardiomyocyte sleeve which surrounds the pulmonary vein (PV), is an important cause of atrial fibrillation. However, the underlying mechanisms for this ectopic activity remain unclear. Recent studies have proposed that sodium channels in the PV cardiomyocytes play a role. Thus, the aim of this thesis was to determine the distribution of the Na^+ channel isoforms, as well as examine their characteristics in the rat PV and for comparative purposes the properties of the Na^+ channel isoforms in the left atrium (LA), using a number of complimentary techniques. Furthermore, the arrhythmogenic activity in the PV and LA was investigated with the use of *Anemonia sulcata* toxin II (ATX-II), a substance that is frequently used as a pro-arrhythmic toxin.

Microelectrode recordings revealed that there was no significant difference in the electrically evoked action potentials in the rat PV and LA tissues. Subsequent voltage clamp experiments on single isolated cardiomyocytes demonstrated that the I_{Na} current density, activation and inactivation properties were also similar between the PV and LA. However, the use of the selective Na^+ channel blocker tetrodotoxin (TTX), to distinguish between Na^+ channel subtypes, revealed a 20% contribution of the TTX-sensitive I_{Na} to the total I_{Na} in PV cardiomyocytes, with the current activated at more depolarised potentials compared to the TTX-resistant I_{Na}. In contrast, there was no evidence of the TTX-sensitive I_{Na} in LA cardiomyocytes. Although, inhibition of the TTX-sensitive Na^+ channels had no effect on the action potential of the PV and LA, a small, but significant, reduction in the contractile response of both tissues was observed.

Arrhythmogenic activity in the form of spontaneous contractions, spontaneous action potentials (which for the purpose of this thesis are used to define contractions or action potentials that occur after treatment of the tissue with ATX-II, and which are independent of electrical stimulation), and early afterdepolarisations (EADs) were

induced in both PV and LA tissues in the presence of ATX-II, which is known to enhance the I_{NaL}. This ATX-II induced arrhythmogenic activity was not affected by block of TTX-sensitive Na^+ channels alone, but was abolished by inhibition of both TTX-sensitive and TTX-resistant Na^+ channels, highlighting the dependence of this arrhythmogenic activity on Na^+ channels. In addition, suppression of the ATX-II induced arrhythmogenic activity using the calcium/calmodulin-dependent protein kinase II (CaMKII) blocker, KN-93, or the Na^+/Ca^{2+} exchanger (NCX) inhibitor, ORM-10103, demonstrated the involvement of CaMKII and the NCX in ATX-II induced spontaneous activity. Thus, the excitability of cells from both the PV and LA is influenced by both the direct and indirect action of Na^+ influx through the action of ATX-II.

Chapter 1

Introduction

1.1 Atrial Fibrillation

1.1.1 Atrial Fibrillation

Atrial Fibrillation (AF) is the most common cardiac arrhythmia, affecting approximately 1% to 2% of the developed world population and it is a major contributor to morbidity and mortality (Murphy *et al.*, 2007; Wilke *et al.*, 2013). This arrhythmia is most common in those over 70 years of age and by 2050 the incidence of AF is expected to triple in line with the increasing elderly population (Miyasaka *et al.*, 2006). Typically, AF is characterised by uncoordinated and disorganized contraction of the atria and can be diagnosed on an electrocardiogram in which the P wave is replaced by irregular fibrillatory waves (Bennett and Pentecost, 1970). During AF, the sinus node no longer controls the heart rate, instead the rate is determined by the interaction of the rapid atrial rate and the filtering ability of the atrioventricular (AV) node (Nattel, 2002). The fibrillating atrium greatly increases the occurrence of blood clots, consequently enhancing the risk of stroke (Wolf *et al.*, 1978).

There are numerous classifications of AF and the American Heart Association and The European Society of Cardiology (Fuster *et al.*, 2006) recommends AF should be classed as:

- First Detected AF – on initial detection by the clinician.
- Recurrent AF – if there are more than two detected episodes of AF.
- Paroxysmal AF – if the recurrent arrhythmia ceases spontaneously.
- Persistent AF – if the recurrent arrhythmia is prolonged beyond 7 days.
- Permanent AF – ongoing recurrent arrhythmia that cannot be attenuated by cardioversion.

Numerous cardiac diseases such as coronary artery disease, hypertension, congestive heart failure and thyrotoxic heart disease can predispose to AF (Wolf *et al.*, 1978;

Forfar *et al.*, 1979). In addition, epidemiological factors such as old age, gender and smoking are thought to be predisposing factors in AF (Allessie *et al.*, 2001).

1.1.2 Atrial action potential

Normally, mammalian atrial action potentials are initiated by the pacemaking activity of the sino-atrial node located in the right atrium. The action potentials are then conducted throughout the atria, to the AV node, through the bundle of His and into the Purkinje fibres of the ventricles. The action potentials are propagated between cardiomyocytes via gap junctions, which are composed of connexin proteins connecting the cytoplasm of adjacent cells (Yeager and Gilula, 1992). As shown in the schematic representation in Figure 1.1, the resting membrane potential (phase 4), which is between -80 to -90 mV in human atrial cardiomyocytes, is maintained by the inward rectifier K^+ currents such as I_{K1} (Koumi *et al.*, 1994, 1995). Phase 4 depolarisation results in the membrane potential reaching a threshold to trigger an action potential. This begins with the action potential upstroke (phase 0), which is the result of a rapid influx of Na^+ into the cardiomyocyte (Sakakibara *et al.*, 1992). Following this, the cell briefly repolarises (phase 1), due to activation of the transient outward K^+ current (I_{to}) (Escande *et al.*, 1987), and then reaches a plateau phase (phase 2) where there is a balance between inward Ca^{2+} currents through L-type Ca^{2+} channels (I_{CaL}) (Li and Nattel, 1997) and outward K^+ currents (Yue *et al.*, 1996; Wettwer *et al.*, 2004). During this phase there is a time dependent activation of the delayed rectifier K^+ current (particularly the rapid delayed rectifier K^+ current, I_{Kr}, and the slowly activating delayed rectifier current, I_{Ks}) resulting in rapid phase 3 repolarisation and termination of the action potential (Wang *et al.*, 1993, 1994). Both the constitutive acetylcholine-dependent potassium current (I_{KACh}) and ultra-rapid delayed rectifier potassium current (I_{Kur}) are also involved in repolarisation (Wang *et al.*, 1993; Wettwer *et al.*, 2004).

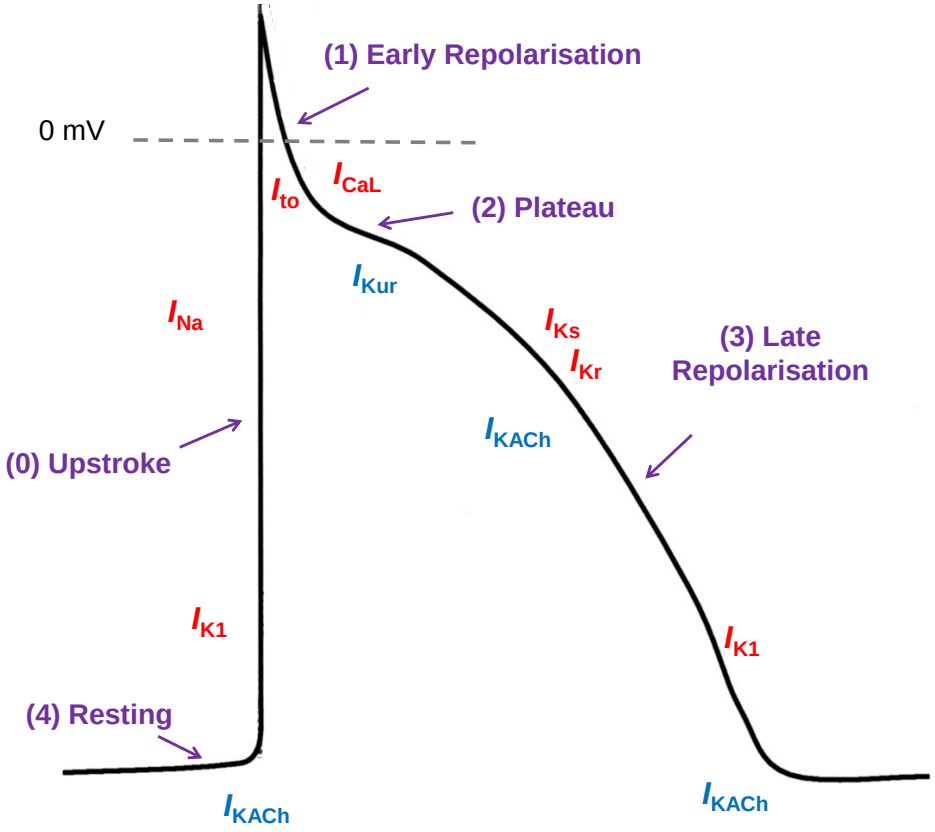

Figure 1.1 **Typical atrial action potential**. Schematic cardiac action potential illustrating phases 0 to 4 (in purple) and the corresponding ionic currents (in red) accounting for the shape and time course of the action potential. The ion currents specific to the atrial action potential are shown in blue (Adapted from Ehrlich *et al.*, 2008).

1.1.3 Ectopic activity

While all cardiac tissue has inherent pacemaking activity, under normal physiological conditions the sino-atrial node is the dominant pacemaker of the heart. This is due to the fact that the sino-atrial node has the highest rate of spontaneous depolarization, and therefore suppresses the pacemaking activity of the other cardiac tissues. However, electrical and structural alterations in cardiac tissue can lead to abnormal spontaneous discharge, which results in ectopic activity (where the pacemaking electrical activity initiates in a site other than the sino-atrial node; Figure 1.2). Such ectopic activity is responsible for the initiation of AF (Haïssaguerre *et al.*, 1998).

In AF patients, the pulmonary vein (PV), which transports oxygenated blood from the lungs to the left atrium (LA), is the most common site of focal ectopic activity (Haïssaguerre *et al.*, 1998), and this will be discussed in more detail later. In addition, ectopic activity can also originate from the vena cava, ligament of Marshall, mitral valve, tricuspid valve and crista terminalis (Wit and Cranefield, 1976; Hwang *et al.*, 1999; Tsai *et al.*, 2000; Liu *et al.*, 2002; Wu *et al.*, 2002). Ectopic activity can be due to enhanced automaticity, afterdepolarisations and triggered activity. Enhanced automaticity (Figure 1.3A) has been shown to be a result of abnormalities in certain currents (such as a decrease in I_{K1} and/or an increase in the pacemaker "funny" current, I_f) during phase 4 of the action potential (Hoppe *et al.*, 1998; Stillitano *et al.*, 2008). Afterdepolarisations are abnormal depolarisations that occur following the action potential upstroke and there are two types:

- Delayed afterdepolarisations (DADs), which occur when action potential repolarisation is complete or almost complete (Figure 1.3B).
- Early afterdepolarisations (EADs), which are evident during phase 2 or phase 3 of the action potential (Figure 1.3C).

Afterdepolarisations can become large enough to reach the threshold potential for activation of a regenerative inward current, resulting in an action potential. This is referred to as triggered activity (Brugada and Wellens, 1984).

1.1.3.1 Delayed afterdepolarisations

In mammalian cardiomyocytes, transmembrane Ca^{2+} entry via L-type Ca^{2+} channels triggers Ca^{2+} release from the sarcoplasmic reticulum into the cytosol through the ryanodine receptor. This is termed Ca^{2+} induced Ca^{2+} release (Fabiato and Fabiato, 1978; Cannell *et al.*, 1995). Cytosolic Ca^{2+} levels are restored by reuptake of Ca^{2+} into the sarcoplasmic reticulum via the sarcoplasmic reticulum Ca^{2+} ATPase (SERCA) pump or by extrusion from the cell via the sodium/calcium exchanger (NCX), which extrudes one Ca^{2+} ion from the cytosol in exchange for three Na^{+} ions (Mackenzie *et al.*, 2004). Generation of a transient inward current (I_{ti}) upon activation of forward mode NCX, as well as Ca^{2+} overload, due to increased Ca^{2+} influx, decreased Ca^{2+} efflux and/or opening of the sarcoplasmic reticulum Ca^{2+} channels can cause substantial depolarisation in cardiomyocytes leading to DADs (Kass *et al.*, 1978; Tweedie *et al.*, 2000; Fujiwara *et al.*, 2008).

1.1.3.2 Early afterdepolarisations

When the action potential duration (APD) becomes unusually prolonged, potentially because of either an increase in I_{CaL}, an enhancement in the late sodium current (I_{NaL}) (Song *et al.*, 2008; Lemoine *et al.*, 2011) or a reduction in the K^{+} current (Ehrlich *et al.*, 2005), this allows *L*-type Ca^{2+} channels to recover from inactivation and re-activate (January and Riddle, 1989; Zeng and Rudy, 1995). The Ca^{2+} influx results in increased Ca^{2+} induced Ca^{2+} release, which may then generate an inward current sufficient enough to overcome the outward repolarising K^{+} currents and generate EADs during phase 2 of repolarisation (January and Riddle, 1989; Zeng and Rudy, 1995). In addition, Burashnikov and Antzelevitch, (2003) reported the appearance of EADs in dog atrial cardiomyocytes during the late stages of repolarisation. These late phase 3 EADs appeared at rapid atrial rates and were associated with an abbreviated APD.

1.1.3.3 Re-entry

Re-entry requires a substrate and a trigger that acts on that substrate (Figure 1.2). If there is a suitable substrate for re-entry then different zones of tissue can continually reactivate each other, producing persistent re-entrant activity (Allessie *et al.*, 1976). Remodelling, which is discussed in more detail in section 1.1.4 can provide a suitable substrate for re-entry, whereas ectopic activity can result in re-entry triggers. There are two key mechanisms of re-entry; spiral wave re-entry and leading circle re-entry which are illustrated in Figure 1.4.

Spiral wave re-entry (Figure 1.4A) involves a fast circulating rotor consisting of a central core of excitable but unexcited tissue, with a circulating curved wavefront which propagates outwards into excitable tissue (Davidenko *et al.*, 1992; Pertsov *et al.*, 1993; Ikeda *et al.*, 1996). Tissue excitability and refractoriness determine the size of the spiral wave. For example, increased excitability and a short effective refractory period (ERP) will allow rapid rotation of the spiral wave around the small core, stabilising rotor maintenance (Comtois *et al.*, 2005). A decrease in excitability or increased refractoriness will enlarge and slow the rotor, enhancing the chance that the rotors will be abolished as they come into contact with refractory tissue or anatomical boundaries (Comtois *et al.*, 2005).

With the leading circle concept (Figure 1.4B), re-entry establishes itself in the minimum sized circuit needed for the maintenance of re-entry. The minimum wavelength (λ; circumference of the circle) of the circuit is calculated by (Allessie *et al.*, 1976; Rensma *et al.*, 1988):

λ = ERP x conduction velocity

If the atria contain a small number of larger circuits, re-entry is unstable and self-terminating. To allow the persistence of a re-entrant circuit, the wavelength has to be shorter than the available conduction path length, which then leaves an excitable gap before the propagating wavefront. For example, a decrease in wavelength (due to a reduction in the ERP or the conduction velocity) results in smaller, more abundant

circuits and maintenance of AF, as simultaneous self-termination of all the circuits is unlikely. An increase in the ERP, potentially due to an antiarrhythmic drug, would result in an increase in the wavelength (Figure 1.4C), decreasing the number of circuits that can be maintained. Therefore AF cannot be sustained (Moe and Abildskov, 1959; Moe, 1962; Allessie *et al.*, 1977).

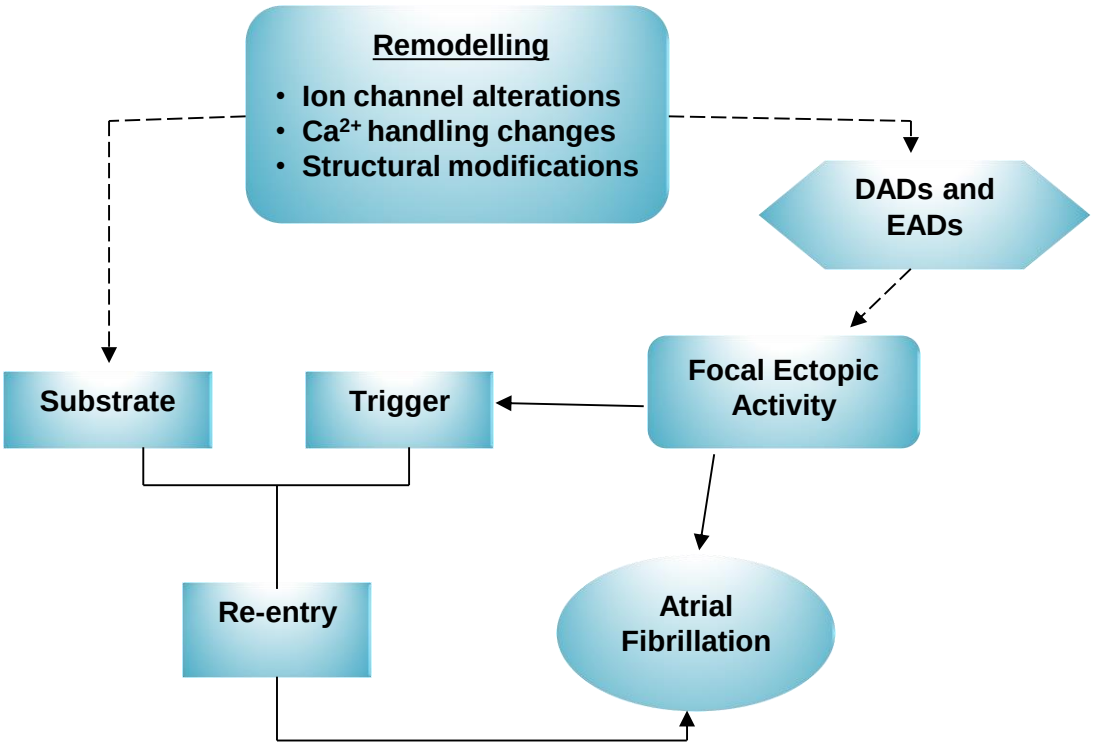

Figure 1.2 **Basic mechanisms of atrial fibrillation**. Remodelling of atrial tissue in the form of ion channel alterations or Ca^{2+} handling changes can generate arrhythmogenic delayed afterdepolarisations (DADs) and early afterdepolarisations (EADs), which can trigger electrical activity in areas outwith the sino-atrial node. The focal ectopic activity can result in the initiation and maintenance of atrial fibrillation (AF). Re-entry which relies on the action of a trigger (typically from an ectopic beat) acting on a susceptible substrate can also lead to AF (Dobrev and Nattel, 2010).

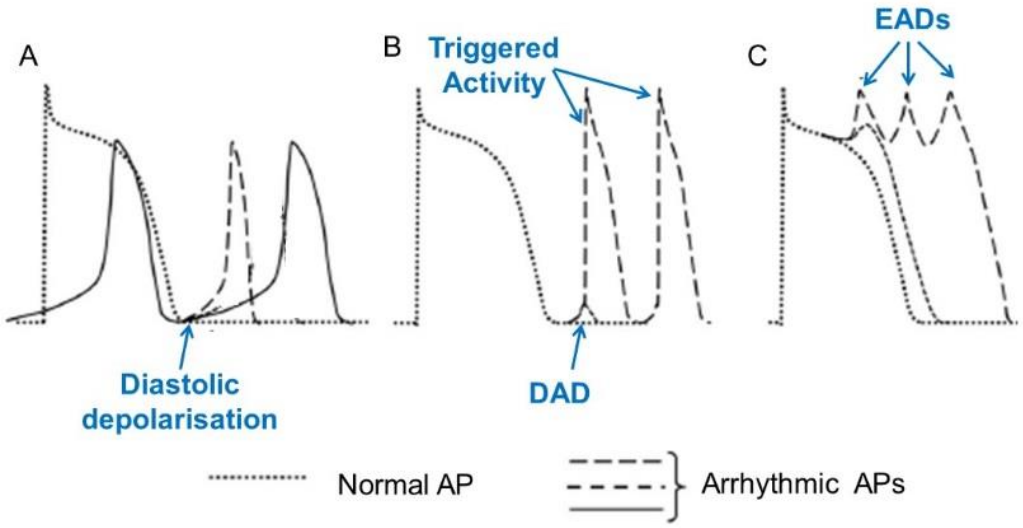

Figure 1.3 **Mechanisms of focal ectopic activity**. (A) Alterations during phase 4 of the action potential such as a decrease in I_{K1} results in diastolic depolarisation induced enhanced automaticity. (B) Delayed afterdepolarisation (DAD) can occur after repolarisation of the action potential and can induce triggered activity. (C) Early afterdepolarisations (EAD) occur during phase 2 or phase 3 of the action potential (Iwasaki *et al.*, 2011).

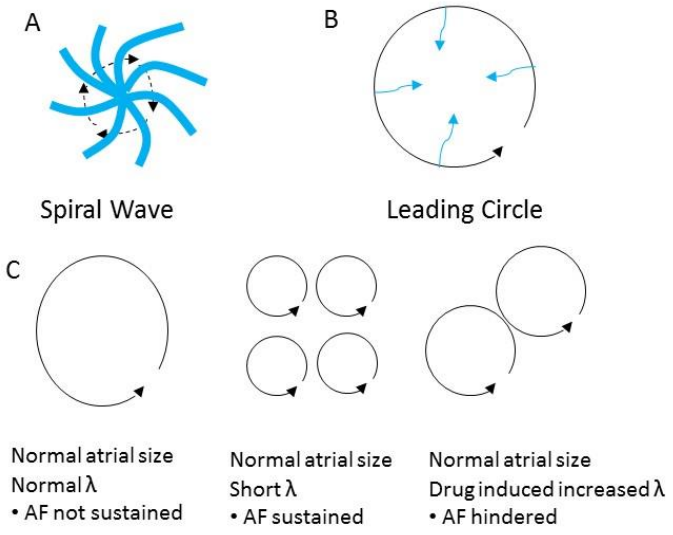

Figure 1.4 **Re-entry Concepts**. (A) Spiral wave model of re-entry, consisting of a core of excitable but unexcited tissue with a circulating curved wavefront which propagates outwards into excitable tissue. (B) Leading circle model of re-entry. Activity establishes itself in the smallest pathway that can support re-entry, with wavelets maintaining the central core in a refractory state. (C) Role of wavelength in AF maintenance according to the leading circle model. Initiation and maintenance of re-entry circuits depends on the length of the wavelength. Shorter wavelengths allow several simultaneous re-entry circuits to be sustained, favouring AF. Antiarrhythmic drugs that increase the refractory period and therefore the wavelength, reduce the number of circuits that can be accommodated, favouring the suppression of AF. λ – wavelength (Nattel, 2002b).

1.1.4 Atrial remodelling and AF

Atrial remodelling, which is defined as any continual alteration in the structure or function of the atria, is thought to be a contributor to the initiation and maintenance of AF (Xu *et al.*, 2013). Cardiac diseases such as heart failure, can lead to atrial remodelling and promotion of AF (Li *et al.*, 1999). The presence of AF itself and the associated rapid atrial tachycardia can also result in further atrial remodelling. It is thought that atrial cardiomyocytes may adapt to AF by facilitating the maintenance of rapid atrial firing with the lowest metabolic cost, although this may result in further promotion of AF. This has been shown in animal models such as those developed as by Wijffels *et al.* (1995). They reported in a goat model of AF that while initially AF is short lived, over time AF itself causes atrial remodelling resulting in a gradual increase of its likelihood to become sustained. This was described as "AF begets AF".

Electrical remodelling, which alters the expression and/or function of ion channels, pumps and exchangers in atrial cardiomyocytes can promote AF (Wagoner *et al.*, 1997; Dobrev *et al.*, 2002; Neef *et al.*, 2010; Voigt *et al.*, 2012). Remodelling of ion channels can abbreviate the cardiac action potential, increasing the tissue vulnerability to the initiation and maintenance of re-entry (Colman *et al.*, 2013). The $I_{K1,}$ which determines the cardiomyocyte resting membrane potential and contributes to the termination of phase 3 repolarisation, has been found to be increased in atrial cells of AF patients (Giles and Imaizumi, 1988; Zhang *et al.*, 2005). This increase in I_{K1} could contribute to a decrease in APD, promoting re-entry (Wagoner *et al.*, 1997; Dobrev *et al.*, 2002). Electrical remodelling can also result in Ca^{2+} overload, due to increased Ca^{2+} influx or decreased Ca^{2+} efflux (Vest *et al.*, 2005; Chelu *et al.*, 2009; Voigt *et al.*, 2012), which leads to afterdepolarisations and ectopic activity. In atrial cardiomyocytes from AF patients, an increased open probability of the ryanodine receptor, which triggered the release of Ca^{2+} from the sarcoplasmic reticulum was reported (Neef *et al.*, 2010; Voigt *et al.*, 2012). This enhanced sarcoplasmic reticulum Ca^{2+} leak resulted in the promotion of arrhythmogenic DADs. An increase in Ca^{2+} overload can also promote further atrial remodelling. For example, I_{CaL} is

reduced in atrial cardiomyocytes from AF animal models (Yagi *et al.*, 2002; Bosch *et al.*, 2003) and human permanent AF patients (Bosch *et al.*, 1999; Workman *et al.*, 2001), potentially as a compensatory mechanism to alleviate the Ca^{2+} overload in AF (Qi *et al.*, 2008). However, a reduction in I_{CaL} could contribute to a reduction in APD, promoting re-entry and maintenance of AF. The AF induced remodelling can also lead to conduction abnormalities as altered connexion expression and distribution has been observed in human AF patients (Kostin *et al.*, 2002; Nao *et al.*, 2003; Firouzi *et al.*, 2004) and in the goat AF model (van der Velden *et al.*, 1998).

Structural remodelling is characterised by increased atrial size and cardiac tissue fibrosis. Sanfilippo *et al.* (1990) investigated the structural remodelling of the atria of AF patients and reported that over time, both atria can become enlarged as a consequence of AF. This increased atrial size is thought to favour re-entry persistence (Zou *et al.*, 2005). Structural changes in the form of increased levels of fibrosis, are also common in the atria of AF patients (Boldt *et al.*, 2004; Oakes *et al.*, 2009), as well as in dog AF models (Li *et al.*, 1999). Fibrosis is the excessive deposition of extracellular matrix components such as collagen and fibronectin, synthesised by fibroblast related cells (Bishop, 1998; Swynghedauw, 1999). The presence of fibrosis is thought to interfere with local conduction and increase tissue susceptibility to re-entry (Li *et al.*, 1999; Verheule *et al.*, 2013). Furthermore, Xu *et al.* (2004) reported a positive correlation in the extent of fibrosis and the persistence of AF, suggesting that AF itself may promote fibrosis.

1.1.5 Pharmacological treatment of AF

There are two main options in the treatment of AF: rate control and rhythm control. With rate control, regulation of ventricular rate is key while the atria remain fibrillating, whereas maintenance of sinus rhythm is the central aim in rhythm control (Fuster *et al.*, 2006). Rhythm or rate control can be achieved by pharmacological treatment in the form of antiarrhythmic drugs. Vaughan Williams, 1984, grouped the antiarrhythmic drugs according to their mechanisms of action (although some can span several classes), namely, Na^+ channel blockade (Class I), β-adrenoceptor antagonism (Class II), K^+ channel blockade (Class III) and Ca^{2+}

channel blockade (Class IV). Alongside antiarrhythmics, aspirin or other anticoagulants are recommended to reduce the risk of stroke in AF patients (Fuster *et al*., 2006). However, the pharmacological treatments available are only moderately effective in the treatment of AF and many trigger unwanted side effects such as ventricular arrhythmia or organ toxicity (Camm *et al.*, 2010).

1.1.6 Non pharmacological treatment of AF

Surgical and ablation techniques can be effective rhythm control treatments for AF when pharmacological therapy is unsuccessful (Calkins *et al.*, 2007). The Cox-Maze III procedure uses a "cut and sew" technique to separate the left and right atrium and isolate the four pulmonary veins (PVs). The resultant scar tissue interrupts electrical impulses and re-entry circuits (Cox *et al.*, 1995a, 1995b). Despite >90% AF termination success rate, few cardiologists perform Cox-Maze III due to the complexity and technical difficulties of the procedure (Prasad *et al.*, 2003; Mokadam *et al.*, 2004). However, surgical advances have allowed for the application of various energy sources such as radiofrequency, ultrasound and cryotherapy, enabling the procedure to be carried out with less tissue damage. This is termed Cox-Maze IV as a similar lesion pattern to the original is used, but with the use of energy sources in place of the "cut and sew" technique, and it is now a widely used surgical treatment for AF (Sandoval *et al.*, 2011; Melby *et al.*, 2013).

Haïssaguerre *et al.* (1998) first discovered that AF triggered by ectopic activity originating from the PV could be terminated by radio-frequency ablation of the PVs. The procedure utilised mapping catheters in the pulmonary vein-left atrial (PV-LA) junction as a guide to establish the areas of PV ectopic activity. This widely used procedure now employs monopolar and bipolar radiofrequency in patients with paroxysmal AF (Camm *et al.*, 2010). However, recurrence of AF is possible after the procedure due to the PVs re-establishing electrical connection with the LA (Shah *et al.*, 2008; Bertaglia *et al.*, 2014).

1.2 The structure of the PV

Brunton and Fayrer, (1876) first observed that on cessation of artificial respiration, the PVs of anaesthetised rabbits and cats continued to pulsate after the heart had ceased beating; thus establishing the ability of the PV to contract independent of the atria. Following this discovery, the anatomical, contractile and electrical properties of the PVs have been the subject of numerous studies (Chen *et al.*, 2002b; Hocini *et al.*, 2002; Ehrlich *et al.*, 2003; Bronquard *et al.*, 2007; Lo *et al.*, 2007; Luk *et al.*, 2008); however the mechanism underlying the PV ectopic activity is not fully elucidated.

1.2.1 Anatomy of the PV

A number of histological studies reported the PV structure of mammalian species (such as human, rat, dog and guinea pig) to consist of several layers of different cell types, including the cardiomyocyte sleeve. Closest to the lumen is the tunica intima comprised of a thin layer of endothelial cells. Then there is the tunica media, which is comprised of both smooth muscle cells and the cardiomyocyte sleeve, separated by a layer of collagenous tissue and finally a tunica externa, or adventitia, comprising of elastic fibrils and collagenous tissue (Nathan and Eliakim, 1966; Ludatscher, 1968; Hashizume *et al.*, 1998; Saito *et al.*, 2000; Hocini *et al.*, 2002; Hassink *et al.*, 2003; Takahara *et al.*, 2011). The cardiomyocytes are believed to be responsible for the veins unique contractile and electrophysiological properties. The physiological relevance of the cardiomyocyte sleeve remains unknown; although it has been hypothesised that the PV contraction could prevent the backflow of blood when the atria contracts (Nathan and Eliakim, 1966). The cardiomyocyte sleeve was described as consisting of one or more layers of cardiomyocytes running in circular, longitudinal, oblique and spiral directions (Nathan and Eliakim, 1966). Further examination of the PVs of several species elaborated on the complexity of the cardiomyocyte sleeve, illustrating the non-uniform and complex arrangement of cardiomyocytes (Figure 1.5) (Hashizume *et al.*, 1998; Ho *et al.*, 2001). In some parts of the tissue, numerous cardiomyocytes are grouped together to form bundles, with several gaps between the bundles interspersed with fibrous tissue (which consists of

extracellular matrix proteins such as type 1 collagen) (Hashizume *et al.*, 1998; Ho *et al.*, 2001). As the sleeve becomes increasingly distal from the junction at which the PV meets the LA (PV-LA junction), the cardiomyocyte bundles diminish, and are replaced with an increasing amount of fibrous tissue (Saito *et al.*, 2000; Hassink *et al.*, 2003). Gap junction proteins are also present in the PV cardiomyocyte sleeve, thereby enabling the conduction of electrical activity between the PV cardiomyocytes (Verheule *et al.*, 2002; Sun *et al.*, 2008). Electron microscopy studies revealed a strong resemblance of PV cardiomyocytes to those of the LA in that they possessed completely developed contractile apparatus (Ludatscher, 1968; Hashizume *et al.*, 1998; Verheule *et al.*, 2002).

In atrial cardiomyocytes transverse-tubules (T-tubules) are thought to be virtually absent in smaller animals such as rat, and present in larger mammals such as sheep and human (Dibb *et al.*, 2009; Lenaerts *et al.*, 2009; Richards *et al.*, 2011). The presence of T-tubules in the PV cardiomyocytes of human and other mammals remains controversial. An electron microscopy study reported sparse T-tubules in the rat PV cardiomyocytes (Masani, 1986), whereas an abundance of T-tubules were observed in the same cells stained with di-8-ANEPPS (Okamoto *et al.*, 2012), and in dog PV sections stained with the surface membrane stain, wheat germ agglutinin (Melnyk *et al.*, 2005). However, Rietdorf *et al.* (2014) reported the absence of T-tubules in mouse PV sections.

The length of the human PV cardiomyocyte sleeve ranges from 0.4-4.8 cm, with a longer and more prominent sleeve present in the superior veins compared to the inferior veins (Saito *et al.*, 2000; Ho *et al.*, 2001; Hassink *et al.*, 2003; Kholová and Kautzner, 2003; Roux *et al.*, 2004). The dog PV sleeve is of similar length to that of human, with both cardiomyocyte sleeves terminating before reaching the lungs (Verheule *et al.*, 2002). However, the PV sleeve in several rodent species such as mouse and rat extends into the lungs (Kramer and Marks, 1965; Mueller-Hoecker *et al.*, 2008). The reason for this difference remains unknown, although it is hypothesised that in humans the pericardium potentially acts as a barrier for PV

cardiomyocytes, preventing further extension of the sleeve (Mueller-Hoecker *et al.*, 2008).

The PV arrhythmogenic propensity could be associated with the length of the cardiomyocyte sleeve, with several groups reporting increased ectopic foci in the longest cardiomyocyte sleeves of human PVs (Haïssaguerre *et al.*, 1998; Ho *et al.*, 2001). The PV sleeves of AF patients were found to be longer and thicker when compared to patients without a history of AF (Hassink *et al.*, 2003; Kholová and Kautzner, 2003). Although, in contrast, Saito *et al.* (2000) reported no such relationship. The complex arrangement of the cardiomyocytes in the PV is also thought to enhance the arrhythmogenicity, as the abrupt changes in cardiomyocyte orientation can disturb electrical conduction, facilitating re-entry (Ho *et al.*, 2001; Hocini *et al.*, 2002; Hamabe *et al.*, 2003; Roux *et al.*, 2004; Tan *et al.*, 2006). This complex and non-uniform arrangement may account for the slower conduction velocity in the guinea pig PV compared to the LA (Takahara *et al.*, 2011). The presence of fibrosis, particularly in the distal areas of the PV sleeve, is also thought to enhance the arrhythmogenic substrate of the PV (Tagawa *et al.*, 2001; Hassink *et al.*, 2003; Steiner *et al.*, 2006). Since fibrotic tissue offers a larger resistance to the propagation of electrical activity, this could potentially slow the conduction and create favourable substrate conditions for re-entry (Hassink *et al.*, 2003).

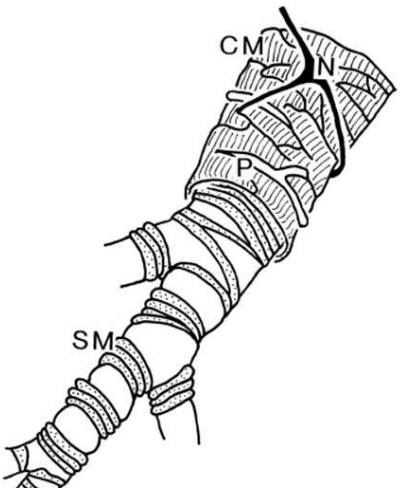

Figure 1.5. **Schematic representation of the rat pulmonary vein**. The pulmonary vein (PV) contains a thin layer of smooth muscle cells (*SM*). Outside of the smooth muscle layer, are several layers of cardiomyocyte cells (*CM*) arranged in a complex manner, creating a cardiomyocyte sleeve on the PV. Capillaries (P) and nerve fibres (N) are present in the cardiomyocyte sleeve (Hashizume *et al.*, 1998).

1.2.2 Origin of PV cardiomyocytes

The origin of the PV cardiomyocyte sleeve has been a subject of great debate and two separate hypotheses have been proposed, the first being that the cardiomyocyte sleeve is an extension of left atrial cells into the PV during neonatal development (Jones *et al.*, 1994; Millino *et al.*, 2000). The second is that the cardiomyocytes are originally part of the PV cell line, which then differentiate into cardiomyocytes during development (van den Hoff *et al.*, 2004). A study utilising genetic profiling at different stages of murine development introduced a biphasic model connecting both hypotheses. It was shown that mouse PV cardiomyocytes originate from PV mesenchymal cells at the connection of the PV and LA and then proliferate, migrate, and expand to form the cardiomyocyte sleeve (Mommersteeg *et al.*, 2007). This is further supported by evidence demonstrating that the PV cardiomyocytes of various species possess a variable distribution, a highly differentiated physiological state and intrinsically pre-set developmental clock, which is different to that of the LA (Mueller-Hoecker *et al.*, 2008; Kracklauer *et al.*, 2013). The difference in origin of the PV cardiomyocytes in comparison to those of the LA, could support the hypothesis that PV cardiomyocytes possess a dissimilar physiology and pharmacology to LA cardiomyocytes and that they are more prone to the initiation of ectopic activity.

1.2.3 Innervation of the PV

The human PV cardiomyocyte sleeve contains a nerve plexus of cardiac origin (Armour *et al.*, 1997; Tan *et al.*, 2006; Vaitkevicius *et al.*, 2008) with autonomic nerves in clusters, which are termed ganglionated plexi (Armour *et al.*, 1997). Pauza *et al.* (2000) identified seven ganglionated subplexuses of the cardiac neural plexus and reported that three of these surrounded the PV. Immunohistochemical staining of human PVs revealed the majority (approximately 60%) of nerve bundles were purely adrenergic, 10% were purely cholinergic, 25% consisted of both cholinergic and adrenergic nerves in the same nerve bundle and 5% of nerve bundles were not immunoreactive to the antibodies used (Tan *et al.*, 2006). However, the innervation pattern varies between species. In dog PVs, Arora *et al.* (2008) reported approximately 67% of nerve bundles contained cholinergic and adrenergic nerves,

with the remaining bundles consisting of purely cholinergic nerves. A mix of cholinergic and adrenergic nerve bundles were also identified in the PVs of guinea-pig, rat and mouse (Fisher, 1965; Cech, 1969; Paes de Almeida *et al.*, 1975; Zarzoso *et al.*, 2013).

Investigations using a number of animal models have suggested that the autonomic nervous system may contribute to the generation of PV ectopic activity. Direct electrical stimulation of the autonomic nerves in dog PV preparations *in vitro,* resulted in a shortening of the APD as well as initiation of afterdepolarisations and triggered activity in the majority of PVs (Schauerte *et al.*, 2001; Patterson *et al.*, 2005, 2007). Similar results were observed *in vivo* in the dog, where autonomic stimulation produced ectopic beats in the PV (Schauerte *et al.*, 2001; Patterson *et al.*, 2005, 2007). The afterdepolarisations and triggered activity were suppressed by cholinergic (atropine) or β-adrenergic (atenolol) receptor block, demonstrating that parasympathetic and sympathetic nerve activation may contribute to the development of the arrhythmogenic activity (Patterson *et al.*, 2005). Block of the ryanodine receptor also inhibited this arrhythmogenic activity, suggesting that autonomic induced ectopic activity is the result of Ca^{2+} release through the ryanodine receptor (Patterson *et al.*, 2005). Arrhythmogenic activity could also be triggered by parasympathetic or sympathetic nerve stimulation alone. Sympathetic stimulation through activation of α- and β-adrenoceptors with noradrenaline produced a positive inotropic effect (Maupoil *et al.*, 2007; Malécot *et al.*, 2014), and induced triggered activity in rat PV preparations (Doisne *et al.*, 2009; Malécot *et al.*, 2014) or in cardiomyocytes isolated from the rat PV (Okamoto *et al.*, 2012). Moreover, microelectrode recordings revealed adrenergic stimulation also induced afterdepolarisations and in some instances triggered activity in PVs from rabbit (Lo *et al.*, 2007), guinea-pig (Cheung, 1981), mouse (Tsuneoka *et al.*, 2012) and dog (Sicouri *et al.*, 2008, 2012), further supporting the notion that the sympathetic neuronal influence alone can induce arrhythmogenic activity. Interestingly, application of noradrenaline did not induce arrhythmic activity in rat LA tissue (Maupoil *et al.*, 2007; Doisne *et al.*, 2009), indicating that PV may be more prone to ectopic activity generated by adrenergic activation. The autonomic nervous system

has also been associated with the promotion of PV ectopic activity in humans. A study in patients with paroxysmal AF and ectopic activity, which originates in the PV, identified an initial increase in adrenergic tone followed by a distinct shift toward vagal dominance directly before AF onset (Zimmermann and Kalusche, 2001). In addition, in patients with paroxysmal AF, activation of the autonomic nervous system by endocardial high frequency stimulation of ganglionated plexi, triggered ectopic activity in human PVs (Lim *et al.*, 2011).

1.2.4 Presence of "pacemaker" cells

The sino-atrial node contains pacemaker (P-cells) which are thought to generate the pacemaker activity of the heart (James *et al.*, 1966; Bleeker *et al.*, 1980). There is increasing evidence that these P-cells may also be present in the PV, with some hypothesising that these cells could contribute to PV ectopic activity (Masani, 1986; Perez-Lugones *et al.*, 2003; Chou *et al.*, 2005). Using electron microscopy, Masani, (1986) identified P-cells distally in the rat PV. In addition, the use of a positive periodic-acid Schiff (PAS) stain as an indicator for P-cells, revealed the presence of P-cells in dog PVs, with an increased presence in close proximity to areas of focal ectopic activity (Chou *et al.*, 2005; Tan *et al.*, 2008). However, there are conflicting reports regarding the presence of P-cells in the human PV. Perez-Lugones *et al.* (2003) observed P-cells in human PVs, but only in those with a history of AF, whereas Nguyen *et al.* (2009) reported PAS-positive cells in the PVs of patients with and without a history of AF.

Pacemaker and other excitable cells, which are not typical cardiac cells have also been identified in the PV, although their role in ectopic activity is unclear. For instance, interstitial Cajal like cells, which are responsible for pacemaker activity in the gastrointestinal tract (Sanders, 1996), have been observed in the PVs of dog AF models (He *et al.*, 2012) and human PVs of those with and without a history of AF (Gherghiceanu *et al.*, 2008; Morel *et al.*, 2008). Melanocyte like cells, which are excitable cells, were also identified in the mouse and human PVs (Levin *et al.*, 2009). Interestingly, atrial arrhythmias could not be induced in genetically modified

mice lacking melanocyte cells in the PV and atrium, suggesting that these cells may play a role in arrhythmogenesis (Levin *et al.*, 2009).

1.3 Electrophysiology of the PV

1.3.1 Action potential and ionic currents of the PV; comparison to the LA and implications for ectopic activity initiation

Both PV and LA tissue can be electrically stimulated to produce action potentials (Cheung, 1981; Sicouri *et al.*, 2008, 2012; Song *et al.*, 2008; Doisne *et al.*, 2009). However, whether there is a difference in the action potential characteristics between both tissues and if this is linked to the greater arrhythmogenic propensity of the PV compared to the LA remains controversial (Doisne *et al.*, 2009; Takahara *et al.*, 2011; Okamoto *et al.*, 2012). With the use of the patch clamp recording technique, Ehrlich *et al.* (2003) demonstrated that the PV cardiomyocytes of dogs had a more depolarised resting membrane potential compared to those of the LA Since the resting membrane potential is maintained by the outward hyperpolarising I_{K1} current (Figure 1.2), the smaller I_{K1} current density observed in dog PV cardiomyocytes compared to those of the LA, is thought to contribute to the less negative membrane potential (Cha *et al.*, 2005; Melnyk *et al.*, 2005). Several groups have also reported that rat PV cardiomyocytes exhibit a more depolarised resting membrane potential compared to the LA (Doisne *et al.*, 2009; Okamoto *et al.*, 2012; Malécot *et al.*, 2014), whereas others observed no difference in the resting membrane potential in both tissues of the rat (Miyauchi *et al.*, 2004, 2005).

Whether there are variations in APD between PV and LA cardiomyocytes also remains controversial (Ehrlich *et al.*, 2003; Cha *et al.*, 2005; Ding *et al.*, 2006; Doisne *et al.*, 2009; Okamoto *et al.*, 2012). A shorter APD was recorded in dog and rat PV cardiomyocytes in comparison to those of the LA (Ehrlich *et al.*, 2003; Cha *et al.*, 2005; Okamoto *et al.*, 2012). The abbreviated APD was attributed to differences in the densities of specific currents in the PV and LA. Smaller I_{CaL} and higher I_{Kr} and I_{Ks} current densities were recorded in the rat and dog PV, than in the LA (Ehrlich *et al.*, 2003; Cha *et al.*, 2005; Okamoto *et al.*, 2012). In addition Melnyk *et al.* (2005)

reported higher expression of hERG (I_{Kr} subunit) and KvLQT1 (I_{Ks} subunit) in dog PV cells. Since the K^+ currents and the inward Ca^{2+} currents are important determinants of the APD (Figure 1.2), an increase in the K^+ current and/or a decrease in the Ca^{2+} current could lead to shortening of the APD. In contrast, others have observed a longer APD in rat, dog and rabbit PVs in comparison to the LA (Arora *et al.*, 2003; Ding *et al.*, 2006; Doisne *et al.*, 2009).

A shorter APD can result in a decrease in the ERP, creating a favourable substrate for re-entry (Nattel, 2002). In human patients without a history of AF, a longer ERP was observed in PV cardiomyocytes compared to those of the LA. However, in AF patients, the ERP was shorter in the PV than in the LA, further suggesting a shortened ERP is associated with arrhythmic activity (Jaïs *et al.*, 2002). A reduced upstroke velocity (dV/dt_{max}) was also established in dog PVs compared to the LA (Ehrlich *et al.*, 2003; Okamoto *et al.*, 2012). The I_{Na} density and activation/inactivation kinetics were comparable in both tissues, thus inactivation of $I_{Na,}$ due to the more depolarised PV cardiomyocyte resting membrane potential, could be responsible for the reduced dV/dt_{max} (Ehrlich *et al.*, 2003; Malécot *et al.*, 2014). In contrast, Doisne *et al.* (2009) recorded no difference in dV/dt_{max} between rat PV and LA cells.

1.3.2 Calcium handling in PV and LA cardiomyocytes

Disruption of Ca^{2+} regulation is thought to enhance the arrhythmogenicity of cardiomyocytes (Honjo *et al.*, 2003; Patterson *et al.*, 2005) and so a number of studies have investigated the Ca^{2+} handling properties in PV cardiomyocytes compared to those of the LA. Changes in intracellular Ca^{2+} can be monitored using Ca^{2+} sensitive fluorescent indicators and wide field or confocal microscopy. The Ca^{2+} sparks are the result of spontaneous Ca^{2+} release from the sarcoplasmic reticulum, due to opening of the ryanodine receptor (Cheng *et al.*, 1993; Blatter *et al.*, 1997); they also represent the fundamental event in excitation contraction coupling in cardiomyocytes. These Ca^{2+} sparks and/or spontaneous Ca^{2+} transients have been observed in PV cardiomyocytes of the mouse (Rietdorf *et al.*, 2014), rat (Logantha *et al.*, 2010), rabbit (Chang *et al.*, 2008) and dog (Coutu *et al.*, 2006).

Although a lone spark is not sufficient for cardiomyocyte excitation; the simultaneous occurrence of numerous sparks, can generate a propagating Ca^{2+} wave (Cheng *et al.*, 1993). Whether there is a difference in Ca^{2+} handling properties between the PV and LA remains controversial. Dog PV and LA cardiomyocytes from control animals and those isolated from dogs which were subjected to 7-days of rapid atrial pacing, exhibited similar electrically evoked Ca^{2+} transient amplitude, half-decay time, beat-to-beat regularity, propensity to generate alternans and caffeine induced Ca^{2+} transients (Coutu *et al.*, 2006). In contrast, Jones *et al.* (2008) observed a number of differences in the Ca^{2+} handling properties of rabbit PV cardiomyocytes compared to those of the LA, such as higher diastolic Ca^{2+} during stimulation and a slower decay to resting diastolic Ca^{2+} on stimulation cessation in PV cardiomyocytes. They also recorded smaller caffeine evoked responses in the PV cardiomyocytes, suggesting that these cells have a smaller sarcoplasmic reticulum Ca^{2+} capacity. Whether these reported differences in PV Ca^{2+} handling are a result of a species difference remains unknown.

1.3.3 Automaticity in the PV

As far as basic science studies are concerned, the existence of automaticity in the PV is a somewhat controversial issue. Automaticity is often referred to as spontaneous action potentials, since they occur in the absence of any applied electrical stimulation. Conflicting results have been reported between different animal species and different research groups. Chen *et al.* (2000, 2001) remain the only group to observe automaticity and afterdepolarisations in dog PV preparations as well as in cardiomyocytes isolated from the PV; while others have observed no such activity in the dog PV (Hocini *et al.*, 2002; Ehrlich *et al.*, 2003; Wang *et al.*, 2003; Patterson *et al.*, 2005; Sicouri *et al.*, 2008). Automaticity has also been observed in the intact PV and single PV cardiomyocytes from the guinea pig (Cheung, 1981; Namekata *et al.*, 2009), rabbit (Chen *et al.*, 2002b, 2004, 2009; Wongcharoen *et al.*, 2006; Chang *et al.*, 2007) and mouse (Tsuneoka *et al.*, 2012), although there is considerable variability in the proportion of cardiomyocytes exhibiting automatic activity. Again, others did not observe automaticity in similar tissues (Honjo *et al.*, 2003; Luk *et al.*, 2008). Doisne *et al.* (2009), reported the absence of intrinsic automatic activity in rat

PV preparations, whereas Egorov *et al.* (2015) observed automatic activity in 36% of rat PV tissues. In addition, Okamoto *et al.* (2012) only observed automatic activity in 2 out of 120 cardiomyocytes isolated from the rat PV. Thus, whether automaticity is a normal intrinsic property of the PV cardiomyocyte sleeve, or the consequence of the experimental conditions and/or cell isolation technique remains unresolved (Wang *et al.*, 2003; Chen *et al.*, 2006a).

1.3.4 The PV pacemaker current

The cardiac hyperpolarisation activated cation current is a mixed Na^+/K^+ inward current known as the "funny" current (I_f). It is thought to be the pacemaker current that contributes to spontaneous diastolic depolarisation, initiating the action potentials in the sino-atrial node (DiFrancesco, 1991). The molecular basis of I_f is a family of hyperpolarisation activated cyclic nucleotide-gated (HCN) channel isoforms, HCN1-4 (Baruscotti *et al.*, 2010). The expression of HCN isoforms and the contribution of I_f to spontaneous action potentials and ectopic activity in the PV is controversial. To begin with, there may be species difference in the expression of HCN isoforms as both HCN2 and HCN4 mRNA expression were observed in rabbit PVs, but absent in rat PVs (Yamamoto *et al.*, 2006). There are also conflicting reports within the same species since Li *et al.* (2014) reported the presence of HCN2 and HCN4 in dog PVs, whereas Tan *et al.* (2008) did not observe either of these isoforms. Patch clamp studies have revealed the presence of I_f in rabbit (Liu *et al.*, 2005) and dog (Li *et al.*, 2012) PV cardiomyocytes. Furthermore, the addition of the selective I_f blocker, ivabradine to rabbit PV cardiomyocytes with automatic activity reduced the frequency of automatic action potentials in a concentration-dependent manner, suggesting the involvement of I_f in PV automaticity (Suenari *et al.*, 2012). In addition, ivabradine reduced the slope of the diastolic depolarisation of spontaneous action potentials in PV cardiomyocytes isolated from rapid atrial paced dogs (Li *et al.*, 2012).

1.4 Arrhythmogenic pulmonary vein pathologies

1.4.1 Cardiac glycoside toxicity

Cardiac glycosides are used in the treatment of heart failure. However, their narrow therapeutic range can easily induce cardiac arrhythmias due to intoxication (Irons and Orgain, 1966). Intracellular recording of the membrane potential revealed that addition of the cardiac glycoside ouabain could induce afterdepolarisations and triggered activity in guinea pig and rabbit PVs (Cheung, 1981; Wongcharoen *et al.*, 2006; Namekata *et al.*, 2009), at concentrations which did not induce arrhythmias in the ventricles (Tanaka *et al.*, 2007). This suggests a possible role for the PV in the initiation of arrhythmias as a consequence of cardiac glycoside intoxication. It was proposed that ouabain induced arrhythmias in the PV through inhibition of the Na^+/K^+-ATPase, resulting in increased intracellular Na^+ accumulation and activation of the reverse mode NCX, leading to intracellular Ca^{2+} overload (Wongcharoen *et al.*, 2006). This was supported by Namekata *et al*. (2009) who reported that block of the NCX or ryanodine receptor reduced the incidence of ouabain induced arrhythmogenic activity in the PV.

1.4.2 Hyperthyroidism

There is a well-known link between hyperthyroidism and AF (Woeber, 1992; Cappola *et al.*, 2006), and thyroid hormones have been shown to shorten the atrial APD increasing the susceptibility for re-entry (Johnson *et al.*, 1973). Treatment of rabbit PV cardiomyocytes with the thyroid hormone L-triiodothyronine reduced the APD of electrically evoked action potentials and induced DADs (Chen *et al.*, 2002a). This hormone also shortened the APD and induced EADs and DADs in the PV cardiomyocytes with automatic activity (Chen *et al.*, 2002a). The ability of L-triiodothyronine to induce arrhythmogenic activity in PV cardiomyocytes suggests an increase in thyroid hormones could trigger ectopic activity in the PVs and the decreased APD may also enhance the PV susceptibility to re-entry.

1.4.3 Renin-angiotensin system

Renin released from the juxtaglomerular cells converts angiotensinogen to angiotensin-I. Angiotensin converting enzyme then converts angiotensin-I to angiotensin-II, which is the major active component of the renin-angiotensin system (RAS). The RAS components can be synthesised in the blood vessels, with the exception of renin, which is thought to be taken up by the circulation (Peach, 1977; Dzau, 1993; Nguyen Dinh Cat and Touyz, 2011). An up-regulation of angiotensin-II receptors was reported in atrial tissue of AF patients, highlighting a potential link between AF and the RAS (Goette *et al.*, 2000). Treatment with angiotensin II induced DADs in electrically evoked action potentials and increased the force of contraction in the rabbit PV, suggesting that activation of angiotensin-II receptors could play a role in PV ectopic activity (Chen *et al.*, 2006b). Patch clamp recording of PV cardiomyocytes from the rabbit revealed angiotensin II increased I_{CaL}, thereby explaining the increased contractile amplitude. Both the I_{ti} and NCX currents were also increased, which are associated with the generation of afterdepolarisations (Chen *et al.*, 2006b). Sicouri *et al*. (2011) reported that inhibition of the RAS reduced arrhythmogenic activity in the PV. They found that losartan (an angiotensin II-receptor blocker) and enalapril (an angiotensin-converting enzyme inhibitor) both displayed antiarrhythmic activity on isoprenaline and high Ca^{2+} induced EADs, DADs and triggered activity in the dog PV (Sicouri *et al.*, 2011).

1.4.4 Oxidative stress

Oxidative stress has also been linked to the initiation of AF (Mihm *et al.*, 2001; Dudley *et al.*, 2005). Induction of oxidative stress by treatment of rabbit PVs with H_2O_2 *in vitro* significantly enhanced PV contractility (Lin *et al.*, 2010). Furthermore, H_2O_2 activation of free radicals induced bursts of spontaneous action potentials and EADs in the rabbit PV (Lin *et al.*, 2010; Hanafy *et al.*, 2013), but not in the LA (Lin *et al.*, 2010) suggesting enhanced oxidative stress could be an underlying mechanism of PV ectopic activity.

1.4.5 The PV and re-entry

Development of a re-entry circuit is also thought to be an underlying mechanism of arrhythmogenic activity in the PV. The complex and non-uniform arrangement of cells in the PV with abrupt changes in their orientation is associated with conduction disturbances, creating a substrate for re-entry (Ho *et al.*, 2001; Hocini *et al.*, 2002). In addition, the shorter APD in PV cardiomyocytes, compared to that of the LA, could lead to a reduced ERP and a decrease in wavelength, favouring the occurrence of re-entry (Li *et al.*, 2001; Hocini *et al.*, 2002; Arora *et al.*, 2003; Ehrlich *et al.*, 2003). This mechanism was further examined in a computational study by Aslanidi *et al.* (2013) who suggested that a combination of action potential heterogeneity as well as conduction anisotropy between the PV and LA provides a substrate for re-entrant activity.

With the use of high-resolution optical mapping, re-entrant activity was observed *in vitro* in dog PV preparations after a combination of atrial electrical extra-stimulation and isoprenaline infusion (Arora *et al.*, 2003). Moreover, a combination of rapid atrial pacing or cholinergic activation with acetylcholine also induced re-entry in dog PV preparations (Po *et al.*, 2005). Re-entrant circuits have also been observed in AF patients, as Kumagai *et al.* (2004a) reported the appearance of unstable re-entrant circuits in the PV of patients with paroxysmal AF. The presence of rapid repetitive focal activity with short cycle lengths resulted in areas of abnormal conduction in the PV, allowing the formation of short lived re-entrant circuits. Therefore the presence of re-entry circuits in the PV may result in the initiation and maintenance of AF.

1.4.6 Remodelling of the PV

Similar to what has been observed in the LA, various pathologies are thought to lead to PV remodelling, enhancing the susceptibility of the PV to arrhythmogenic activity and the maintenance of AF. For example, an increase in fibrosis could disrupt the electrical propagation in the PV (Luo *et al.*, 2007). In the PVs of a chronic AF model, increased fibrosis was thought to contribute to the down regulation of gap junction proteins, connexins CX40 and C43 as well as a change in their distribution

pattern (Sun *et al.*, 2008). In addition, enhanced fibrosis was reported in the PVs of AF patients in comparison to those without a history of AF (Tagawa *et al.*, 2001; Hassink *et al.*, 2003; Steiner *et al.*, 2006). Therefore the remodelling of the PV due to increased fibrosis, and the alterations in gap junctions, may lead to disturbances in the propagation of electrical activity and local conduction block creating a substrate for arrhythmia.

Amyloidosis is characterised by the presence of abnormal protein deposits which, like fibrosis, are thought to cause conduction abnormalities in cardiac tissues of AF patients (Röcken *et al.*, 2002, 2002). Amyloidosis was present in 58.5% of PVs from AF patients (Steiner *et al.*, 2006). Incubation of single rabbit PV cardiomyocytes with the amyloid peptide beta-amyloid ($A\beta_{25\text{-}35}$) significantly reduced the APD, demonstrating the ability of amyloid peptides to alter the PV cardiomyocyte action potential (Tsao *et al.*, 2012). The resultant shortened APD could enhance the susceptibility of the PV for re-entry.

Cardiac diseases related to AF, such as heart failure, have been shown to induce remodelling in the PV from animal models. An increase in NCX activity, I_{ti} and I_{NaL}, as well as larger Ca^{2+} transients and a higher incidence and frequency of Ca^{2+} sparks, were recorded in the PV cardiomyocytes from a rabbit heart failure model (Chang *et al.*, 2011). In addition, heart failure resulted in a higher rate of automaticity and an increased incidence of DADs in rabbit PV cardiomyocytes (Chang *et al.*, 2011). These findings suggest that heart failure induced remodelling could enhance the capability of the PV to produce ectopic activity. Heart failure also induced autonomic remodelling, with PVs of a dog chronic heart failure model exhibiting a significant increase in sympathetic nerve fibre density (Ng *et al.*, 2011).

The presence of AF is also thought to promote PV remodelling. A reduction in I_{to} and I_{CaL} and an increase in I_{K1} were observed in PV cardiomyocytes from a dog 7-day atrial tachycardia pacing model, suggesting that rapid atrial beating during AF could lead to ionic remodelling in the PV cardiomyocytes (Cha *et al.*, 2005). In addition, a decrease in I_{to} and a shorter APD was also observed in the PV of dogs

subject to long term (6-8 weeks) rapid atrial pacing (Chen *et al.*, 2001; Li *et al.*, 2012). It is thought that AF induced remodelling in the PVs of AF patients results in abnormal conduction and action potential shortening (Jaïs *et al.*, 2002; Takahashi *et al.*, 2003; Rostock *et al.*, 2008). Furthermore, Rostock *et al.* (2008) demonstrated in humans that the susceptibility to induce AF was significantly enhanced after short term AF exposure, particularly by pacing from within the PVs, suggesting that "AF begets AF in the PVs".

1.5 Sodium ion channels as therapeutic targets in AF

1.5.1 Sodium channels

During the cardiac cycle the key contributors to Na^+ entry are the voltage gated sodium (Na_v) channels and the NCX, with Na^+ efflux maintained through the Na^+/K^+ ATPase. Opening of the Na^+ channels allows for flow of Na^+ into the cell, further depolarising the cell membrane, and so the Na^+ channels are involved in the upstroke of the action potential in excitable cells such as cardiomyocytes (Draper and Weidmann, 1951; Cohen *et al.*, 1984). Therefore, the larger the $I_{Na,}$ the greater the dV/dt_{max} (Cohen *et al.*, 1984). In addition, the activation and inactivation of cardiac Na^+ channels can contribute to the determination of the conduction velocity as well as the refractory period between action potentials (Papadatos *et al.*, 2002). The Na^+ channels consist of the principal α-subunit, which is the major contributor to channel function and one or more β-subunits. Figure 1.6 illustrates the α-subunit of the Na_v channel, a glycosylated membrane protein, which consists of four homologous domains (DI-DIV), each of which has six transmembrane segments (S1-S6) (Noda *et al.*, 1984; Sato *et al.*, 1998). The four domains fold to create a central ion conducting pore which is lined by the four S5 and S6 segments and the intervening pore loop (Pérez-García *et al.*, 1996; Payandeh *et al.*, 2011). The channel's selectivity for Na^+ ions is governed by the pore loop (Guy and Seetharamulu, 1986; Heinemann *et al.*, 1992; Pérez-García *et al.*, 1997). The four S4 transmembrane segments act as the voltage sensor as they contain positive amino acids motifs, such as arginine and lysine, within the membrane electric field which undergo outward displacement upon depolarisation, triggering opening of the central pore of the channel (Stühmer *et al.*, 1989; Auld *et al.*, 1990; Kontis *et al.*, 1997). The work of Hodgkin and

Huxley, (1952a, 1952b) showed that the Na_v channel exists in three states: deactivated (closed), activated (open), and inactivated (closed). The Na^+ channel also has an activation gate as well as an inactivation gate. As shown in Figure 1.7, at the resting membrane potential the channel is deactivated, the pore is closed by the activation gate and so the open probability of the channel is low in this state. During membrane depolarisation the channel activates and opens (both the activation and inactivation gates are open) and it allows selective entry of Na^+ ions into the cell. The channel then rapidly inactivates after 1-2 ms by folding of the intracellular inactivation gate into the channel, closing the pore. The repolarisation of the cell membrane allows recovery from inactivation to occur and the Na^+ channels return to the deactivated (closed) state.

Ten genes encode the Na^+ channel α-subunits, nine are voltage gated and the other is a leak Na^+ channel which is involved in salt sensing and so it is not voltage gated (Watanabe *et al.*, 2000; Tremblay *et al.*, 2011). The Na_v 1.1, 1.2 and 1.3 channels are mainly located in the central nervous system of various species (Noda *et al.*, 1984; Kayano *et al.*, 1988; Ahmed *et al.*, 1992; Lu *et al.*, 1992). The Na_v1.6 isoform is also located in the central nervous system and has also been observed in the peripheral nervous system such as the sciatic nerves and nodes of Ranvier (Schaller *et al.*, 1995; Plummer *et al.*, 1998; Smith *et al.*, 1998). Na_v 1.7, 1.8 and 1.9 are the primary sodium channels in the peripheral nervous system, with a number of studies reporting the presence of these channels in the dorsal root ganglia (Akopian *et al.*, 1996; Sangameswaran *et al.*, 1996; Toledo-Aral *et al.*, 1997; Dib-Hajj *et al.*, 1998). The Na_v 1.4 channel is the primary Na^+ channel in skeletal muscle (Trimmer *et al.*, 1989). The major cardiac sodium channel is Na_v1.5 as it is thought to establish the key electrophysiological and pharmacological properties of the cardiac I_{Na} (Gellens *et al.*, 1992; Lu *et al.*, 1992). Immunofluorescence studies in ventricular cardiomyocytes from a number of species, such as mouse, rat and dog, revealed Na_v1.5 channels are clustered at intercalated discs where they could interact with gap junctions to transmit action potentials, as well as at z-lines (Cohen, 1996; Maier *et al.*, 2002; Haufe *et al.*, 2005a, 2005b; Xi *et al.*, 2009). In rat and human atrial cardiomyocytes, Na_v1.5 was observed to be distributed in a striated pattern similar to

the z-lines (Cohen, 1996; Kaufmann *et al.*, 2013). The subcellular location of $Na_v1.5$ in the PV cardiomyocytes has yet to be elucidated.

The Na^+ channels can be modulated by a number of physiological factors such as intracellular Ca^{2+}, pH, reactive oxygen species, temperature, stretch and phosphorylation (Rook *et al.*, 2012; Remme, 2013). In addition there are a number of intracellular proteins such as ankyrin-G, syntrophin and calmodulin, which can modulate Na^+ channels (Abriel, 2010).

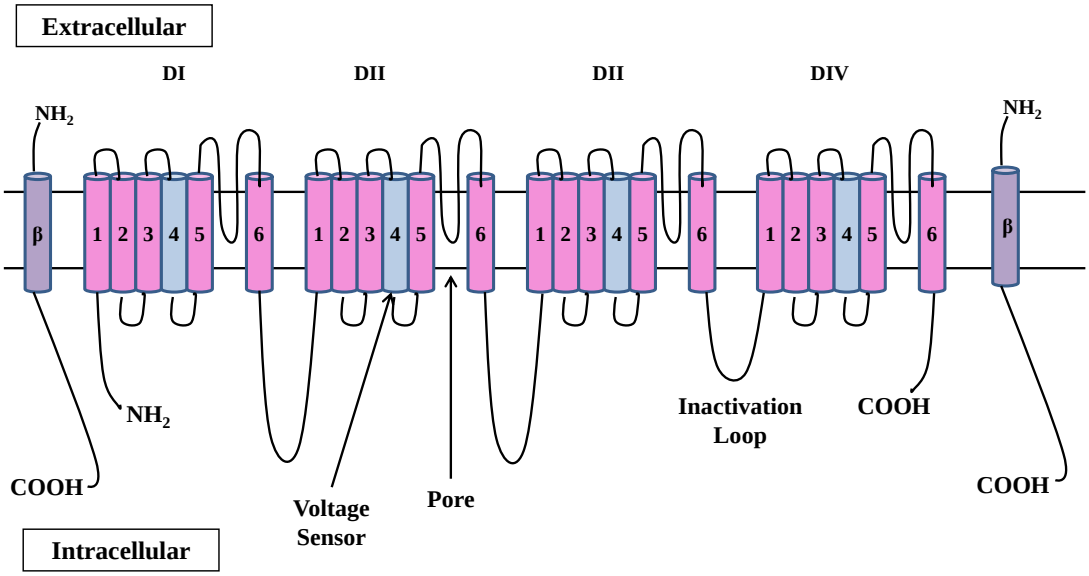

Figure 1.6. **General voltage gated sodium (Na_v) channel structure**. DI-DIV characterizes the four conserved domains, each consisting of six transmembrane segments (S1-S6) with S4 acting as a voltage sensor in each segment. The four domains are connected by three linker loops. Na_v channels also contain one or more β-subunits (Brackenbury and Isom, 2011).

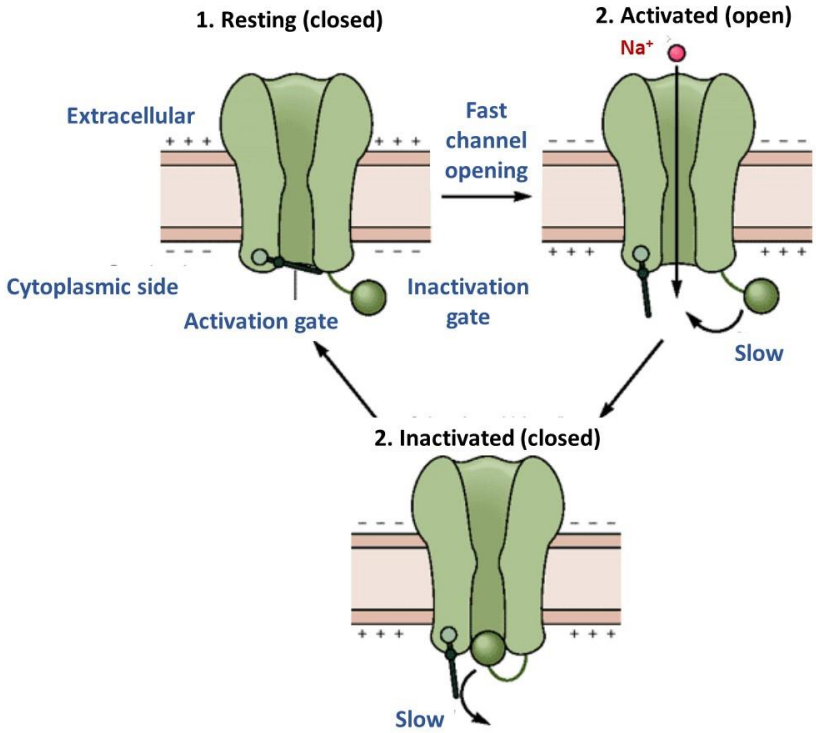

Figure 1.7 **The Na^+ channel gating.** During the resting (closed) state the activation gate is closed while the inactivation gate is open. Rapid opening of the activation gate upon depolarisation of the cell membrane allows Na^+ to flow through the channel. The inactivation gate rapidly closes and the Na^+ channels move into the inactivated (closed) state. Repolarisation of the cell allows the channel to return to the resting state from (Kandel *et al.*, 2000).

1.5.2 The β-subunits

So far, five β-subunits have been identified in mammals: β1 and its splice variant β1B (previously known as β1A), β2, β3 and β4 (Isom *et al.*, 1992; Kazen-Gillespie *et al.*, 2000; Qin *et al.*, 2003; Yu *et al.*, 2003; Maltsev *et al.*, 2009; Hakim *et al.*, 2010a). Four genes, SCN1B-SCN4B each encode for one of the β-subunits. Both β2 and β4 can be disulphide linked to the α-subunit of the Na_v channel, whereas β1 and β3 associate non-covalently with the α-subunit (Isom *et al.*, 1992; Yu *et al.*, 2003). Increasing evidence has demonstrated that the β-subunits have more influence of the α-subunit than first thought as they can alter the gating, voltage dependence, and kinetics of the Na^+ channel α-subunit (Brackenbury and Isom, 2011).

1.5.2.1 The β1-subunit

There are conflicting reports as to whether or not co-expression of the β1-subunit with $Na_v1.5$ affects the Na^+ channel function. While some studies have reported that expression of the β1 subunit in cells such as *Xenopus* oocytes can increase $Na_v1.5$ current density with no effect on the channel kinetics, others saw a β1-mediated change in $Na_v1.5$ gating and kinetics (Makielski *et al.*, 1996; Dhar Malhotra *et al.*, 2001). Using knockout mice to further study the effect of β1 on the Na^+ current, Lopez-Santiago *et al.* (2007) reported an increase in the I_{Na} and I_{NaL} density in ventricular cardiomyocytes of *Scn1b*$^{-/-}$ mice. Mutations in β-subunits may affect the cardiac I_{Na} and contribute to the maintenance of cardiac arrhythmias, as genetic screening studies identified mutations in the β1-subunit in patients with Brugada syndrome and in a small set of AF patients (Watanabe *et al.*, 2008, 2009). Expression of these mutant β1-subunits in CHO cells resulted in a reduction in the I_{Na} current (Watanabe *et al.*, 2008, 2009).

1.5.2.2 The β2-subunit

Co-expression of β2 with $Na_v1.5$ in transformed human kidney cells (TsA201) or Chinese hamster ovary (CHO) cells had no effect on the I_{Na} current density or the ion channel kinetics (Dhar Malhotra *et al.*, 2001; Watanabe *et al.*, 2009). However, two mutations in the SCN2B gene were identified in a small set of AF patients. Co-

expression of the mutated β2-subunit with $Na_v1.5$ in CHO cells reduced the peak I_{Na} and produced a positive shift in the voltage dependence of activation and inactivation (Watanabe *et al.*, 2009). This shows that mutations in the β2-subunit could contribute to arrhythmogenic activity, as the resultant reduction in peak I_{Na} could shorten the ERP and slow conduction, potentially creating a substrate for re-entry.

1.5.2.3 The β3-subunit

The β3-subunit is also thought to contribute to the regulation of the I_{Na}. Co-expression of β3 mutants, which were present in a sub-set of AF patients, with $Na_v1.5$ in CHO or HEK293 cells resulted in a reduction in I_{Na} density, although there was no effect on the activation or inactivation kinetics of the current (Wang *et al.*, 2010; Olesen *et al.*, 2011). The role of the β3-subunit was also examined in Langendorff-perfused hearts from *Scn3b*$^{-/-}$ mice (Hakim *et al.*, 2008, 2010a). The absence of the β3 subunit produced shorter cardiomyocyte ERPs due to the resultant effect on I_{Na} (Hakim *et al*., 2008, 2010a). The *Scn3b*$^{-/-}$ mouse hearts also displayed an increased susceptibility to arrhythmias, as burst pacing of the right atrial appendage resulted in AF in all *Scn3b*$^{-/-}$ hearts, but not in the wild type hearts (Hakim *et al.*, 2010a, 2010b).

1.5.2.4 The β4-subunit

The β4-subunit can also alter the cardiac Na^+ channel as co-expression of β4 with $Na_v1.5$ in HEK cells was found to increase the peak I_{Na} (Scicluna *et al.*, 2008). Compared to the other β-subunits, there is less information on the link between β4 mutations, the cardiac Na^+ channel and AF. However, recently mutations in the β4 subunit were identified in familial AF (Li *et al.*, 2013).

1.5.3 The PV and atrial sodium current in AF and associated pathologies

The presence of AF or associated pathologies can alter the I_{Na}. A reduction in I_{Na} density and downregulation of SCN5A mRNA, which encodes for the main cardiac Na^+ channel $Na_v1.5$, was observed in atrial cardiomyocytes from the dog AF model

(Gaspo *et al.*, 1997; Yue *et al.*, 1999; Yagi *et al.*, 2002). In addition, *in vivo* recordings showed a slowed atrial conduction velocity in the dog AF model (Gaspo *et al.*, 1997). This was attributed to the decrease in I_{Na} since I_{Na} is one of the key determinants of the conduction velocity in cardiac tissue (Buchanan *et al.*, 1985). This slowing of conduction could lead to the promotion of re-entry. Similar results were observed in humans as a 10-16% reduction in the I_{Na} density as well as a 26% decrease in the expression of SCN5A was reported in cardiomyocytes isolated from the right atrial appendage of patients with permanent AF, in comparison to patients in sinus rhythm (Bosch *et al.*, 1999; Sossalla *et al.*, 2010). It was hypothesised that the reduction may be a consequence of the increased intracellular Ca^{2+} concentration that occurs during arrhythmic conditions, since this has been shown to down regulate Na^+ channel expression (Duff *et al.*, 1992). Although there is a general lack of information regarding the effect of AF on the I_{Na} in PVs, in animal models and humans, a decrease in I_{Na} density was recorded in PV cardiomyocytes from the rabbit heart failure model, which is a condition known to predispose to AF (Chang *et al.*, 2011). A reduction in conduction velocity was also observed in the PV of AF patients (Jaïs *et al.*, 2002; Takahashi *et al.*, 2003; Rostock *et al.*, 2008); however, whether a decrease in I_{Na} contributed to this awaits further study.

1.5.4 The late sodium current

In addition to the 'peak' I_{Na} which is responsible for phase 0 of the action potential, the I_{Na} also contains a smaller sustained component known as the late Na^+ current (I_{NaL}), which persists during prolonged depolarization. A number of mechanisms are proposed to contribute to the generation of I_{NaL}, namely: 1) slow or failed inactivation of Na^+ channels after their initial opening (Gintant *et al.*, 1984); 2) single and/or bursts of Na^+ channel openings that are in an unstable inactivated state during the plateau or repolarisation phase of the action potential (Patlak and Ortiz, 1985; Maltsev *et al.*, 1998); 3) rapid recovery of channels from inactivation during non-equilibrium conditions (Clancy *et al.*, 2003). The I_{NaL} is a reverse rate-dependent current, which means that the current magnitude decreases as the electrical simulation frequency increases (Zygmunt *et al.*, 2001; Guo *et al.*, 2011). Therefore, the involvement of I_{NaL} in the electrophysiology of cardiomyocytes is

thought to be of greater importance when the APD is longer and the heart rate is slower (Zygmunt *et al.*, 2001; Grandi *et al.*, 2007; Guo *et al.*, 2011). Although I_{NaL} is small in cardiomyocytes, the overall amount of Na^+ carried by I_{NaL} can be similar to that carried by peak I_{Na} due to the prolonged persistence of I_{NaL} (100-300 ms; (Li *et al.*, 2000; Huang *et al.*, 2001; Maltsev *et al.*, 2007) . The I_{NaL} can be enhanced by cardiac pathologies. An increased I_{NaL} was observed in LA cardiomyocytes from a rabbit left ventricular hypertrophy model, which is an associated AF pathology (Guo *et al.*, 2010). An enhanced I_{NaL} was also recorded in PV cardiomyocytes from a rabbit heart failure model (Chang *et al.*, 2011). In addition, Sossalla *et al.* (2010) reported an enhancement of I_{NaL} (by 26%) in right atrial cardiomyocytes from permanent AF patients, when compared to patients without a history of AF. Although, in contrast, Poulet *et al.* (2015) recently reported no significant difference in the I_{NaL} in cardiomyocytes from the right atrial appendage of patients in sinus rhythm in comparison to those with chronic AF.

The I_{NaL} can be directly or indirectly enhanced pharmacologically by a variety of agents such as H_2O_2, aconitine, veratridine or *Anemonia sulcata* toxin II (ATX-II), all of which prevent the Na^+ channels entering their inactivated state (Scherf *et al.*, 1948; Isenberg and Ravens, 1984; Nánási *et al.*, 1994; Lin *et al.*, 2011). Using these pharmacological tools to increase I_{NaL} has indicated that this current may contribute to automaticity in cardiomyocytes. Specifically, addition of ATX-II or H_2O_2 accelerated diastolic depolarisation and increased automaticity in guinea-pig isolated atrial cardiomyocytes (Song *et al.*, 2009). Similarly ATX-II enhanced the automaticity in rabbit PV preparations (Lu *et al.*, 2012; Chen *et al.*, 2014). The involvement of I_{NaL} in automaticity was further supported by the finding that both the diastolic depolarisation and automaticity were reduced by the I_{NaL} blocker ranolazine (Song *et al.*, 2009; Lu *et al.*, 2012). An increase in I_{NaL} can also induce arrhythmogenic activity in atrial cardiomyocytes which did not display any inherent spontaneous activity (Song *et al.*, 2008; Wolkowicz *et al.*, 2014). For example, pharmacological increase in the I_{NaL} prolonged the APD of electrically evoked action potentials and induced EADs, DADs and triggered activity in rat atrial tissue

(Wolkowicz *et al.*, 2014) and guinea pig isolated atrial cardiomyocytes (Song *et al.*, 2008, 2009).

One proposal for the mechanism by which the increase in I_{NaL} enhances arrhythmogenic activity is through an increase in the intracellular Na^+ concentration (Hoey *et al.*, 1994; Sossalla *et al.*, 2008). The consequence of the increase in intracellular Na^+ is that it would reduce Ca^{2+} efflux via the NCX, or it may drive the NCX into reverse mode bringing Ca^{2+} into the cell. Activation of the reverse mode NCX and dysregulation of Ca^{2+} homeostasis leads to Ca^{2+} overload, which both contribute to the initiation of DADs (Faber and Rudy, 2000; Song *et al.*, 2008; Sossalla *et al.*, 2008; Undrovinas *et al.*, 2010). An increase in I_{NaL} can also prolong the APD, leading to arrhythmogenic EADs. The prolonging of the APD allows the Ca^{2+} channels to recover from inactivation, leading to increased Ca^{2+} influx, which if sufficient can reverse the repolarisation and generate EADs (January and Riddle, 1989; Zeng and Rudy, 1995).

1.5.5 Effect of sodium channel blockers on atrial and PV arrhythmogenic activity

Although Na^+ channel blockers are widely used as an anti-arrhythmic treatment for AF, their mechanism of action in terminating the ectopic activity from the PV is complex and not fully elucidated. Reduction of both peak I_{Na} and I_{NaL} is exhibited by Na^+ channel blockers, with many displaying enhanced potency for I_{NaL} in comparison to peak I_{Na} (Carmeliet and Mubagwa, 1998). Low concentrations of Na^+ channel blockers such as lidocaine, quinidine and ranolazine can selectively inhibit I_{NaL} with minimal effect on the peak I_{Na} (Ju *et al.*, 1992; Antzelevitch *et al.*, 2004).

In the atrium, Na^+ channel block is thought to treat AF by suppression of re-entry (Brugada *et al.*, 1993). In dogs, rapid atrial pacing resulted in atrial re-entry and AF, which was prevented or terminated by the Na^+ channel blockers flecainide (Wang *et al.*, 1992), pilsicainide (Hayashi *et al.*, 1998) or propafenone (Wang *et al.*, 1993). Similar results were observed in human AF patients with the Na^+ channel blockers cibenzoline (Brugada *et al.*, 1993), disopyramide (Ishibashi *et al.*, 1995), flecainide

(Kirchhof *et al.*, 2005) and procainamide (Fujiki *et al.*, 2001). Generally, the Na^+ channel blockers in these studies reduced excitability and suppressed re-entry by increasing the ERP and in some cases increasing the wavelength. A number of class I drugs (e.g. flecainide, propafenone) also inhibit the repolarising K^+ currents, which would be expected to increase the ERP, due to an increase in the APD (Duan *et al.*, 1993; Slawsky and Castle, 1994; Yue *et al.*, 2000). However, in some cases block of I_{Na} alone increased the atrial ERP even though the APD was not prolonged, resulting in post repolarisation refractoriness (Kanki *et al.*, 1998). This could be due to suppression of I_{Na} reactivation in the atrial cardiomyocytes and an increase in the diastolic threshold for excitation.

The Na^+ channel blockers may also treat AF by suppression of PV ectopic activity. Hirose *et al.* (2007a) reported pre-treatment of anaesthetised dogs with pilsicainide prevented the induction of AF by rapid pacing of the left superior PV. The reduction in excitability was thought to create a conduction block between the PV and the LA (PV-LA junction), therefore suppressing PV ectopic activity. Clinical studies have also demonstrated the antiarrhythmic action of Na^+ channel blockers in the PVs of AF patients. Procainamide significantly decreased the ectopic activity originating from the PV, in paroxysmal AF patients (Chen *et al.*, 1999). In addition, Kumagai *et al.* (2004b) utilised basket catheter mapping to monitor the effect of pilsicainide on the PVs and PV-LA junction in patients with paroxysmal AF. Addition of pilsicainide terminated AF in 5 out of 8 patients with sustained AF by significantly prolonging the ERP, suggesting that Na^+ channel blockers may suppress the substrate for re-entry in the PV. Moreover, PV-LA junction conduction block just before AF termination was also observed in a number of patients (Kumagai *et al.*, 2004b).

Afterdepolarisations and triggered activity in atrial and PV cardiomyocytes were also suppressed by Na^+ channel inhibition, with the reduction in intracellular Na^+ thought to decrease Na^+ dependent Ca^{2+} overload. The highly selective Na^+ channel blocker tetrodotoxin (TTX; 2 μM) abolished ATX-II induced EADs, DADs and triggered activity in guinea-pig LA cardiomyocytes (Song *et al.*, 2008). In addition,

microelectrode recording from PVs of dogs subjected to 6-8 weeks of rapid atrial pacing revealed the presence of high frequency irregular triggered activity, which was suppressed by 3 μM TTX (Chen *et al.*, 2000).

Although they are not currently approved for AF treatment, multichannel blockers that potently inhibit I_{NaL}, such as ranolazine, have shown great potential as antiarrhythmics for AF (Murdock *et al.*, 2008; Miles *et al.*, 2011; Scirica *et al.*, 2015). Ranolazine is thought to exhibit its antiarrhythmic effect in atrial cardiomyocytes through inhibition of I_{NaL} and peak I_{Na}, as well as block of I_{Kr} (Antzelevitch *et al.*, 2004). Treatment with ranolazine suppressed the arrhythmic activity in rabbit and human atrial cardiomyocytes (Sossalla *et al.*, 2010; Aidonidis *et al.*, 2013). Block of I_{NaL} with ranolazine can also suppress PV ectopic activity as automaticity and EADs in rabbit PVs, induced by an increased I_{NaL}, were inhibited by ranolazine (Lu *et al.*, 2012). In addition, DADs, late phase 3 EADs and triggered activity in dog PVs induced by acetylcholine or isoprenaline in combination with rapid pacing were attenuated by ranolazine as well as the selective I_{NaL} inhibitor GS-458967 (Sicouri *et al.*, 2008, 2013).

1.5.6 Atrial selective sodium channel block

A major problem with a number of antiarrhythmic drugs in the treatment of AF, is the risk of pro-arrhythmic activity in the ventricles (Camm *et al.*, 2010). In recent years studies have focused on investigating the atrial selectivity of anti-arrhythmics. The Na^+ channel blockers have been a main focus, due to the difference in Na^+ channel characteristics between atrial and ventricular cardiomyocytes. Atrial cardiomyocytes from dog and guinea pig display a more negative half- inactivation voltage and a more positive membrane potential (so a greater proportion of Na^+ channels are in the inactivated state), in comparison to those from the ventricle (Li *et al.*, 2002; Burashnikov *et al.*, 2007). The affinity of Na^+ channel blockers is higher when the channels are in their activated or inactivated state as opposed to their resting state (Hondeghem and Katzung, 1984; Starmer *et al.*, 1984). In addition, Na^+ channel blockers with relatively rapid unbinding kinetics such as amiodarone, ranolazine and vernakalant display atrial selective I_{Na} block (Burashnikov *et al.*,

2007, 2008). These anti-arrhythmics exert greater inhibition of parameters associated with the peak I_{Na} such as dV/dt_{max}, conduction velocity and excitability, in the atria compared to the ventricles (Burashnikov *et al.*, 2007, 2008; Zygmunt *et al.*, 2011). Certain Na^+ channel blockers also display selectivity for PV cardiomyocytes over ventricular cardiomyocytes, as dog PVs treated with amiodarone displayed a greater suppression of dV/dt_{max} and conduction velocity in comparison to the left ventricular wedge (Sicouri *et al.*, 2009). Although further study is needed to support this, it is feasable that Na^+ channel blockers could be used to suppress PV ectopic activity with minimal ventricular pro-arrhythmic effects.

1.5.7 Sodium channel mutations and AF

Acquired and inherited mutations of the Na^+ channel α-subunits particularly $Na_v1.5$ (SCN5A), can alter the kinetics of Na^+ channels (Darbar *et al.*, 2008). This change in kinetics could result in arrhythmic activity. Many Na^+ channel mutations are unique to AF patients and not present in those without a history of AF, while others are thought to enhance the risk of developing AF (Darbar *et al.*, 2008; Chen *et al.*, 2011). Loss of function Na^+ channel mutations could result in a decrease in peak I_{Na}, diminished Na^+ entry, and a reduction in conduction velocity in cardiomyocytes (Figure 1.8). A study of a large Finnish family in which conduction defects and atrial arrhythmias were common, revealed a missense mutation D1275N in the SCN5A gene in all affected individuals (Laitinen-Forsblom *et al.*, 2006). In addition, the loss of function H558R polymorphism of the human SCN5A gene was associated with an increased incidence of AF (Chen *et al.*, 2011). Gain of function Na^+ channel mutations are associated with enhanced I_{NaL} and arrhythmogenic afterdepolarisations (Figure 1.8). Novel gain of function SCN5A mutations were discovered in familial AF patients and the biophysical properties were examined by transfection of heterologous cell lines with the mutations (Makiyama *et al.*, 2008; Li *et al.*, 2009). Transfection of one of these SCN5A coding variants, K1493R, into tsA201 cells resulted in a positive shift in the voltage dependence of inactivation and an increased I_{NaL} (Li *et al.*, 2009). In addition, after transfection of the Na^+ channel mutation into HL-1 atrial cardiomyocytes, spontaneous action potentials and a reduced threshold for action potential triggering were observed (Li *et al.*, 2009).

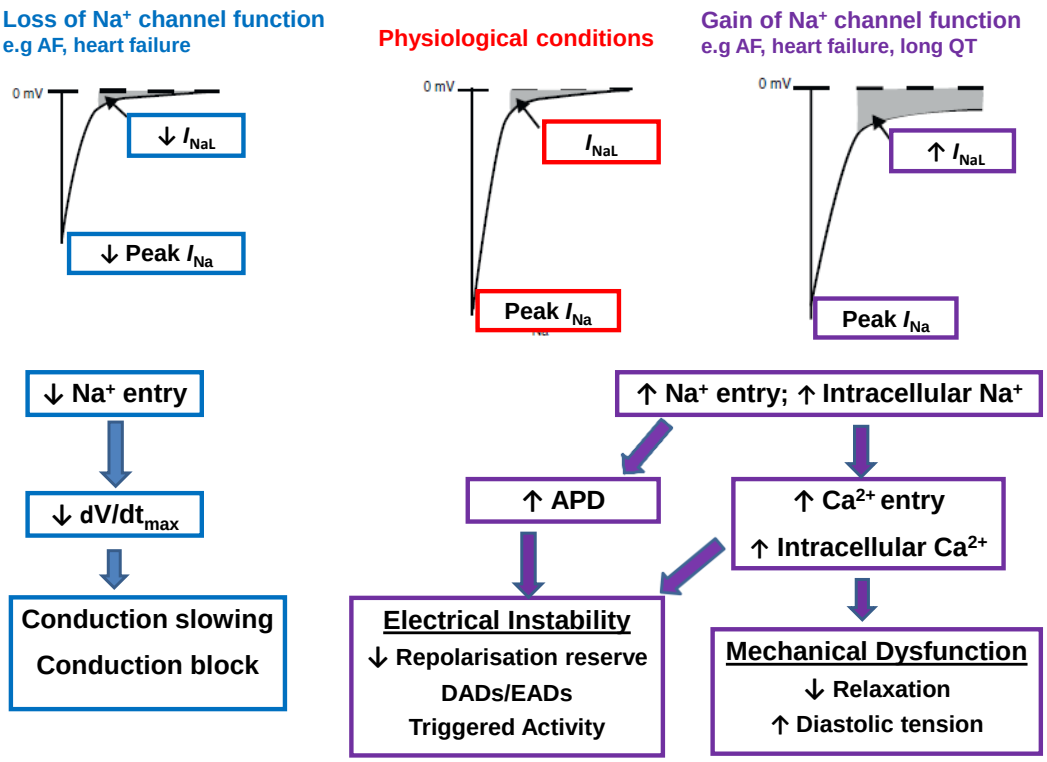

Figure 1.8. **Consequences of Na^+ channel alteration**. Schematic representation of the proposed AF promoting consequences of peak I_{Na} reduction and increase in I_{NaL} in cardiomyocytes. A decrease in peak I_{Na} can lead to a reduction in Na^+ entry, V_{max} and therefore conduction slowing in cardiac tissues as a consequence. Gain of function mutations are associated with an increase in I_{NaL} which can increase Na^+ entry and generate accumulation of intracellular Na^+. The resultant increase in APD leads to electrical instability and EADs. In addition the Na^+ dependant Ca^{2+} overload can trigger afterdepolarisations as well as mechanical dysfunction in cardiomyocytes. APD, action potential duration; DAD, delayed afterdepolarisation; EAD, early afterdepolarisation; dV/dt_{max}, maximum upstroke velocity (Adapted from Remme and Wilde, 2014).

1.6 Aims

Since Na^+ channels are thought to play a key role in the generation of arrhythmic activity in cardiomyocytes, then this study hypothesised that the Na^+ channels could contribute to PV ectopic activity. Differences in Na^+ channel expression, distribution, kinetics or density may account for the PVs susceptibility to ectopic activity in comparison to the LA.

The aims of this study were to compare the functional characteristics of the rat PV and LA cardiomyocytes by comparing the electrically evoked contractile properties, as well as the action potential characteristics in both tissues. In order to further understand the properties of Na^+ channels, the distribution of the Na^+ channel isoforms, as well as the I_{Na} properties were examined in the PV compared to that of the LA. This was explored further by a comparison of the contribution of the TTX-sensitive I_{Na} to the total I_{Na} in PV and LA cardiomyocytes as well as determining if the TTX-sensitive I_{Na} is significantly involved in the action potential and contractile properties of both tissues. Lastly, the ability of ATX-II, which increases I_{NaL}, to induce arrhythmogenic activity in the PV and LA was investigated, with the aim of establishing the contribution of TTX-sensitive Na^+ channels, CaMKII and the NCX to ATX-II mediated arrhythmogenic activity.

Chapter 2

Morphological and Electrophysiological Comparison of the PV and LA

2.1 Introduction

2.1.1 The mammalian PV sleeve

The PVs contain several layers of cardiomyocytes, which form a sleeve surrounding the external aspect of the blood vessel. This arrangement has been found to exist in mammalian PVs, such as those of human (Moubarak *et al.*, 2000; Saito *et al.*, 2000; Ho *et al.*, 2001; Hassink *et al.*, 2003; Perez-Lugones *et al.*, 2003), rat (Kramer and Marks, 1965; Paes de Almeida *et al.*, 1975; Masani, 1986; Hashizume *et al.*, 1998; Miyauchi *et al.*, 2004), guinea pig (Takahara *et al.*, 2011) and dog (Hocini *et al.*, 2002). Since Haïssaguerre *et al*. (1998) discovered that ectopic activity originating from the PV cardiomyocyte sleeve causes AF, the PV has been the subject of intense investigation in order to better understand its role in disease processes.

Brunton and Fayer first observed that the PVs of anaesthetised rabbits and cats would continue to pulsate after the cessation of artificial respiration and the heart had stopped beating, indicating that the PV had inherent contractile activity (Brunton and Fayrer, 1876). Since then various groups have utilised myography techniques to measure electrically evoked contractions of the rabbit and rat PVs (MacLeod and Hunter, 1967; Bronquard *et al.*, 2007; Maupoil *et al.*, 2007; Luk *et al.*, 2008). The contractile properties of the PV have been shown to be more like cardiac tissue than smooth muscle tissue and it is thought that the smooth muscle does not play a major role in the contraction of the PV (Bronquard *et al.*, 2007). In addition, the associated endothelium appears not to contribute significantly to the contractile or relaxant response to the PV (Bronquard *et al.*, 2007).

The electrical activity of the PV cardiomyocyte sleeve has also been the focus of a number of studies (Cheung, 1981; Wang *et al.*, 2003; Po *et al.*, 2005). Several groups have reported that there is heterogeneity in the action potentials recorded in PV cardiomyocytes located proximal and distal to the atrium in a number of different species (Cheung, 1981; Po *et al.*, 2005). This has led to the hypothesis that certain regions of the PV may be more prone to ectopic activity than others. Distal cardiomyocytes in guinea pig and dog PVs were found to exhibit a more depolarised resting membrane potential in comparison to cardiomyocytes proximal to the LA

(Cheung, 1981; Po *et al.*, 2005). In addition, a shorter action potential duration (APD) was recorded in the distal region of the guinea pig PV (Cheung, 1981). However, others have reported in the dog PV that there was no difference in the action potential characteristics along the length of the cardiomyocyte sleeve (Wang et al., 2003).

There has been some comparison of the action potential characteristics in the PV and LA, in order to try and establish if the cardiomyocytes from these two tissues have any distinguishing characteristics. However, these studies have also tended to produce quite variable results (Ehrlich *et al.*, 2003; Miyauchi *et al.*, 2004, 2005; Cha *et al.*, 2005). A number of groups reported no significant difference between the action potentials recorded from the rat PV and LA (Miyauchi *et al.*, 2004, 2005), while others recorded differences such as a more depolarised resting membrane potential in rat (Doisne *et al.*, 2009; Okamoto *et al.*, 2012; Malécot *et al.*, 2014) and dog PVs (Ehrlich *et al.*, 2003), or a shorter APD in rat (Okamoto *et al.*, 2012) and dog PVs (Ehrlich *et al.*, 2003; Cha *et al.*, 2005).

The aims of this chapter were to histologically examine and compare the arrangement of cardiomyocytes in the PV and LA from both rat and human tissue species. Following this, the contractile properties of the rat PV and LA tissue were compared. Lastly, the electrophysiology of the rat PV and LA tissues were compared to determine if there is a difference in the evoked action potential characteristics between the tissues.

2.2 Methods

2.2.1 Animals and dissection

The rat was chosen for this study as the rat PV adventitia consists of only a thin layer of collagenous tissue, allowing microelectrode impalement to be carried out with relative ease. Male Sprague-Dawley rats (200-400 g) were sacrificed by cervical dislocation and the heart and lungs were carefully removed and placed in ice cold, oxygenated bath solution of the following composition: 150 mM NaCl, 5.4 mM KCl, 10 mM HEPES, 10 mM glucose, 1.2 mM $MgCl_2$, 1.8 mM $CaCl_2$, pH 7.4 with NaOH. The tissue was pinned out on a Sylgard®184 (Dow Corning Corporation, Midland, USA) coated petri dish containing cold bath solution. The PVs were then carefully dissected from the left lobe and the posterior or median right lobe (Figure 2.1).

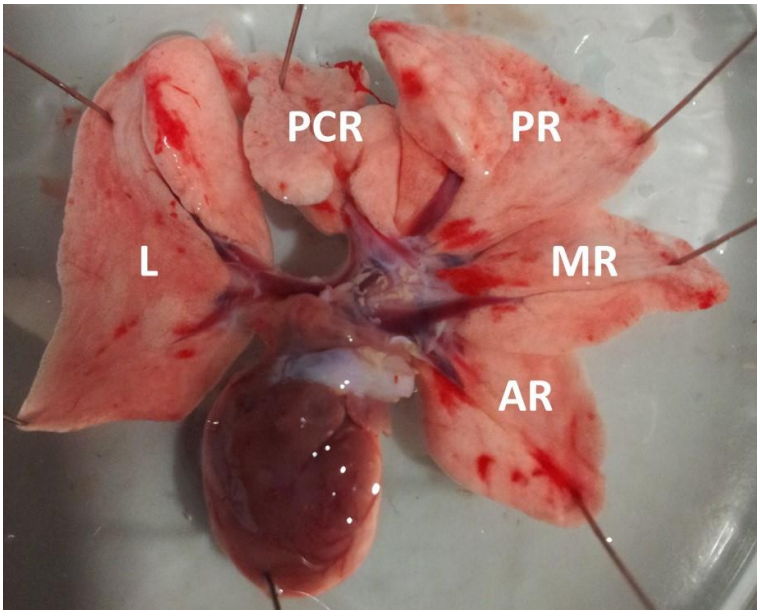

Figure 2.1 **Rat heart and lungs**. The heart and lung were removed *en bloc* from the rat and pinned out on a Sylgard®184 coated petri dish. The five lobes of the rat lungs are: left (L); postcaval right (PCR); posterior right (PR); median right (MR) and anterior right (AR). The blood vessels that are visible in the lungs in this image are the PVs.

2.2.2. Human tissue

Human hearts were provided by Biopta Ltd, Glasgow, UK and they were obtained with ethical consent. The human tissue was obtained from transplant donors, for whom there was no suitable recipient or which weren't used in transplant procedures because of logistical reasons. The donor hearts used in this study were from a 21 year old male and a 60 year old male. The hearts were 24-48 hours post donation at the time of formalin fixation. Patients were screened for blood-borne diseases and were not accepted by Biopta if considered to be positive. There were no reports of cardiovascular disease in the medical history of the 21 year old male. The medical history of the 60 year old male is unknown. The LA and ventricular tissue were identified by a member of Biopta and a 1-2 cm section was dissected. The veins were identified by their position in relation to the LA, and a 0.5-1 cm long ring of PV was cut from the heart tissue. Electrophysiological examination of the PV was not possible due to the lack of availability of tissue necessary to carry out these experiments.

2.2.3 Histology of cardiac sections

2.2.3.1 Preparation of tissues

The PVs and the LA from rat or humans were fixed in 10% formalin solution for a minimum of 24 hours. Tissues were then processed in a Citadel 1000 tissue processor (Thermofisher, UK) under in the following conditions: 3 hours in 70% ethanol; 3.5 hours in 90% ethanol; 3 hours in 100% ethanol; 1 hour in a 1:1 mixture of ethanol and Histo-Clear (Thermofisher, UK); 3 hours in 100% Histo-Clear and 4 hours in paraffin wax. After which the tissue was paraffin wax embedded using a Leica paraffin embedding station, model EG1140H. The wax blocks were cut into 4 μm thick sections using a Leica RM2125RTS rotary microtome and floated onto polarised glass slides in a water bath set to 50^{o}C. The slides were polarised beforehand by 10 minute washes with each of the following: acetone; 5% (v/v) (3-aminopropyl)triethoxysaline (APTES) in acetone; running tap water and then covered and air dried for 48 hours. To clear excess wax before staining, the slides were placed in an oven set at 60-65°C for 30-40 minutes. Prior to staining, the tissue sections were rehydrated using a Varistain 24-4 auto stainer (Thermo Shandon, UK)

using the following conditions: 10 minute wash in Histo-Clear (repeated 3 times), 10 minute wash with 100% ethanol (repeated 3 times) and a 5 minute wash in distilled water.

2.2.3.2 Masson's trichrome stain

Following rehydration, the tissues were stained using Masson's trichrome stain according to the following procedure: 10 minutes in Weigert's iron haematoxylin solution; 10 minutes in warm running tap water; 10 minutes in Biebrich-Scarlet acid fuschin solution; 15 minutes in phosphomolybdic-phosphotungstic acid solution; 8 minutes in aniline blue solution; 1 minute wash in distilled water; 4 minutes in 1% acetic acid solution and a 1 minute wash in distilled water. The tissues were then dehydrated by a 2 second exposure to each of the following solutions: 95% ethanol; 100% ethanol and then Histo-Clear. Thereafter the tissues were mounted with Histomount (ThermoFisher, UK) and 24x50 mm coverslips. The slides were left to dry overnight before viewing with a Leica DM LB2 microscope equipped with a Leica DFC 320 camera. Scale bars were added to the images using Image J software (Version 1.48).

2.2.4 Contraction studies

Once the heart and lungs were removed *en bloc* from the rat, the left or posterior right PVs were carefully dissected from the lungs in ice cold bath solution, oxygenated with medical oxygen, and excess connective tissue was removed. In addition, the LA was separated from the heart. Surgical silk suture was looped onto the LA or the section of the PV proximal to the LA and fixed onto a hook inside a 10 mL organ bath filled with oxygenated bath solution and warmed to 37^{o}C. The other end of the tissue was attached by silk thread to a force displacement transducer (FT03C, Grass Instrument Co., USA), so that the tissue was positioned vertically in the organ bath. To record force, the transducer was connected to a Grass model 79H polygraph whose output was digitized via a national instruments PCR-6221 data acquisition board. Platinum wire electrodes, connected to a stimulus isolation unit (model SIU 5A, Grass Instrument Co., USA), were lowered into the bath and encircled around the PV or LA tissue, to allow delivery of an electrical stimulus.

Contractions were evoked by a single stimulus, which was twice that of the threshold voltage, and 2 ms duration at 0.1 Hz using a Grass stimulator (Model S88, Grass Instrument Co., USA). The resting tension of the tissue was gradually increased until the maximal contraction was observed and this was typically around 0.5 g. The tissue was allowed to equilibrate for 30-40 minutes, to allow the contractions to stabilise. Data was recorded at 1 kHz using Chart Software (Dr. J. Dempster, University of Strathclyde) and converted into a text file in WinEDR (Version 3.4.3 Dr J. Dempster, University of Strathclyde) to enable analysis of the contractions. The text file was then opened with Chart 5 software (ADInstruments, Dunedin, New Zealand), which allowed for identification of contractions by only detecting the response which occurred above a certain threshold amplitude. The contraction amplitudes were analysed over a 5 minute period, with the average during this time period being used for comparison. The WINWCP (Version 4.6.5 Dr J. Dempster, University of Strathclyde) software was used for measurement of the following contraction parameters:

- Contraction duration - The time taken from initiation of contraction until return to baseline.

- Time to peak contraction - The time taken for the contraction to rise from 10% to 90% of the peak amplitude.

2.2.5 Microelectrode studies

Once the heart and lungs were removed *en bloc* from the rat, the LA was carefully dissected from the heart. Following this the lungs were separated from the heart and the left, posterior right and median right lung lobes were cut at the PV-LA junction to provide the individual lobes. The PV was not dissected from the lobes; instead excess lung parenchyma was removed to allow the lobe of the lung to fit inside the recording chamber. The additional lobes of the lung and LA were stored in ice cold oxygenated bath solution (until required, which was not longer than 8 hours). Each lung or LA preparation was pinned onto a Sylgard®184 (Dow Corning, USA) coated recording chamber and continuously perfused with oxygenated bath solution heated to 37ºC using a temperature regulator (HSE Temperature Regulator, Type 319, Hugo

Sachs, Germany). The tissue was allowed to equilibrate for 30 minutes before commencing any recording.

Action potential recordings were made using the conventional microelectrode technique. For microelectrode fabrication, borosilicate glass capillaries (1.5 mm outer diameter, 0.86 mm inner diameter, Warner Instruments, USA) were pulled using a vertical micropipette puller (model P-30, Sutter Instrument Co., Novato, USA) to produce electrodes with a resistance of 20-50 MΩ. These were then backfilled with 3 M KCl. A mechanical micromanipulator (Leitz, Wetzlar, Germany) was used to position the microelectrode prior to insertion into the cell. In order to reduce mechanical vibration and electrical noise, the recording chamber and micromanipulator were fixed onto an air table (Model AVT 701, Wentworth Laboratories LTD, Bedford, UK) and enclosed in a Faraday cage. A silver/silver chloride bead type reference electrode was positioned in the recording chamber. The potential difference between the reference electrode and the recording microelectrode in the cell was measured by a unitary gain high input impedance electrometer (model Electro 705, World Precision Instruments, Hertfordshire, UK).

Electrical signals were amplified using a CED1902 amplifier (Cambridge Electronic Design LTD, Cambridge, UK) and data was sampled at 16 kHz by a computer controlled data acquisition system (National Instruments PCI-6221 data acquisition board) connected to the computer using a bespoke BNC interface. The amplified signals were displayed using WinEDR electrophysiology software (Version 3.3.4, Dr. J. Dempster, University of Strathclyde) and simultaneously stored on the hard disk of a desktop computer for later analysis.

Platinum electrodes, placed at least 1 cm from the recording electrode (to minimise artefacts), were used to electrically stimulate the tissue. A Grass S44 stimulator supplied rectangular voltage pulses via a stimulus isolation unit (model SIU 5A, Grass Instrument Co., USA). Following impalement of the cell, the stimulation voltage was increased in 5 V steps until the threshold voltage capable of eliciting an action potential was reached. All experiments were carried out at twice the threshold

voltage and a pulse duration of 2 ms, with a stimulation frequency of 1 Hz (unless otherwise stated). The membrane potential was continuously monitored, although recordings were typically made over a 1-5 minute period. Cells were rejected if the membrane potential was more depolarised than -60 mV. The tissue was constantly perfused with oxygenated bath solution at a rate of 5 mL/min.

Action potentials were identified using WinEDR software and exported to WinWCP software (Version 4.6.5 Dr. J. Dempster, University of Strathclyde) for further analysis. The membrane potential and the following action potential parameters were measured (Figure 2.2A):

- Peak amplitude – The peak action potential amplitude measured relative to the resting membrane potential
- Rise time – The time taken for the action potential to rise from 10% to 90% of the peak amplitude
- Rate of rise (dV/dt_{max}) – The maximum rate of voltage change during the upstroke of the action potential
- APD_{90} – The action potential duration at 90% repolarisation

Action potential characteristics were calculated from the average of 5 consecutive action potentials for each experimental observation.

The effective refractory period (ERP) was determined by stimulating tissues with a double pulse protocol comprising of an initial pulse (S_1) which was followed by a second pulse (S_2) of the same magnitude (Figure 2.2B). The S_1-S_2 interval was progressively shortened in 2 ms steps and the ERP was defined as the longest S_1-S_2 interval which failed to elicit an S_2 action potential.

The data was transferred to GraphPad Prism (Version 4.03, GraphPad Software Inc., USA) to plot graphs and produce representative recordings.

2.2.6 Statistics

Graphs were produced using GraphPad Prism (version 4.03, GraphPad Software Inc., San Diego, CA, USA). Electrophysiological data, where more than one recording was made from the same tissue, are expressed as mean ± standard error of the mean (s.e.m) of *N* technical replicates (number of recordings), from *n* biological replicates (number of rats). Statistical comparisons were made using Student's unpaired *t*-test and $P<0.05$ was considered to be statistically significant.

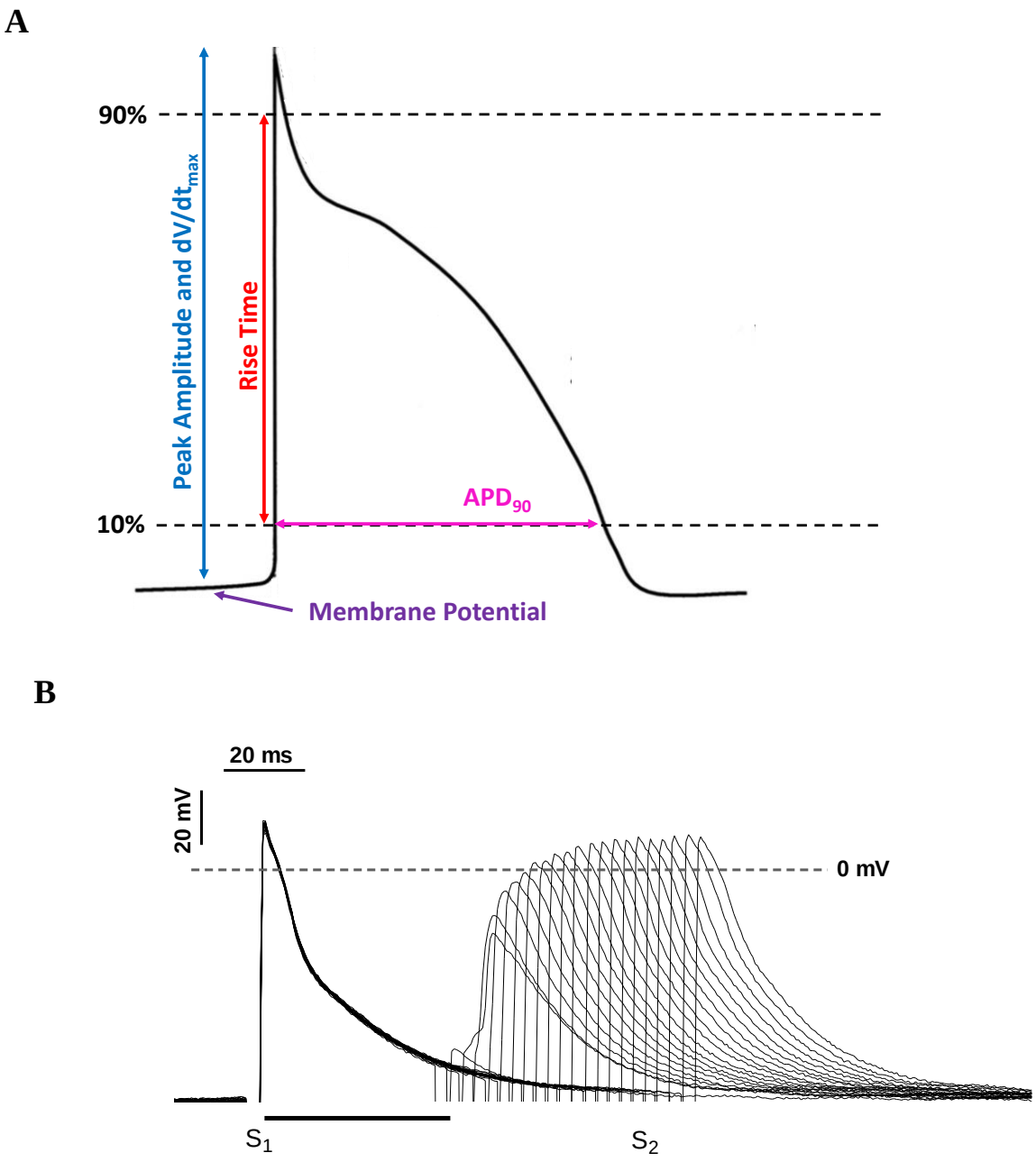

Figure 2.2. **Illustration of the electrically evoked action potential parameters in cardiomyocytes.** (A) Illustration of the action potential in the PV illustrating the measured parameters: the membrane potential; peak amplitude, rise time, rate of rise (dV/dt_{max}) and the action potential duration at 90% repolarisation (APD_{90}). (B) Superimposed action potentials of the initial pulse (S_1) with each pulse followed by a second pulse (S_2). The S_1-S_2 interval was progressively shortened in 2 ms increments. The effective refractory period (ERP) is indicated by the solid bar.

2.3 Results

2.3.1 Histological Examination of the rat and human PV and LA tissue.

Rat and human PVs and LA were sectioned and Masson's trichrome stained to differentiate the musculature (stained red) and connective tissue (stained blue). The rectangular and striated appearance of the cardiomyocytes distinguished them from smooth muscle cells. Figure 2.3A shows the cardiomyocyte sleeve extending along the length of the rat left PV. The sleeve becomes gradually thinner and diminishes at the distal part of the vein, which is located within the lung (intrapulmonary). The magnified PV sleeve sections in Figures 2.3 illustrate a mixture of cell arrangements with some cardiomyocytes observed in a uniform arrangement (Figure 2.3B), orientated parallel to each other, while other cardiomyocytes display a non-uniform arrangement, where groups of cardiomyocytes cross over each other (Figure 2.3C, D) .

The circumferential arrangement of cardiomyocytes around the vein was confirmed in transverse sections of the rat PV. Figures 2.3 E and F show a transverse section of the left PV proximal to the LA. The sections show that, several layers of cardiomyocytes encircle the vein. Moving toward the lumen, the cardiomyocyte sleeve diminishes and is replaced with connective tissue and a layer of small thin cells in the tunica intima, which are morphologically distinct from the cardiomyocytes.

Examination of the human left superior PV revealed a similar arrangement of cardiomyocytes to that of the rat PV. In the same PV, the cardiomyocyte arrangement varied from a uniform arrangement (Figure 2.4A), with typical cardiomyocyte striations are visible at higher magnification in Figure 2.4D, to a non-uniform and complex arrangement with cardiomyocytes running in different directions (Figure 2.4B,C). In addition, bundles of cardiomyocytes were often observed, separated by collagenous tissue. Similar to the rat PV, transverse sections of the human PV revealed the cardiomyocytes surrounding the lumen, although unsurprisingly the cardiomyocyte sleeve of the human PV appeared to be several

layers thicker than that of the rat (Figure 2.4E). The cardiomyocyte bundles are also evident in the transverse sections.

A complex arrangement of cardiomyocytes was also observed in the LA of rat (Figure 2.5A) with cardiomyocytes orientated uniformly in some areas as well as in differing planes in other sections. Higher magnification of the rat LA cardiomyocytes showed the striated appearance of the cells (Figure 2.5B). In addition, a similar arrangement was observed in the human LA (Figure 2.5C), with the striations of the cardiomyocytes evident at a higher magnification (Figure 2.5D).

2.3.2. Contraction of rat PV and LA tissues

Both the PV and LA tissues could be electrically stimulated to evoke contractions. The representative examples in Figure 2.6A illustrate the similarities in time course of the PV and LA contractions, as well as the greater amplitude of the LA contraction. Figure 2.6B shows that during electrical stimulation at 0.1 Hz, the LA contraction amplitude (0.3 ± 0.06 g) was significantly greater than that of the PV (0.2 ± 0.03 g, $P<0.05$). However, there was no significant difference in the time to peak contraction between the PV (29.4 ± 0.7 ms) and LA (27.1 ± 1.5 ms; Figure 2.6C). In addition, the duration of both contractions were similar, with the contraction duration determined as 92.0 ± 4.4 ms in the PV, compared to 84.6 ± 5.4 ms in the LA (Figure 2.6D). Contractions were creased in the absence of electrical activity.

2.3.3 Action potential characteristics of the PV and LA

The characteristics of electrically evoked action potentials which were recorded 0-0.5 cm proximal to the PV-LA junction, and those >0.5 cm from PV-LA junction (hereafter referred to as distal) were investigated in the rat PV. The membrane potential was similar in proximal (-73.3 ± 2.0 mV) and distal regions of the PV (-68.3 ± 1.6 mV, $P=0.0615$; Figure 2.7A). Figure 2.7B shows the peak amplitude of the action potential in distal PV cardiomyocytes was significantly smaller (74.8 ± 1.9 mV) when compared to proximal regions of the PV (80.6 ± 1.9 mV, $P<0.05$). The rise time (Figure 2.7C), dV/dt_{max} (Figure 2.7D), and APD_{90} (Figure 2.7E) were not significantly different in either region of the PV. In addition, a similar ERP was

recorded in proximal (35.2 ± 2 ms) and distal regions of the PV (35.5 ± 1.4 ms; Figure 2.7F).

The action potential parameters of the proximal PV and those of the LA from the same rat were also compared, demonstrating the similarity in the shape of the action potential between both tissues (Figure 2.8A). The membrane potential of both tissues was similar, being -73.3 ± 2.2 mV in the PV and -71.9 ± 0.8 mV in the LA (Figure 2.8B). Figure 2.8 shows the peak amplitude (Figure 2.8C) and rise time (Figure 2.8D) were also similar in the PV and LA. Although it was not significant, the dV/dt_{max} was slightly higher in the PV (213.1 ± 15.2 mV/ms) compared to the LA (185.8 ± 9.4 mV/ms; Figure 2.8E). There was no significant difference in the APD_{90} between the PV (32.9 ± 1.0 ms) and LA preparations (33.8 ± 1.2 ms; Figure 2.8F). The ERP was also no different in PV (36.1 ± 1.6 ms) and LA (32.3 ± 1.6 ms) tissues (Figure 2.8G).

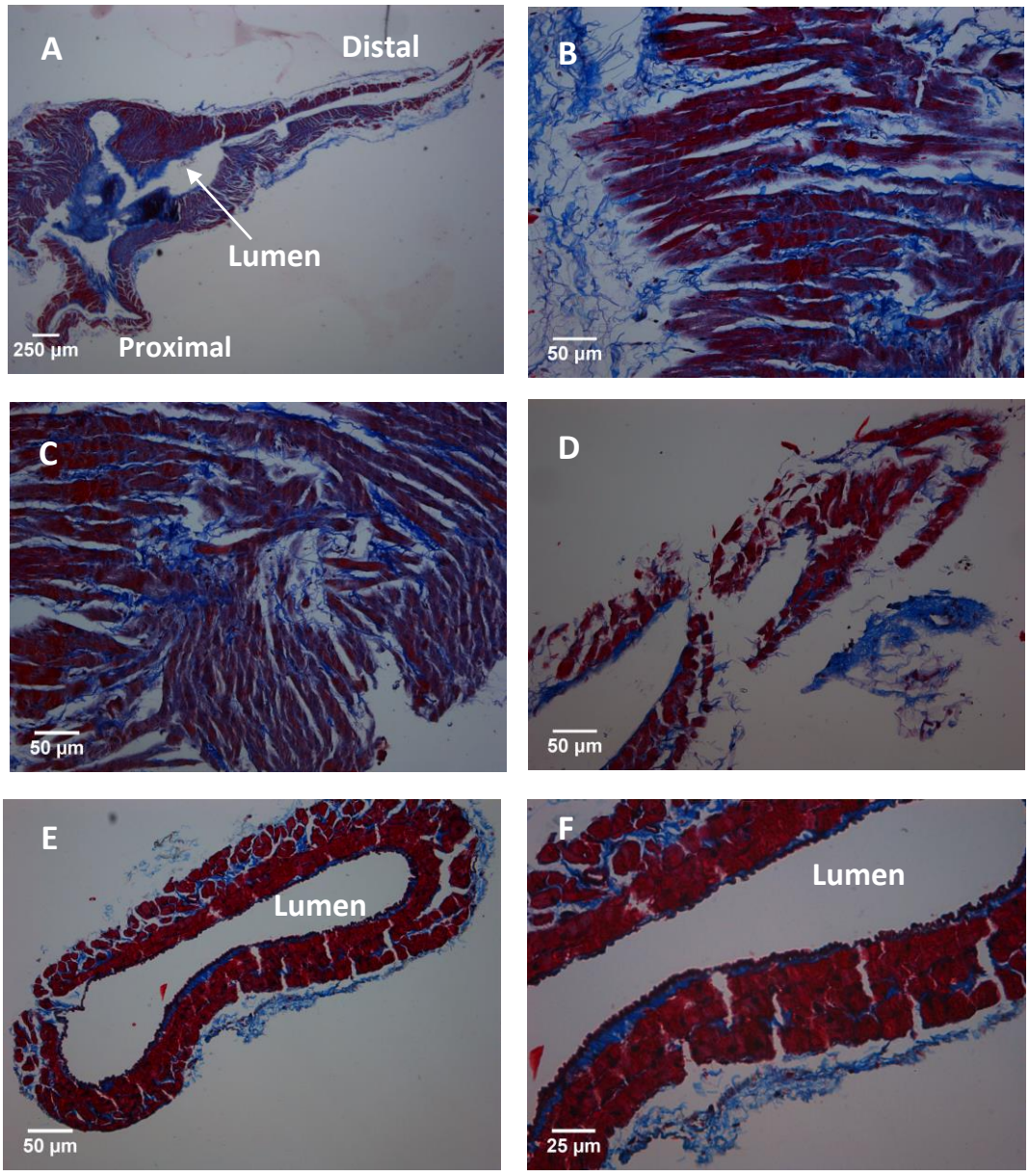

Figure 2.3 **Histological sections of the rat PV.** Formalin fixed rat PVs were wax embedded, sectioned and Masson's trichrome stained. Collagen is stained blue, muscle cells red and nuclei black. (A) Longitudinal section shows the cardiomyocyte sleeve extends along the length of the left PV. The proximal, middle and distal areas are shown at higher magnification in (B), (C) and (D) respectively. (E) Transverse section of the PV shows layers of cardiomyocytes encircling the lumen of the vein and shown at higher magnification in (F). Scale bar values are noted on each image.

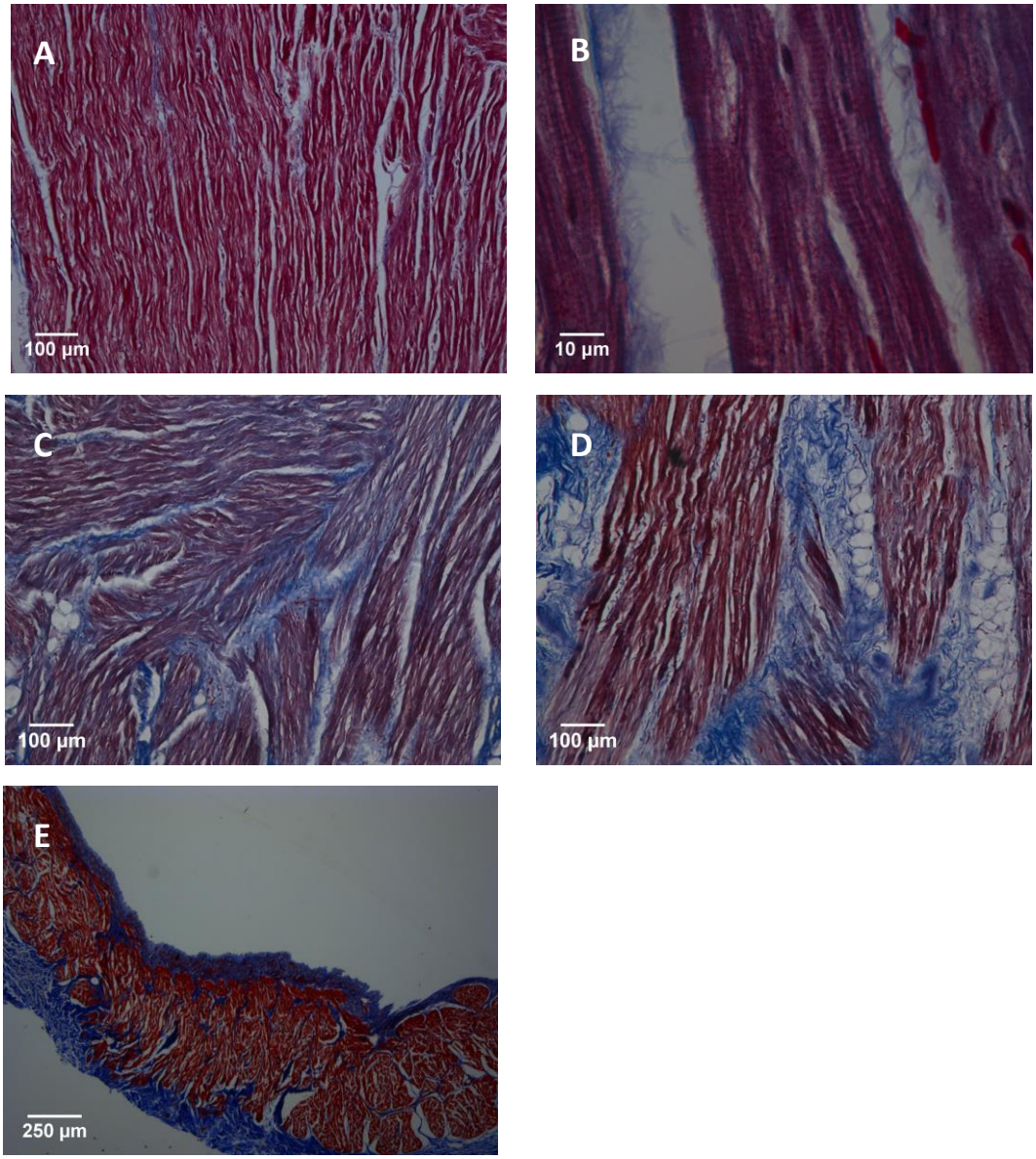

Figure 2.4 **Histological sections of the human PV.** Formalin fixed human PVs were wax embedded, sectioned and Masson's trichrome stained. Collagen is stained blue, muscle cells red and nuclei black. (A) Longitudinal section showing the uniform arrangement of cardiomyocytes in one area, and the striated cardiomyocytes are shown at higher magnification in (B). (C) and (D) Longitudinal sections showing the non-uniform arrangement of cardiomyocytes in the PV of two different patients. (E) Transverse section of the human PV. Scale bar values are noted on each image.

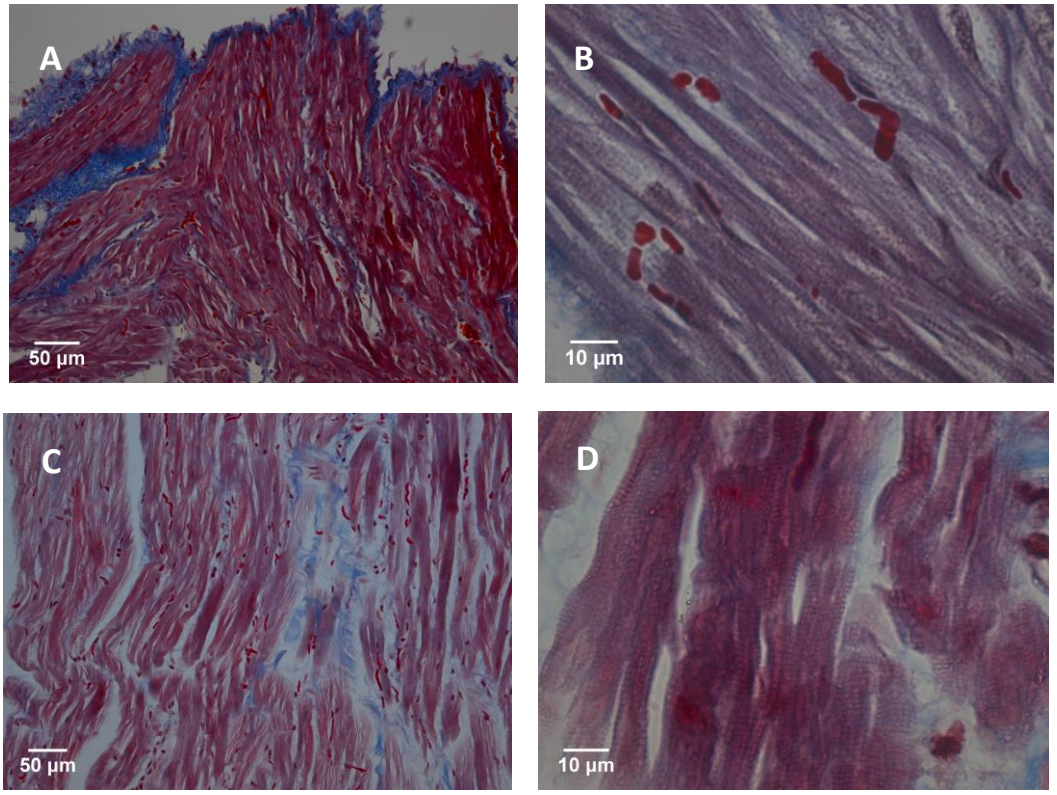

Figure 2.5. **Histological sections of the rat and human LA.** Formalin fixed tissues were wax embedded, sectioned and Masson's trichrome stained. Collagen is stained blue, muscle cells red and nuclei black. (A) Rat LA and (C) human LA sections demonstrating the arrangement of the cardiomyocytes and shown at a higher magnification in (B) and (D) respectively. Scale bar values are noted on each image.

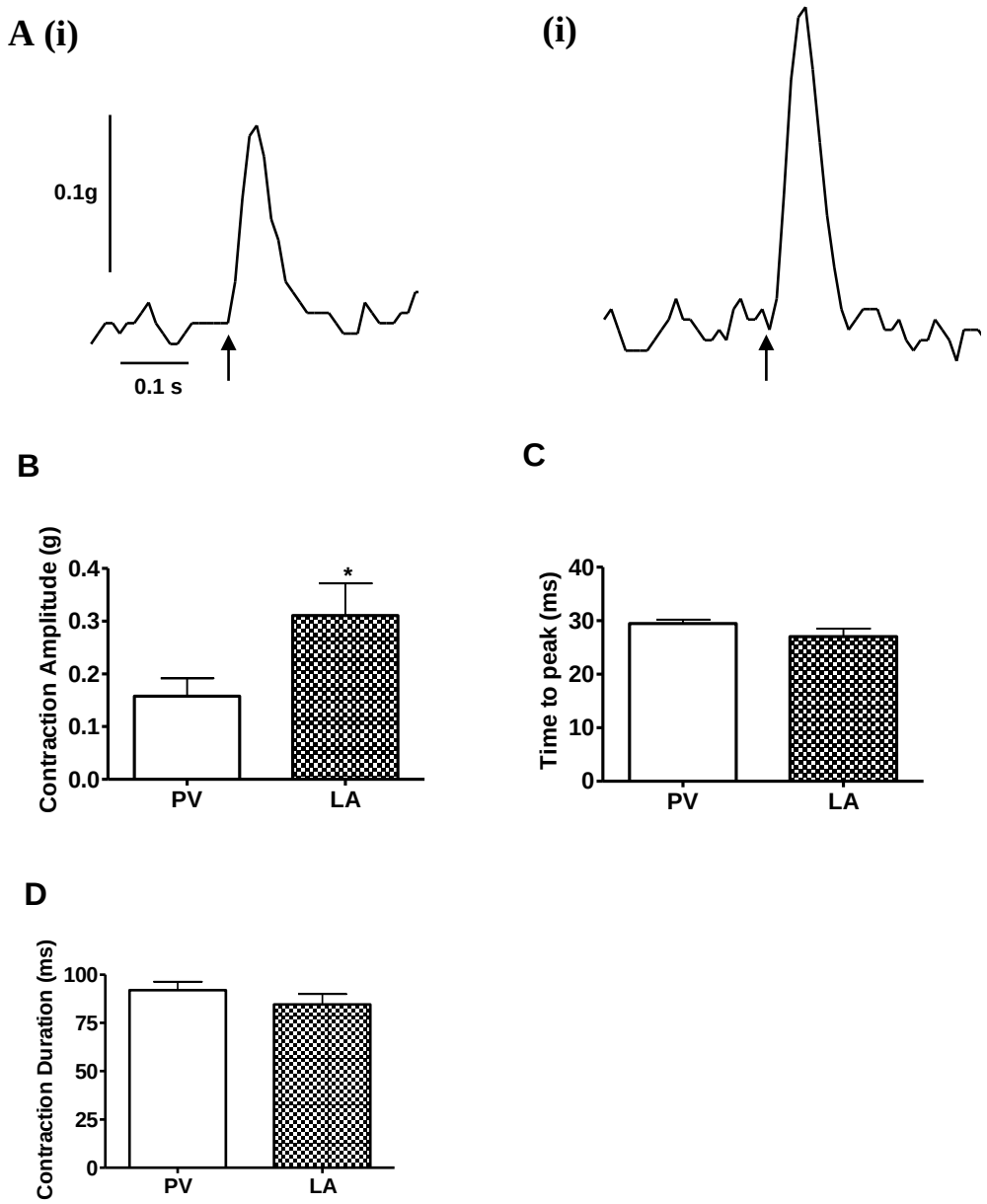

Figure 2.6 **Electrical stimulation evoked contractions of the rat PV and LA tissues.** (A) Representative recording of the rat PV (i) and LA (ii) contraction elicited by electrical stimulation at 0.1 Hz. Bar charts show the contraction amplitude (B), time to peak contraction (C) and contraction duration (D) in PV (n=7) and LA (n=7) tissues evoked by electrical stimulation at 0.1 Hz. All data are presented as mean ± s.e.m. * indicates $P<0.05$ for PV *vs.* LA. Arrows represent the electrical stimulus.

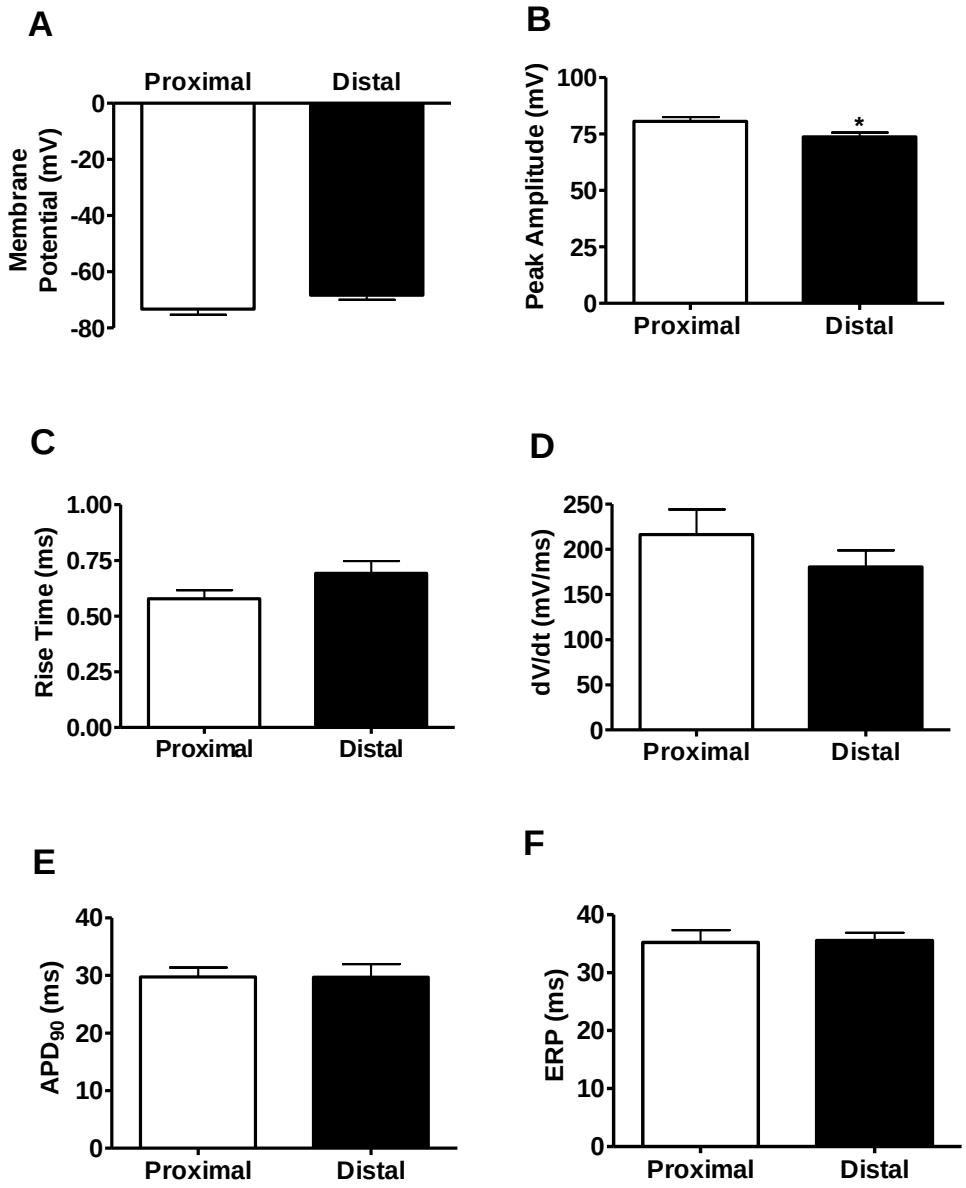

Figure 2.7 **Action potential characteristics of PV cardiomyocytes proximal and distal to the LA**. At a simulation frequency of 1 Hz, the membrane potential (A); and action potential peak amplitude (B); rise time (C); dV/dt_{max} (D); APD_{90} (E); and ERP (F) in PV cardiomyocytes located within 0.5 cm of the PV-LA junction (n=12/4) and cardiomyocytes located >0.5 cm from the PV-LA junction (n=11/4). All data are presented as mean ± s.e.m. * indicates P<0.05 for proximal *vs*. distal.

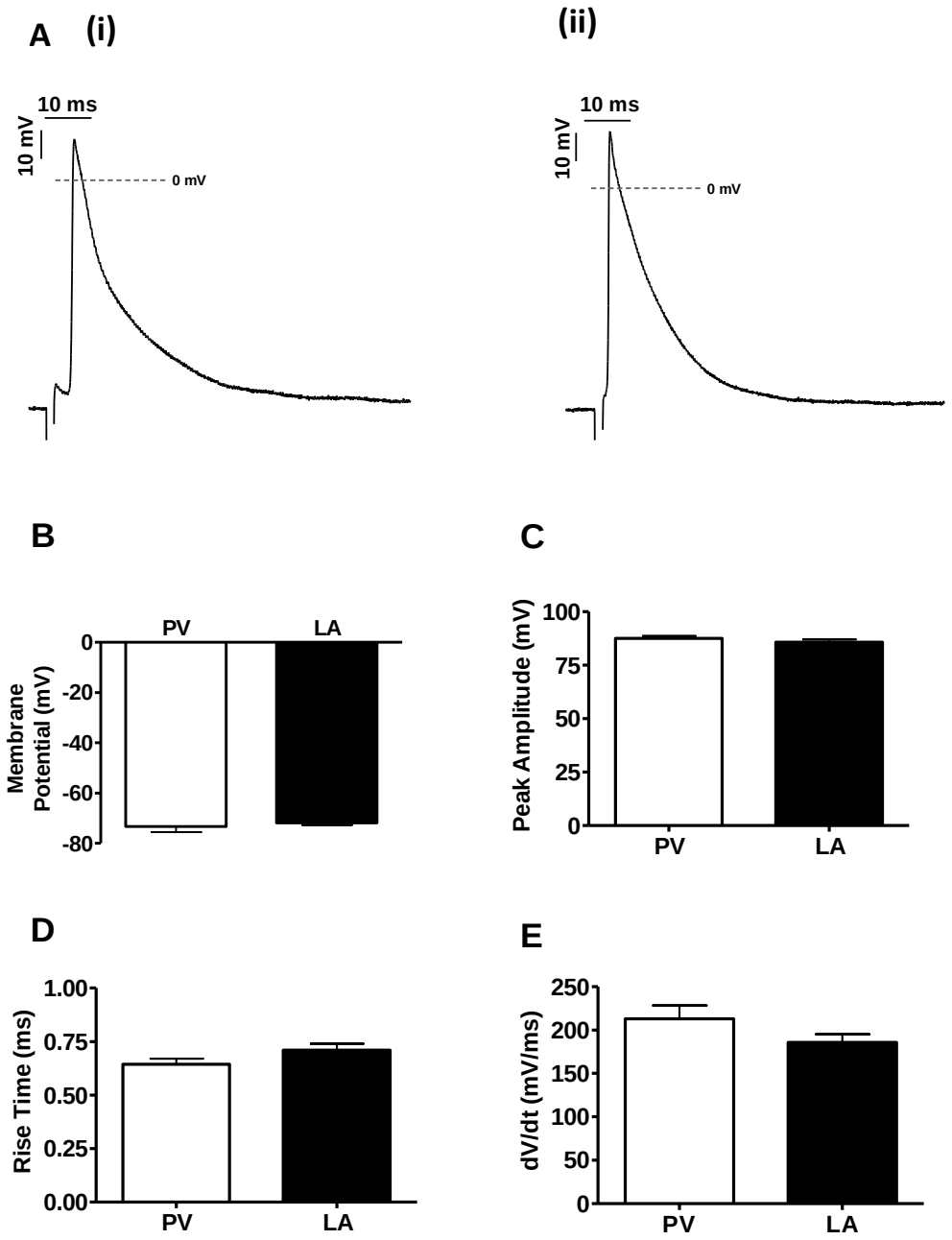

Figure 2.8 **Action potential characteristics of the PV and LA.** (A) Typical microelectrode action potential recording of a PV cardiomyocyte located within 0.5 cm of the PV-LA junction (proximal) (i) and LA cardiomyocyte (ii) evoked by electrical stimulation at 1 Hz. Membrane potential (B); action potential peak amplitude (C); rise time rise time (D) and dV/dt (E) in PV tissue located proximal to the PV-LA junction (n=54/21 rats) and LA (n=57/21) tissues. All data are presented as mean ± s.e.m.

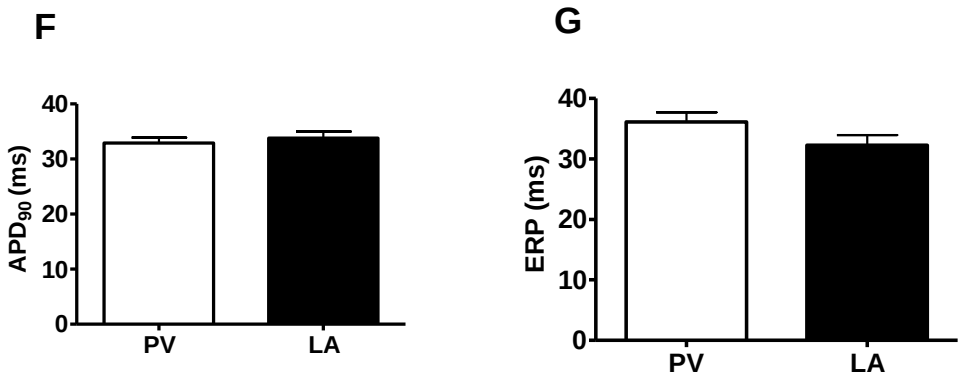

Figure 2.8 (Cont'd) **The action potential characteristics of the PV and LA.** The APD_{90} (F) and ERP (G) in PV located within 0.5 cm of the PV-LA junction (n=54/21) and LA (n=57/21) cardiomyocytes. All data are presented as mean ± s.e.m.

2.4 Discussion

2.4.1 The arrangement of cardiomyocytes in PV and LA tissues

Both the rat and human PV and LA were examined histologically after staining with Masson's trichrome. Longitudinal sections of the rat PV showed extension of the cardiomyocyte sleeve from the atrium, and into the intrapulmonary sections of the vein. Previous histological studies of the PV of rat and other rodents also reported the extension of the cardiomyocyte sleeve into the intrapulmonary sections of the PV (Kramer and Marks, 1965; Mueller-Hoecker *et al.*, 2008). However, in larger mammals the cardiomyocyte sleeve does not extend as far. The human and dog PV cardiomyocyte sleeve is reported to be around 0.4–4.8 cm long and terminates before reaching the lungs (Saito *et al.*, 2000; Ho *et al.*, 2001; Verheule *et al.*, 2002; Hassink *et al.*, 2003; Kholová and Kautzner, 2003; Roux *et al.*, 2004). However, this could not be confirmed in the present study, because sections of the PV obtained were too short in length. Some of the basic ultrastructural characteristics of the PV cardiomyocyte sleeve are similar in rat and humans. Both the rat and human PV sleeve possessed a complex arrangement of cardiomyocytes with areas of non-uniformity, where cardiomyocytes were orientated in differing directions, although this complex arrangement was possibly more prominent in the human PV compared to that of the rat. This histological observation is consistent with previous examinations of PVs and the complex PV architecture is a common feature in mammals (Kramer and Marks, 1965; Ludatscher, 1968; Hashizume et al., 1998; Mueller-Hoecker et al., 2008; Nathan and Eliakim, 1966; Moubarak et al., 2000; Saito et al., 2000; Ho et al., 2001; Hassink et al., 2003; Perez-Lugones et al., 2003; Roux et al., 2004). This complex and non-uniform arrangement of cardiomyocytes in areas of the PV will likely affect electrical conduction in the vein since the conduction velocity is influenced by the cardiomyocyte arrangement (Spach *et al.*, 2000). For example, detailed examination of cardiac conduction has demonstrated the existence of anisotropic conduction as electrical signals are propagated more rapidly over the longitudinal axis of the cardiomyocytes, compared to transverse cardiomyocyte paths (Sano *et al.*, 1959; Clerc, 1976; Roberts *et al.*, 1979). This is thought to be a consequence of the greater number of cell boundaries per unit distance encountered in the transverse direction, which can slow the conduction

velocity (Sano *et al.*, 1959). Microelectrode array recordings on the dog PV revealed that conduction abnormalities arose in areas where there was abrupt changes in cardiomyocyte orientation (Hocini *et al.*, 2002; Hamabe *et al.*, 2003). Such conduction abnormalities may also create a favourable substrate for re-entry in the PV.

Transverse sections demonstrated that the PVs of both species had several layers of cardiomyocytes surrounding the vein. Due to the nature of the Masson's trichrome stain, the cell type of the thin layer of cells close to the lumen was not clear. However, previous confocal and electron microscopy studies of the rat PV showed that close to the lumen there was a thin layer of endothelial cells, with an adjacent layer of smooth muscle cells which stained positive for α-smooth muscle actin (Hashizume *et al.*, 1998; Hosoyamada *et al.*, 2010). Further immunostaining of the PV with F-actin confirmed that several layers of striated cardiomyocytes encircled the smooth muscle layer (Hosoyamada *et al.*, 2010). A similar arrangement was also observed in the PVs from human (Saito *et al.*, 2000), guinea pig (Takahara *et al.*, 2011) and dog (Verheule *et al.*, 2002).

2.4.2 Contractile properties of PV and LA tissues

Electrical stimulation elicited a PV contraction, which on average was similar in time to peak and duration, but smaller in amplitude when compared to the LA. The similarity in contraction duration between both tissues suggests the PV contraction is due to the cardiomyocyte sleeve as vascular smooth muscle contraction has a much longer timecourse compared to cardiac muscle. The lack of contractions, in the absence of electrical stimulation, in the rat PV and LA preparations was in agreement with previous studies (Maupoil et al., 2007; Luk et al., 2008). This also further highlights the lack of intrinsic automaticity in the rat PV sleeve.

The underlying mechanism of excitation contraction coupling, which initiates contraction, is thought to be similar in PV and LA tissues. This could account for the similarity in the contraction timecourse of both tissues. The greater contractile magnitude observed in the LA compared to the PV presumably reflects the greater

muscle mass of this tissue. Previously, the Ca^{2+} dependence of contraction was demonstrated by Luk *et al.* (2008), who reported that the amplitude of the electrically evoked contraction of the rabbit PV was dependent on the Ca^{2+} concentration in the external solution. Similar findings were reported in rabbit and guinea pig LA preparations (Winegrad and Shanes, 1962; Toda, 1969).

2.4.3 Action potential characteristics of the PV and LA

As to whether or not there is heterogeneity in the action potential characteristics along the cardiomyocyte sleeve is controversial (Cheung, 1981; Wang *et al.*, 2003; Po *et al.*, 2005). In this study, the smaller action potential peak amplitude in distal PV cardiomyocytes compared to those in the proximal regions suggests there is some degree of heterogeneity along the length of the sleeve. Recently, Egorov *et al.* (2015) also reported heterogeneity in the PV sleeve as they observed a more depolarised resting membrane potential in the distal areas of the PV, compared to those proximal, although this was measured in the absence of electrical stimulation. Previous studies in other species also observed action potential heterogeneity along the PV as a smaller amplitude, a more depolarised resting membrane potential and a shorter APD was recorded in the distal PV cardiomyocytes from the guinea pig (Cheung, 1981). A more depolarised resting membrane potential was also reported in the distal regions of the dog PV (Po *et al.*, 2005). Conversely others reported no difference in AP characteristics along the PV sleeve of dogs (Wang *et al.*, 2003).

There was no discernible difference in the action potential characteristics between proximal regions of the PV and the LA in this study. This is in agreement with previous studies on the rat, which reported that there was no difference in the electrically evoked action potentials in these two tissues (Miyauchi *et al.*, 2004, 2005). Therefore, the PVs susceptibility to arrhythmogenic activity is not simply due to a difference in the action potential characteristics compared to the LA. However, others have observed a slower dV/dt_{max} and shorter APD Okamoto *et al.* (2012) in rat PV cardiomyocytes compared to those of the LA. A more depolarised resting membrane potential in rat PV cardiomyocytes was also reported, although this was measured in the absence of electrical stimulation and the membrane potential

became more negative and of a similar value to the LA upon initiation of electrical stimulation (Doisne *et al.*, 2009; Malécot *et al.*, 2014; Egorov *et al.*, 2015).

In conclusion, a similar arrangement of cardiomyocytes was observed in rat and human PVs, with a mix of uniform and non-uniform arrangements of cardiomyocytes in both species. Functional studies of the rat PV demonstrated the ability of rat PVs to contract during electrical stimulation with a similar timecourse to that of the LA. Further electrophysiological characterisation of the rat PV revealed the peak amplitude of electrically evoked action potentials was significantly smaller in the distal regions of the PV, compared to those proximal. In addition, the electrically evoked action potentials in PV cardiomyocytes proximal to the LA, were not significantly different from those of the LA.

Chapter 3

The Properties of Na^+ Channels in the PV and LA

3.1 Introduction

3.1.1 Na^+ channel subtypes in cardiomyocytes

The nine voltage gated Na^+ channels (Na_v) display diverse distribution and differing pharmacological properties. The subtypes can be distinguished by their sensitivity to the selective Na^+ channel blocker, tetrodotoxin (TTX) (Renaud *et al.*, 1983). The Na^+ channel isoforms which are sensitive to inhibition by nanomolar concentrations of TTX are termed TTX-sensitive Na^+ channels (Na_v1.1, 1.2, 1.3, 1.4, 1.6 and 1.7) whereas those which require micromolar concentrations of TTX for inhibition are termed TTX-resistant Na^+ channels (Na_v1.5, 1.8 and 1.9). This difference in TTX-sensitivity is due to the presence of a cysteine residue in the pore region of the Na_v1.5 isoform and the presence of serine in Na_v1.8 and Na_v1.9, instead of phenylalanine or tyrosine, which reduces their sensitivity to TTX (Satin *et al.*, 1992; Sivilotti *et al.*, 1997). The Na_v1.1, 1.2, 1.3, 1.6 and 1.7 subunits are expressed primarily in the nervous system (Kayano *et al.*, 1988; Ahmed *et al.*, 1992; Lu *et al.*, 1992; Schaller *et al.*, 1995), while the Na_v1.4 isoform, is mainly present in skeletal muscle (Trimmer *et al.*, 1989). Two of the TTX-resistant isoforms, Na_v1.8 and 1.9, are primarily located in the peripheral nervous system (Akopian *et al.*, 1996; Toledo-Aral *et al.*, 1997; Dib-Hajj *et al.*, 1998). The Na_v1.5 isoform is the major cardiac Na^+ channel isoform, establishing the key electrophysiological and pharmacological properties of the cardiac I_{Na} (Gellens *et al.*, 1992). However, using tritiated ethylenediamine TTX ([^{3}H]) in binding assays, Renaud *et al.* (1983) reported the existence of a small fraction of Na^+ channels with a high affinity for TTX, as well as a larger fraction with a low affinity for TTX in neonatal ventricular rat cardiomyocytes. Subsequent, patch clamp recordings in rat ventricular cardiomyocytes revealed that 14% of the total I_{Na} was TTX-sensitive (Brette and Orchard, 2006), indicating that Na_v1.5 is not the only contributor to the cardiac I_{Na}. The TTX-sensitive current was found to contribute 8% of the total I_{Na} in mouse (Haufe *et al.*, 2005a) and 10-22% in dog ventricular cardiomyocytes (Haufe *et al.*, 2005b), while 27% of the total I_{Na} in human right atrial cardiomyocytes was TTX-sensitive (Kaufmann *et al.*, 2013).

Expression of $Na_v1.1$, $Na_v1.2$, $Na_v1.3$ and $Na_v1.4$ mRNA, and the corresponding proteins, has been reported in the ventricles of rat, mouse, dog, pig and human (Sills *et al.*, 1989; Schaller *et al.*, 1995; Dhar Malhotra *et al.*, 2001; Zimmer *et al.*, 2002; Haufe *et al.*, 2005a; Gaborit *et al.*, 2007; Blechschmidt *et al.*, 2008; Sossalla *et al.*, 2010). This adds further support to the notion that $Na_v1.5$ is not the only Na^+ channel isoform present in cardiomyocytes. The localisation of the TTX-sensitive channels in comparison to the $Na_v1.5$ channels has also been examined. Immunocytochemistry studies revealed that $Na_v1.5$ is present at the T-tubules, as well as the intercalated discs of ventricular cardiomyocytes suggesting they are involved in rapid depolarisation and conduction of the action potential (Cohen, 1996; Maier *et al.*, 2002, 2004; Haufe *et al.*, 2005a; Xi *et al.*, 2009). Furthermore $Na_v1.5$ was observed in a uniform striated pattern in the atria (Cohen, 1996; Kaufmann *et al.*, 2013). The TTX-sensitive channels $Na_v1.1$, $Na_v1.2$, and $Na_v1.6$ were observed in a striated pattern in ventricular cardiomyocytes of mouse (Maier *et al.*, 2002, 2004; Haufe *et al.*, 2005a; Westenbroek *et al.*, 2013) and dog (Haufe *et al.*, 2005b), indicative of a location at the T-tubules, and in some studies they were also located at the intercalated discs. The $Na_v1.3$ channel displays a species difference in distribution, with a striated T-tubular location reported in mouse ventricular cardiomyocytes (Maier *et al.*, 2002, 2004; Westenbroek *et al.*, 2013), and a more diffuse distribution throughout the cell in dog ventricular cardiomyocytes (Haufe *et al.*, 2005b). The TTX-sensitive isoforms were located differently in human atrial cells, with $Na_v1.1$, 1.3 and 1.6 located in a diffuse pattern on the cell surface and $Na_v1.2$ observed at the intercalated discs (Kaufmann *et al.*, 2013).

3.1.2 Role of TTX-sensitive Na^+ channels in cardiomyocytes

Whether, as hypothesised by Maier *et al.* (2002), a difference in the localisation of the Na^+ channel isoforms suggests specific physiological roles for the TTX-sensitive and TTX-resistant Na^+ channel isoforms remains controversial. The presence of TTX-sensitive Na^+ channels at the intercalated discs and T-tubules suggests a potential role in both the excitation contraction coupling and propagation of the action potential in ventricular cardiomyocytes. This hypothesis was supported by Maier *et al.* (2002) who reported that low concentrations of TTX (100-200 nM)

decreased left ventricular contraction in mouse and guinea pig whole hearts, when studied *in vitro*. In addition, a reduction in the conduction velocity was observed in the ventricles of $Na_v1.6$ null mice (Noujaim *et al.*, 2012). The TTX-sensitive Na^+ channels are also thought to be somehow involved in triggering the release of Ca^{2+} from the sarcoplasmic reticulum, as inhibition of TTX-sensitive Na^+ channels reduced the maximum rate of rise, as well as the amplitude of the Ca^{2+} transients in rabbit ventricular cardiomyocytes (Torres *et al.*, 2010). In contrast, (Brette and Orchard, 2006) found that low concentrations of TTX did not affect the Ca^{2+} transients or contraction of rat ventricular cardiomyocytes.

The TTX-resistant $Na_v1.8$, may also contribute to the cardiac I_{Na}, as expression of mRNA from the SCN10A gene, which encodes $Na_v1.8$, was identified in the atria and ventricle of mice and humans (Chambers *et al.*, 2010; Facer *et al.*, 2011). It has been shown that A-803467, a $Na_v1.8$ blocker, reduced the I_{NaL} in mouse ventricular cardiomyocytes, shortened the APD and suppressed EADs (Yang *et al.*, 2012). Thus, it was suggested that $Na_v1.8$ contributes to I_{NaL} and could be involved in arrhythmogenic activity. This was further supported by genome wide association studies, which linked mutations in the SCN10a gene to an altered PR interval and QRS duration in the ECG (Chambers *et al.*, 2010; Holm *et al.*, 2010; Pfeufer *et al.*, 2010; Sotoodehnia *et al.*, 2010). Furthermore, Pfeufer *et al.* (2010) identified a link between variations in the $Na_v1.8$ gene and AF.

3.1.3 Aims

The aims of this chapter were to examine the role of I_{Na} in the generation of the action potential and gain further insight into the effect of inhibition of Na^+ channels on the excitability of PV and LA cardiomyocytes. A method was then developed to isolate cardiomyocytes from the PV and LA, which were then subsequently studied in order to compare the I_{Na} characteristics in both cell types. The contribution of TTX-sensitive Na^+ channels to the total I_{Na}, as well as the individual Na^+ channel isoform expression and localisation in PV and LA cardiomyocytes was also investigated. The potential role of TTX-sensitive Na^+ channels in the contraction as well as the generation of action potentials was also examined in both tissues.

3.2 Methods

3.2.1 Microelectrode studies

Male Sprague Dawley rats were sacrificed by cervical dislocation and the heart and lungs removed. The PV and LA were dissected and action potentials recorded using the microelectrode technique described in Section 2.2.5. The tissues were allowed to equilibrate in bath solution, consisting of 150 mM NaCl, 5.4 mM KCl, 10 mM HEPES, 10 mM glucose, 1.2 mM $MgCl_2$, 1.8 mM $CaCl_2$, pH 7.4 with NaOH, warmed to 37^{o}C for 30 minutes before commencing any recording. Action potentials were elicited by stimulating at twice the threshold voltage, with a 2 ms pulse at a rate of 1 Hz. To determine the action potential threshold voltage, the stimulation voltage was increased in 5 V increments under control conditions until an action potential was elicite; this was also repeated in the presence of TTX. To investigate the effect of TTX on PV and LA action potentials, the tissues were stimulated at 1 Hz and recordings (1 minute in duration) were obtained in the same cell before and after 15 minutes in the presence of TTX. Data was acquired using WinEDR software (Version 3.3.4, Dr. J. Dempster, University of Strathclyde), which was subsequently exported to WinWCP software (Version 4.6.5 Dr. J. Dempster, University of Strathclyde) to enable the action potential characteristics and effective refractory period (ERP) to be measured as described in section 2.2.5.

3.2.2 Cell isolation – The Chunk method

The chunk method alone (where the PV or LA tissue was cut into chunks and incubated with digestive enzymes) was first adopted for cardiomyocyte isolation, with a number of different enzyme combinations and incubation time periods tested. The tissue was incubated in Ca^{2+} free isolation solution 1 (see appendix, Table 6.1) with a combination of papain (1 mg/mL) and dithiothreitol (DTT, 1 mg/mL) for 10 minutes to 1 hour and then transferred to isolation solution 1 containing Type VIII collagenase for periods of 15 minutes to 1 hour, similar to the method used by Michelakis *et al.* (2001). However this resulted in cardiomyocytes which were not viable for patch clamping due to a low yield of Ca^{2+} tolerant cardiomyocytes, with a "blebby" appearance. The Ca^{2+} tolerance was determined by the observation of cells

rounding up after the re-introduction of Ca^{2+}. Different approaches to the chunk method were then adopted in order to try and improve the yield and Ca^{2+} tolerance. The PV tissues were digested using Type I, II or VIII collagenase in a number of different Ca^{2+} free isolation solutions (see appendix, Table 6.1) for periods of 20, 40 or 60 minutes. However, this did not yield single cardiomyocytes, without the aid of vigorous trituration, which rendered the cells non-viable. In a number of digestions, approximately 50 µM $CaCl_2$ was also added during collagenase digestion to aid with collagenase activation and perhaps improve the Ca^{2+} tolerance, but this also did not produce viable single cardiomyocytes. A combination of digestive enzymes was then tested in order to reduce the trituration needed to produce single cells. Incubation of the PV with collagenase (Type I, II or VIII) in combination with elastase or protease, in a Ca^{2+} free isolation solution for 20-60 minutes, in some cases produced a higher yield of cardiomyocytes, with minimal trituration, in comparison to digestion with collagenase alone. In particular, dissociation with Type I collagenase and Type XIV protease for 20 minutes resulted in rod shaped cardiomyocytes. However, the cardiomyocytes were not Ca^{2+} tolerant and not viable for patch clamping. Incubation of isolated cells in KB solution (Honjo *et al.*, 1996); 70 mM L-glutamic acid, 25 mM KCl, 20 mM taurine, 10 mM KH_2PO_4, 3mM $MgCl_2$, 10 mM glucose, 10 mM HEPES, 0.5 mM EGTA, pH 7.4 with KOH) for at least one hour at 4ºC, which has been shown previously to improve Ca^{2+} tolerance in cardiomyocytes (Isenberg and Klockner, 1982; Honjo *et al.*, 1996), also did not improve cardiomyocyte viability with the different chunk methods tested. A similar outcome was also observed when Ca^{2+} was reintroduced stepwise every 10 minutes from 0.01 mM to 0.05, 0.1, 0.5, 0.9, 1.3 and 1.8 mM, even after the cells were pre-incubated for 1 hour with KB solution prior to the Ca^{2+} reintroduction.

Previous studies also reported a poor cell yield with the use of the chunk method to isolate dog PV cardiomyocytes (Sicouri *et al.*, 2011). Therefore, in order to try and improve the cardiomyocyte yield and quality, the Langendorff technique was utilised. Several other groups have reported success with the use of the Langendorff technique in the dissociation of rat PV cardiomyocytes (Okamoto *et al.*, 2012, 2014) and rat LA cardiomyocytes (Xu and Best, 1990; Kim, 1993; Bond *et al.*, 2014).

3.2.3 Cell isolation – The Langendorff method

All solutions used in this section were prepared with commercially supplied sterile water (VWR, UK) as this was found to improve the Ca^{2+} tolerance of the isolated cardiomyocytes, in comparison to solutions prepared with water from the laboratory Purite Milli-Q® system. The Langendorff apparatus was primed with 200 mL of VWR water, followed by 200 mL of Ca^{2+} free isolation solution (120 mM NaCl, 20 mM HEPES, 5.4 mM KCl, 0.52 mM NaH_2PO_4, 3.5 mM $MgCl_2$, 20 mM taurine, 10 mM creatine, glucose 11.1 mM, pH 7.4 with NaOH) in which 1 mM EGTA was also added to chelate any excess Ca^{2+}. For the isolation, all solutions were warmed to 37ºC before perfusion and the perfusate was maintained at 37ºC throughout by the use of a heated coil (see Figure 2.1A). Male Sprague-Dawley rats (200-400 g) were anesthetised by intraperitoneal injection of Euthatal (100 mg/kg), to allow transportation from the Biological Procedures Unit (BPU) to the laboratory where they were euthanised by cervical dislocation. The heart and lungs were quickly removed, briefly immersed in Ca^{2+} free isolation solution containing around 1-2% heparin (5000 IU/mL, Leo Pharma, UK) and mounted via the aorta to the Langendorff apparatus (Figure. 3.1A, B), while the heart was still beating. The tissue was then perfused with 50 mL oxygenated Ca^{2+} free isolation solution, to clear the heart and lungs of blood, at a flow rate of 6 mL/min using a Watson Marlow peristaltic pump. The removal of Ca^{2+} from the solution is thought to aid in the dissociation of the cardiomyocytes by disrupting intercellular connections at the intercalated discs (Muir, 1967). The position of the cannula was adjusted, so that it was reaching as far down as the beginning of the left ventricle, and care was taken to check the solution was able to flow in the coronary circulation as well as within the PVs. A small incision was also made in the pulmonary artery to aid clearing of the blood from the lungs. For enzymatic digestion, the perfusate was replaced with oxygenated Ca^{2+} free isolation solution containing 0.66 mg/mL Type I collagenase (Worthington, New Jersey, USA) and 0.04 mg/mL Type XIV protease (Sigma, UK) for 7-10 minutes. After digestion, the enzymes were removed by perfusion with 50 mL of Ca^{2+} free isolation solution containing 0.8 mg/mL BSA (Sigma, UK). The heart and lungs were then removed from the apparatus and the LA was cut into 1-2 mm cubes, transferred to KB solution containing 0.8 mg/mL BSA (70 mM L-

glutamic acid, 25 mM KCl, 20 mM taurine, 10 mM KH_2PO_4, 3mM $MgCl_2$, 10 mM glucose, 10 mM HEPES, 0.5 mM EGTA, pH 7.4 with KOH) and gently triturated 5-10 times with a fire polished glass pipette. The PVs could not be fully digested with the Langendorff method alone, as even an increase in the perfusion time did not yield single PV cardiomyocytes, and resulted in over digested LA cardiomyocytes. Therefore, following the Langendorff perfusion the PVs were carefully dissected from the lungs and further digested by incubating in Ca^{2+} free isolation solution containing 0.8 mg/mL Type I collagenase and 0.08 mg/mL Type XIV protease for 15-20 minutes in a slowly shaking waterbath set at 37ºC. Following this, the PVs were cut into 1-2 mm chunks and gently triturated 5-10 times with a fire polished glass pipette into KB solution containing 0.8 mg/mL BSA. To improve Ca^{2+} tolerance, isolated PV and LA cells were stored at 4ºC in KB solution for at least one hour before use.

Isolated cells were viewed with an Olympus CK2 inverted microscope. Cell images were acquired using a Tuscen IS1000 digital microscope camera (Xintu Photonics Co., Ltd, China) and cell length and width were measured with the use of Tsview version 7 software. Measurements were taken during resting conditions and only Ca^{2+} tolerant cardiomyocytes with clear striations and ‘non-blebby’ membranes were used.

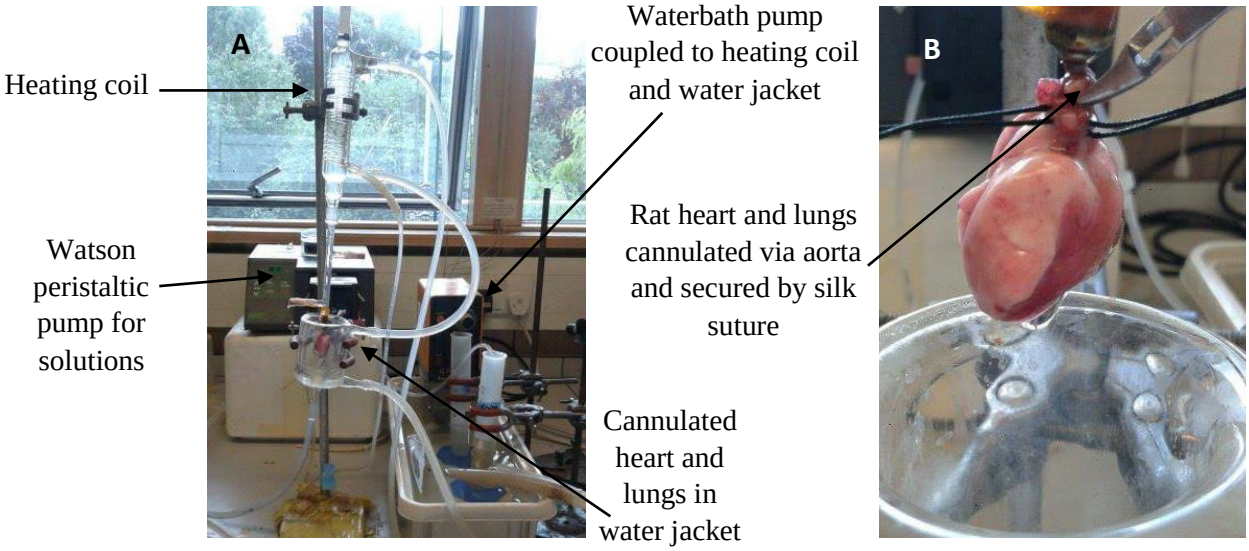

Figure 3.1. **The Langendorff apparatus.** Cannulation of the rat aorta, which was held in place with silk suture thread and a bulldog clamp, allowed retrograde perfusion of the heart with Ca^{2+} free and enzyme containing solutions by constant flow perfusion. Solutions were pre-heated to 37^{o}C in a waterbath and passed through a 37^{o}C heating coil before reaching the heart and lungs, which were suspended in a water jacketed glass vessel at 37^{o}C.

3.2.4 Patch Clamp

3.2.4.1 Whole cell recording

After storage for 1 hour at 4^{o}C in KB solution, a drop of freshly isolated PV or LA cardiomyocytes was allowed to adhere for 10-15 minutes onto a cover glass that formed the bottom of a 1.5 mL circular chamber, which was mounted onto the stage of an Olympus CK2 inverted microscope. Investigations were carried out on Ca^{2+} tolerant cardiomyocytes, using the whole-cell configuration of the patch clamp technique. Experiments were carried out at room temperature (18-23^{o}C) to reduce the magnitude of the I_{Na} and thereby ensure adequate voltage control (Colatsky, 1980; Makielski *et al.*, 1987). An Axopatch 1D (Axon Instruments, USA) patch clamp amplifier connected via a BNC-2110 connector block to a NI PCI-6221 data acquisition card (National Instruments, Texas, USA), was used throughout. Data acquisition and analysis was achieved using WinWCP software (Version 4.6.5). Currents were filtered at 5 kHz (-3 dB) before digitization at 20 kHz and stored electronically on the hard drive of a desk top computer. The microscope and manipulators (three-axis oil hydraulic, MMO 203, Narishige, Japan) were mounted onto an air table (Model AVT 701, Wentworth Laboratories LTD, Bedford, UK) to minimise vibrations and enclosed in a Faraday cage.

External and internal solutions containing a low Na^{+} concentration were used in order to reduce the magnitude of I_{Na}, which improves the voltage control of the cell membrane potential (Colatsky, 1980). A Nanion (Nanion, Germany) perfusion system perfused the low Na^{+} external solution (Undrovinas *et al.*, 2006), which consisted of 5 mM NaCl, 133 mM CsCl, 2 mM $MgCl_2$, 1.8 mM $CaCl_2$, 0.002 nM nifedipine, 5 mM HEPES, 5 mM glucose, pH 7.3 with CsOH, at a rate of 1-2 mL/min. Osmolarity of the solution was measured with an Osmomat 030 cryoscopic osmometer (Gonotec, Germany) and adjusted to 300-310 mOsm with sucrose. The inclusion of CsCl and nifedipine was added to avoid contamination of overlapping K^{+} and Ca^{2+} currents respectively. Patch pipettes (1.2-2.5 MΩ) were fabricated using borosilicate glass (1.5 mm outer diameter, 0.86 mm inner diameter, Clark

Electromedical Instruments, UK) and a horizontal micropipette puller (Model P-87, Sutter Instruments Co, Novato, California). The pipette solution contained 133 mM CsCl, 5 mM NaCl, 5 mM Mg_2ATP, 20 mM TEACl, 5 mM HEPES, 10 mM EGTA, pH 7.3 with CsOH and an osmolarity of 290-300 mOsm. The current was zeroed when the pipette was placed in the bath solution to correct for liquid junction potentials between the bath solution and the pipette solution. After obtaining the whole cell recording configuration, the cell membrane capacitance was measured by integrating the capacitance current recording during a 5 mV hyperpolarising step from -80 mV. The cell capacitance was significantly greater in PV cardiomyocytes (114.0 ± 5.2 pF, n=42) than LA cardiomyocytes (68.9 ± 4.3 pF, n=34; $P<0.001$). The amplifier was limited to capacitance compensation for cells up to 100 pF. Capacitance and series resistance were adjusted to obtain minimal contribution of the capacitive transients. Series resistance was compensated by 80-85% without ringing. A P/4 protocol was used to subtract residual linear leak and capacitance currents.

3.2.4.2 Voltage protocols and curve fitting

Recording began 5-10 minutes after establishing the whole-cell recording configuration. Cells were rejected if the leak current was >-11 pA/pF at a holding potential of -120 mV. The electronic series resistance compensation (ER_s) was adjusted to a point just before ringing occurred. The current-voltage (*I*-V) relationship for peak I_{Na} was then used to determine the maximum peak I_{Na} (I_{max}). Voltage clamp quality was also assessed for each cell using a method adapted from (Maltsev and Undrovinas, 1997), and the deviation from voltage command (V_{dev}) was estimated using the following equation:

$$V_{dev} = I_{max} \times R_s \times (100\% - ER_s)/100\% \quad (1)$$

where R_s is the non-compensated series resistance. If V_{dev} was <6 mV, adequate voltage control was assumed and only these cells were included in the study.

Currents are expressed as the current density (pA/pF), to account for the variability in cell size. The current voltage relationship and steady state activation were determined using a series of 25 ms depolarising test pulses, from a holding potential

of -120 mV, to voltages between -90 mV and +50 mV in 5 mV increments. For steady-state activation curves, the Boltzmann equation was fitted:

$$G/G_{max} = 1/(1+\exp((V_{½}-V)/k)) \quad (2)$$

where G_{max} is the maximal peak Na^+ conductance, $V_{½}$ the voltage of half maximal activation and k the slope factor.

To determine the steady-state inactivation, the cells were held at -120 mV and a 500 ms conditioning prepulse was applied in 5 mV increments between -130 and -30 mV, followed by a 20 ms test pulse to -20 mV. The following equation was fitted to the steady state inactivation curves:

$$I/I_{max} = 1/(1+\exp((V_{½}-V)/k)) \quad (3)$$

where $V_{½}$ is the voltage of half maximal inactivation and k is the slope factor.

The inactivation fast (τ_f) and slow (τ_s) time constants were determined during the steady state inactivation protocol, by fitting the decay phase of the current elicited by a test potential to -30 mV with the following bi-exponential equation:

$$I/I_{max} = A_f \exp(-t/\tau_f)+A_s \exp(-t/\tau_f)+Ss \quad (4)$$

where A_f and A_s represent the relative amplitudes of the fast and slow inactivation time constants.

To determine recovery from inactivation, cells were held at -120 mV followed by a step to -20 mV (P1) for 500 ms, and then stepped to the recovery potential of -120 mV, for 1-1000 ms. After the specified recovery period, the potential was again stepped to -20 mV (P2) for 20 ms. The peak Na^+ current measured during P2 was normalised to the peak Na^+ current measured during P1. The fractional current was then plotted as a function of the recovery time between the 2 test pulses. The time course of recovery from inactivation was measured after fitting the following bi-exponential equation:

$$P2/P1 = 1-A_f*\exp(-x/\tau_f)-(1-A_f)\exp(-x/\tau_s) \quad (5)$$

where τ_f and τ_s represent the fast and slow recovery time constants respectively and A_f is the relative fraction of the fast recovery time component. The relative fraction of slow recovery time component (A_s) can be calculated by:

$$A_s = (1-A_f) \quad (6)$$

An F-test comparison of the absolute sum of squares of both single and bi-exponential fit of the recovery of inactivation data, confirmed that the bi-exponential equation resulted in a better fit.

The TTX-sensitive Na^+ channels were distinguished from the TTX-resistant Na^+ channels with the use of two different test potentials. Cardiomyocytes were held at -120 mV and stepped to -60 mV for 25 ms and then back to -120 mV for a recovery period. Following this the cardiomyocytes were stepped to -10 mV for 25 ms. The TTX-resistant Na^+ channels are activated at -60 mV, whereas the TTX-sensitive channels are activated at more depolarised potentials (Lei *et al.*, 2004; Haufe *et al.*, 2005a; Brette and Orchard, 2006). When stepping to -10 mV, the probability of all Na^+ channels being in the activated state is the greatest. The peak I_{Na} at each test potential under control conditions and in the presence of TTX was determined with WinWCP (Version 4.6.5) and the TTX concentration response curve was plotted with GraphPad Prism (Version 4.03, Graph Pad Software Inc., San Diego, CA, USA). The concentration response curve for TTX-resistant activation was fitted with an equation (Brette and Orchard, 2006):

$$I_{Na\ TTX}/I_{Na\ Control} = 1-(1/(10\text{^}(K_{D,R}-[TTX])+1)) \quad (7)$$

where $K_{D,R}$ is the dissociation constant of the TTX-resistant I_{Na} and [TTX] is the TTX concentration. The TTX concentration response curve when Na^+ channels are fully activated (holding at -120 mV and stepping to -10 mV) was fitted with the following Hill type equation:

$$I_{Na\ TTX}/I_{Na\ Control} = 1-(f/(10\text{^}(K_{D,S}-[TTX])+1)) - ((1-f)/(10\text{^}(K_{D,R}-[TTX])+1)) \quad (8)$$

Where $K_{D,S}$ is the dissociation constant of the TTX-sensitive I_{Na} and f is the fraction of the total I_{Na} which is TTX-sensitive.

3.2.5 cDNA Preparation and Reverse Transcription PCR

The PVs were dissected from the lungs in bath solution and excess connective tissue and lung parenchyma removed. The LA was separated from the heart. Tissues were then placed separately into RNA Later (Qiagen, UK) and stored overnight at 4^{o}C. Following this, RNA Later was removed and the tissues stored at -80^{o}C until use. Total RNA was extracted from the tissues using an RNAqueous-Micro Kit (Ambion, UK). A cone ball (RETSCH, Germany) and 0.1 mL of Lysis Solution per 10 mg of tissue was added and then rapidly shaken for 1 minute with a Beadmill Grinder (RETSCH, Germany). This was repeated 3 times until the tissue was homogenised. Thereafter, 100 µl of the homogenised sample was added to 200 µl RNAse free water and 3.3 µl Proteinase K (Qiagen, UK), and incubated at 55^{o}C for 10 minutes in a DriBlock (Techne). The samples were centrifuged for 3 minutes at 10,000 g, at room temperature and the supernatant transferred to a DNase free microcentrifuge tube. Following this, 50 µl of ethanol per 100 µl of lysate was added to each sample and the lysate/ethanol mixture was loaded into a microfilter cartridge and centrifuged for 10 seconds at 16,000 g. The filter was washed by adding 180 µl of Wash Solution 1 to the microfilter cartridge and centrifuging for 10 seconds. This was repeated twice with Wash Solution 2. The flow through was discarded and the microfilter cartridge and collection tube centrifuged at 16,000 g for 1 minute to dry the filter. The microfilter cartridge was then transferred to a new micro elution tube and 10 µl Elution Solution, preheated to 75^{o}C, was added. After a 1 minute incubation at room temperature the column was centrifuged for 1.5 minutes to elute the RNA from the filter. The RNA filtrate, 2 µl of 10X DNase I Buffer and 1 µl of DNase I was transferred to a centrifuge tube and incubated for 30 minutes at 37^{o}C. Afterwards, 2 µl DNase inactivation reagent was added to the centrifuge tube, vortexed once to disperse the agent and then stored at room temperature for 2 minutes. The tube was centrifuged for 1.5 minutes at 16,000 g and the RNA was transferred to an RNase free tube. The Nanodrop (ThermoScientific, UK) was utilised for RNA concentration and purity determination. Only samples with an A260/280 > 1.85 were used.

A Tetro cDNA Synthesis Kit (Bioline, UK) was used for cDNA generation. The reaction was carried out on ice and each sample consisted of a positive (+) and negative (-) (deficient of reverse transcriptase) reaction. To each tube, 1 µl of oligo $(DT)_{18}$, 1 µl of 10 mM DNTP mix, 1 µg of RNA and RNase free water was added to make up a total volume of 10 µl. To generate the single stranded RNA, the tubes were incubated at 70^{o}C for 5 minutes and cooled on ice for 1 minute. To each tube, 4 µl of First Strand Buffer and 1 µl of Ribosafe RNAase inhibitor were added. Then 1 µl of reverse transcriptase was added to (+) tubes only, along with DNAse free water to both tubes to give a final reaction volume of 20 µl. Samples were incubated for 30 minutes at 45^{o}C and then 15 minutes at 75^{o}C in a DNA thermal cycler. The generated cDNA was used in a PCR reaction or stored at -20^{o}C for future use.

For the reverse transcription PCR reaction, 1 µl of cDNA, 1 µl of a forward and reverse primer for one subunit (Table 3.1) at a concentration of 10 pmol/µl, 25 µl of KOD Hot Start Mastertmix (Merck, USA) and RNase free water were added to a PCR reaction tube to make a final total volume of 50 µl. The reaction was heated to 95^{o}C for 2 minutes in a Primus 96 Plus Thermocycler (MWG AG Biotech, Germany) and was then subject to the following conditions: 95^{o}C for 20 seconds, 55^{o}C for 10 seconds, 70^{o}C for 5 seconds for 30-35 cycles. Products were viewed with the use of SYNGENE Inventory (SYNGENE Bioimaging) on a 2% ethidium bromide (Sigma, UK) stained agarose gel with Hyperladder II (Bioline, UK) as a size marker.

GenElute Gel Extraction Kit (Sigma, UK) solutions and columns were used for gel extraction and purification. Products were excised from a 1% ethidium bromide stained, agarose gel and then 3 gel volumes of Gel Solubilisation Solution were added to each gel slice. After a 10 minute incubation at 55^{o}C, 1 gel volume of isopropanol was added and 700 µl of the dissociated gel solution at a time was added to the binding column and centrifuged at 16,000 g for 1 minute. This was repeated with 700 µl of Wash Solution G. The flow through was discarded and the column was centrifuged for 1 minute to remove excess ethanol. The column was incubated with 50 µl of Elution Solution for 3 mins and centrifuged for 1.5 mins to elute the

DNA. Nanodrop (ThermoScientific) was utilised for DNA concentration and purity determination. Extracted DNA was stored at -20^{o}C until sequencing. Samples were then sequenced with the use of the LightRun (GATC Biotech, Germany) sequencing service. The generated sequence was checked using Nucleotide Blast (NCBI) and compared to the predicted PCR sequence with MUSCLE Multiple Sequence Alignment (EBI).

Table 3.1. **Primer pair sequences and expected products.** Primer pairs were designed in-house with the use of Gene-Runner (Version 3.0) and purchased from Eurofins (Germany).

Gene	Primer Pair (forward/reverse primer)	Amplicon (bp)
rSCN1A ($Na_v1.1$)	GGAACCAGAAGAAACCCTTGAGC/ CCTAACAGGGCATTCACAACCAC	519
rSCN3A ($Na_v1.3$)	AGAGCCGATGGAGACAGGTTTC/ TGGTGTTGGTCAGGATACTGGC	451
rSCN5A ($Na_v1.5$)	GCCTTGGCACAGAGGAAGAGTCC/ TTGTCCGCGTACTCCAGCAGAAC	532 and 373
rSCN10A ($Na_v1.8$)	GACCATTTCCAGATTCAGTGCCAC/ GTCTATCGCTGCACCCACATCG	325
rSCN1B (β1)	GCTGCGTGGAGGTGGATTCTG/ TCTCGGAAGTAATGGCCAGGTATTC	561
rSCN2B (β2)	AATGCACAGGGATGCCTGGCTAC / CCACTGAGGCACCCACGATGAC	500
rSCN3B (β3)	GCTCATCTACTGGGTCAGAGTCTGC/ CTCCACAGGTACCACAGAGTTCTCC	601
rSCN4B (β4)	GAGGCAATACTCAGGCGAGATGG/ AGCCCGTTCTCTGTGTTGTCG	625

3.2.6 Immunocytochemistry and Immunohistochemistry

3.2.6.1 Antibodies

Anti-Na_v 1.1, anti-Na_v 1.3, anti-Na_v 1.4, anti-Na_v 1.5 and anti-Na_v 1.6 primary antibodies were obtained from Alomone (Jerusalem, Israel) and, as stated by Alomone, are specific against each Na^+ channel epitope. The secondary antibody, goat anti-rabbit Alexa 488 was obtained from Life Sciences (Invitrogen, UK).

3.2.6.2 Single cell immunofluorescence

For maximal cell adhesion, glass coverslips were coated with Poly-l-lysine (Sigma, UK) and allowed to oven dry for one hour. Freshly isolated PV, LA or ventricular cardiomyocytes were fixed with 1% paraformaldehyde for 20 minutes. After fixation the cells were washed 3 times with phosphate buffered saline (PBS; Tablets purchased from Sigma, UK) for 10 minutes, permeabilised for 20 minutes at room temperature with 0.1% Triton-X100 in PBS and then washed in PBS for 10 minutes. Non-specific antibody binding sites were blocked by incubating with a blocking solution (10% goat serum in PBS) for 1 hour at room temperature. Primary antibodies were diluted 1:100 in blocking serum and 25 µl of the antibody solution was applied to parafilm in the chambers of a 6-well plate. Coverslips were laid face down onto the antibody and stored overnight at 4^{o}C. A moist paper towel was placed inside the lid of the plate to create a humidifying environment, preventing evaporation of the solution. Thereafter, the cells were washed three times for 10 minutes each in PBS. Secondary antibodies were diluted 1:200 in PBS and 50 µl of solution added to parafilm. Coverslips were laid face down onto the antibody and incubated for 1 hour at room temperature. The cells were washed three times for 10 minutes each in PBS and mounted onto glass slides using VECTASHIELD hard set mounting medium with DAPI (Vector Laboratories, USA). To obtain negative controls, a similar procedure was followed, except the primary antibody was omitted. The slides were stored at 4^{o}C in a dark box until imaged.

3.2.6.3 Whole tissue immunofluorescence

Human PV and LA tissue slides were prepared and rehydrated as in section 2.1 of the previous chapter. Heat induced epitope retrieval was then performed in order to facilitate epitope unmasking in the formalin fixed tissue. For this, the slides were placed in pre-heated Tris/EDTA buffer (10 mM Tris Base, 1.3 mM EDTA, pH 9.0) in a pressure cooker and microwaved for 17 minutes. Afterwards the tissues were washed in PBS and tissue sections were circled with a hydrophobic barrier using a wax pen (Vector Laboratories, USA). Non-specific antibody binding was decreased by incubation of the tissue for 1 hour at room temperature in blocking serum (10% goat serum and 0.5 % Triton X-100 in PBS). The tissues were then incubated with

primary antibodies diluted 1:100 with blocking serum overnight at 4^{o}C. A moist paper towel was added to the chamber to create a humidifying environment. Tissues were washed three times in PBS for 10 minutes each time and incubated at room temperature in a dark humidifying chamber for 2.5 hours with the secondary antibody, which was diluted 1:200 with PBS. Tissues were mounted with VECTASHEILD mounting medium with added DAPI. To obtain negative controls, a similar procedure was followed, except the primary antibody was omitted. Slides were stored at 4^{o}C in a dark box until imaged.

3.2.6.4 Confocal microscopy

Presented images were obtained using a Leica TCS SP5 confocal microscope (Leica Microsystems, Mannheim, Germany) with either a 60.66 µm or 95.55 µm pin hole. For Alexa 488 the filters used were, excitation 488 nm and emission 499-588 nm. The filters used for DAPI were, excitation 405 nm and emission 499-463 nm. Scale bars were added with Image J software (Version 1.48).

3.2.7 Contraction studies

The rat PV and LA tissues were obtained and set up for contraction studies as described in section 2.2.4. Contractions were evoked using field stimulation via ring electrodes at twice the threshold voltage and 2 ms duration, delivered at 1 Hz using a Grass stimulator (Model S88, Grass Instrument Co.,USA). The tissue was allowed to equilibrate at 37^{o}C for at least 40 minutes before beginning the experiments. To determine the effect of TTX on the electrically evoked contractions, recordings were obtained for 5 minute periods under control conditions and then after 15 minutes in the presence of TTX. Contractions were recorded via a DAQ PCI 6221 analogue to digital converter (National Instruments, Texas, USA) and displayed continuously using Chart Software (Version 5.0.7, Dr. J. Dempster, University of Strathclyde). The data were converted to a text file using WinEDR (Version 3.4.3, Dr. J. Dempster, University of Strathclyde) and the contraction height was determined using Chart5 software (ADInstruments, Dunedin, New Zealand).

3.2.8 Chemicals and Drugs

TTX (Alomone, Israel) was dissolved in water at a stock concentration of 1 mM, and stored at -20^{o}C until required. All digestive enzymes were purchased from Sigma, UK with the exception of Type I Collagenase, which was purchased from Worthington, New Jersey, USA.

3.2.9 Statistics

Graphs were produced using GraphPad Prism (Version 4.03, Graph Pad Software Inc., San Diego, CA, USA). Electrophysiological data, where more than one recording was made from the same tissue, are expressed as mean ± standard error of the mean (s.e.m) of *N* technical replicates (number of recordings), from *n* biological replicates (number of rats). Prism was also used to carry out Student's paired and unpaired *t*-tests on the data. For each group of experiments, PV and LA data were obtained from at least three different animals. A Student's unpaired *t*-test determined the statistical significance of the Na^{+} current kinetics in the PV and LA cardiomyocytes, with the exception of current density which was analysed using a nonparametric test (Mann-Whitney U test). In both tissues, a Student's paired *t*-test was used when comparing the effect of TTX on the action potential characteristics and the effect of TTX on I_{Na} at two different test potentials.

3.3 Results

3.3.1 The effect of TTX on the PV and LA action potentials.

In order to determine the effect of Na^+ channel inhibition on the PV and LA action potentials, 10 µM TTX was utilised. This concentration of TTX (10 µM) provides a full and partial block of TTX-sensitive and TTX-resistant Na^+ channels, respectively. Treatment with TTX (10 µM), altered a number of key characteristics of the electrically evoked action potential in the rat PV and LA, with similar effects exhibited in both tissues (Figure 3.2A). In addition, in comparison to control conditions, the presence of TTX (10 µM) resulted in a noticeable lag in the period following electrical stimulation to the initiation of the action potential in both tissues (Figure 3.2A). Detailed examination of the action potentials revealed that the membrane potential of both tissues was not significantly affected by the presence of TTX (Figure 3.2B), whereas treatment with TTX resulted in a significant reduction in action potential peak amplitude from 94.7 ± 1.3 mV to 67.1 ± 7.7 mV ($P<0.05$) in the PV and from 83.1 ± 5.9 mV to 71.4 ± 4.9 mV ($P<0.05$) in the LA (Figure 3.2C). The rise time was also significantly increased in both tissues, increasing from 0.6 ± 0.1 ms to 1.4 ± 0.2 ms ($P<0.05$) in the PV in the presence of TTX and from 0.7 ± 0.1 ms to 1.8 ± 0.3 ms ($P<0.05$) in the LA in the presence of TTX (Figure 3.2D). Furthermore, the dV/dt was significantly slower in the presence of TTX (10 µM) in the PV, being reduced from 212.9 ± 18.3 mV/ms to 80.0 ± 18.9 mV/ms, ($P<0.05$) and in the LA, being reduced from 162.7 ± 79.6 mV/ms to 45.8 ± 22.9 mV/ms, ($P<0.05$, Figure 3.2E). The APD_{90} of either tissue was not significantly affected by TTX (Figure 3.2 F), although the presence of TTX increased the ERP from 35.8 ± 2.6 ms to 159.5 ± 34.8 ms, ($P<0.05$) in the PV and from 28.8 ± 3.0 ms to 121.5 ± 27.4 ms, ($P<0.05$) in the LA (Figure 3.2G). The action potential excitation threshold in both tissues was altered by the presence of TTX (10 µM). An example of this is shown in Figure 3.3, where the voltage needed to elicit an action potential in the PV was 40 V under control conditions and increased to 80 V in the presence of TTX (10 µM).

3.3.2 Morphology of enzymatically dissociated rat PV and LA cardiomyocytes.

The Langendorff method yielded single cardiomyocytes from the rat PV and LA, which were identified by their striated appearance. The morphology of both PV (Figure 3.4A) and LA (Figure 3.4B) cardiomyocytes was varied, with some of the rod shaped cardiomyocytes displaying smooth tapered ends, whereas others had bifurcations. Measurement of cell size (Figure 3.4C) revealed a difference in cell size as rat PV cardiomyocytes were significantly longer (117.8 ± 4.0 µm) in comparison LA cardiomyocytes (104.0 ± 4.2 µm). In addition, the PV cardiomyocytes were also significantly wider (19.4 ±1.0 µm) compared to those of the LA (15.0 ± 0.5 µm; $P<0.01$, Figure 3.4D).

3.3.3 Comparison of I_{Na} kinetics in PV and LA cardiomyocytes.

Detailed patch clamp examination of the I_{Na} in cardiomyocytes isolated from the rat PV and LA revealed similarities in I_{Na} properties between both tissues. The I-V relationship recorded from PV and LA cardiomyocytes shows both the adequate voltage control as well as a similar peak I_{Na} density in PV and LA cardiomyocytes (Figure 3.5A). A normalised peak density of -62.2 ± 5.3 pA/pF in the PV and -63.5 ± 5.6 pA/pF in the LA was recorded while holding cells at -120 mV and stepping to -40 mV for 25 ms (Figure 3.5B). In addition, there was no significant difference in the voltage of half activation ($V_{½}$) in both tissues, being -54.0 ± 2 mV in the PV and -55.5 ± 1.1 mV in the LA (Figure 3.5C). The inactivation properties of the I_{Na} in PV and LA cardiomyocytes were also similar, as there was no difference in the inactivation $V_{½}$ between PV (-98.3 ± 1.8 mV) and LA (-100.0 ± 2.4 mV) cardiomyocytes (Figure 3.6A, B). The fast and slow inactivation time constants (Figure 3.6C) and the relative amplitude of the inactivation components of the I_{Na} were also similar (Figure 3.6D) in both tissues. The recovery of the I_{Na} from inactivation was also studied (Figure 3.7A), which revealed the similarities in recovery from inactivation in PV cardiomyocytes compared to those of the LA (Figure 3.7B). Fitting Equation (5) yielded two inactivation time constants; a fast recovery time constant (τ_f : PV, 9.3 ± 1.2 ms *vs* LA, 10.5 ± 2.8 ms), which was similar in both tissues (Figure 3.7C) and a slow recovery time constant (τ_s) which

was higher in the PV (272.1 ± 65.8 ms) than the LA (114.2 ± 22.8 ms), although this was not statistically significant (P=0.058).

3.3.4 The presence of TTX-resistant and TTX-sensitive I_{Na} in PV and LA cardiomyocytes.

To establish the presence of TTX-sensitive I_{Na} and determine its contribution to the total I_{Na} in PV and LA cardiomyocytes, a concentration response curve for TTX inhibition of I_{Na} at two different test potentials was determined. Holding the cardiomyocyte membrane potential at -120 mV and stepping to -60 mV activates TTX-resistant channels. During this voltage step, the TTX-sensitive channels are closed as they are activated at more depolarised potentials (Lei *et al.*, 2004; Haufe *et al.*, 2005a; Brette and Orchard, 2006). Stepping to -10 mV, from a holding potential of -120 mV, activates both the TTX-resistant and TTX-sensitive channels. Therefore, if the cardiomyocyte I_{Na} consists of both a TTX-resistant and a TTX-sensitive $I_{Na,}$ the concentration response curves at the two different test potentials should display a deviation in the presence of nanomolar concentrations of TTX (Lei *et al.*, 2004; Haufe *et al.*, 2005a). In PV cardiomyocytes inhibition of I_{Na} with 10 nM or 100 nM TTX was significantly greater at a test potential of -10 mV than a test potential of -60 mV (Figure 3.8A,B). This showed that TTX-resistant and TTX-sensitive I_{Na} both contribute to the I_{Na} in PV cardiomyocytes. It was not possible to complete a full concentration response experiment on each cell (particularly in the PV cells). Instead only one concentration of TTX was added per cell. Fitting Equation 7 to the data points in the concentration response curve at a step potential to -60 mV yields a K_D value of 650 nM for TTX-resistant I_{Na} (Figure 3.8B). The TTX concentration response curve for the step potential to -10 mV was fitted with Equation 8 giving a K_D value of 5 nM for the TTX-sensitive I_{Na} and the fraction of TTX-sensitive current as 0.2 (20%) (Figure 3.8B). Conversely, in LA cardiomyocytes there was not a significant difference in TTX inhibition at the two different test potentials (Figure 3.8C) and so TTX-sensitive I_{Na} was not measurable in the LA cardiomyocytes.

In PV cardiomyocytes, the activation characteristics of the TTX-sensitive and the TTX-resistant I_{Na} were characterised by their sensitivity to TTX; a low concentration of TTX (100 nM) has been shown to inhibit TTX-sensitive Na^+ channels with minimal effect on TTX-resistant Na^+ channels. Inhibition of the I_{Na} with 100 nM TTX, leaves only the TTX-resistant I_{Na} and then subtraction of the TTX-resistant I_{Na} from the control I_{Na} gives the TTX-sensitive I_{Na} (Figure 3.9A,B). Fitting the Boltzmann equation to the activation curves (Figure 3.9C) of both I_{Na} currents revealed the TTX-sensitive I_{Na} was activated at more positive potentials, with an activation $V_{½}$ of -53.0 ± 2.3 mV in comparison to an activation $V_{½}$ of -62.3 ± 1.6 mV ($P<0.05$) for the TTX-resistant I_{Na}. The effect of TTX (100 nM) was reversible upon washing with external bath solution. This was not repeated in LA cardiomyocytes as the TTX-sensitive I_{Na} was not measurable in these cells.

3.3.5 Detection of Na^+ channel subunits in the rat PV and LA

The mRNA for a number of Na^+ channel α- and β-subunits was identified in rat PV and LA tissues using reverse transcriptase PCR. These investigations showed that there was a difference in Na^+ channel mRNA expression, with the $Na_v1.1$ subunit mRNA being detected in PV (Figure 3.10A) but not in LA tissues (Figure. 3.10B), whereas $Na_v1.3$ mRNA was present in both tissues (Figure 3.10A,B). A primer was designed to recognise $Na_v1.5$ (573 bp) and one splice variant $Na_v1.5a$ (352 bp), which were both identified in the PV (Figure 3.10A) and LA (Figure 3.10B). The band between $Na_v1.5$ and $Na_v1.5a$ is thought to represent a $Na_v1.5/Na_v1.5a$ heteroduplex which is common in primers detecting both $Na_v1.5$ and $Na_v1.5a$ (Zimmer *et al.*, 2002; Blechschmidt *et al.*, 2008). The presence of each of these α-subunits was confirmed by sequencing of the DNA in each band after reverse transcription PCR (see appendix, Figure 6.1-Figure 6.4). The mRNA of the four β-subunits: β1, β2, β3 and β4 were present in both PV (Figure 3.10A) and LA (Figure 3.10B) tissues. The presence of each β-subunit was confirmed by sequencing of the DNA in each band after reverse transcription PCR (see appendix, Figure 6.5-Figure 6.8). The TTX-resistant $Na_v1.8$ mRNA was absent in PV and LA tissues (Figure 3.10C). Since, other Na^+ channel subunits were observed in the tissues used, then the negative result was not due to issues with the tissue. The $Na_v1.8$ primer was

validated using rat dorsal root ganglion tissue (Figure 3.10D), as previous studies have detected $Na_v1.8$ mRNA in this tissue (Joshi *et al.*, 2006).

3.3.6 Localisation of Na^+ channel α-subunits in rat and human PV and LA cardiomyocytes.

To determine the cellular location of Na^+ channels, rat PV and LA cardiomyocytes were isolated and labelled with antibodies recognising individual Na^+ channel α-subunits. The $Na_v1.1$ and $Na_v1.3$ channels were located in a diffuse pattern throughout the PV and LA cardiomyocytes (Figure 3.11A,B). There was a difference in the $Na_v1.4$ localisation between both tissues as in the PV, $Na_v1.4$ was widely distributed throughout the cardiomyocyte in a striated pattern which was perpendicular to the long axis of the cells, whereas in the LA $Na_v1.4$ was diffuse in the cytoplasm (Figure 3.11C). In both PV and LA cardiomyocytes, $Na_v1.5$ was located in a striated pattern as well as around the periphery of the cell (Figure 3.11D) and the $Na_v1.6$ subunit was located in a diffuse pattern (Figure 3.11E). Staining was absent when the primary antibodies were omitted (Figure 3.11F). Some nuclear labelling was observed with $Na_v1.1$, $Na_v1.3$ and $Na_v1.6$; this was presumably non-specific labelling (Lei *et al*., 2004, Xi *et al*., 2009).

Human PV and LA samples were also labelled with antibodies recognising individual Na^+ channel α-subunits, to allow comparison of Na^+ channel distribution between species. Similar to the rat, $Na_v1.1$ was diffuse throughout the human PV and LA tissues (Figure 3.12A). In contrast to their location in the rat, $Na_v1.3$ and $Na_v1.6$ isoforms were localised in a striated pattern throughout the human PV and LA cardiomyocytes (Figure 3.12B, E). The $Na_v1.4$ and $Na_v1.5$ Na^+ channels were also observed in a striated pattern in the human PV and LA (Figure 3.12C,D). In the human tissues there was no difference in Na^+ channel distribution between the PV and LA. Again, in the negative controls, when the primary antibody was omitted, there was an absence of positive staining (Figure 3.12F).

3.3.7 Effect of TTX-sensitive Na^+ channel block on the action potential and contraction in the rat PV and LA

To determine whether TTX-sensitive Na^+ channels had a physiological function, the effect of TTX-sensitive Na^+ channel inhibition on electrically evoked action potentials and contractions of the PV and LA were investigated. A lack of effect of TTX (100 nM) on the action potential was observed in both tissues, as the presence of TTX (100 nM) had no effect on the membrane potential of the PV (-79.1 ± 4.2 mV in control conditions and -78.7 ± 3.7 mV in the presence of TTX) and the LA (-78.7 ± 0.8 mV in control conditions and -78.2 ± 1.0 mV in the presence of TTX, Figure 3.13A). There was also no significant difference in the action potential peak amplitude (Figure 3.13B), rise time (Figure 3.13C), dV/dt (Figure 3.13D) and ERP (Figure 3.13F), in either tissue in the presence of TTX (100 nM). In addition, the PV APD_{90} was not altered by the presence of 100 nM TTX (from 31.2 ± 3.4 ms in control conditions to 30.7 ± 2.9 ms in the presence of TTX, Figure 3.13E), nor was that of the LA (from 39.4 ± 6.1 ms in control conditions to 38.8 ± 4.8 ms, in the presence of TTX; Figure 3.13E). However, the treatment with TTX did alter the contraction amplitude of both tissues with a small but significant decrease in the contraction amplitude from 0.064 ± 0.01 g to 0.056 ± 0.01 g in PV tissues ($P<0.05$) and from 0.092 ± 0.005 g to 0.078 ± 0.005 g in LA tissues ($P<0.05$; Figure 3.14B). This decrease in contraction amplitude was reversible after washing with bath solution.

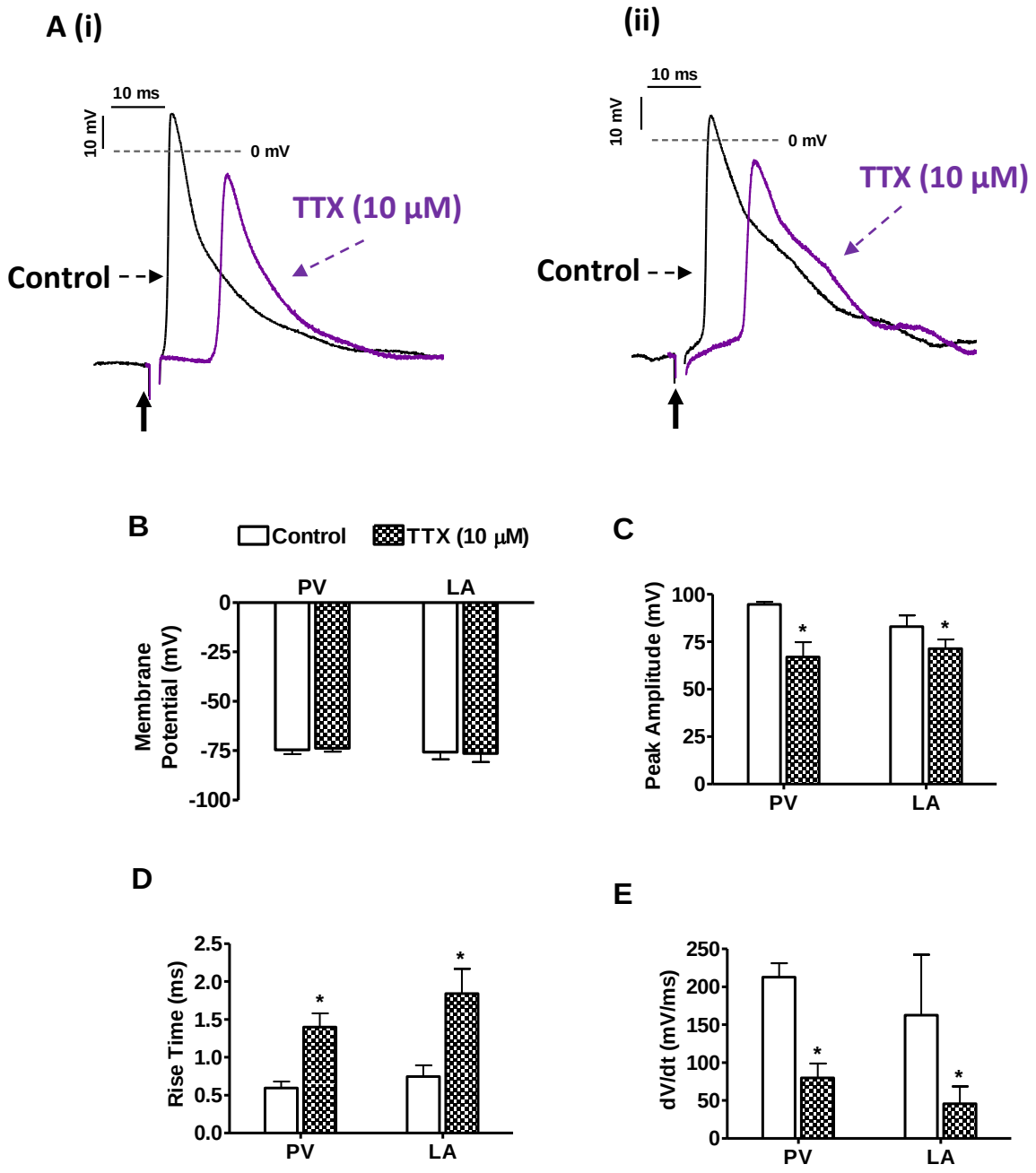

Figure 3.2 **The effect of TTX on rat PV and LA action potentials**. (A) Superimposed microelectrode recordings of PV (i) and LA (ii) action potentials elicited by electrical stimulation at 1 Hz under control conditions and in the presence of TTX (10 µM). The PV (n=4) and LA (n=4) membrane potential (B); action potential peak amplitude (C); rise time (D) and dV/dt_{max} (E) under control conditions and in the presence of TTX (10 µM). All data are presented as mean ± s.e.m. * indicates $P<0.05$ for control *vs*. TTX. Solid black arrows represent the onset of electrical stimulus.

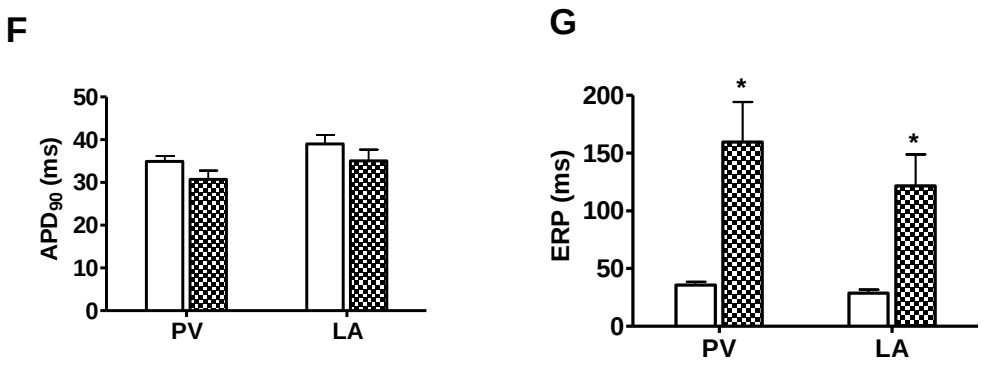

Figure 3.2 (Cont'd.) **The effect of TTX on rat PV and LA cardiomyocyte action potentials.** The PV (n=4) and LA (n=4) cardiomyocyte APD_{90} (F) and ERP (G) under control conditions and in the presence of TTX (10 μM). All data are presented as mean ± s.e.m. * indicates $P<0.05$ for control *vs*. TTX.

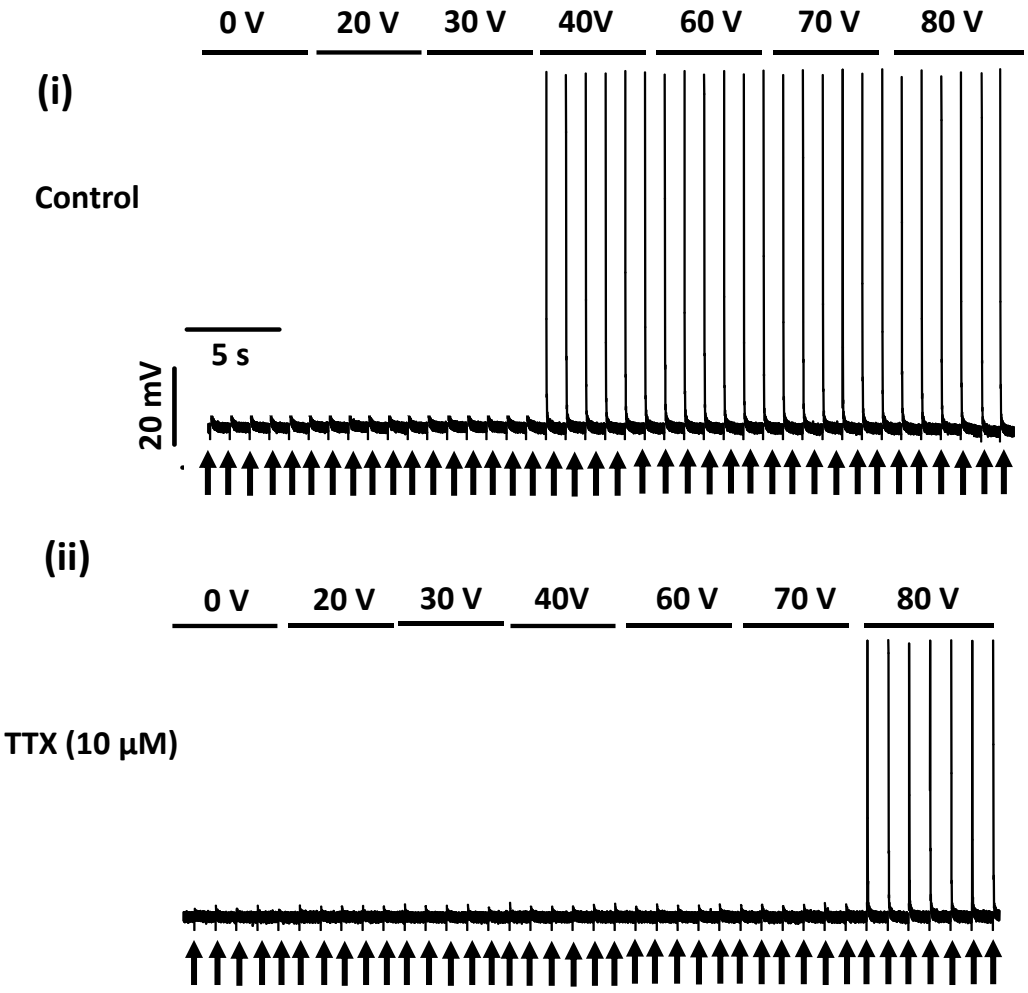

Figure 3.3 **The effect of TTX on the stimulus voltage required to elicit an action potential.** Shown are representative microelectrode recordings from PV tissue under control conditions (i) and in the presence of 10 µM TTX (ii). Action potentials were elicited at 1 Hz electrical stimulation and with the increasing stimulation voltages shown by each bar. Solid black arrows represent the onset of electrical stimulus.

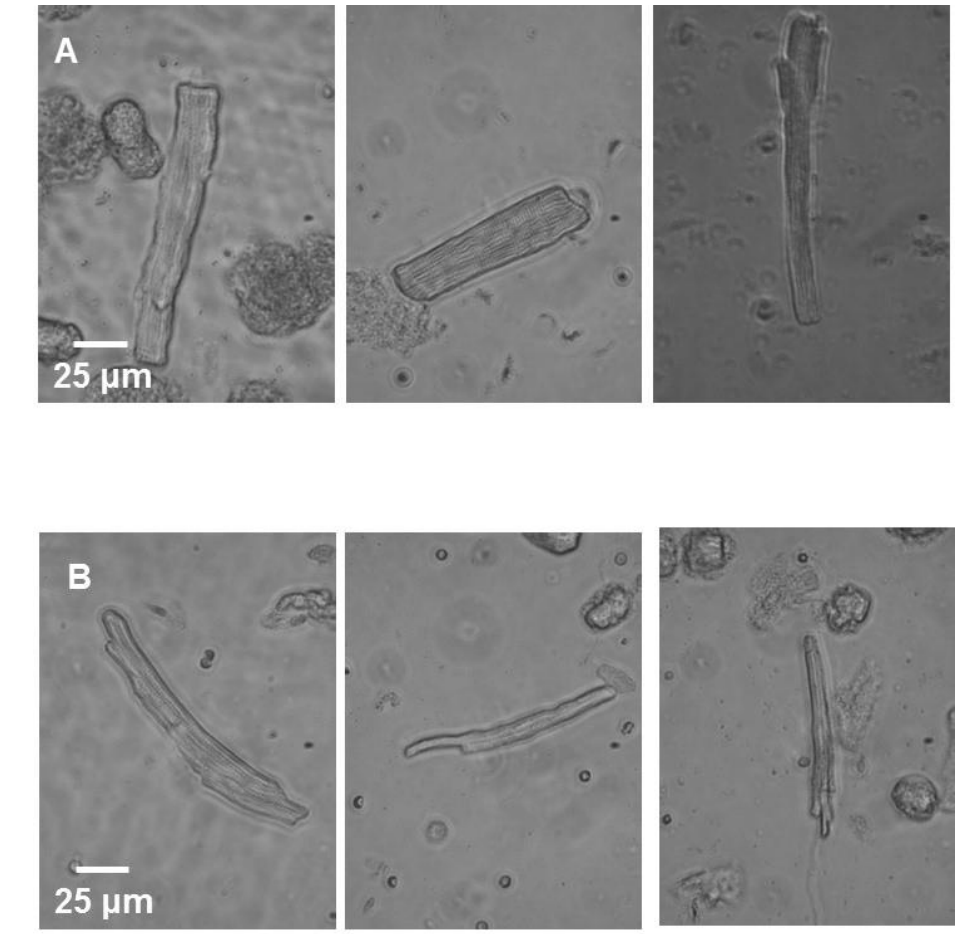

Figure 3.4 **The morphology of cardiomyocytes isolated from the rat PV and LA**. Rat PV (A) and LA (B) cardiomyocytes were isolated via the Langendorff method. Measurement of cell length (C) and cell width (D) of Ca^{2+} tolerant, quiescent rat PV (n=28) and LA (n=25) cardiomyocytes. All data are presented as mean ± s.e.m.* indicates P<0.05 PV *vs.* LA and ** indicates P<0.01 PV *vs.* LA.

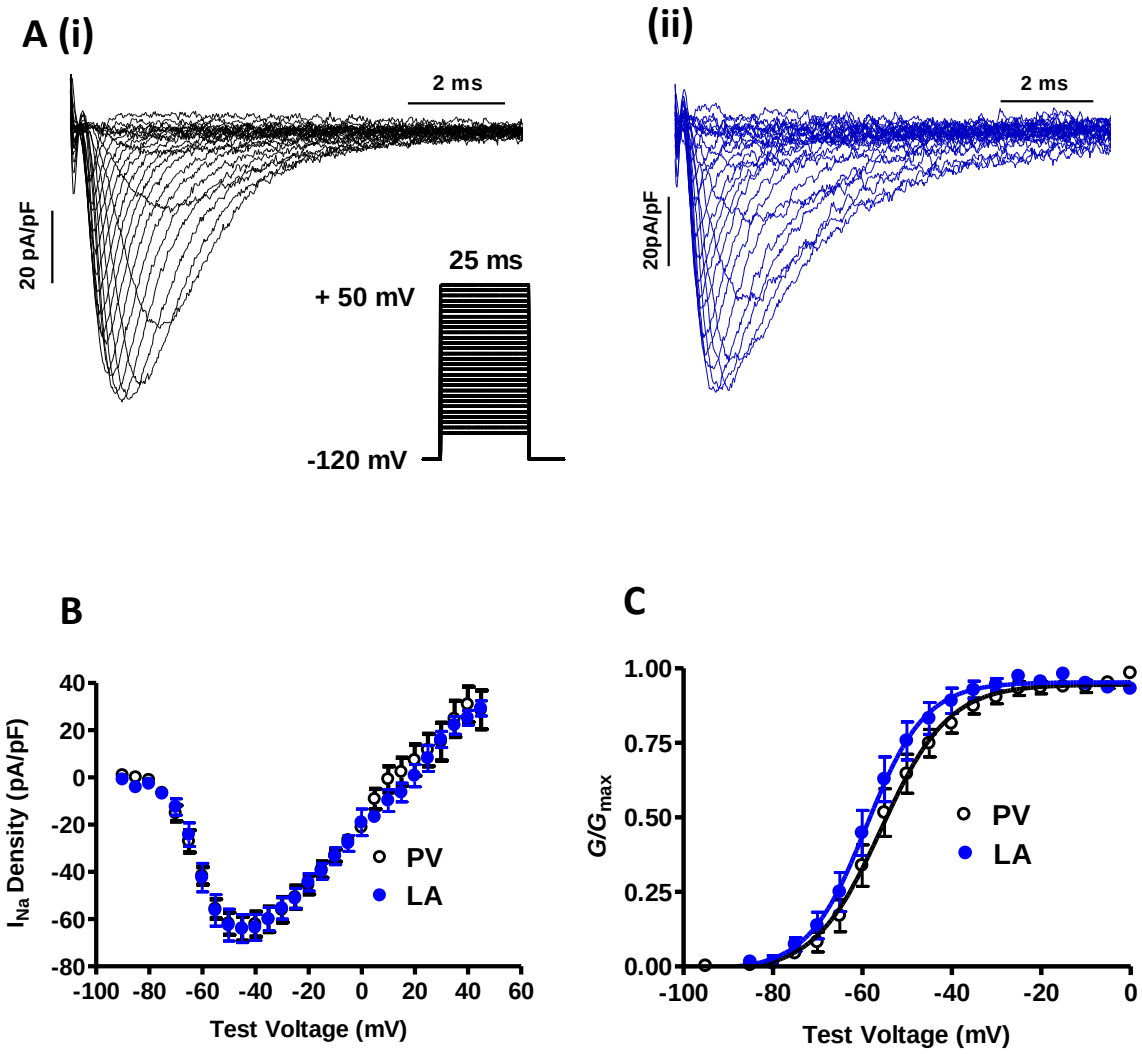

Figure 3.5 **Current density and activation properties of the I_{Na} in PV and LA cardiomyocytes.** (A) Superimposed recordings of I_{Na} in PV (i) and LA (ii) cardiomyocytes. The voltage protocol is shown in the inset, the I-V was measured using a series of 25 ms depolarising test pulses to a range of voltages between -90 mV and +50 mV in 5 mV increments, from a holding potential of 120 mV. (B) Average peak I_{Na} I-V curve for PV (n=10) and LA (n=8) cardiomyocytes. (C) Average steady state activation curve of PV (n=10) and LA (n=8) cardiomyocytes. The activation $V_{½}$ was calculated by fitting the Boltzmann equation (Equation 2). All data are presented as mean ± s.e.m.

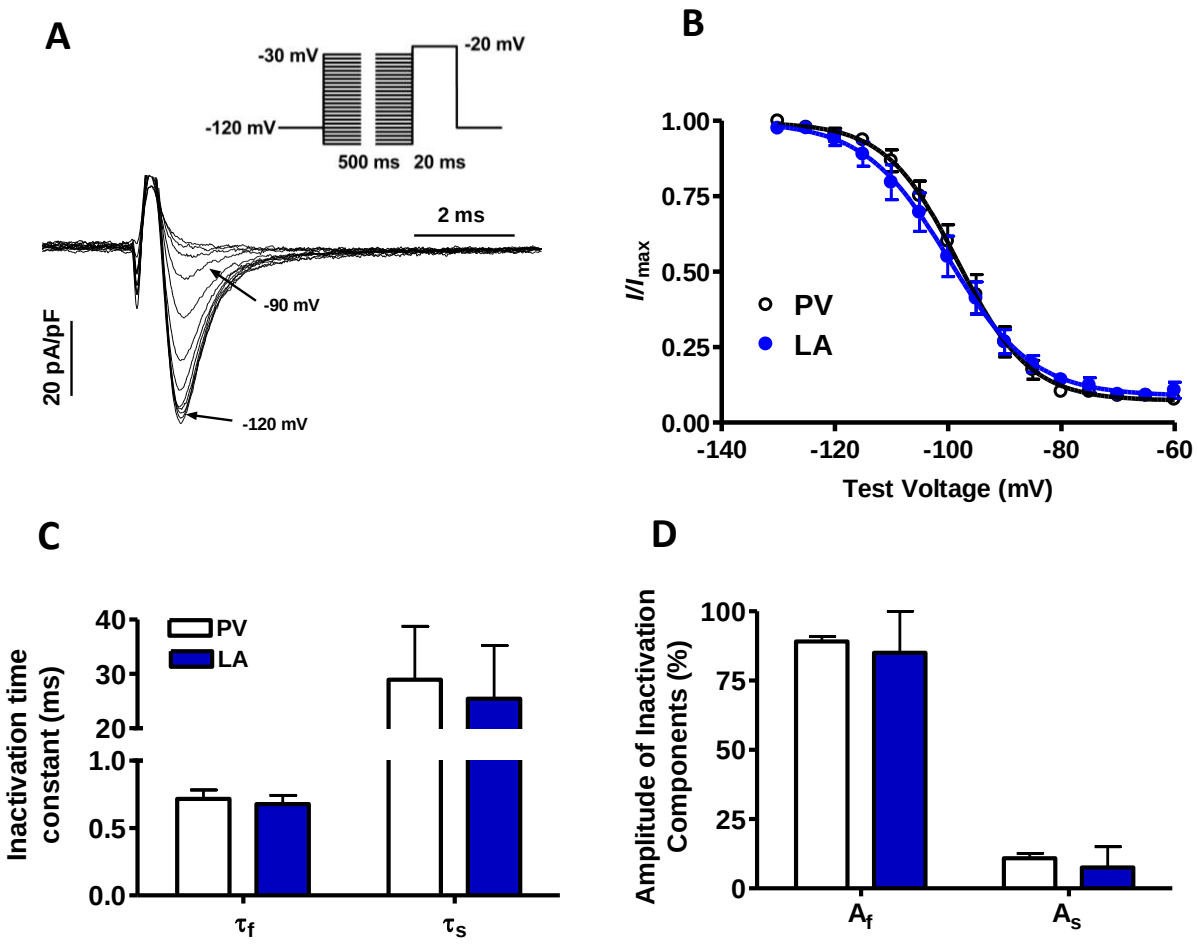

Figure 3.6 **Inactivation of I_{Na} in PV and LA cardiomyocytes.** (A) Representative I_{Na} recording showing the inactivation protocol in a PV cardiomyocyte. Cardiomyocytes were held at a holding potential of -120 mV and a 500 ms conditioning prepulse was applied in 5 mV increments between -130 and -30 mV, followed by a 20 ms test pulse to -20 mV. The voltage protocol is shown in the inset. (B) Average data of the steady state inactivation curve of the Na^+ current in PV (n=7) and LA (n=6) cardiomyocytes. (C) Values for the fast (τ_f) and slow (τ_s) inactivation time constant for PV and LA cardiomyocytes at a test potential of -30 mV. (D) The relative amplitudes (%) of the fast (A_f) and slow (A_s) inactivation components of the I_{Na}. All data are presented as mean ± s.e.m.

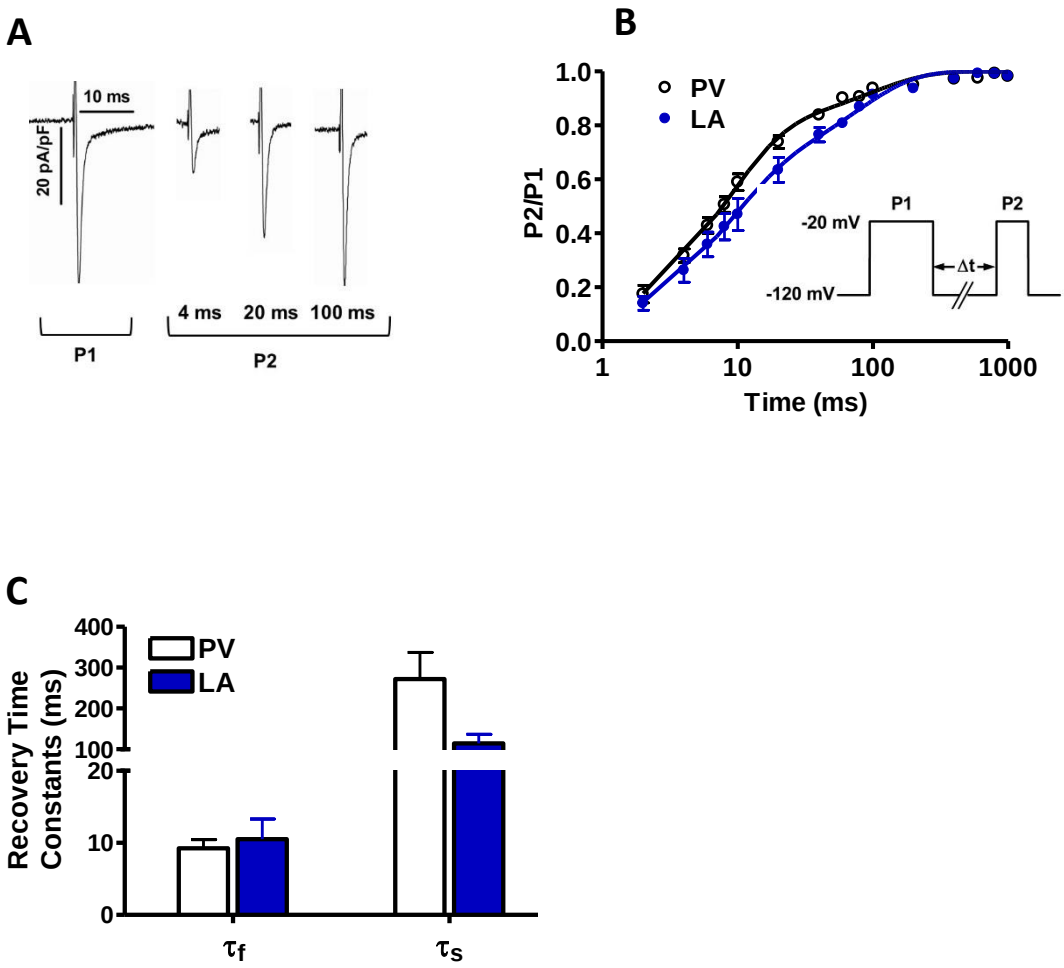

Figure 3.7 **Recovery from inactivation in PV and LA cardiomyocytes.** (A) Representative recording from a PV cardiomyocyte showing the Na^+ current recovery from inactivation. (B) The recovery from inactivation of the Na^+ current in PV (n=7) and LA (n=8) cardiomyocytes. The voltage protocol is shown in the inset. The currents were elicited by holding the cells at -120 mV and stepping to -20 mV for 500 ms (P1), then stepping back to the holding potential for 1-1000 ms. After the recovery period, the potential was again stepped to -20 mV (P2) for 20 ms. (C) Fitting the bi-exponential equation 5 yielded fast (τ_f) and slow (τ_s) recovery time constants. All data are presented as mean ± s.e.m.

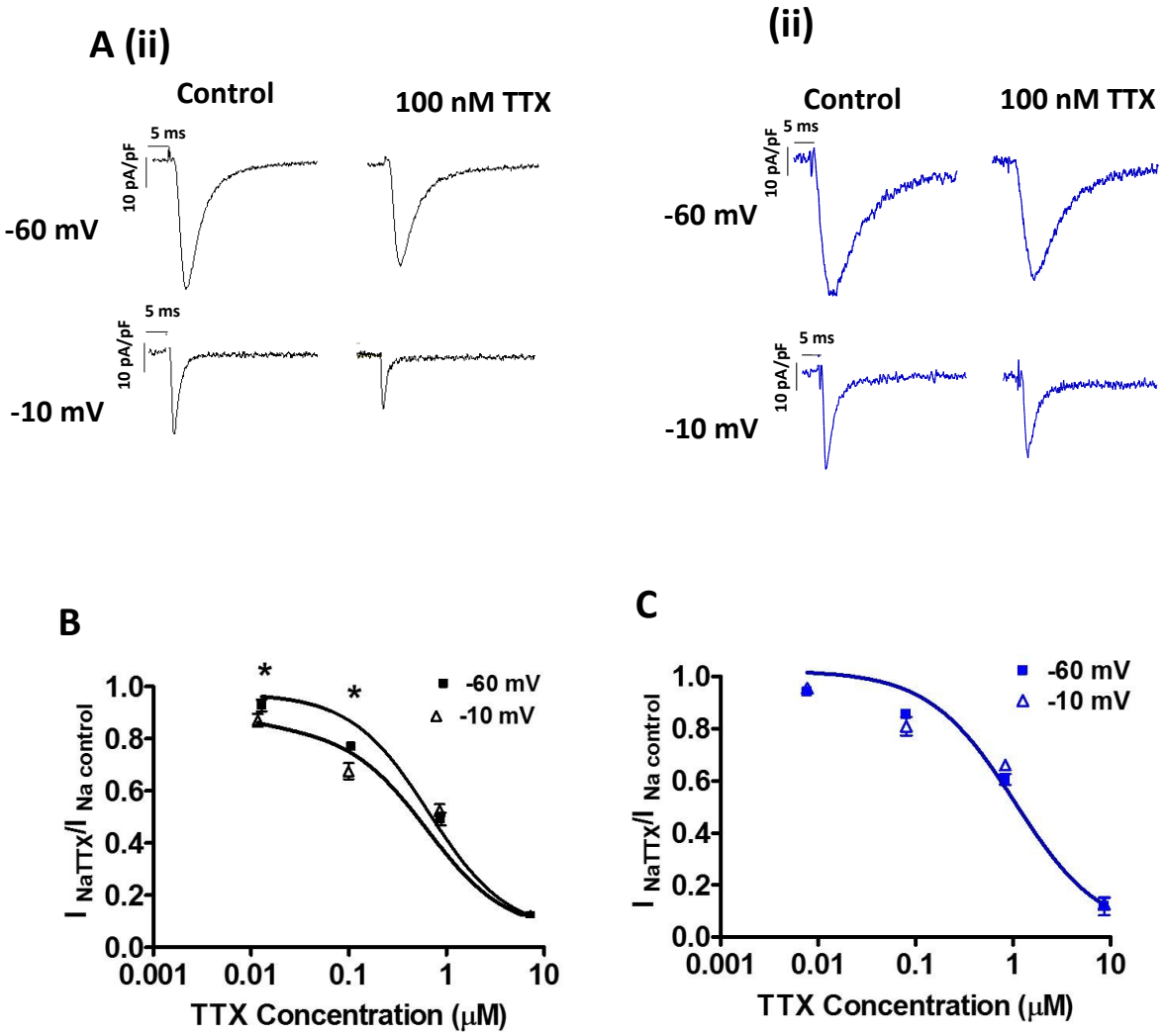

Figure 3.8 **Concentration response curves for TTX block of I_{Na} in PV and LA cardiomyocytes.** (A) Representative recordings from a PV (i) and a LA (ii) cardiomyocyte during control conditions and in the presence of TTX (100 nM) at the two test potentials. Cells were held at -120 mV and stepped to a test potential of -60 mV, activating TTX-resistant channels only. Following a recovery period at -120 mV, cells were stepped to -10 mV, activating TTX-resistant and TTX-sensitive channels. Concentration response curves showing the effect of TTX on I_{Na} in PV (B, n=3-7 cells for each concentration) and LA (C, n=3-6 cells for each concentration) cardiomyocytes at test potentials of -60 mV and -10 mV. All data are presented as mean ± s.e.m. * indicates $P<0.05$ for the current magnitude of the step to -10 mV *vs.* the step to -60 mV.

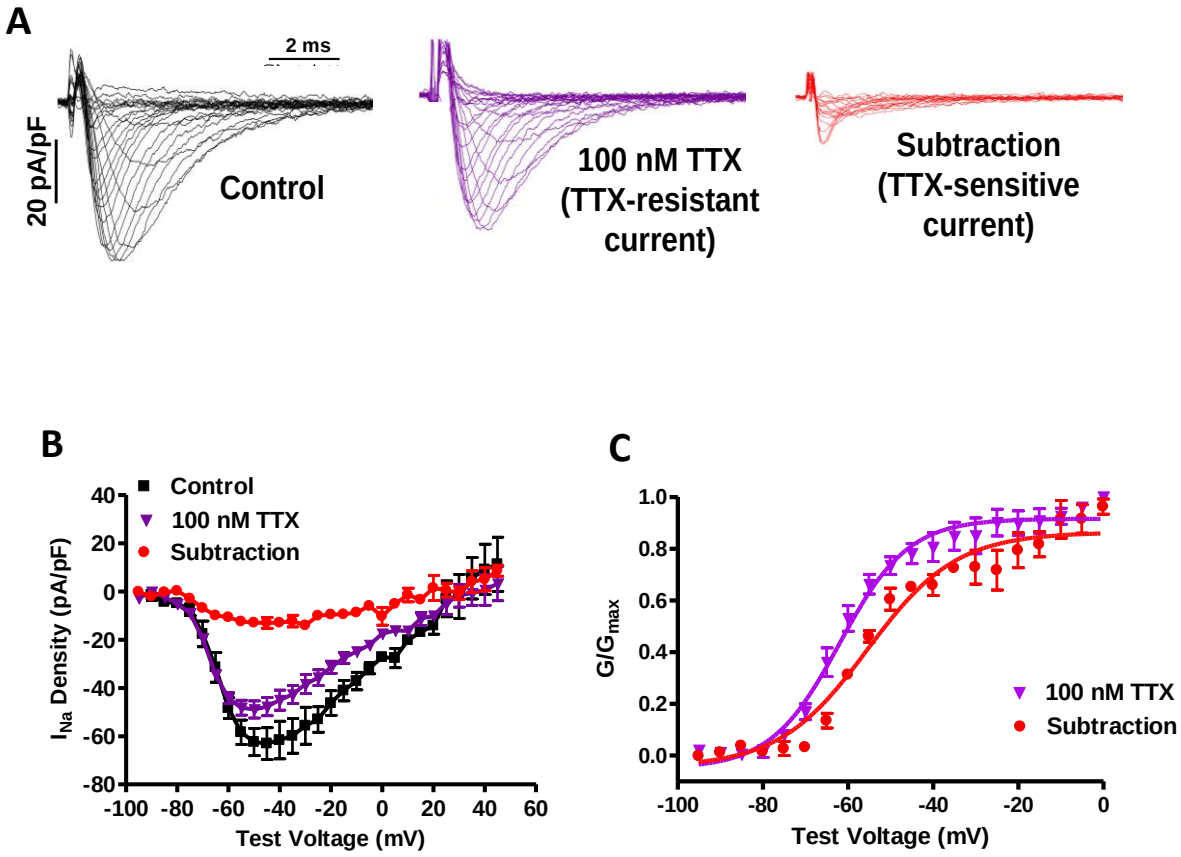

Figure 3.9 **Current density and activation properties of TTX-resistant and TTX-sensitive I_{Na} in PV cardiomyocytes.** (A) Superimposed recordings of I_{Na} in a PV cardiomyocyte under control conditions (left), in the presence of 100 nM TTX (middle) and the TTX-sensitive I_{Na} (obtained by subtraction of the TTX-resistant I_{Na} from the control current; right). The I_{Na} was elicited by using a series of 25 ms depolarising test pulses to a range of voltages between -90 mV and +50 mV in 5 mV increments from a holding potential of -120 mV (B) I-V relationships for total I_{Na} (control), TTX-resistant I_{Na} (in the presence of 100 nM TTX) and TTX-sensitive I_{Na} (the current which is blocked by 100 nM TTX) (n=4). (C) Activation curves of the TTX-resistant and TTX-sensitive I_{Na} from PV cardiomyocytes (n=4). All data are presented as mean ± s.e.m.

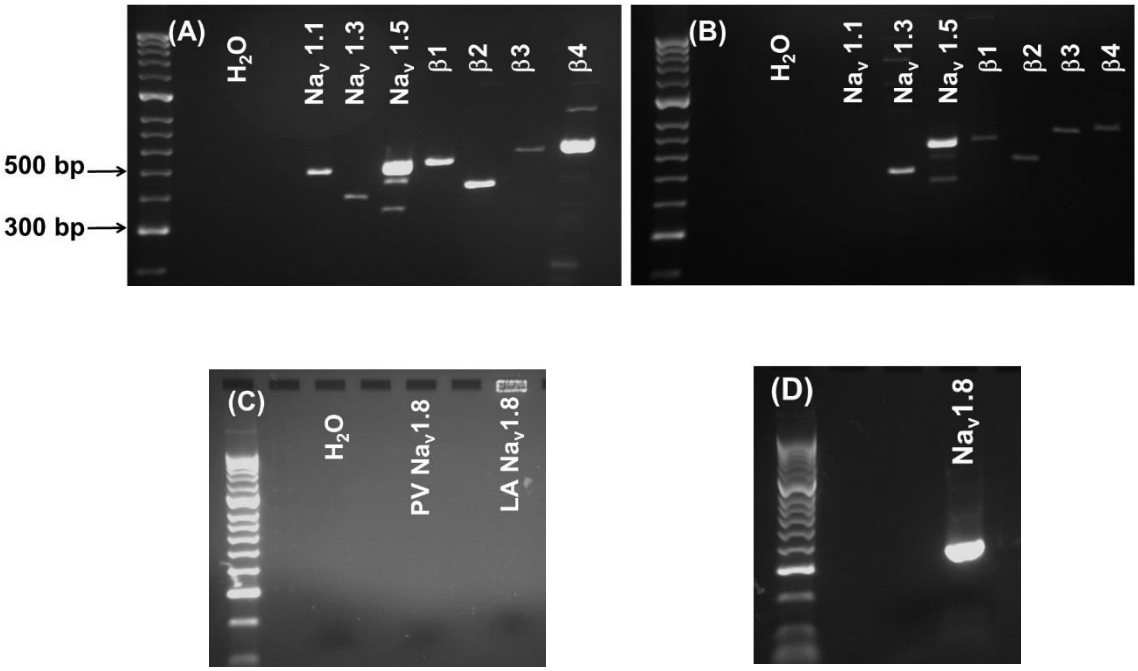

Figure 3.10 **Reverse transcriptase PCR demonstrating the presence of Na^+ channels mRNA in rat tissue**. The reverse transcription PCR products were generated through the use of gene specific primers and then separated on a 2% agarose gel. In PV (A) and LA (B) tissue, primers for $Na_v1.1$ (519 bp product); $Na_v1.3$ (416 bp product); $Na_v1.5$ (535 bp product) and the splice variant (373 bp product); β1 (561 bp); β2 (457 bp); β3 (601 bp) and β4 (625 bp) were used to determine the presence of Na^+ channel subunit mRNA. Primers were also used to determine the presence of $Na_v1.8$ (325 bp) mRNA in (C) PV and LA tissue and in (D) dorsal root ganglion tissue, as a positive control. This was repeated using tissue from three separate rats.

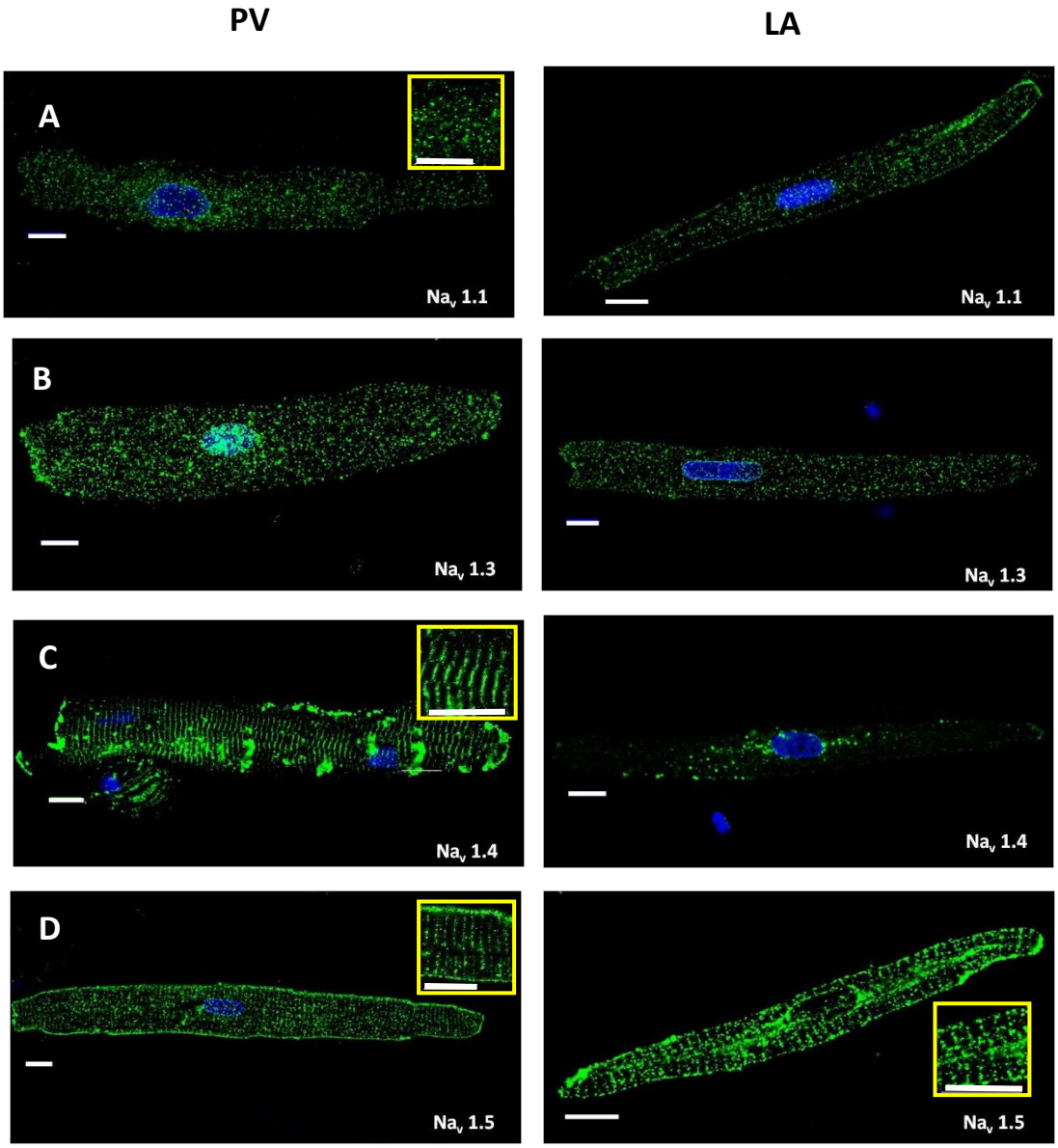

Figure 3.11 **Immunostaining of Na^+ channel α-subunits in rat PV and LA cardiomyocytes.** Rat PV (*left panels*) and LA (*right panels*) cardiomyocytes were isolated using the Langendorff method and labelled with: (A) $Na_v1.1$, (B) $Na_v1.3$, (C) $Na_v1.4$, and (D) $Na_v1.5$ primary antibodies and an Alexa 488 secondary antibody (green). DAPI staining of the nucleus is shown in blue. For these images, the plane of focus was within the cell. In some cells, magnified sections are shown inset in the yellow box. Scale bars are 10 µm. This was repeated using cells from three separate rats.

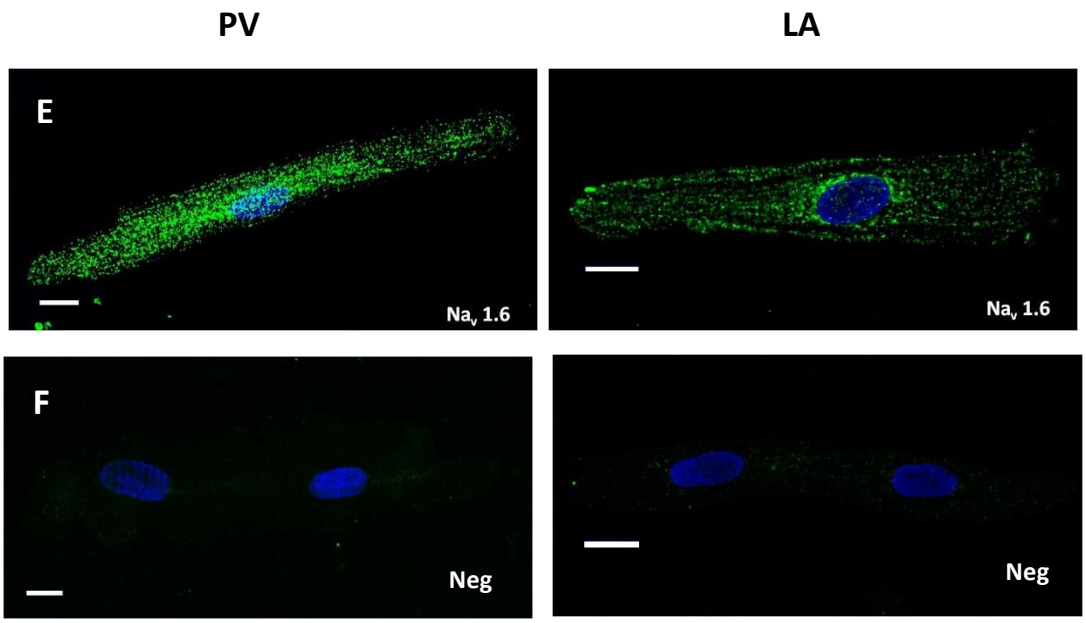

Figure 3.11 (cont'd) **Immunostaining of Na^+ channel α-subunits in rat PV and LA cardiomyocytes.** Rat PV (*left panels*) and LA (*right panels*) cardiomyocytes were isolated using the Langendorff method and labelled with a $Na_v1.6$ antibody (E) and an Alexa 488 secondary antibody (green). (F) Negative controls in which the primary antibody was omitted are also shown. DAPI staining of the nucleus is shown in blue. For these images, the plane of focus was within the cell. Scale bars are 10 µm. This was repeated using cells from three separate rats.

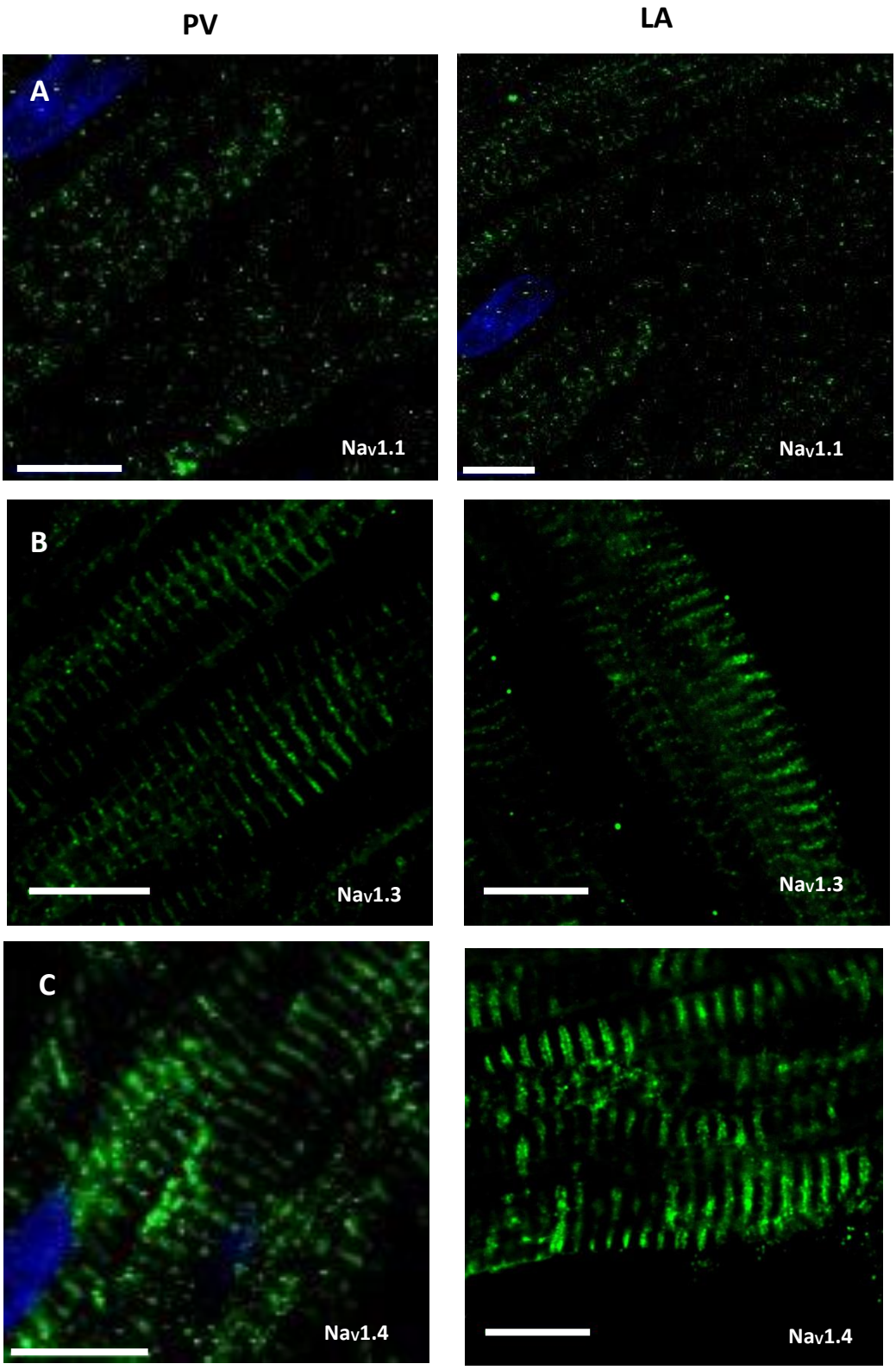

Figure 3.12 **Immunostaining of Na^+ channel α-subunits in human PV and LA tissue.** Left superior PV (*left panels*) and LA (*right panels*) tissue sections were labelled with (A) $Na_v1.1$, (B) $Na_v1.3$ and (C) $Na_v1.4$ antibodies and Alexa 488 secondary antibody (green). DAPI staining of the nucleus is shown in blue. Scale bars are 10 μm. Staining was carried out in tissue from two human patients.

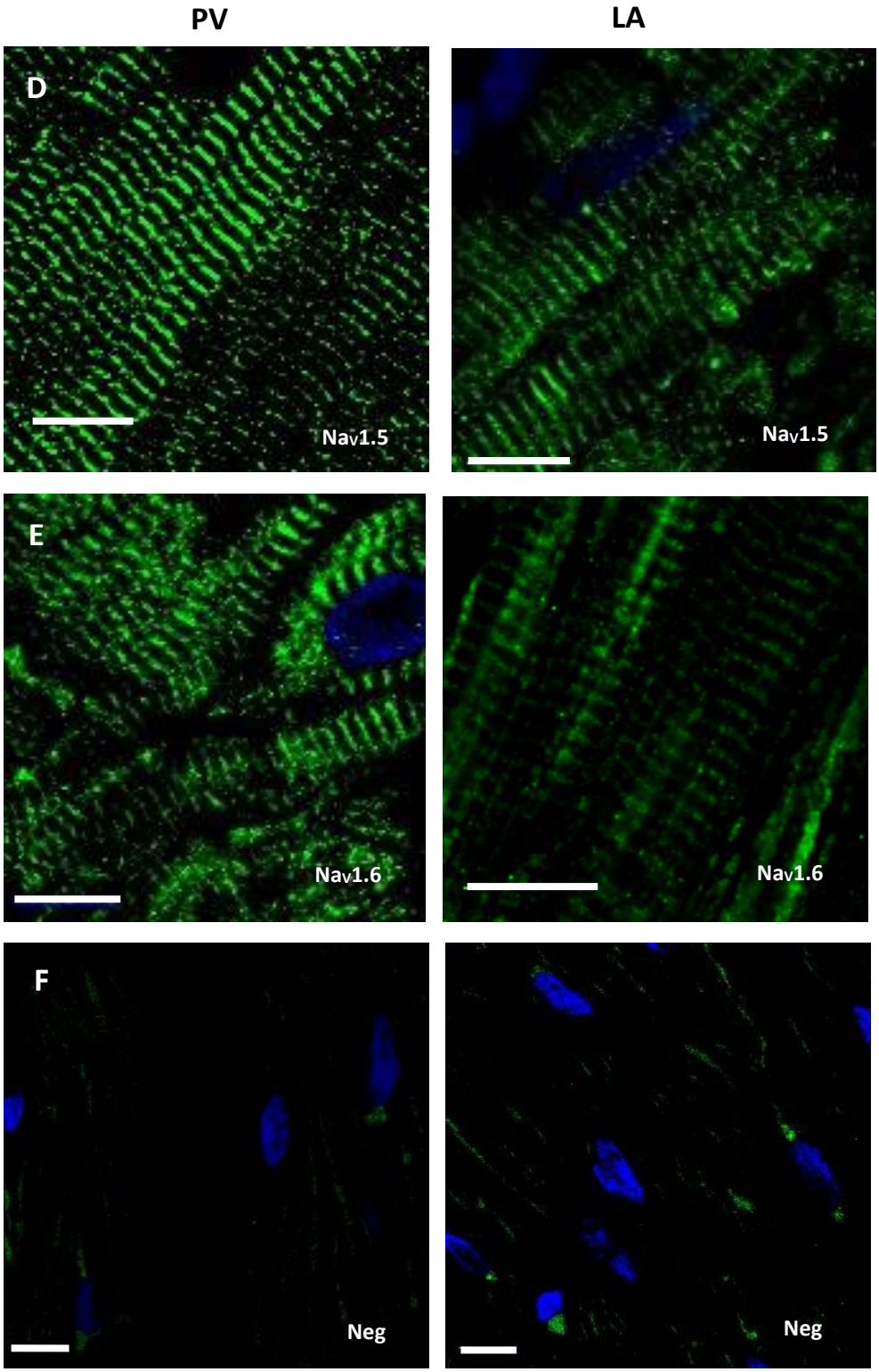

Figure 3.12 (cont'd) **Immunostaining of Na^+ channel α-subunits in human PV and LA tissue.** Left superior PV (*left panels*) and LA (*right panels*) tissue sections were stained with (D) $Na_v1.5$ and (E) $Na_v1.6$ antibodies and Alexa 488 secondary antibody. (F) Negative controls in which the primary antibody was omitted are also shown. DAPI staining of the nucleus is shown in blue. Scale bars are 10 µm.

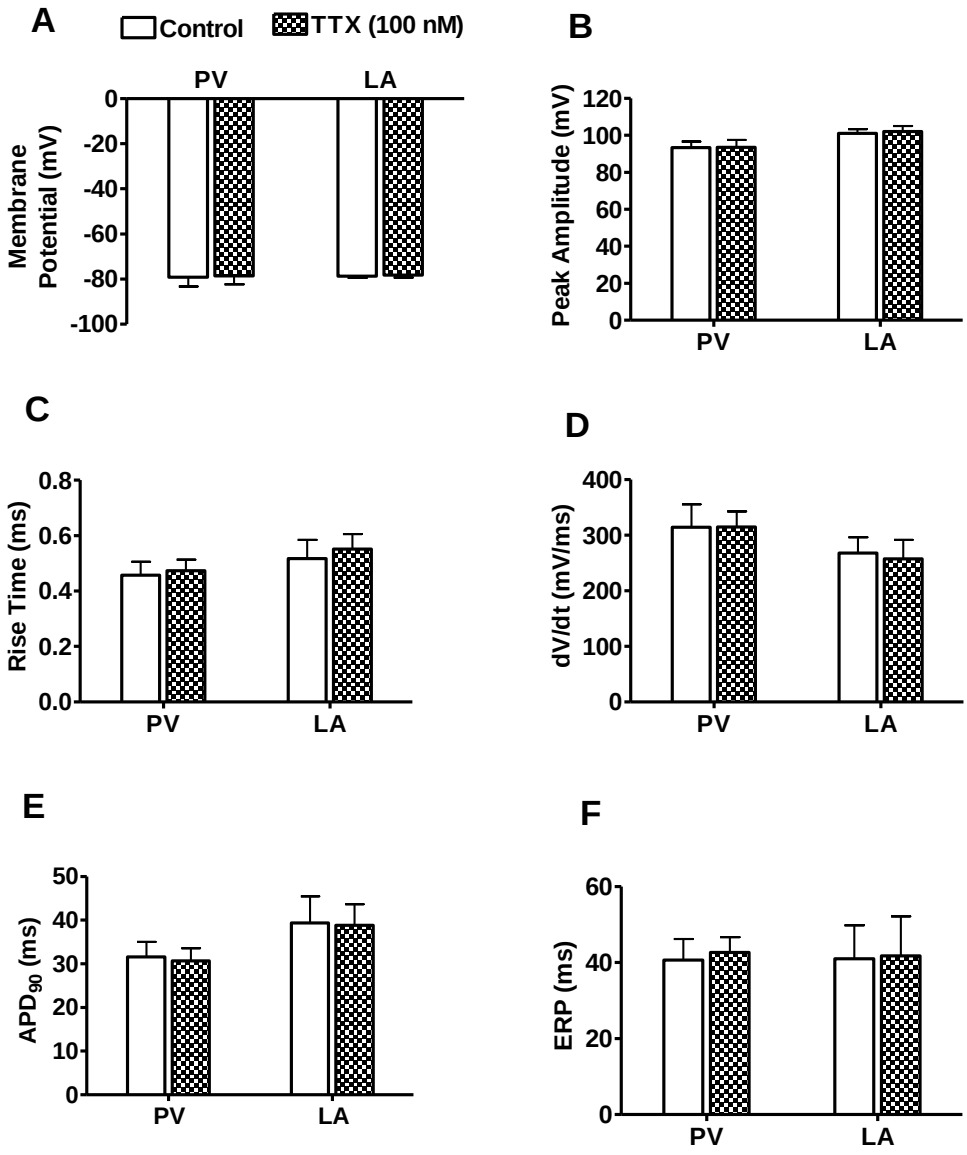

Figure 3.13 **The effect of TTX-sensitive Na^+ channel block on PV and LA action potential characteristics.** Action potentials were elicited by electrical stimulation at 1 Hz and the membrane potential (A); and action potential peak amplitude (B); rise time (C); dV/dt_{max} (D); APD_{90} (E) and ERP (F) of PV (n=5) and LA (n=3) cardiomyocytes under control conditions and in the presence of TTX (100 nM) were measured. All data are presented as mean ± s.e.m.

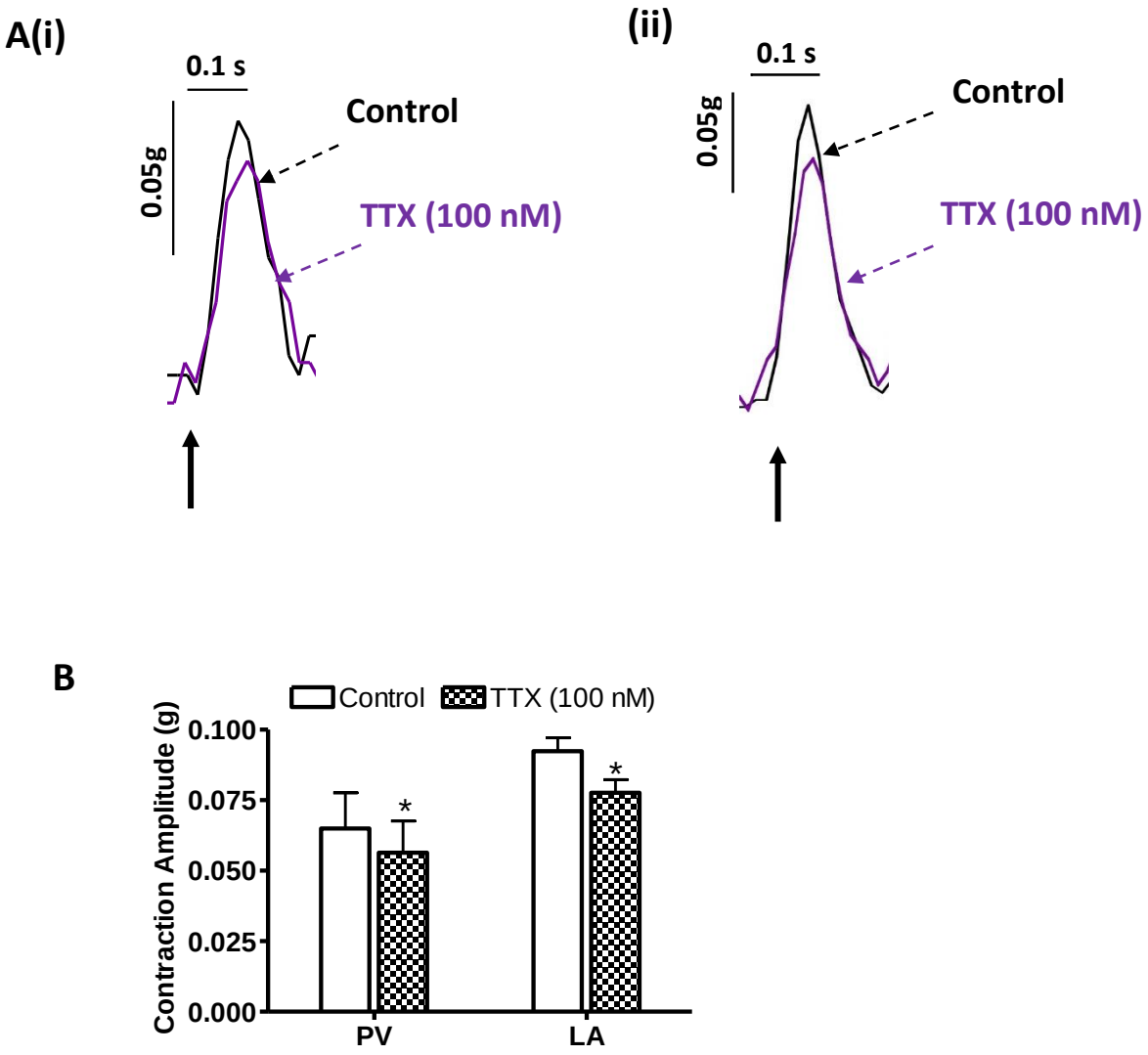

Figure 3.14 **The effect of TTX-sensitive Na^+ channel block on PV and LA contraction amplitude.** (A) Representative recording of the rat PV (i) and LA (ii) contraction elicited by electrical stimulation at 1 Hz during control conditions and in the presence of TTX (100 nM). Solid black arrows represent the onset of electrical stimulus. (B) The graph shows PV (n=4) and LA (n=5) contractions evoked by electrical stimulation at 1 Hz, under control conditions and in the presence of TTX (100 nM). All data are presented as mean ± s.e.m. * indicates P<0.05 for control *vs.* TTX (100 nM).

3.4 Discussion

3.4.1 The role of Na^+ channels in excitability of PV and LA tissues

It is widely accepted that Na^+ channels are involved in the upstroke of the action potential in atrial and ventricular cardiomyocytes (Sakakibara *et al.*, 1992). The present study demonstrated their importance in the upstroke of the PV action potential, as inhibition of both TTX-sensitive and TTX-resistant Na^+ channels with TTX (10 µM) reduced the action potential peak amplitude and dV/dt_{max} in PV cardiomyocytes. The effect of TTX on the PV action potential was similar to what was observed in LA cardiomyocytes in the current study, as well as earlier studies in which TTX reduced the action potential amplitude in atrial preparations from guinea pig and human (Fabiato and Fabiato, 1971; Jakob and Nawrath, 1988; Luk *et al.*, 1988). This is also in agreement with Takahara *et al.* (2012) who reported similar results in guinea pig PV and LA tissues with the Class I antiarrhythmic pilsicainide, and further supports the notion that Na^+ channels are involved in the upstroke of the action potential in PV cardiomyocytes. The involvement of Na^+ channels in the excitability of PV and LA cardiomyocytes was also demonstrated in the present study, as the threshold electrical stimulation voltage, which elicited an action potential, was almost doubled in both tissues when TTX was present. This reduction in excitability could explain the lag observed between electrical stimulation of the tissue and the upstroke of the action potential in both tissues, in the presence of TTX (10 µM).

The increase in ERP without any change in the APD observed in the presence of TTX (10 µM), shows that Na^+ channel block also results in post repolarisation refractoriness in PV cardiomyocytes as well as the LA. Previous studies in atrial tissues have shown that Na^+ channel blockers such as pilsicainide mainly exert their antiarrhythmic action due to the induction of post repolarisation refractoriness (Kanki *et al.*, 1998; Fukuda *et al.*, 2011). The post repolarisation refractoriness induced by Na^+ channel blockers has been reported to decrease the incidence of ectopic activity in the PV, since pilsicainide suppressed AF induced by electrical

stimulation of the PV in both dog (Hirose *et al.*, 2007b) and human AF patients (Kumagai *et al.*, 2004b; Yasuda *et al.*, 2010).

3.4.2 Properties of I_{Na} in PV and LA cardiomyocytes

Investigation of the I_{Na} revealed no significant difference in I_{Na} density and activation kinetics in PV and LA cardiomyocytes. This is consistent with a recent study by Malécot *et al.* (2015) who also reported no difference in I_{Na} current density or activation kinetics in rat PV cardiomyocytes compared to those of the LA. In addition, similar I_{Na} current density and activation properties were also observed in dog PV cardiomyocytes compared to those of the LA (Ehrlich *et al.*, 2003). The calculated activation $V_{½}$ in the current study was slightly more negative compared to those reported in previous studies in rat PV (-50.01 ± 1.32 mV) and LA (-46.93 ± 1.24 mV) cardiomyocytes as well as the dog PV (-48.2 ± 4.3 mV) and LA (-49.9 ± 3.6 mV) cardiomyocytes (Ehrlich *et al.*, 2003; Malécot *et al.*, 2015).

The I_{Na} steady state inactivation was also similar in the PV and LA cardiomyocytes, with the inactivation $V_{½}$ consistent with what has been reported previously (Ehrlich *et al.*, 2003; Malécot *et al.*, 2015). The steady state inactivation had a fast and a slow inactivation component. There was no significant difference in the τ_f or τ_s components of inactivation in the PV and LA cardiomyocytes. The presence of both the τ_f and τ_s inactivation time constants were also reported in atrial cardiomyocytes of human and dog (Sakakibara *et al.*, 1992; Baba *et al.*, 2006).

In this study there was no significant difference in the recovery from inactivation (τ_f or τ_s) in the PV and LA. This is consistent with Ehrlich *et al.* (2003) who also reported similar recovery from inactivation time constants in the dog PV and LA, whereas Malécot *et al.* (2015) measured a slower τ_f of recovery from inactivation in the rat PV (6.52 ± 0.62 ms) in comparison to the LA (4.95 ± 0.34 ms).

3.4.3 The TTX-sensitive I_{Na} in PV and LA cardiomyocytes

This study also revealed the presence of TTX-sensitive I_{Na} in rat PV cardiomyocytes as there was a deviation in block of the I_{Na} by nanomolar concentrations of TTX

when the cardiomyocytes were held at -120 mV and stepped to two different test potentials of -60 mV and -10 mV. The difference in TTX inhibition observed at the two test potentials is unlikely to be due to block of $Na_v1.5$ alone as Haufe *et al.* (2005) demonstrated, with the expression of $Na_v1.5$ in HEK293 cells, that nanomolar concentrations of TTX exhibit similar block of $Na_v1.5$ at both test potentials. The calculated TTX K_D value of 5 nM for TTX-sensitive Na^+ channels and 650 nM for TTX-resistant Na^+ channels is in agreement with previous K_D values for TTX in mouse and rat ventricular cardiomyocytes, in which solutions with low concentrations of Na^+ were used (Maier *et al.*, 2002; Brette and Orchard, 2006). However, the K_D for the TTX-resistant component is lower compared to a number of earlier studies, which generally report a K_D value in the micromolar range when physiological Na^+ concentrations are used (White *et al.*, 1991; Tate *et al.*, 1998). Since the affinity for TTX is dependent on the extracellular Na^+ concentration (Reed and Raftery, 1976; Doyle *et al.*, 1993), the discrepancy in K_D values is most likely a consequence of the differing Na^+ concentrations used in the extracellular solutions of these studies. The TTX-sensitive Na^+ channels were found to contribute 20% of the total I_{Na} in PV cardiomyocytes, which is similar to the 8-22% contribution to the total I_{Na} reported in rat, mouse and dog ventricular cardiomyocytes (Haufe *et al.*, 2005a, 2005b; Brette and Orchard, 2006).

Characterisation of the TTX-sensitive I_{Na} in rat PV cardiomyocytes demonstrated that the TTX-sensitive Na^+ channels were activated at more depolarised potentials compared to TTX-resistant Na^+ channels. Utilising a similar technique Brette and Orchard, (2006) reported a difference in activation properties in rat ventricular cardiomyocytes. This difference in activation properties is in agreement with the idea that different Na^+ channel isoforms contribute to the TTX-sensitive and TTX-resistant I_{Na}. It has been hypothesised that the more depolarised activation properties of the TTX-sensitive Na^+ channels may aid in preserving normal cardiac conduction in disease conditions in which there is a depolarised myocardium, such as myocardial infarction (Huang *et al.*, 2001; Protas *et al.*, 2009; Anyukhovsky *et al.*, 2011). For example, Huang *et al.* (2001) reported an increased expression of $Na_v1.1$ mRNA and a larger TTX-sensitive Na^+ current in mouse ventricular cardiomyocytes

after myocardial infarction, compared to control cardiomyocytes. Furthermore, rat and mouse cardiomyocytes transfected with the TTX-sensitive $Na_v1.4$ isoform were more effective than control cardiomyocytes at preserving dV/dt_{max} when the extracellular K^+ was increased, depolarising the membrane potential (Protas *et al.*, 2009; Anyukhovsky *et al.*, 2011).

In the LA cardiomyocytes, there was no deviation in the I_{Na} inhibition in the presence of nanomolar concentrations of TTX, when the cells were held at -120 mV and stepped to the two different test potentials. Thus, there was no evidence of the TTX-sensitive I_{Na} in LA cardiomyocytes. An earlier patch clamp study in human right atrial cardiomyocytes identified the presence of high and low affinity TTX binding sites, by fitting a two-binding-site model to the TTX concentration response curve (Sakakibara *et al.*, 1992). In addition, using two different test potentials to differentiate the TTX-sensitive and TTX-resistant I_{Na}, Kaufmann *et al.* (2013) reported that 27% of the I_{Na} was attributed to the TTX-sensitive I_{Na} in human right atrial cardiomyocytes. These findings may simply reflect species differences in the expression of TTX-sensitive Na^+ channels.

3.4.4 Expression and distribution of TTX-sensitive Na^+ channel isoforms in the PV and LA

Reverse transcriptase PCR demonstrated the presence of mRNA for $Na_v1.5$ and the TTX-sensitive Na^+ channel isoform $Na_v1.3$ in the PV and LA. The mRNA for $Na_v1.1$ was identified in the PV but not the LA. Using real time PCR, Marionneau *et al.* (2005) reported the presence of $Na_v1.1$ and $Na_v1.3$ in mouse atrial tissue (from pooled left and right atrial tissue), indicating that $Na_v1.1$ is present in the atria of other rodents. Since the present study only used reverse transcriptase PCR, the mRNA expression levels of the different Na^+ channel isoforms in the PV and LA could not be deduced. However, previous studies have reported a difference in the Na^+ channel isoform expression in atrial and ventricular cardiomyocytes. With the use of real time PCR, a higher expression of $Na_v1.4$ mRNA was identified in mouse ventricular tissue in comparison to atrial tissue (Marionneau *et al.*, 2005), and increased $Na_v1.3$ mRNA expression levels were detected in human ventricular tissue

compared to atrial tissue (Gaborit *et al.*, 2007). Whether there is a difference in the TTX-sensitive Na^+ channel transcript level in rat PV and LA tissues, which would explain the observed difference in TTX-sensitive Na^+ channel current, requires further investigation. It should also be taken into account that the preparations could also contain mRNA from nerve terminals in the PV and LA. This could be an additional source of Na^+ channel RNA for the $Na_v1.1$, Na_v 1.3 and Na_v 1.6 isoforms, which can be located in neurons (Noda *et al.*, 1984; Kayano *et al.*, 1988; Ahmed *et al.*, 1992; Lu *et al.*, 1992).

The immunofluorescence studies determined the location of $Na_v1.1$, 1.3, 1.4, 1.5 and 1.6 in the PV and LA of both rat and human. The results demonstrated a variation in localisation of the $Na_v1.5$ isoform and the TTX-sensitive Na^+ channels. As hypothesised by Maier *et al.* (2002), this variation in localisation may suggest a difference in physiological roles for the TTX-sensitive and TTX-resistant Na^+ channels. In rat PV and LA cardiomyocytes, $Na_v1.5$ was distributed in a striated pattern presumably along the z-lines, as well as around the cell periphery. This localisation is similar to what was observed in rat ventricular cardiomyocytes in this study (see appendix, Figure 6.9D), as well as previous studies in ventricular cardiomyocytes from rat (Xi *et al.*, 2009) and mouse (Haufe *et al.*, 2005a). This striated distribution, which is in register with the z-lines of cardiomyocytes, is thought to demonstrate the role of Na^+ channels in the rapid depolarisation of the action potential (Cohen, 1996; Kaufmann *et al.*, 2013; Xi *et al*., 2009).

There were no discernible differences between rat PV and LA cardiomyocytes in the localisation of $Na_v1.1$ or Na_v 1.3, which were diffuse throughout the cell. In contrast, these TTX-sensitive channels were observed in a striated pattern along the z-lines of rat (see appendix, Figure 6.9A,B) and mouse ventricular cardiomyocytes (Maier *et al.*, 2002, 2004; Haufe *et al.*, 2005a; Westenbroek *et al.*, 2013), although Haufe *et al.* (2005b) reported a diffuse distribution of $Na_v1.3$ in dog ventricular cardiomyocytes. The $Na_v1.1$ mRNA was not detected in the LA in the PCR study, yet $Na_v1.1$ was identified in the LA with immunocytochemistry. Whether this is due to an antibody specificity issue remains to be elucidated. In rat PV cardiomyocytes, $Na_v1.4$ was

observed in a striated pattern similar to the localisation of $Na_v1.5$. In contrast, in LA cardiomyocytes, $Na_v1.4$ was observed in a diffuse pattern. In ventricular cardiomyocytes, $Na_v1.4$ had a similar localisation to the PV as it was observed in a striated pattern throughout the cell (appendix, Figure 6.9C), although a previous study in mouse ventricular cardiomyocytes reported that $Na_v1.4$ was only present at the intercalated discs (Ednie *et al.*, 2013). The $Na_v1.6$ isoform was also localised in a diffuse pattern throughout the PV and LA cardiomyocytes, as well as in rat ventricular cardiomyocytes (see appendix, Figure 6.9E). Xi *et al*. (2009) also observed this staining pattern in rat ventricular cardiomyocytes.

In the human PV and LA tissue there was no difference in the diffuse distribution of $Na_v1.1$ and the striated pattern of $Na_v1.5$ when compared to the rat. The striated distribution of the $Na_v1.4$ isoform in the human PV of the current study, is also comparable to that of the rat PV. However the striated localisation of $Na_v1.4$ in the human LA is in distinction to the diffuse distribution observed in the rat LA cardiomyocytes. A species difference in the location of $Na_v1.3$ and $Na_v1.6$ was evident, as unlike the diffuse distribution observed in the rat PV and LA, they were observed in a striated distribution, potentially at the z-lines, of the human PV and LA tissue. The distribution of TTX-sensitive Na^+ channel isoforms can vary between the left and right atrial cardiomyocytes. For example, Kaufmann *et al.* (2013) reported that $Na_v1.3$ and $Na_v1.6$ were localised in a diffuse pattern with no overlap with the z-lines in right atrial cardiomyocytes, which is in contrast to the striated distribution observed in the human LA in the present study.

3.4.5 Function of TTX-sensitive Na^+ channels in PV and LA tissues

The variation in localisation of Na^+ channel isoforms could be an indication that they possess distinct physiological functions, as hypothesised by Maier *et al.* (2002). However, the present study showed that inhibition of the TTX-sensitive I_{Na} with 100 nM TTX had no effect on the action potential characteristics in the rat PV or LA. Brette and Orchard, (2006) observed a very small decrease in the action potential amplitude and dV/dt in rat ventricular myocytes treated with TTX, although they used a slightly higher concentration of TTX (200 nM), which could have produced a

slight block of $Na_v1.5$. Thus, under physiological conditions, TTX-resistant channels are the major contributors to the action potential peak amplitude, dV/dt_{max}, rise time and the ERP in the rat PV and LA. However, a potential contribution of TTX-sensitive Na^+ channels to action potential characteristics when cardiomyocytes are depolarised cannot be ruled out (Protas *et al.*, 2009; Anyukhovsky *et al.*, 2011).

In general, it is known that the I_{Na} is involved in the contractility of cardiomyocytes as opening of Na_v channels triggers the upstroke of the action potential (Bers and Despa, 2009). In the current study, inhibition of the TTX-sensitive Na^+ channels with TTX (100 nM) decreased the contraction amplitude in the PV and LA suggesting involvement of the TTX-sensitive Na^+ channels in contractility. This is in agreement with previous studies which reported that block of TTX-sensitive channels reduced the contraction amplitude in human right atrial muscle (Kaufmann *et al.*, 2013) and decreased the maximal rate of rise of left ventricular pressure (dP/dt_{max}), a measurement of cardiac contractility, in guinea pig hearts (Maier *et al.*, 2002). The presence of a low concentration of TTX also altered the latency and amplitude of Ca^{2+} transients in ventricular cardiomyocytes isolated from the rat (Lines *et al.*, 2006), mouse (Radwański *et al.*, 2015), and rabbit (Torres *et al.*, 2010) further indicating that TTX-sensitive Na^+ channels play a role in excitation contraction coupling in ventricular cardiomyocytes. Moreover, Torres *et al.* (2010) demonstrated that sarcoplasmic reticulum Ca^{2+} release could be modulated by the TTX-sensitive Na^+ channels as inhibition of TTX-sensitive Na^+ channels decreased the rate of rise and amplitude of the Ca^{2+} transient. They proposed that TTX-sensitive Na^+ channels may reside within couplons, which are regarded as the functional unit of ion channels and receptors that generate a Ca^{2+} spark (Franzini-Armstrong *et al.*, 1999). The presence of the Na^+ channels could result in Na^+ accumulation, activating the reverse mode NCX and thereby priming the dyadic cleft with Ca^{2+}. This could enhance the probability of the ryanodine receptor opening, following the influx of Ca^{2+} via the L-type Ca^{2+} channels. Conversely, Brette and Orchard, (2006) reported inhibition of TTX-sensitive channels had no effect on the contraction or Ca^{2+} handling in rat ventricular cardiomyocytes. The rat PV and LA are both highly innervated (Paes de Almeida *et al.*, 1975; McLean *et al.*, 1983;

Cheng *et al.*, 1997) and so there is the possibility that block of the TTX-sensitive channels in neurons prevents neurotransmitter release, leading to the observed decrease in contractility, particularly since a TTX-sensitive I_{Na} was not present in the LA.

3.4.6 $Na_v1.8$ and β-subunits

The lack of $Na_v1.8$ mRNA expression in both rat PV and LA tissue is consistent with previous studies in which northern blot and real time PCR did not detect $Na_v1.8$ in the rat whole heart (Akopian *et al.*, 1996; Rabert *et al.*, 1998). In addition, using immunohistochemistry, Verkerk *et al.* (2012) reported that $Na_v1.8$ was absent in mouse atrial and ventricular cardiomyocytes, but was present in cardiac neurons.

This study also confirmed the presence of mRNA for the four β-subunits β1, β2, β3 and β4 in both rat PV and LA tissue. Previous studies have reported the presence of the four β-subunits in human atrial tissue (Gaborit *et al.*, 2007; Kaufmann *et al.*, 2013). However, their localisation, particularly in relation of the Na^+ channel α-subunits, in the cardiomyocytes of rat PV and LA cardiomyocytes remains to be elucidated

3.4.7 Summary

In summary, there are no differences in the total Na^+ current properties in rat PV and LA cardiomyocytes. The Na^+ channels contribute to the upstroke of the action potential in both tissues and block of these channels can result in post repolarisation refractoriness. In PV cardiomyocytes, the TTX-sensitive Na^+ channels contribute 20% of the total I_{Na} and they are activated at more depolarised potentials compared to the TTX-resistant channels. However, there was no evidence of the TTX-sensitive current in LA cardiomyocytes. As well as the cardiac $Na_v1.5$, the TTX-sensitive $Na_v1.1$, $Na_v1.3$, $Na_v1.4$, and $Na_v1.6$ isoforms were also observed in both rat PV and LA tissues, with a variation in their localisation, particularly between the rat and human PV and LA cardiomyocytes. The TTX-sensitive channels did not contribute to the action potential upstroke of rat PV and LA cardiomyocytes; but may play a small role in the tissue contraction.

Chapter 4

ATX-II Induced Arrhythmic Activity in the PV and LA

4.1 Introduction

4.1.1 The Na^+ channel isoforms and the cardiac I_{NaL}

Gain of function mutations in the SCN5A gene, which encodes for the main cardiac Na^+ channel $Na_v1.5$, are linked to AF (Makiyama *et al.*, 2008; Li *et al.*, 2009) and long QT syndrome (LTQS), which is associated with a high incidence of AF (Benito *et al.*, 2008; Zellerhoff *et al.*, 2009). The arrhythmogenic activity associated with SCN5A gain of function mutations is thought to be due mainly to an increase in the cardiac late Na^+ current (I_{NaL}). This was demonstrated in a number of studies, which reported that heterologous expression of human gain of function $Na_v1.5$ mutations in HEK293 cells resulted in an increase in I_{NaL} and prolongation of the APD (Bennett *et al.*, 1995; Wang *et al.*, 1995). The contribution of $Na_v1.5$ to I_{NaL} was further supported by evidence demonstrating that knockdown of $Na_v1.5$ in dog ventricular cardiomyocytes resulted in a 60% decrease in I_{NaL} (Maltsev *et al.*, 2007). There is an increasing body of evidence suggesting that the TTX-sensitive Na^+ channel isoforms as well as $Na_v1.8$ and $Na_v1.9$ may also contribute to the cardiac I_{NaL}. Utilising (2-aminoethyl)mehanethiosulfonate (MTSEA) to selectively inhibit $Na_v1.5$, Biet *et al.* (2012) reported a 44% contribution of the other Na^+ channel isoforms to the I_{NaL} in dog ventricular cardiomyocytes.

The contribution of TTX-sensitive Na^+ channels to the I_{NaL} is thought to increase in disease states such as heart failure. For example, Mishra *et al.* (2014) reported an upregulation of $Na_v1.1$ expression in ventricular cardiomyocytes isolated from a dog heart failure model. Furthermore, siRNA silencing of $Na_v1.1$ in cardiomyocytes isolated from the dog heart failure model revealed that $Na_v1.5$ was not the main contributor to I_{NaL}, instead $Na_v1.1$ contributed approximately 60% of I_{NaL} (Maltsev *et al.*, 2008; Mishra *et al.*, 2014). Additionally, an increase in I_{NaL} in ventricular cardiomyocytes from a rat model of heart failure was thought to be a consequence of a 2.5 fold increase in the expression of $Na_v1.1$ and $Na_v1.6$ mRNA (Xi *et al.*, 2009). A 60% decrease in $Na_v1.5$ mRNA was measured in the same cells, suggesting that the enhanced I_{NaL} was not linked to $Na_v1.5$ (Xi *et al.*, 2009). The neuronal Na^+ channel isoforms may also be of importance in the development of arrhythmogenic activity induced by I_{NaL}. This was shown by Yang *et al.* (2012) who reported that

EADs induced by an enhanced I_{NaL} in isolated rabbit and mouse ventricular cardiomyocytes were suppressed by addition of the highly selective $Na_v1.8$ blocker, A-803467.

Investigations of mutations present in human patients have also linked the TTX-sensitive Na^+ channels as well as $Na_v1.8$ with the I_{NaL}. Missense mutations in TTX-sensitive Na^+ channels such as $Na_v1.1$, $Na_v1.2$ and $Na_v1.4$, which are associated with epilepsy and paramyotonia congenita, result in altered biophysical properties of Na^+ channels and increased I_{NaL} in neurons and skeletal muscle cells (Sugawara *et al.*, 2001a, 2001b; Akalin *et al.*, 2003). Notably, a prolonged QT interval was also observed in hereditary epilepsy patients (Christidis *et al.*, 2006), epileptic children (Akalin *et al*., 2003), and paramyotonia congenita (Péréon *et al.*, 2003) suggesting that Na^+ channels, which were thought to be normally expressed in neuronal tissue and skeletal muscle cells, are also involved in the cardiac action potential. Furthermore, SCN10A gene variants, which encodes for $Na_v1.8$, have been identified in AF patients. Expression of the $Na_v1.8$ mutations in ND7/23 cells revealed an enhanced I_{NaL} in comparison to the wild type $Na_v1.8$ isoform (Savio Galimberti *et al.*, 2012; Savio-Galimberti *et al.*, 2014).

4.1.2 Pharmacological enhancement of I_{NaL}

One well established pharmacological tool that is used to enhance I_{NaL} is *anemonia sulcata* toxin II (ATX-II). This toxin has been shown to selectively increase I_{NaL} in isolated atrial and ventricular cardiomyocytes (Isenberg and Ravens, 1984; Song *et al.*, 2004, 2009; Fischer *et al.*, 2015). The ATX-II induced increase in I_{NaL} results in prolongation of the APD, with evidence of this effect apparent in whole tissue studies, as well as in single cells isolated from the ventricle (Isenberg and Ravens, 1984; Hoey *et al.*, 1994; Studenik *et al.*, 2001), atria (Song *et al.*, 2008), and PVs (Lu *et al.*, 2012). However, the effect of ATX-II on action potential parameters such as the peak amplitude and rise time is unknown in atrial and PV preparations.

Enhancement of I_{NaL} by ATX-II leads to the generation of EADs, DADs and triggered activity in dog and guinea pig ventricular preparations (Boutjdir and el-

Sherif, 1991; Song *et al.*, 2004). This ATX-II induced arrhythmogenic activity was also observed in guinea pig atrial (Song *et al.*, 2004, 2009) as well as rabbit and rat PV preparations (Lu *et al.*, 2012; Chen *et al.*, 2014). The ATX-II mediated arrhythmogenic activity is thought to be due to an increase in the intracellular Na^+ concentration (Hoey *et al.*, 1994; Sossalla *et al.*, 2008). Sossalla *et al.*, 2008 demonstrated using the Na^+ sensitive fluorescence dye SBFI that treatment of rabbit ventricular cardiomyocytes with ATX-II (40 nM) resulted in a 4 fold increase in the intracellular Na^+ concentration. Moreover, in rat ventricular cardiomyocytes, a 50% and a 70% increase in intracellular Na^+ was observed after addition of 10 nM and 30 nM ATX-II respectively (Yao *et al.*, 2011). The increased intracellular Na^+ concentration has been shown to drive the NCX in reverse mode, leading to cellular Ca^{2+} overload, which in turn contributes to the generation of DADs (Faber and Rudy, 2000; Sossalla *et al.*, 2008; Undrovinas *et al.*, 2010). The ATX-II induced prolongation of the APD also allows the L-type Ca^{2+} channels to recover from inactivation, leading to increased Ca^{2+} entry, which if sufficient enough can reverse the repolarising K^+ currents and generate EADs during phase 2 of the action potential (January and Riddle, 1989; Zeng and Rudy, 1995).

The ATX-II induced Ca^{2+} overload can also lead to contraction abnormalities in cardiac tissues. Addition of ATX-II to rat and guinea pig LA preparations resulted in the presence of ATX-II induced spontaneous contractions (Alsen *et al.*, 1976, 1982; Wolkowicz *et al.*, 2014).

4.1.3 The effect of CaMKII on the cardiac I_{NaL}

CaMKII is a serine/threonine protein kinase involved in the regulation of Ca^{2+} signalling (Witcher *et al.*, 1991; Dzhura *et al.*, 2000; Maier *et al.*, 2003). Intracellular Ca^{2+} binds to calmodulin (CaM), and the Ca^{2+}/CaM complex binds to CaMKII resulting in a conformational change that enables kinase activity, by freeing the catalytic domain of CaMKII from its autoinhibitory pseudosubstrate (Witcher *et al.*, 1991; Dzhura *et al.*, 2000; Maier *et al.*, 2003). Typically, in cardiomyocytes CaMKII exerts its action by the phosphorylation of various key Ca^{2+} transport proteins and

ion channels such as the type 2 ryanodine receptor (RyR2; Witcher *et al*., 1991; Maier et al., 2003), L-type Ca^{2+} channels (Dzhura *et al*., 2000) and K^+ channels (Tessier *et al.*, 1999).

CaMKII has also been shown to phosphorylate Na^+ channels (Tan *et al.*, 2002; Wagner *et al.*, 2006). This was confirmed by Aiba *et al.* (2010) who showed that CaMKII phosphorylated $Na_v1.5$ predominately at the I-II linker region, as well as at the carboxyl terminus of the α-subunit. Phosphorylation by CaMKII can alter Na^+ channel gating. This was shown by Wagner *et al*. (2006) who reported that overexpression of CaMKII in mouse and rabbit ventricular cardiomyocytes slowed Na^+ channel inactivation and recovery from inactivation, which was reversed by inhibition of CaMKII. This slowed Na^+ channel inactivation could lead to an increase in I_{NaL}. Adenovirus-mediated overexpression of the cytosolic CaMKII isoform, CaMKII*δ,* in rabbit isolated ventricular cardiomyocytes and *in vivo* by transgenic overexpression of CaMKII*δ* in mice resulted in a rise in the intracellular Na^+ concentration and an increased I_{NaL} (Wagner *et al*., 2006, 2011). It is thought that the CaMKII mediated increase in I_{NaL} could lead to arrhythmogenic activity in cardiomyocytes. This was supported by studies in transgenic mice overexpressing CaMKII*δ,* where a prolonged QT interval (which is typical of increased I_{NaL}), and an enhanced susceptibility to develop ventricular tachycardia was observed (Wagner *et al.*, 2006). Furthermore, papillary muscles from transgenic mice overexpressing CaMKII*δ* displayed extra contractions, which were abolished by the I_{NaL} inhibitor ranolazine (Sossalla *et al.*, 2011). An increase in I_{NaL} can also in turn activate CaMKII. Western blot analysis of ATX-II treated rat neonatal ventricular cardiomyocytes and adult mouse ventricular cardiomyocytes revealed an increased autophosphorylation of CaMKII, which was reduced by treatment with ranolazine or the specific CAMKII blocker autocamtide-2-related inhibitory peptide (AIP) (Yao *et al.*, 2011; Sag *et al.*, 2014). As recently demonstrated in a computational model of mouse ventricular cardiomyocyte electrophysiology, this could result in a positive feedback loop of CaMKII activation and increased I_{NaL}, which could enhance cardiac arrhythmogenicity (Morotti *et al.*, 2014).

Expression of CaMKII has been shown to be upregulated in dogs with pacing-induced atrial tachycardia (Wakili *et al.*, 2010), in goats with induced AF (Greiser *et al.*, 2009), and in the right atrial appendage of AF patients (Tessier *et al.*, 1999; Neef *et al*., 2010; Voigt *et al*., 2012), suggesting that increased CaMKII expression may be linked to AF. Two CaMKII inhibitors, N-[2-[[[3-(4-chlorophenyl)-2-propenyl]methylamino]methyl]phenyl]-N-(2-hydroxyethyl)4methoxybenzenesulpho namide (KN-93) and AIP have been shown to inhibit I_{NaL} in cardiomyocytes isolated from guinea pig (Horvath *et al.*, 2013), rabbit (Wagner *et al*., 2006) and rat (Yoon *et al.*, 2009). Both KN-93 and AIP can also reduce arrhythmogenic activity induced by ATX-II in cardiomyocytes. Treatment with AIP decreased ATX-II induced DADs in mouse ventricular cardiomyocytes (Sag *et al*., 2014) and prevented ATX-II induced arrhythmogenic activity in the rat Langendorff perfused heart (Yao *et al*., 2011). Pre-incubation with KN-93 also prevented ATX-II induced extra contractions in rat LA preparations (Wolkowicz *et al*., 2014).

4.1.4 NCX and I_{NaL}

The forward mode NCX, which extrudes one Ca^{2+} ion in exchange for three Na^{+} ions, aids in the regulation of intracellular Ca^{2+} in cardiomyocytes. Generation of a transient inward current (I_{Ti}) upon activation of forward mode NCX, as well as Ca^{2+} overload, due to increased Ca^{2+} influx, decreased Ca^{2+} efflux and/or opening of the sarcoplasmic reticulum Ca^{2+} channels can cause substantial depolarisation in cardiomyocytes leading to DADs (Kass *et al.*, 1978; Tweedie *et al.*, 2000; Fujiwara *et al.*, 2008). In addition, a rise in I_{NaL} drives the NCX into reverse mode, which can also lead to Ca^{2+} overload, contributing to the generation of DADs (Faber and Rudy, 2000; Sossalla *et al.*, 2008; Undrovinas *et al.*, 2010). The NCX has also been linked to AF, since NCX expression and I_{Ti} is increased is increased in atrial tissue of AF patients (Schotten *et al.*, 2002; Voigt *et al.*, 2012).

Honjo *et al.* (2003), reported the NCX current as a key contributor to pacing induced spontaneous activity in rabbit PVs, as block of the NCX with Ni^{2+} reduced the pacing induced spontaneous action potentials. The antiarrhythmic effects of the NCX blockers KB-R7943 and SEA-0400 have also been reported in various cardiac

tissues (Watano *et al.*, 1999; Wongcharoen *et al.*, 2006; Milberg *et al.*, 2008; Song *et al.*, 2008; Namekata *et al.*, 2009). Ouabain, a Na^+ pump inhibitor which has been shown to indirectly increase the I_{NaL} (Hoyer *et al.*, 2011; Wu *et al.*, 2015), induced arrhythmogenic activity which was suppressed by KB-R7943 in guinea pig atria (Watano *et al.*, 1999) and rabbit PV (Wongcharoen *et al.*, 2006), as well as by SEA-0400 in the guinea pig PV (Namekata *et al.*, 2009). In addition, pre-incubation with KB-R7943 abolished ATX-II induced DADs in guinea pig atrial cardiomyocytes (Song *et al.*, 2008). These studies demonstrate the potential involvement of the NCX in the generation of ATX-II induced arrhythmogenic activity in the atria and PV. However, KB-R7943 and SEA-0400 can also inhibit I_{Na} and I_{CaL} (Watano *et al.*, 1999; Tanaka *et al.*, 2002; Birinyi *et al.*, 2005), casting doubt on the mechanism of action underlying their antiarrhythmic properties. Recently, a more specific NCX inhibitor, ORM-10103 has been developed. This inhibitor reduced both the inward and outward NCX currents, with no effect on I_{CaL}, the Na^+/K^+ pump, or the main K^+ currents at concentrations up to 10 μM in dog ventricular cells, although there was a small reduction in I_{Kr} (Jost *et al.*, 2013). Treatment of dog ventricular preparations with ORM-10103 reversed the ATX-II induced increase in Ca^{2+} transient amplitude, which was thought to be due to NCX inhibition preventing the Na^+ induced Ca^{2+} overload (Nagy *et al.*, 2014).

Since the majority of investigations with ATX-II have focused on ventricular cardiomyocytes, the aim of this chapter was to examine the ATX-II mediated arrhythmogenic activity in rat PV and LA tissues. The ability of ATX-II, which has been shown in previous studies to directly increase the I_{NaL} (Isenberg and Ravens, 1984), to induce spontaneous contractions, spontaneous action potentials and afterdepolarisations at various stimulation frequencies was investigated. In addition, the contribution of TTX-sensitive Na^+ channels, CaMKII and the NCX to ATX-II mediated arrhythmogenic activity was also determined.

4.2 Methods

4.2.1 Contraction studies

The rat PV and LA tissues were obtained and set up for contraction studies as described in section 2.2.4. Contractions were evoked using field stimulation via ring electrodes at twice the threshold voltage and 2 ms duration, delivered at the indicated frequency (from 0.1 Hz – 10 Hz) using a Grass stimulator (Model S88, Grass Instrument Co. USA). The tissue was allowed to equilibrate in bath solution, consisting of 150 mM NaCl, 5.4 mM KCl, 10 mM HEPES, 10 mM glucose, 1.2 mM $MgCl_2$, 1.8 mM $CaCl_2$, pH 7.4 with NaOH, at 37^{o}C for at least 40 minutes before beginning the experiments. Contractions were recorded via a DAQ PCI 6221 analogue to digital converter (National Instruments, Texas, USA) and displayed continuously using Chart Software (Version 5.0.7, Dr. J. Dempster, University of Strathclyde).

4.2.1.1 Determination of the effect of ATX-II on PV and LA contraction

For the purpose of the results in this chapter, the term spontaneous contraction or spontaneous action potential is used to define contractions or action potentials that occur after treatment of the tissue with ATX-II (15 nM), and which are independent of electrical stimulation. For the majority of studies with ATX-II the tissues were incubated with ATX-II for 15-20 minutes, to allow development of the spontaneous contractions, prior to commencing any subsequent steps in the protocol.

Initially the influence of concomitant electrical stimulation on the ability of ATX-II to induce spontaneous contractions in both tissues was examined. To determine this, the PV or LA was subject to a period of electrical stimulation at 0.1, 0.3, 1, 3 or 10 Hz for 2-5 minutes at each frequency. The tissue was then treated with ATX-II (15 nM) and the electrical stimulation at the different frequencies was repeated in the presence of ATX-II.

To examine the effect of CaMKII inhibition on the spontaneous contractions induced by ATX-II, the CaMKII blocker KN-93 was utilised. The tissues were pre-treated

with KN-93 as previous studies have shown that KN-93 is more successful at preventing the onset arrhythmogenic activity rather than suppressing arrhythmogenic activity once it has developed (Anderson *et al.*, 1998; Lo *et al.*, 2007; Wolkowicz *et al.*, 2014). In PV and LA preparations, control recordings were obtained over 5 minute periods in the absence of electrical stimulation and then during stimulation at 0.1 Hz. This was repeated in the presence of KN-93 (10 µM or 20 µM) allowing 30 minutes for equilibration with the tissue before recordings. Following this tissues were treated with ATX-II (15 nM) and the recordings repeated.

The selective NCX inhibitor ORM-10103 was used to determine the involvement of the NCX in the ATX-II induced spontaneous contractions. Control recordings were initially obtained from the PV or LA, over 5 minute periods, in the absence of electrical stimulation and then during stimulation at 0.1 Hz. The recordings were then repeated in the presence of ATX-II (15 nM). Thereafter, the tissue was treated with ORM-10103 (10 µM) for 20 minutes to determine what effect it had on the ATX-II induced spontaneous activity. The ORM-10103 concentration was subsequently increased to 20 µM.

4.2.1.2 Analysis of the Contractile Response

The data acquired using Chart software was converted to a text file using WinEDR (Version 3.4.3, Dr. J. Dempster, University of Strathclyde), which was subsequently converted to the Chart 5 software (ADInstruments, Dunedin, New Zealand) to enable analysis of the spontaneous contractions. To calculate the number of spontaneous contractions induced by ATX-II, the number of electrically evoked contractions per minute under control conditions was subtracted from the total number of contractions per minute in the presence of ATX-II. The contraction time to peak and duration were determined as per section 2.2.4.

4.2.2 Microelectrode studies

The rat PV and LA were dissected and action potentials recorded using the microelectrode technique described in Section 2.2.5. The tissues were allowed to equilibrate in bath solution, consisting of 150 mM NaCl, 5.4 mM KCl, 10 mM

HEPES, 10 mM glucose, 1.2 mM $MgCl_2$, 1.8 mM $CaCl_2$, pH 7.4 with NaOH, heated to 37^{o}C for 30 minutes before commencing any recording. Action potentials were elicited by electrically stimulating the tissue at twice the threshold voltage, with a 2 ms pulse and a stimulation frequency of 0.1 or 1 Hz. To determine the action potential threshold voltage, the stimulation voltage was increased in 10 V increments under control conditions until an action potential was elicited.

4.2.2.1 Determination of the effect of ATX-II, KN-93 and ORM-10103 on the characteristics of the electrically evoked action potential

Action potentials were elicited by electrical stimulation at 1 Hz, and 1 minute recordings were made from 2-5 individual sites in each tissue before and then in the presence of each drug treatment. When assessing the effect of ATX-II (15 nM or 40 nM) on the action potential characteristics of the PV or LA, the preparations were incubated with ATX-II for 15-20 minutes, before obtaining recordings.

To investigate the effect of KN-93 on the ATX-II induced changes in the action potential characteristics, recordings were obtained under control conditions, then after a 20 minute pre-treatment with 10 µM or 20 µM KN-93. Thereafter tissues were treated with ATX-II (40 nM) and the recordings repeated.

To determine the effect of ORM-10103 on the ATX-II induced changes in the action potential characteristics, the electrically evoked action potentials were recorded under control conditions and then in the presence of ATX-II (40 nM). The recordings were then repeated after a 20 minute treatment with 10 µM ORM-10103, and once again upon increasing the ORM-10103 concentration to 20 µM.

For examination of the effect of the presence of KN-93 or ORM-10103 alone on the action potential characteristics of the PV and LA, action potentials were elicited by electrical stimulation at 1 Hz and recordings, 1 minute in duration, were obtained in the same cell, before and then 15 minutes after the addition of each drug.

4.2.2.2 Determination of the ability of ATX-II to induce spontaneous action potentials in the PV and LA

The term EAD is used to describe afterdepolarisations, which occur during the repolarisation phase of the action potential, in the presence of ATX-II. For the following studies, the PV and LA tissues were treated with ATX-II (40 nM) for 15-20 minutes, to allow the spontaneous action potentials and EADs to develop, before continuing subsequent steps in the protocol.

For the following microelectrode studies, 1-2 minute recordings were made from 2-5 individual sites in the PV and LA before and then in the presence of each treatment. The ability of ATX-II to induce spontaneous action potentials and EADs in the PV and LA preparations was assessed. Control recordings were made when the tissue was electrically stimulated at 0.1 Hz and 1 Hz for periods of 1-2 minutes. The stimulation frequencies were then repeated in the presence of ATX-II (40 nM). As spontaneous action potentials were observed in both tissues in the absence of electrical stimulation and during stimulation at 0.1 Hz, then these stimulation protocols were chosen for subsequent studies.

Control recordings were obtained in the PV and LA in the absence of electrical stimulation and at a stimulation frequency of 0.1 Hz. This was repeated in the presence of 10 µM or 20 µM KN-93, allowing 30 minutes for equilibration with the preparation, before treatment with ATX-II (40 nM).

The effect of ORM-10103 on the spontaneous action potentials and EADs was also examined. Control recordings were made in both tissues in the absence of electrical stimulation as well as when the tissue was stimulated at 0.1 Hz and were then repeated in the presence of ATX-II (40 nM). Following this the tissues were treated with 10 µM ORM-10103 for 20 minutes, which was subsequently increased to 20 µM ORM-10103.

4.2.2.3 Analysis of electrically evoked and ATX-II induced spontaneous action potentials

Electrophysiological data was acquired using WinEDR software (Version 3.3.4, Dr. J. Dempster, University of Strathclyde), which was subsequently exported to WinWCP software (Version 4.6.5 Dr. J. Dempster, University of Strathclyde) to enable the action potential characteristics and effective refractory period (ERP) to be measured as described in section 2.2.5. The number of spontaneous action potentials and EADs were manually counted over a 1 minute period.

4.2.3 Chemicals and drugs

TTX and ATX-II (Alomone, Israel) were dissolved in water to provide stock concentrations of 1 mM and 100 µM respectively, and they were then stored at -20^{o}C until required. KN-93 (Sigma, UK) was dissolved in dimethyl sulfoxide (DMSO) to a stock concentration of 5 mM and stored at -20^{o}C. ORM-10103 (Sigma, UK) was dissolved in DMSO to a stock concentration of 20 mM and stored at room temperature.

4.2.4 Statistics

Graphs were produced using GraphPad Prism (Version 4.03, Graph Pad Software Inc., San Diego, CA, USA). Electrophysiological data, where more than one recording was made from the same tissue, are expressed as mean ± standard error of the mean (s.e.m) of *N* technical replicates (number of recordings), from *n* biological replicates (number of rats). All other data are expressed as mean ± standard error of the mean (s.e.m) of *n* biological replicates. The PV and LA data from at least three different animals were used for each group of experiments. A Student's paired *t*-test was used when comparing the effect of ATX-II, KN-93 or ORM-10103 alone on action potential characteristics. For all other experimental results two way multilayer ANOVAs were performed in Minitab (Version 17.1.0, Minitab Inc., State College, Pennsylvania, USA) in order to determine the statistical significance between treatment groups as well as the statistical significance between the PV and LA. This was followed by Tukey's post hoc test. The difference was considered to be statistically significant when $P<0.05$.

4.3 Results

4.3.1 ATX-II induced spontaneous contractions in the rat PV and LA

The ability of ATX-II to induce spontaneous contractions at a range of stimulation frequencies was investigated, in order to determine the optimum stimulation frequency for use in subsequent experiments. This also gave further insight into the relationship between ATX-II induced spontaneous activity and the electrical stimulation frequency. Representative recordings in Figure 4.1 show that when ATX-II is not present, there are no spontaneous contractions in the rat PV (A) or LA (B), in the absence of electrical stimulation and when the tissue was electrically stimulated at 0.1 Hz or 1 Hz. Under these conditions, only the electrically evoked contractions were observed. However, the presence of ATX-II (15 nM) induced spontaneous contractions in both the PV (Figure 4.1A) and LA (Figure 4.1B), which appeared in an irregular manner. The ATX-II induced spontaneous contractions were observed at a rate of 22.2 ± 2.7 min^{-1} in the absence of stimulation and a rate of 21.0 ± 6.8 min^{-1} at a stimulation frequency of 0.1 Hz, in the PV (Figure 4.1C). However, spontaneous contractions were not apparent in the PV, at electrical stimulation frequencies of 0.3 Hz and above. The presence of ATX-II also induced spontaneous contractions in the LA in the absence of electrical stimulation at a rate of 15.7 ± 2.8 min^{-1} and at a rate of 16.0 ± 3.6 min^{-1} when the tissue was electrically stimulated at a frequency of 0.1 Hz. In contrast to the PV, spontaneous contractions were observed at electrical stimulation frequencies of 0.3 Hz and 1 Hz in LA preparations at rates of 19.6 ± 7.9 and 28.1 ± 8.7 min^{-1} respectively (Figure 4.1D). However, the spontaneous contractions were not apparent at the higher electrical stimulation frequencies of 3 Hz and 10 Hz. The sustainability of the effect of ATX-II over time was also examined and Figure 4.1E shows that the spontaneous contractions in the PV and LA were sustained 1 hour after the addition of ATX-II, under conditions where the tissues were electrically stimulated at 0.1 Hz. In addition, the ATX-II induced spontaneous contractions were not affected by the presence of 0.1% DMSO (Appendix Figure 6.11). Table 4.1 summarises the time to peak tension and timecourse of the contraction in the PV and LA under control conditions and in the

presence of ATX-II (15 nM). No statistically significant change was detected in the contraction parameters.

Treatment with 15 nM ATX-II was deemed the optimum concentration for contraction studies as increasing the ATX-II concentration to 40 nM appeared to hinder both the stimulated and spontaneous contractions.

4.3.2 Effect of 15 nM ATX-II on action potentials of the PV and LA

The effect of ATX-II (15 nM) on the electrically evoked action potential characteristics was also determined, whilst stimulating the tissue at 1 Hz. In Figure 4.2A, representative microelectrode recordings of the PV and LA action potentials, show the prolonged APD in the presence of ATX-II (15 nM), which is accompanied by an increase in ERP (Figure 4.2B). Detailed analysis of the PV and LA action potentials demonstrated that ATX-II (15 nM) had no effect on the membrane potential (Figure 4.2C) or action potential peak amplitude (Figure 4.2D). The presence of ATX-II, significantly increased the action potential rise time of the PV from 0.6 ± 0.02 ms to 1.1 ± 0.1 ms (P<0.05 Figure 4.2E), but did not alter the rise time of the LA (Figure 4.2E). In the PV, ATX-II decreased the rate of rise (dV/dt_{max}) from 188.0 ± 10.1 mV/ms to 111.1 ± 7.2 mV/ms (P<0.05, Figure 4.2F). In contrast, no such effect was observed in the LA (Figure 4.2F). The presence of ATX-II significantly prolonged the APD_{90} in both tissues, with an increase from 37.8 ± 0.9 ms to 365.3 ± 6.8 ms in the PV, and from 32.3 ± 1.4 ms to 203.2 ± 11.4 ms in the LA (P<0.05; Figure 4.2G). Moreover, the prolongation of the APD_{90} was significantly greater in the PV compared to the LA (P<0.05). The prolonged APD_{90} was accompanied by a significant increase in the ERP in the PV from 38.9 ± 2.8 ms to 368.3 ± 35.6 ms (P<0.05) and in the LA from 39.0 ± 4.1 ms to 141.7 ± 41.7 ms (P<0.05, Figure 4.2H). The ATX-II induced ERP prolongation was greater in the PV than in the LA (P<0.05).

4.3.3 The effect of Na^+ channel blockade on ATX-II induced spontaneous contractions and action potential parameters

The presence of 100 nM TTX inhibits the TTX-sensitive channels with minimal effect of the TTX-resistant channels (Doyle *et al.*, 1993). Therefore, to assess the contribution of TTX-sensitive Na^+ channels to ATX-II induced spontaneous contractions and action potentials, 100 nM TTX was utilised. An electrical stimulation frequency of 0.1 Hz was chosen, as the spontaneous contractions were observed in both tissues in the presence of ATX-II at this stimulation frequency. Treatment with TTX (100 nM) had no effect on the spontaneous contractions in the PV, with a rate of 11 ± 2 min^{-1} observed in ATX-II alone and a rate of 11 ± 3 min^{-1} with ATX-II and 100 nM TTX. Similar results were observed in LA tissues with spontaneous contractions remaining at a rate of 23 ± 8 min^{-1} in ATX-II alone and at 16 ± 3 min^{-1} in the presence of ATX-II and 100 nM TTX (Figure 4.3A). In addition, the ATX-II induced alterations in the PV action potential rise time (Figure 4.3B) and dV/dt (Figure 4.3C) were not reversed by TTX. However, in the PV, the prolonged APD_{90}, was significantly attenuated from 386.6 ± 12.1 ms to 327.7 ± 9.2 ms in the presence of TTX ($P<0.05$; Figure 4.3D).

The TTX concentration was increased to 10 µM in order to inhibit both TTX-sensitive and TTX-resistant Na^+ channels. As shown in Figure 4.4A, increasing the TTX concentration to 10 µM TTX significantly reduced the spontaneous contractions from a rate of 15.4 ± 1.7 min^{-1} to 0.9 ± 0.5 min^{-1} in the PV ($P<0.05$; Figure 4.4B). Similarly, in the LA the spontaneous contractions were significantly suppressed from 19.1 ± 7.4 min^{-1} to 0.5 ± 0.03 min^{-1} ($P<0.05$; Figure 4.4B) by 10 µM TTX.

4.3.4 The effect of 40 nM ATX-II on action potentials of the PV and LA

In microelectrode studies, the ATX-II concentration was increased to 40 nM, to determine whether higher concentrations of ATX-II had an effect on the LA action potential rise time and rate of rise. In Figure 4.5A, the representative PV (i) and LA (ii) recordings show the effect of ATX-II (40 nM) on the action potentials evoked by electrical stimulation at 1 Hz. Treatment with ATX-II (40 nM) had no effect on the

resting membrane potential (Figure 4.5B), nor the action potential peak amplitude (Figure 4.5C) in both the PV and LA. However, ATX-II significantly increased the action potential rise time in the PV from 0.6 ± 0.04 ms to 1.2 ± 0.2 ms (P<0.05), and in the LA from 0.8 ± 0.1 ms to 1.3 ± 0.2 ms (P<0.05, Figure 4.5D). In the presence of ATX-II the action potential dV/dt_{max} decreased significantly from 232.5 ± 15.7 mV/ms to 141.7 ± 12.8 mV/ms (P<0.05) in the PV, and from 189.1 ± 12.9 mV/ms to 120.5 ± 6.5 mV/ms (P<0.05) in the LA (Figure 4.5E). Treatment with ATX-II also significantly prolonged the APD_{90}, from 31.8 ± 0.5 ms to 373.0 ± 23.1 ms (P<0.05) in the PV, and from 29.1 ± 1.5 ms to 322.2 ± 63.3 ms (P<0.05) in the LA (Figure 4.5F). This was accompanied by an increase in ERP from 35.8 ± 2.3 ms to 365.8 ± 16.0 ms (P<0.05) in the PV, and from 30.3 ± 0.1 ms to 332.0 ± 66.7 ms (P<0.05) in the LA (Figure 4.5G).

Since ATX-II was shown to induce arrhythmogenic activity in the form of spontaneous contractions in the PV and LA, the ability of ATX-II to induce spontaneous action potentials and EADs in both tissues was also examined. The occurrence of the spontaneous contractions and EADs was studied at various electrical stimulation rates in order to determine the optimum electrical stimulation protocol to use in subsequent experiments. This also allowed for the examination of the relationship of the electrical stimulation frequency to the spontaneous activity. Under control conditions, no spontaneous action potentials were observed in the rat PV (Figure 4.6A) or LA (Figure 4.6B) in the absence of electrical stimulation, or when the tissue was electrically stimulated at 0.1 Hz or 1 Hz. However the presence of ATX-II induced spontaneous action potentials and EADs in the PV (Figure 4.6A) and LA (Figure 4.6B). In the PV, ATX-II (40 nM) induced spontaneous action potentials were observed at a rate of 11.8 ± 1.3 min^{-1}, in the absence of electrical stimulation and at a rate of 12.1 ± 1.7 min^{-1} when the tissue was electrically stimulated at 0.1 Hz (Figure 4.6C). However, no spontaneous action potentials were present at an electrical stimulation frequency of 1 Hz (Figure 4.6C). Similar to what was observed in the PV, ATX-II induced spontaneous action potentials appeared at a rate of 9.1 ± 1.4 min^{-1} in the LA in the absence of electrical stimulation and at a rate of 16.4 ± 6.3 min^{-1} when the tissue was stimulated at a frequency of 0.1 Hz (Figure

4.6D). However, in contrast to the PV, spontaneous action potentials were still observed in the LA when the stimulation frequency was increased to 1 Hz (Figure 4.6D).

As summarised in Table 4.2, there was also a difference in the ability of ATX-II to induce EADs at various electrical stimulation frequencies in the PV compared with the LA. In the PV, treatment with ATX-II induced EADs in the absence of electrical stimulation and when the tissue was stimulated at 0.1 Hz, but EADs were not present at the higher stimulation frequency of 1 Hz. In the LA, ATX-II also induced EADs in the absence of electrical stimulation and at a stimulation frequency of 0.1 Hz. Although unlike the PV, ATX-II induced EADs were exhibited in the LA at the higher stimulation frequency of 1 Hz.

4.3.5 The effect of KN-93 on ATX-II induced arrhythmogenic activity in PV and LA preparations

The CaMKII inhibitor, KN-93 was utilised to gain insight into the contribution of CaMKII to ATX-II induced arrhythmogenic activity. Both 10 µM and 20 µM KN-93 was chosen for this study as these concentrations have previously been reported to reduce ATX-II induced arrhythmic activity in rat cardiac tissue (Wolkowicz *et al.*, 2014). The PV contraction recordings in Figure 4.7A, show that at a stimulation frequency of 0.1 Hz, pre-incubation with KN-93 (20 µM) reduced the number of ATX-II induced spontaneous contractions, with an average reduction from 21.9 ± 6.4 min^{-1} to 3.9 ± 1.9 min^{-1} (P<0.05; Figure 4.7B). Similarly, in the LA, spontaneous contractions were reduced from 15.6 ± 3.7 min^{-1} to 1.2 ± 0.4 min^{-1} (P<0.05) by the presence of KN-93 (20 µM; Figure 4.7B). In the absence of electrical stimulation, pre-incubation with KN-93 (10 µM) did not alter the ATX-II spontaneous contractions in either tissue (Figure 4.7C). However, increasing the KN-93 concentration to 20 µM significantly attenuated the rate of spontaneous contractions from 25.8 ± 6.3 min^{-1} to 10.9 ± 2.8 min^{-1} (P<0.05) in the PV, and from 13.9 ± 3.2 min^{-1} to 5.6 ± 1.2 min^{-1} (P<0.05) in the LA (Figure 4.7C).

Table 4.3 shows that treatment of either tissue with KN-93 (20 μM) had no effect on the action potentials elicited by 1 Hz electrical stimulation. The higher ATX-II concentration (40 nM) was chosen for subsequent studies, since its effect on the electrically evoked action potentials in the PV and LA was similar. The consequence of CaMKII inhibition on ATX-II (40 nM) induced changes to the electrically evoked action potential were studied by pre-incubation of tissues with KN-93 prior to addition of ATX-II (40 nM). In PV tissues, the increase in action potential rise time due to ATX-II, was slightly, but not significantly reduced from 1.2 ± 0.2 ms to 0.9 ± 0.1 ms (Figure 4.8A) by 10 μM KN-93, with a significant reduction to 0.8 ± 0.1 ms (P<0.05) upon increasing KN-93 to 20 μM (Figure 4.8A). The ATX-II induced increase in rise time in LA preparations was also slightly attenuated by KN-93 (10 μM or 20 μM; Figure 4.8A), although this was without significance. Pre-incubation with KN-93 (10 μM or 20 μM) failed to prevent the ATX-II induced decrease in rate of rise of the action potential in both the PV and LA (Figure 4.8B). In the PV, the ATX-II induced prolongation of the APD_{90} was significantly reduced from 373 ± 23.1 ms to 225.0 ± 31.2 ms (P<0.05) in the presence of 10 μM KN-93 and to 261.1 ± 24.8 ms in the presence of 20 μM KN-93 (P<0.05, Figure 4.8C). In the LA, the ATX-II induced APD_{90} prolongation was not altered by pre-incubation with 10 μM KN-93; however increasing KN-93 to 20 μM significantly reduced the APD_{90} from 322.2 ± 63.3 ms to 227.8 ± 22.9 ms (P<0.05, Figure 4.8C).

The effect of pre-treatment of the PV and LA with KN-93 (10 μM or 20 μM) on the ability of ATX-II (40 nM) to induce spontaneous action potentials and EADs was examined. The representative PV recording in Figure 4.9A shows that, at 0.1 Hz electrical stimulation, prior treatment with KN-93 (20 μM) considerably suppressed the spontaneous action potentials. Figure 4.9B demonstrates that the spontaneous action potentials in the PV were reduced from 12.1 ± 1.7 min^{-1} to 6.5 ± 1.5 min^{-1} following pre-treatment with 10 μM KN-93, with a further inhibition to 1.0 ± 0.6 min^{-1} (P<0.05) in the presence of 20 μM KN-93 (Figure 4.9B). Incubation with KN-93 exhibited similar results in the LA, as spontaneous action potentials were attenuated from 16.4 ± 6.3 min^{-1} to 5.3 ± 0.9 min^{-1} (P<0.05) in the presence of 10 μM KN-93 and to 5.0 ± 1.9 min^{-1} in the presence of 20 μM KN-93 (P<0.05, Figure 4.9B). Pre-treatment with KN-93 also reduced the incidence of ATX-II (40 nM)

induced EADs in both tissues. In the PV, 10 µM KN-93 decreased the incidence of EADs from 53 ± 3% to 6 ± 6% (P<0.05) and no EADs were observed in the presence of 20 µM KN-93 (Table 4.4). In LA preparations, 10 µM KN-93 had no effect on EADs, whereas pre-incubation with 20 µM KN-93 suppressed the incidence of EADs from 81 ± 19% of cells to 18 ± 10% of cells (P<0.05, Table 4.4).

The effect of pre-incubation of KN-93 on ATX-II (40 nM) induced spontaneous action potentials and EADs was also studied in the absence of electrical stimulation. In the PV, spontaneous action potentials were reduced from 12.2 ± 1.0 min^{-1} to 4.2 ± 1.1 min^{-1} by pre-treatment with 20 µM KN-93 (P<0.05, Figure 4.9C). In contrast, prior treatment with KN-93 (10 µM or 20 µM) did not reduce the spontaneous action potentials in LA preparations (Figure 4.9C). No ATX-II induced EADs were observed after pre-incubation with KN-93 (10 µM or 20 µM) in PV tissues whereas only the higher concentration of KN-93 (20 µM) significantly suppressed the EADs in LA tissues (Table 4.4).

4.3.6 The effect of ORM-10103 on ATX-II induced arrhythmogenic activity in the PV and LA

To investigate if the NCX contributes to the ATX-II induced spontaneous contractions in the PV and LA, the NCX inhibitor ORM-10103 was utilised. A concentration of 10 µM ORM-10103 was initially selected as a number of studies reported a suppression in arrhythmic activity with minimal effect on other ion currents at this concentration (Jost *et al.,* 2013, Nagy *et al* 2014). The ORM-10103 concentration was increased to 20 µM to examine if the anti-arrhythmic effect may be enhanced. When the PV was electrically stimulated at 0.1 Hz, the ATX-II induced spontaneous contractions were reduced from 22.9 ± 6.4 min^{-1} to 10.8 ± 3.5 min^{-1} in presence of 10 µM ORM-10103, although this was without significance, and significantly reduced to 10.3 ± 3.8 min^{-1} (P<0.05) by 20 µM ORM-10103 (Figure 4.10A, B). Repetition of this experimental protocol in the LA produced similar results, with a decrease in spontaneous contractions from 15.6 ± 3.7 min^{-1} to 7.9 ± 1.2 min^{-1} in the presence of 10 µM ORM-10103, but this was without significance, and a significant reduction to 5.3 ± 1.7 min^{-1} in the presence of 20 µM ORM-10103

(P<0.05, Figure 4.10B). In contrast, when the same experiment was carried out in the absence of electrical stimulation, ORM-10103 (10 µM or 20 µM) had no effect on the spontaneous contractions in the PV, and only a small non-significant decrease in LA preparations (Figure 4.10C).

Before examining the ability of ORM-10103 to modify ATX-II (40 nM) induced changes to the action potential characteristics, the effect of ORM-10103 alone on the PV and LA electrically evoked action potential was investigated. Microelectrode studies demonstrated ORM-10103 (20 µM) had no effect on action potentials evoked by 1 Hz electrical stimulation in PV and LA tissues (Table 4.5). Detailed examination of the electrically evoked action potentials revealed the presence of ORM-10103 (10 µM or 20 µM) did not alter the ATX-II (40 nM) induced increase in rise time (Figure 4.11A), the decrease in the rate of rise (Figure 4.11B) or the ATX-II dependent APD_{90} prolongation (Figure 4.11C) in either tissue.

The ability of ORM-10103 to suppress ATX-II (40 nM) induced spontaneous action potentials and EADs was also examined. The example PV recording in Figure 4.12A demonstrates ATX-II (15 nM) induced spontaneous action potentials, when the tissue was electrically stimulated at 0.1 Hz, were suppressed by treatment with ORM-10103 (20 µM) from 12.1 ± 1.8 min^{-1} to 6.3 ± 2.1 min^{-1} (P<0.05, Figure 4.12B). Likewise, in LA tissues, spontaneous action potentials were significantly suppressed from 15.4 ± 6.3 min^{-1} to 3.8 ± 1.8 min^{-1} after treatment with 10 µM ORM-10103 and then to 3.7 ± 1.0 min^{-1} when ORM-10103 was increased to 20 µM (P<0.05, Figure 4.12B). However, the anti-arrhythmic ability of ORM-10103 was suppressed when the same experiments were carried out in the absence of electrical stimulation as treatment with ORM-10103 (10 µM or 20 µM) did not significantly reduce spontaneous action potentials in the PV or LA (Figure 4.12C). The presence of ORM-10103 had no effect on the ATX-II induced EADs in either tissue when they were electrically stimulated at 0.1 Hz or in the absence of electrical stimulation (Table 4.6).

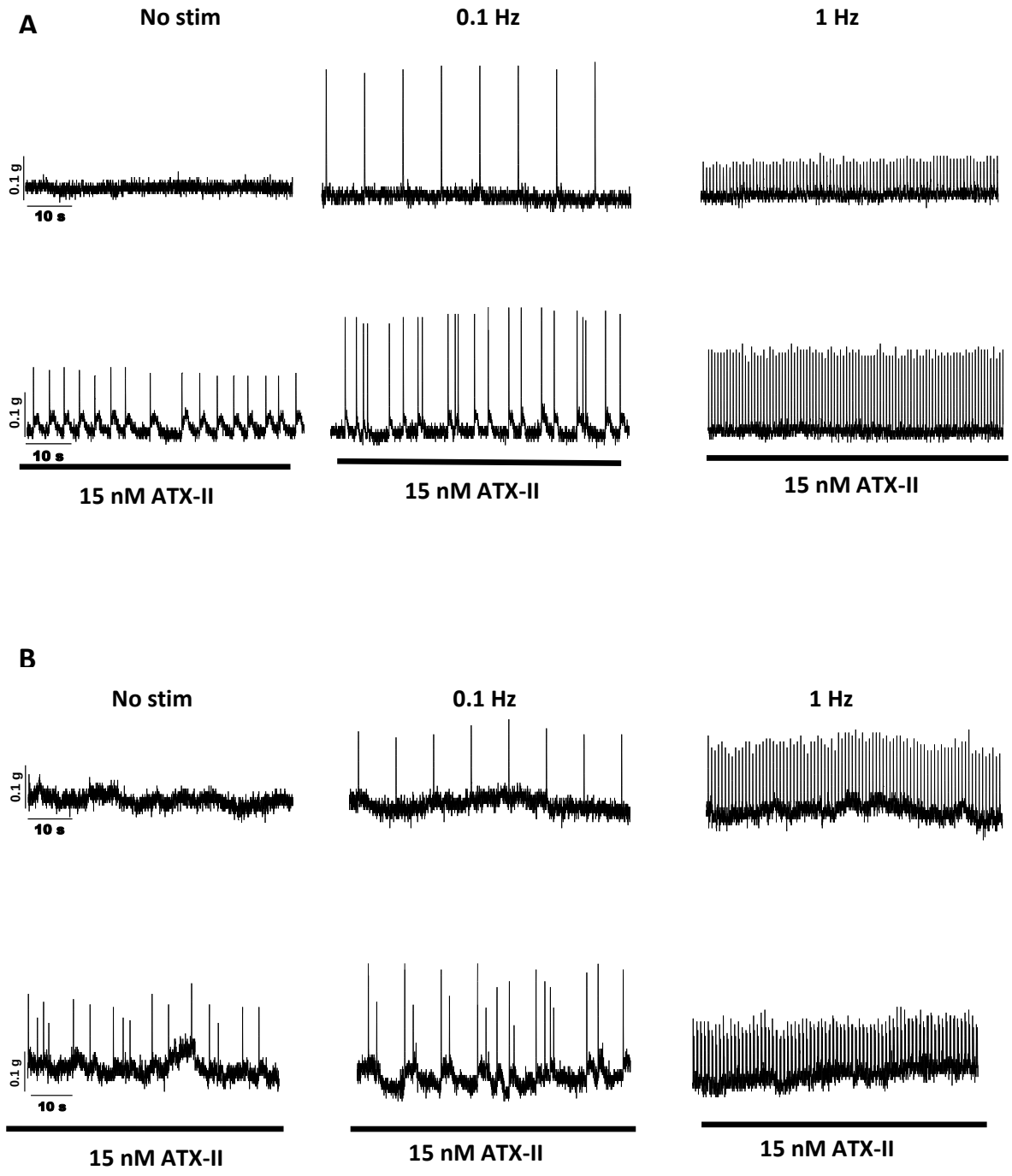

Figure 4.1. **The influence of electrical field stimulation on the contraction response of the rat PV and LA in the presence of ATX-II.** Representative recordings showing contraction of the PV (A) and LA (B) in the absence of electrical stimulation (no stim) and when electrically stimulated at 0.1 Hz or 1 Hz. The top panels in A and B represent contractions under control conditions and the bottom panels show the same tissue in the presence of ATX-II (15 nM).

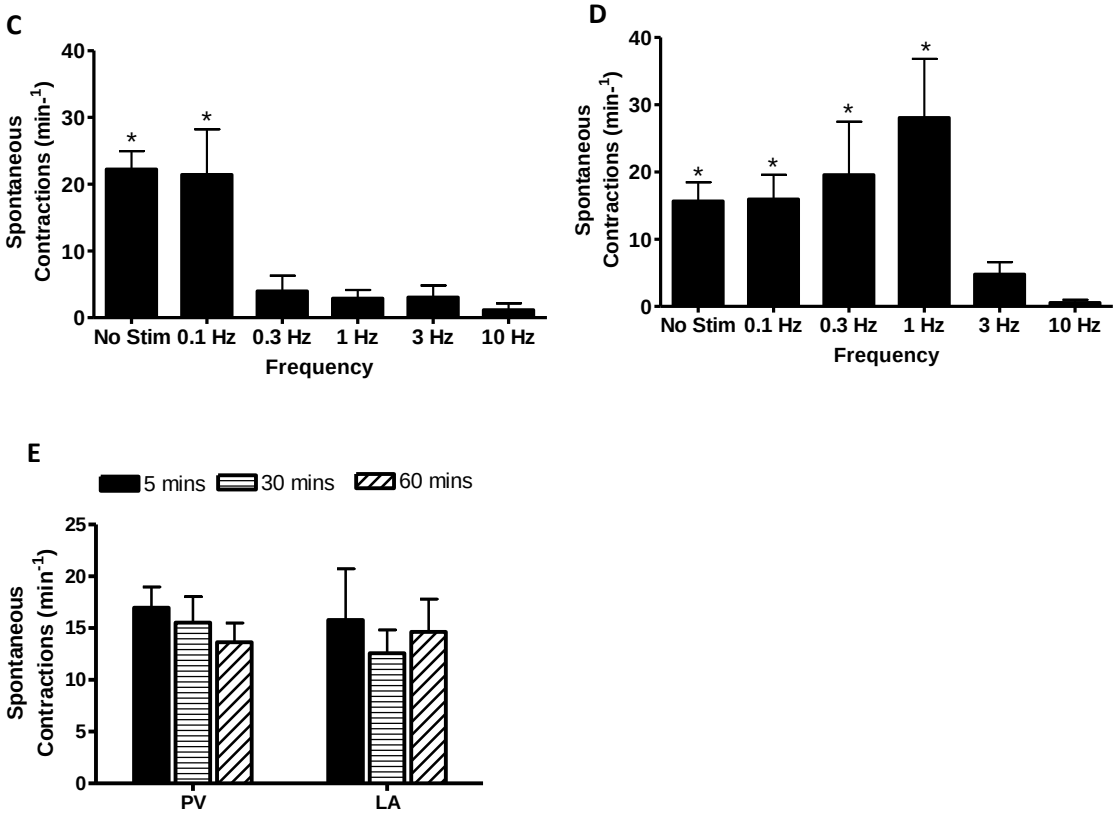

Figure 4.1 (Cont'd) **The influence of electrical field stimulation on the contraction response of the rat PV and LA in the presence of ATX-II.** The number of ATX-II (15 nM) induced spontaneous contractions in PV (C; n=6) and LA (D; n=7) preparations were determined when there was no electrical stimulation and when the frequency of electrical stimulation was varied. (E) The number of spontaneous contractions per minute in PV (n=4) and LA (n=3) tissues at various time points after addition of ATX-II, during electrical stimulation at 0.1 Hz. All data are presented as mean ± s.e.m. * indicates $P<0.05$ for control conditions *vs.* ATX-II treatment.

Table 4.1. **The effect of ATX-II (15 nM) on the PV and LA contraction parameters, when electrically stimulated at 0.1 Hz.**

	PV (n=6)		LA (n=7)	
	Control	ATX-II (15 nM)	Control	ATX-II (15 nM)
Time to Peak Tension (ms)	28.3 ± 0.9	29.5 ± 1.8	28.2 ± 1.0	30.7 ± 1.7
Duration of Contraction (ms)	83.5 ± 5.2	76.1 ± 4.9	79.2 ± 6.7	74.9 ± 3.6

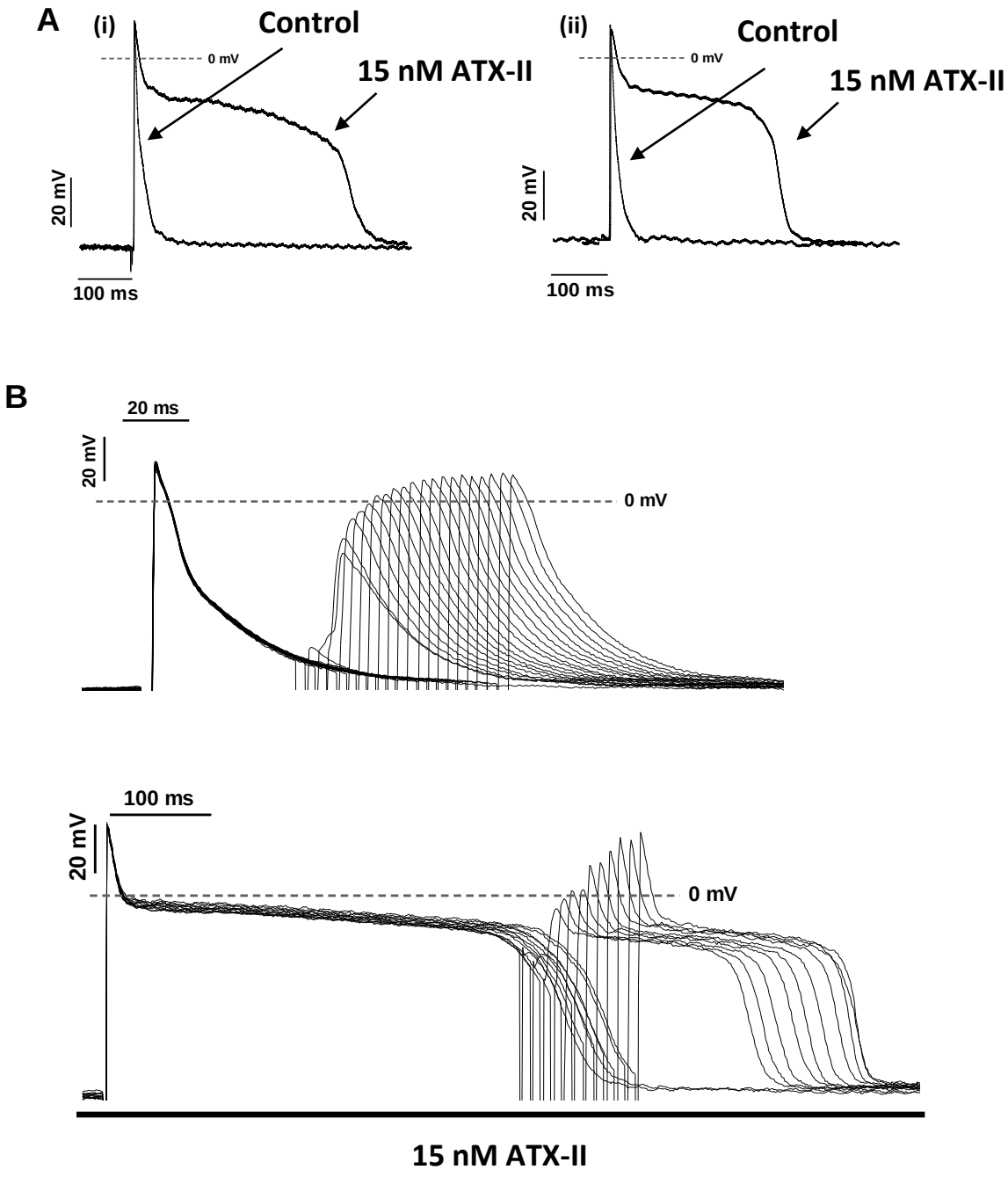

Figure 4.2 **The effect of ATX-II on action potential characteristics of the rat PV and LA.** (A) Superimposed recordings of PV (i) and LA (ii) action potentials elicited by electrical stimulation at 1 Hz, during control conditions and in the presence of ATX-II (15 nM). (B) Superimposed recordings of PV action potentials depicting the effective refractory period (ERP) under control conditions (*top panel*) and in the presence of ATX-II (15 nM) (*bottom panel*).

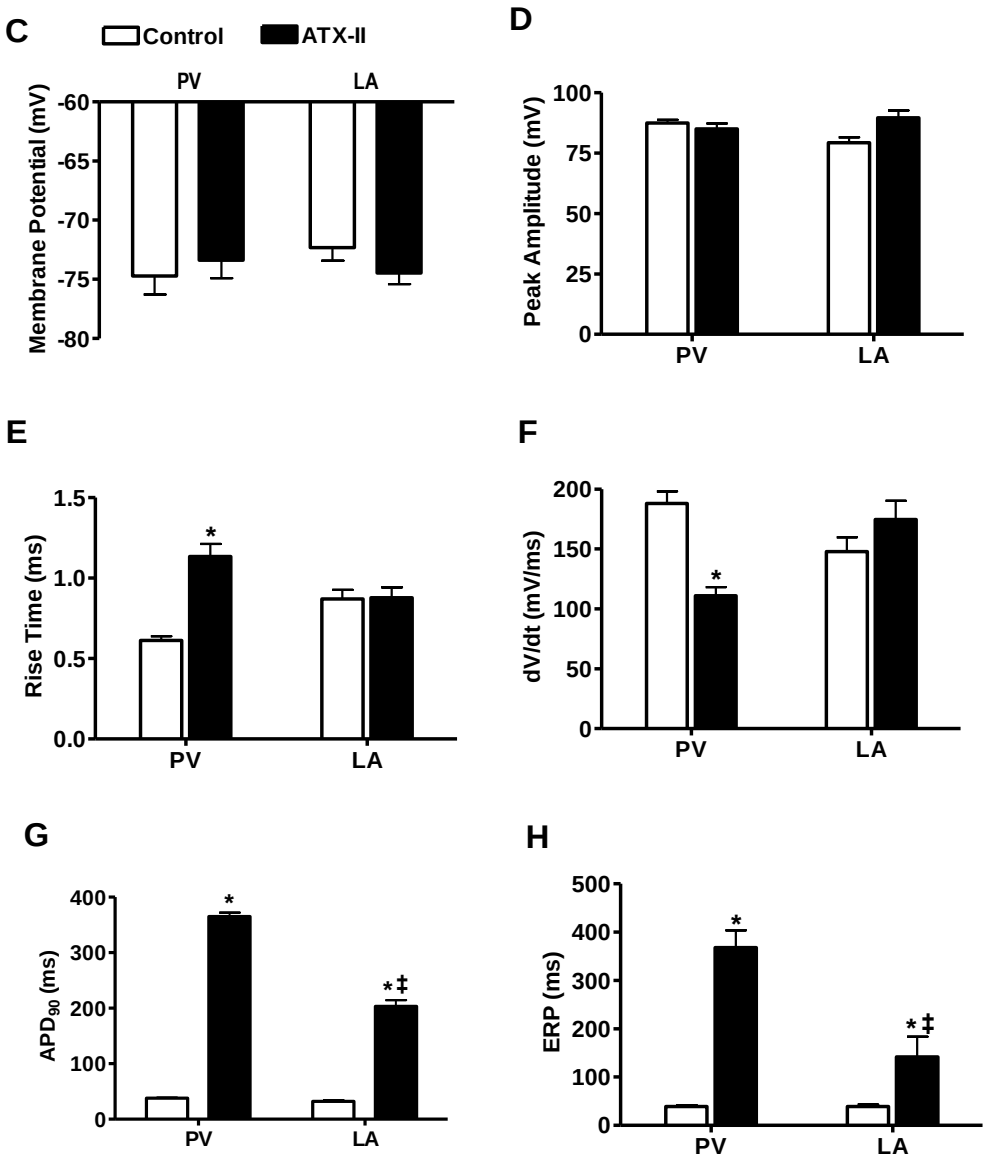

Figure 4.2 (Cont'd) **The effect of ATX-II (15 nM) on action potential characteristics of the rat PV and LA.** Action potential membrane potential (C); peak amplitude (D); rise time (E); dV/dt_{max} (F); APD_{90} (G) elicited by electrical stimulation at 1 Hz and ERP (H) under control conditions (PV, n=15/4; LA, n=17/4) and in the presence of 15 nM ATX-II (PV, n=20/4 rats; LA, n=15/4). All data are presented as mean ± s.e.m. * indicates P<0.05 for control conditions *vs.* ATX-II treatment, ‡ indicates *P*<0.05 for PV *vs.* LA.

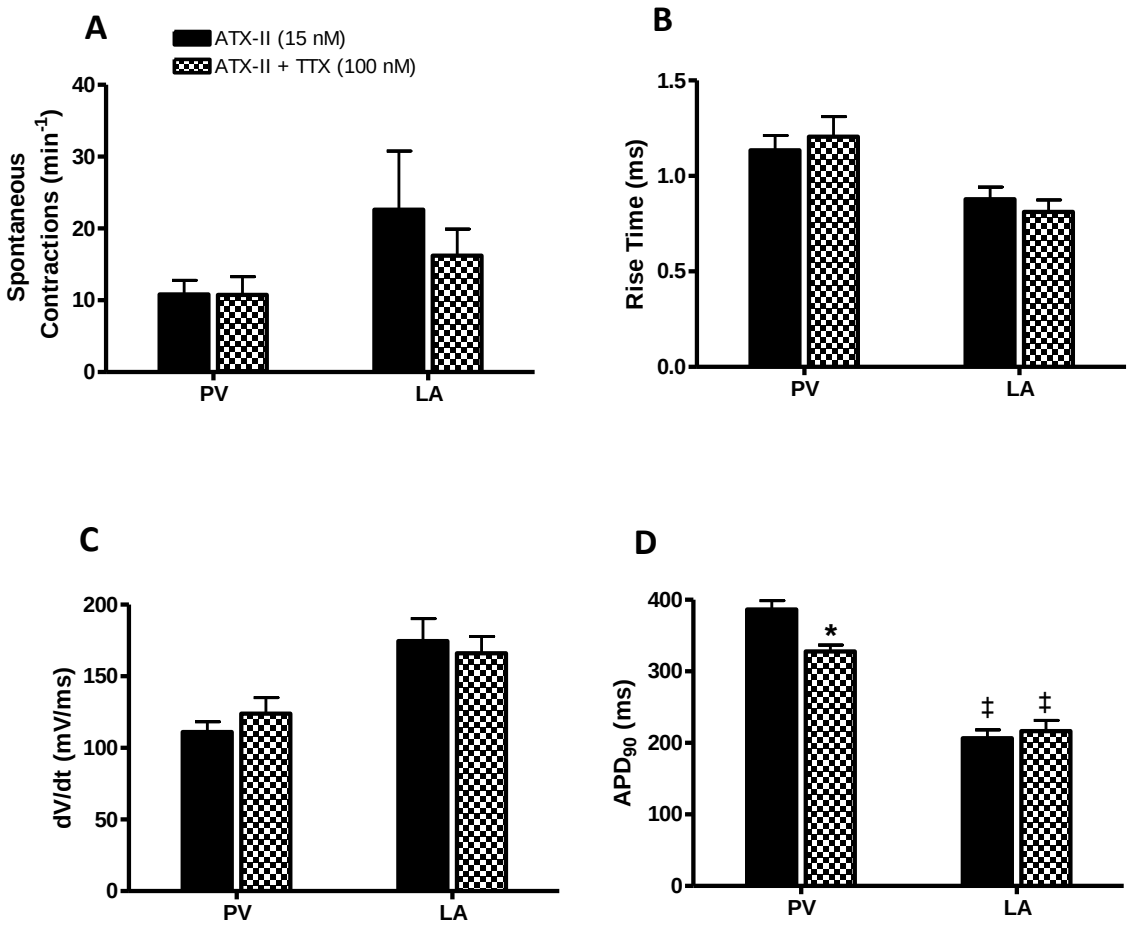

Figure 4.3 **Effect of TTX-sensitive Na^+ channel block on ATX-II induced spontaneous contractions and ATX-II induced changes in action potential characteristics of the PV and LA.** (A) The rate of ATX-II induced spontaneous contractions in PV (n=7) and LA (n=5) tissues before and after the addition of TTX (100 nM) at an electrical stimulation frequency of 0.1 Hz. Action potential rise time (B); dV/dt_{max} (C); and APD_{90} (D) elicited by electrical stimulation at 1 Hz, in the presence of ATX-II (15 nM) (PV, n=20/4; LA, n=15/4) and TTX (100 nM) in the presence of ATX-II (15 nM) (PV, n=18/4; LA, n=15/4). All data are presented as mean ± s.e.m. * indicates $P<0.05$ for ATX treatment *vs.* ATX treatment + TTX treatment. ‡$P<0.05$ PV *vs.* LA.

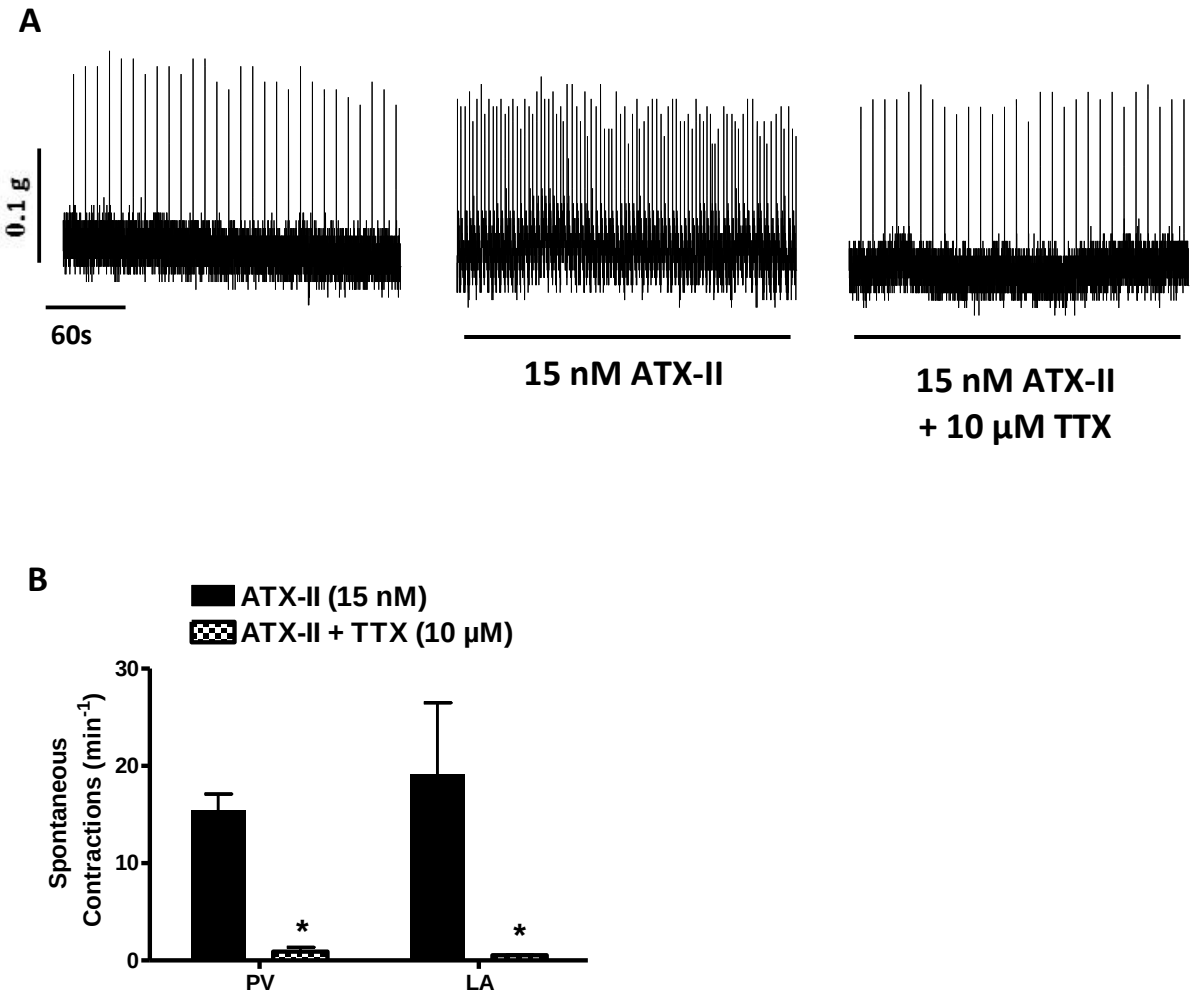

Figure 4.4 **Effect of TTX-sensitive and TTX-resistant Na^+ channel block on ATX-II induced spontaneous contractions.** (A) Representative recording of PV contractions at a stimulation frequency of 0.1 Hz under control conditions (*left panel*), in the presence of ATX-II (15 nM; *middle panel*) and in the presence of ATX-II and TTX (10 µM; *right panel*) (B) The rate of ATX-II induced spontaneous contractions in PV (n=3) and LA (n=3) tissues before and after the treatment with TTX (10 µM) at an electrical stimulation frequency of 0.1 Hz. All data are presented as mean ± s.e.m. * indicates $P<0.05$ for ATX treatment *vs.* ATX treatment + TTX treatment.

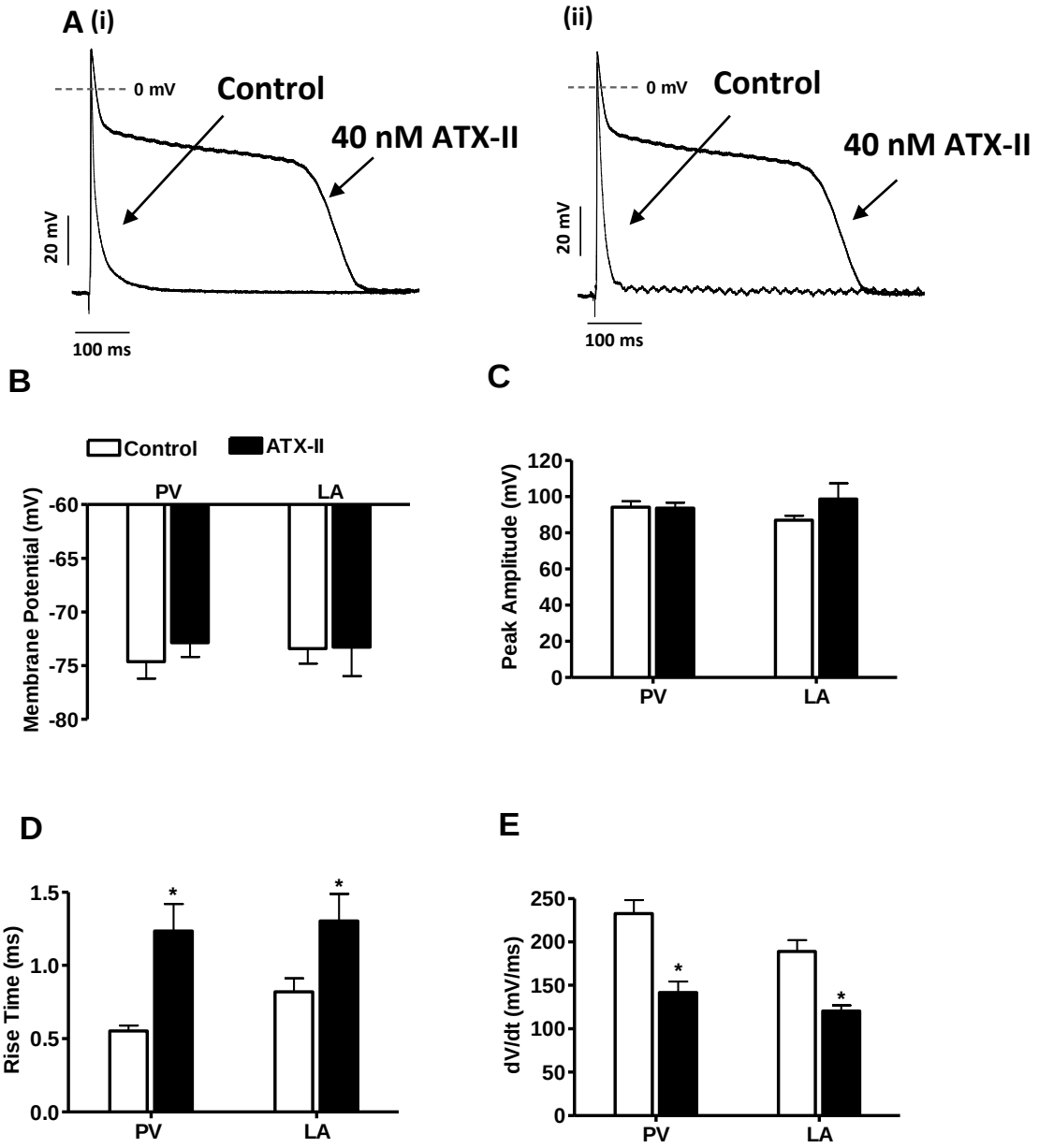

Figure 4.5. **The effect of ATX-II (40 nM) on action potential characteristics of the rat PV and LA.** (A) Superimposed recordings of PV (i) and LA (ii) action potentials elicited by electrical stimulation at 1 Hz during control conditions and in the presence of ATX-II (40 nM). The membrane potential (B); and action potential peak amplitude (C); rise time (D); and dV/dt_{max} (E) elicited by a 1 Hz electrical stimulation frequency, under control conditions (PV, n=10/4; LA n=10/3) and in the presence of 40 nM ATX-II (PV n=11/4; LA n=6/3). All data are presented as mean ± s.e.m. * indicates $P<0.05$ for control *vs.* ATX-II treatment.

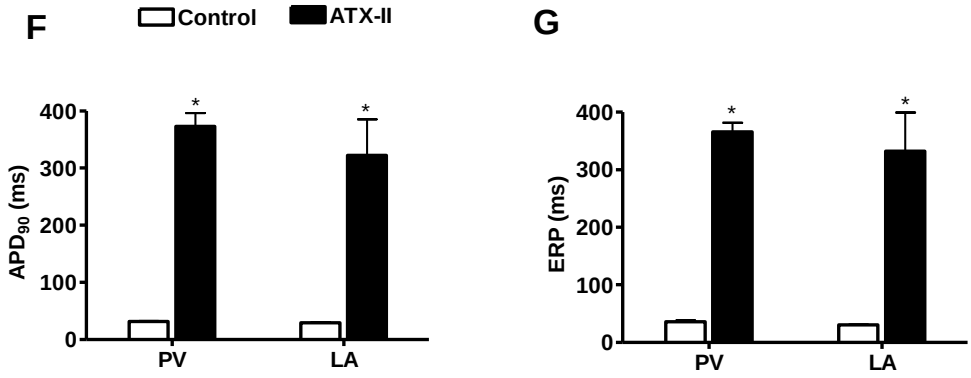

Figure 4.5 (Cont'd). **The effect of ATX-II (40 nM) on action potential characteristics of the rat PV and LA.** The APD_{90} at 1 Hz stimulation (F) and ERP (G), under control conditions (PV, n=10/4; LA n=10/3) and in the presence of 40 nM ATX-II (PV n=11/4; LA n=6/3). All data are presented as mean ± s.e.m. * indicates $P<0.05$ for control *vs.* ATX-II treatment.

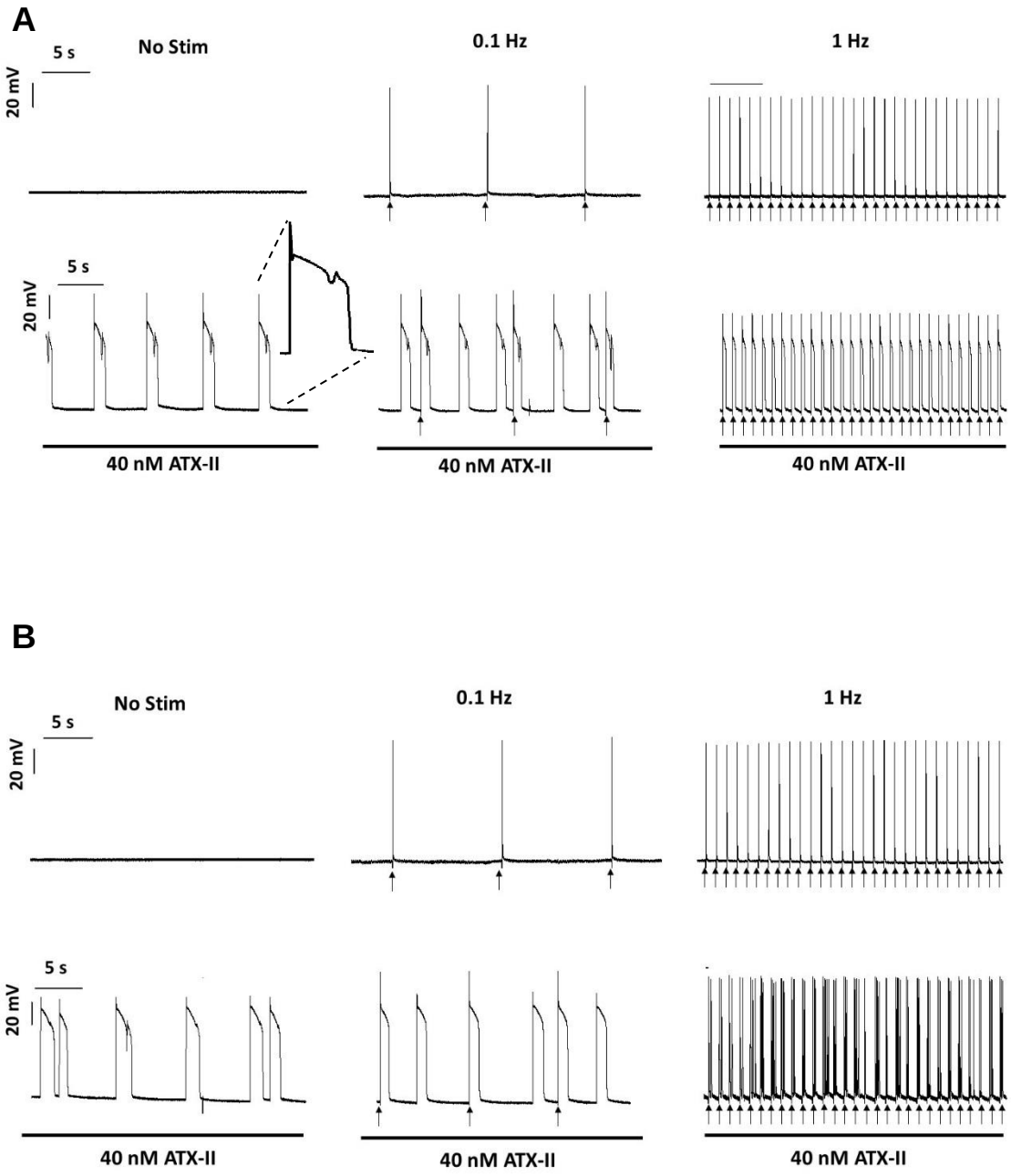

Figure 4.6 **The influence of electrical field stimulation on the ability of ATX-II to induce spontaneous action potentials in the rat PV and LA.** Representative recordings showing ATX-II (40 nM) induced spontaneous action potentials and EADs recorded from the rat PV (A) and LA (B) in the absence of electrical stimulation (no stim) or when electrically stimulated at 0.1 Hz or 1 Hz. The top panels in A and B represent action potentials under control conditions and the bottom panels show the same tissue in the presence of ATX-II (40 nM). An example of an action potential with an EAD is shown inset in A. Arrows represent the electrical stimulus.

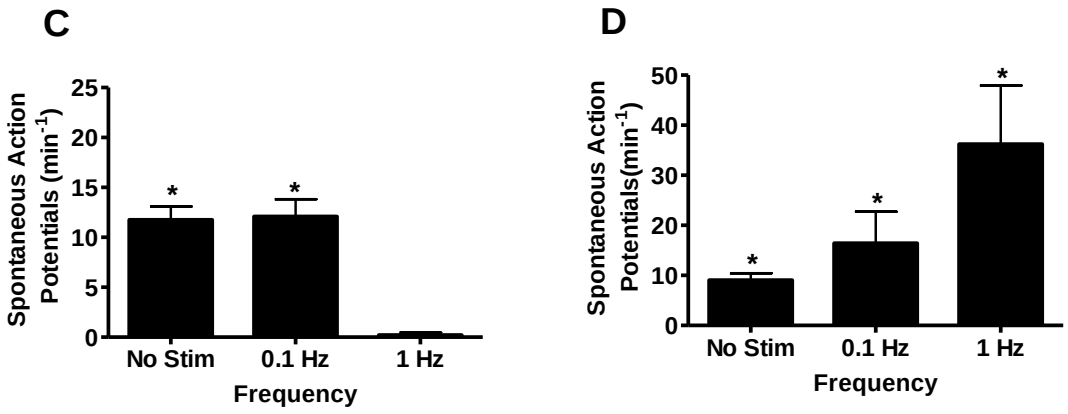

Figure 4.6 (Cont'd) **The influence of electrical field stimulation on the ability of ATX-II to induce spontaneous action potentials in the rat PV and LA.** The number of spontaneous action potentials in PV (C) or LA (D) preparations in the absence of electrical stimulation (PV n=13/4; LA n=13/4), at 0.1 Hz (PV n=10/4; LA n=12/4) and at 1 Hz electrical stimulation (PV n=18/4; LA n=18/4). All data are presented as mean ± s.e.m. * indicates P<0.05 for control *vs.* ATX-II treatment.

Table 4.2 **The effect of increasing the electrical simulation frequency on the generation of ATX-II (40 nM) induced EADs in PV and LA tissues**.

	PV cells with EADs (%)		LA cells with EADs (%)	
	Control	ATX-II (40 nM)	Control	ATX-II (40 nM)
No stim	None detected (n=12/4)	58 ± 22* (n=13/4)	None detected (n=12/4)	81 ± 19* (n=13/4)
0.1 Hz	None detected (n=12/4)	55 ± 6* (n=10/4)	None detected (n=12/4)	81 ± 19* (n=12/4)
1 Hz	None detected (n=20/4)	None detected (n=18/4)	None detected (n=20/4)	18 ± 13 (n=18/4)

The *n* number is reported as: the number of recordings/number of rats. * indicates P<0.05 for control *vs.* ATX-II.

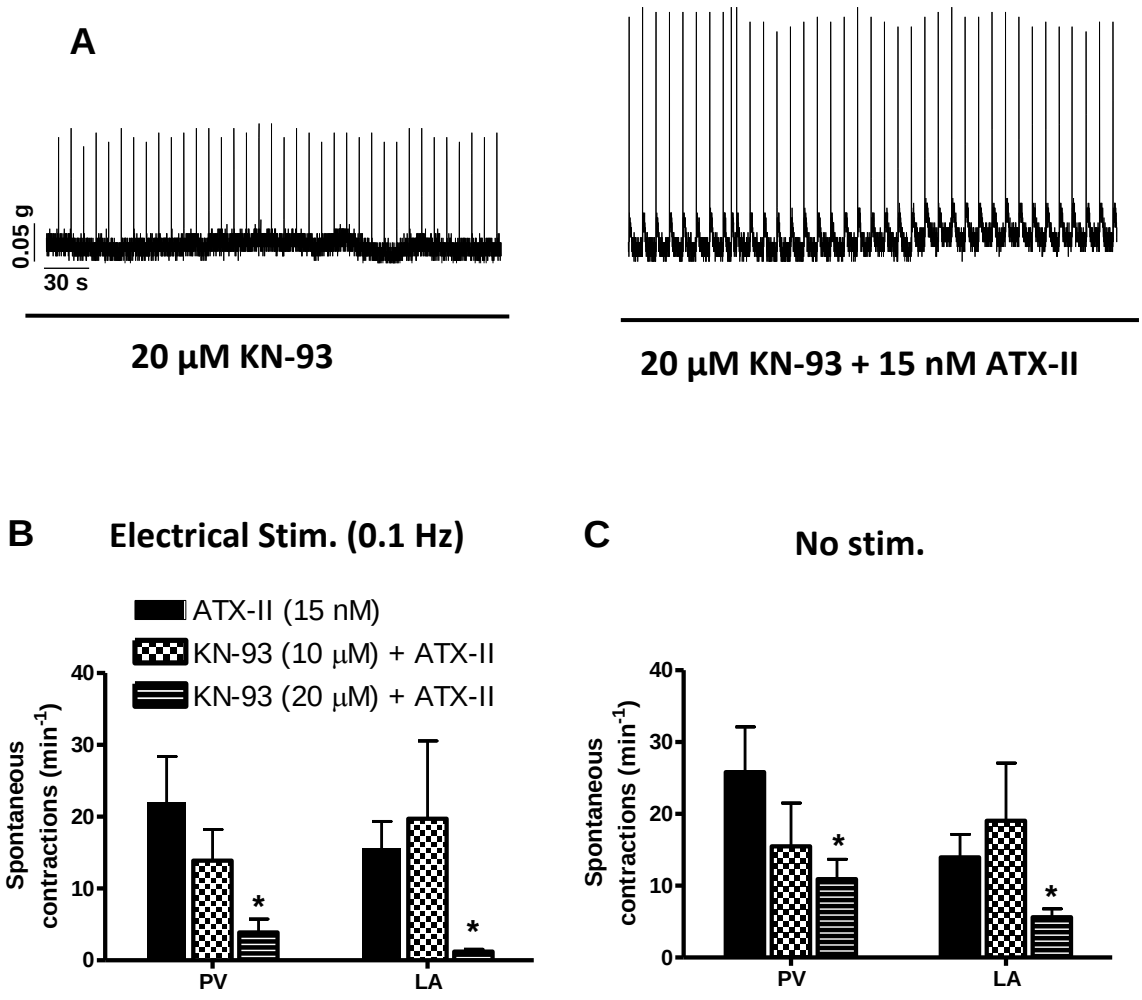

Figure 4.7 **Effect of KN-93 on ATX-II induced spontaneous contractions in the PV and LA.** (A) Representative recordings showing PV contractions during treatment with KN-93 (20 µM) and in the presence of ATX-II (15 nM) after pre-treatment with KN-93, at a stimulation frequency of 0.1 Hz. The number of spontaneous contractions were determined with ATX-II treatment (data obtained from separate group of rats, PV, n=4; LA, n=4) and then examined after 30 minute pre-incubation with KN-93 (10 µM or 20 µM) in the PV (n=4) and LA (n=4) tissues at (B) 0.1 Hz electrical stimulation and (C) no electrical stimulation (no stim.). All data are presented as mean ± s.e.m. * indicates $P<0.05$ for KN-93 treatment *vs.* ATX-II treatment.

Table 4.3 **The effect of KN-93 (20 μM) on the action potentials evoked at 1 Hz electrical stimulation**

	PV (n=3)		LA (n=3)	
	Control	KN-93 (20 μM)	Control	KN-93 (20 μM)
Peak (mV)	91.8 ± 1.6	88.9 ± 4.2	96.9 ± 9.3	98.0 ± 7.8
Rise Time (ms)	0.6 ± 0.1	0.6 ± 0.2	0.7 ± 0.1	1 ± 0.3
dV/dt (mV/ms)	191.5 ± 25.4	194.0 ± 38.2	215.0 ± 40.1	204.7 ± 38.5
APD_{50} (ms)	8.2 ± 1.2	8.9 ± 1.3	8.6 ± 2.8	10.0 ± 3.4
APD_{90} (ms)	31.2 ± 2.5	32.5 ± 3.1	29.9 ± 5.2	34.2 ± 6.4
Membrane Potential (mV)	-72.5 ± 1.3	-71.4 ± 1.7	-78.4 ± 3.1	-78.0 ± 3.4

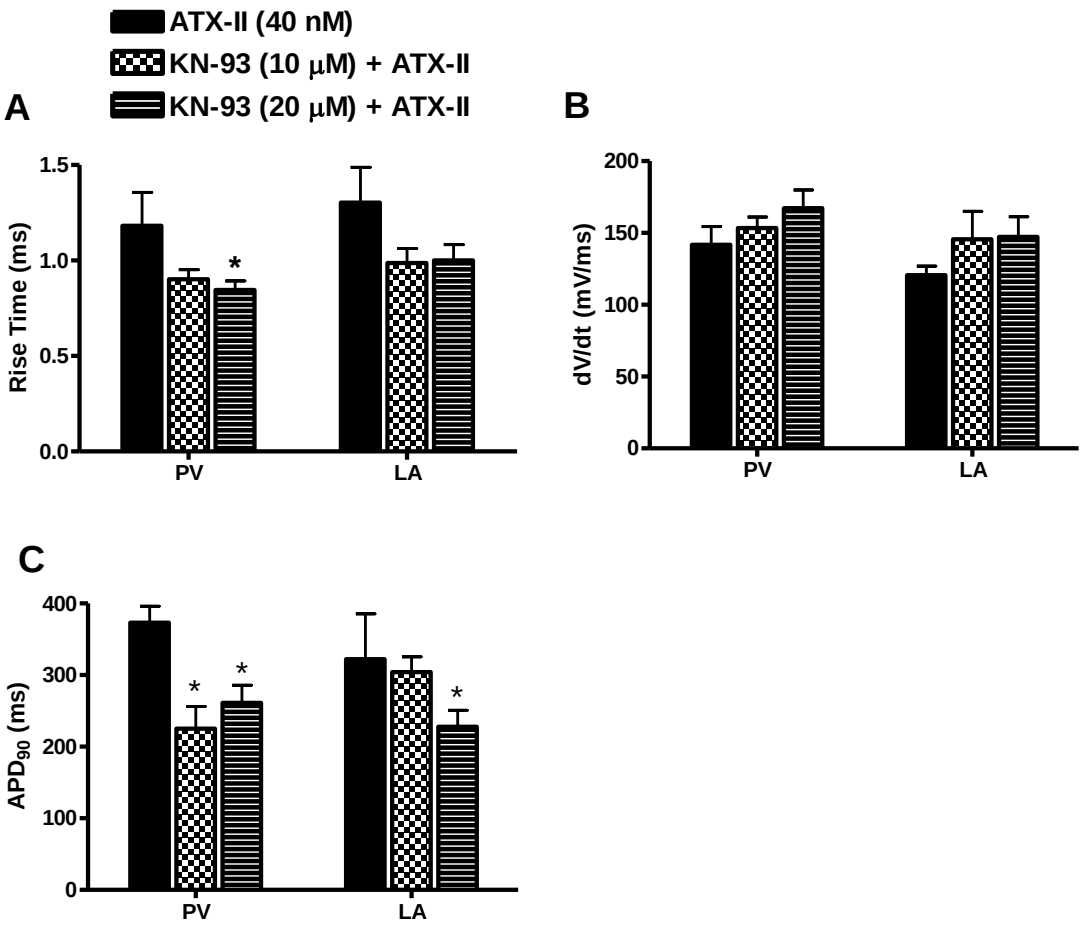

Figure 4.8 **The effect of KN-93 on the ATX-II-induced changes in action potential characteristics of the PV and LA.** Action potential rise time (A); dV/dt_{max} (B); and APD_{90} (C) elicited by stimulation at 1 Hz, in the presence of 40 nM ATX-II (data obtained from separate group of rats, PV, n=11/4; LA, n=6/3). The effect of ATX-II (40 nM) was then examined after incubating the tissue for 30 minutes with 10 μM KN-93 (PV, n=14/4; LA, n=11/4) or 20 μM KN-93 (PV, n=13/3; LA, n=7/3). All data are presented as mean ± s.e.m. * indicates $P<0.05$ for KN-93 + ATX-II treatment *vs.* ATX-II treatment.

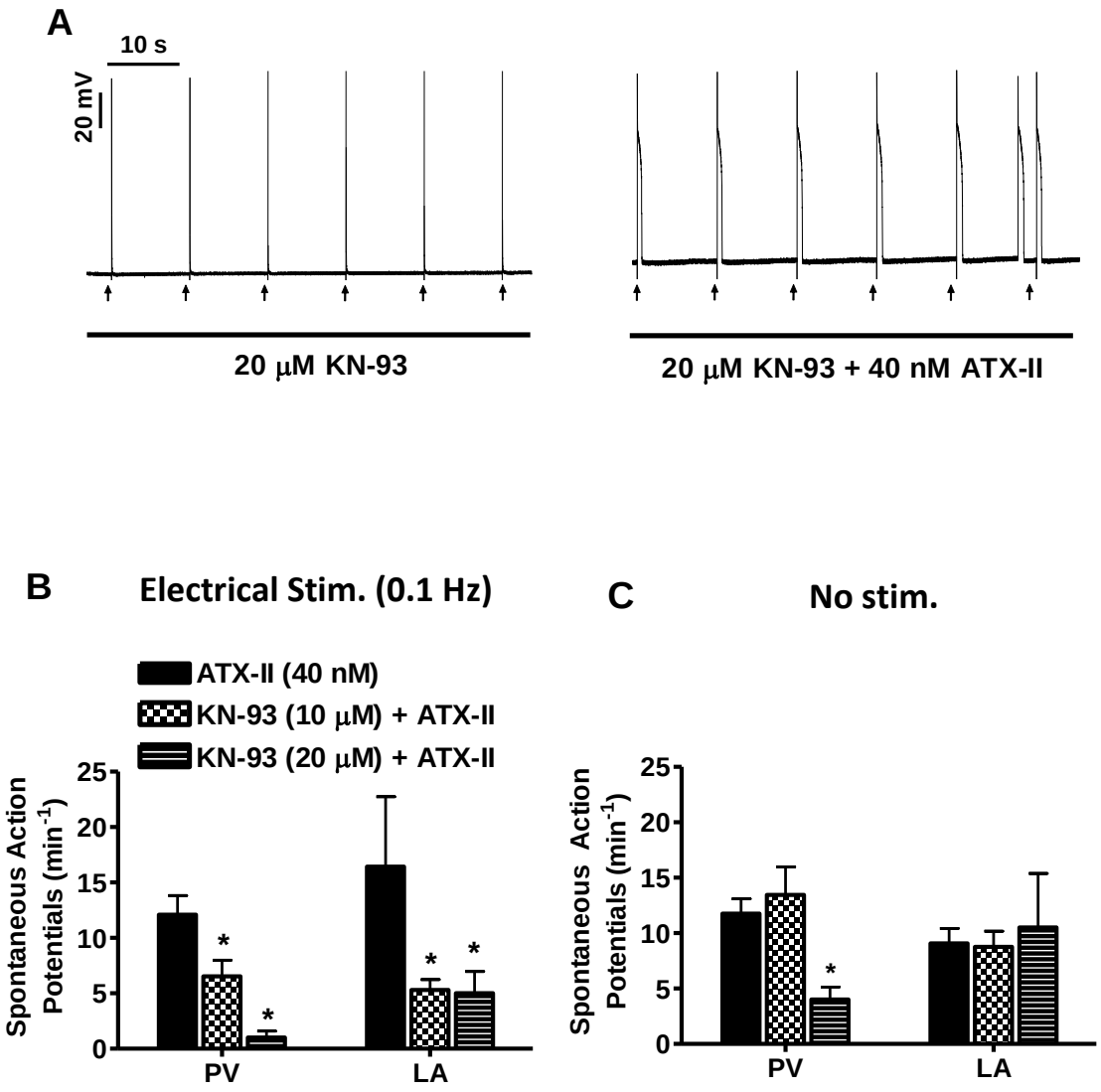

Figure 4.9. **The effect of KN-93 on ATX-II induced spontaneous action potentials.** (A) Representative PV recordings showing action potentials in the presence of KN-93 alone (20 μM, *left panel*) and ATX-II (40 nM) after pre-incubation with KN-93 (20 μM, *right panel*). (B) The rate of ATX-II induced spontaneous action potentials at 0.1 Hz electrical stimulation, in the presence of 40 nM ATX-II (data obtained from separate group of rats, PV, n=10/4; LA, n=12/4) was recorded. The effect of ATX-II (40 nM) was reassessed after incubation with 10 μM KN-93 (PV, n=16/4; LA, n=10/4) or 20 μM KN-93 (PV, n=11/4; LA, n=7/4). (C) Spontaneous action potentials (PV, n=13/4; LA, n=13/4) in the absence of electrical stimulation (no stim.) were also recorded. The effect of ATX-II was examined after pre-incubation with 10 μM (PV, n=16/4; LA, n=8/4) or 20 μM KN-93 (PV, n=13/4; LA, n=7/4). All data are presented as mean ± s.e.m. * indicates $P<0.05$ for KN-93 + ATX-II treatment *vs.* ATX-II treatment. Arrows represent the electrical stimulus.

Table 4.4 **The effect of KN-93 on ATX-II induced EADs in PV and LA tissues**

	PV cells with EADs (%)			LA cells with EADs (%)		
	ATX-II (40 nM)	KN-93 (10 µM) + ATX-II	KN-93 (20 µM) + ATX-II	ATX-II (40 nM)	KN-93 (10 µM) + ATX-II	KN-93 (20 µM) + ATX-II
0.1 Hz	53 ± 3 (n=10/4)	6 ± 6* (n=16/4)	None detected* (n=11/4)	81 ± 19 (n=12/4)	34 ± 19* (n=10/4)	18 ± 10* (n=7/4)
No Stim	58 ± 22 (n=13/4)	None detected* (n=16/4)	None detected* (n=13/4)	81 ± 19 (n=13/4)	42 ± 8 (n=8/4)	None detected* (n=7/4)

The *n* number is reported as: the number of recordings/number of rats.

*indicates P<0.05 for KN-93 treatment *vs.* ATX-II alone.

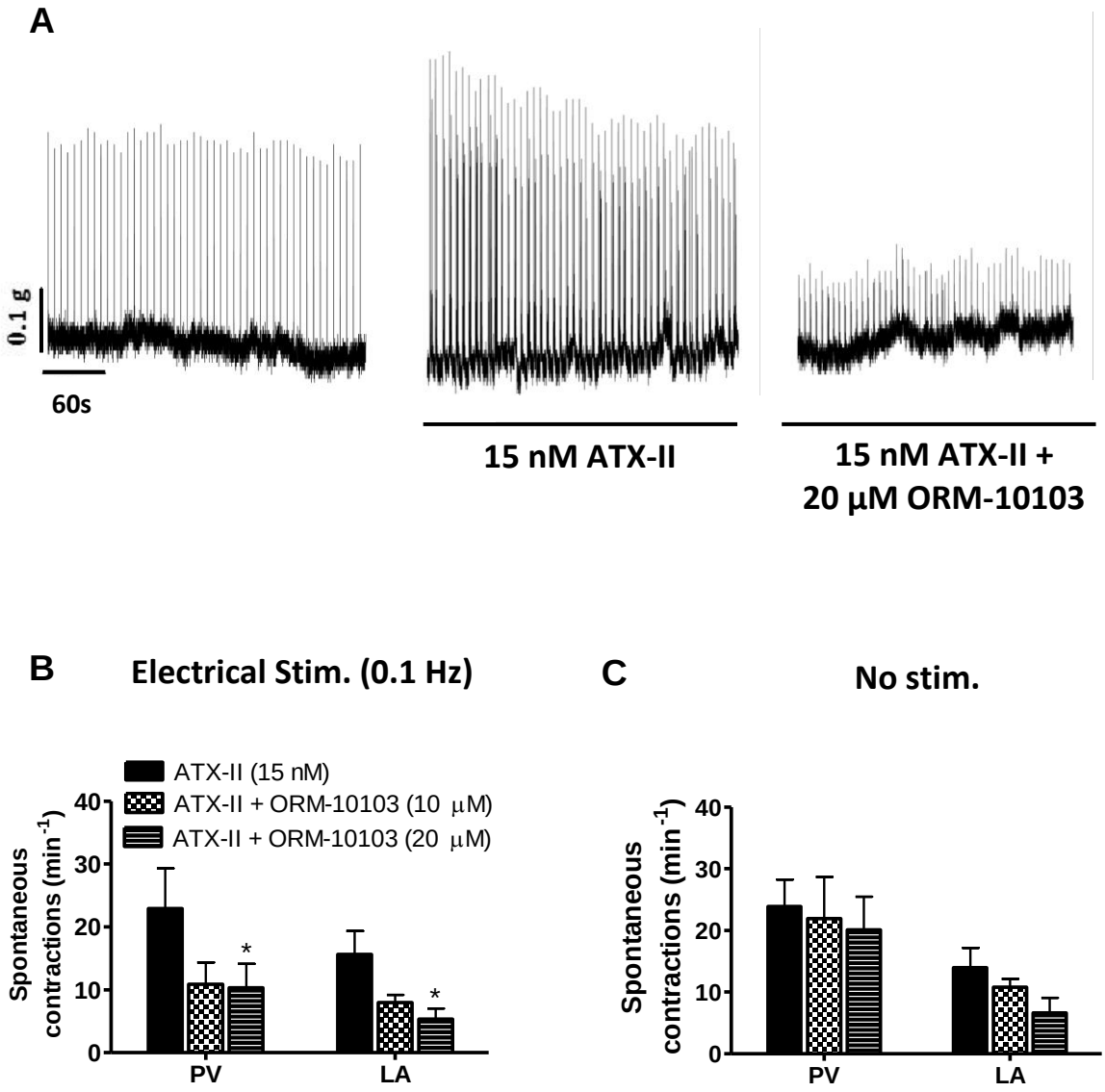

Figure 4.10 **Effect of ORM-10103 on ATX-II induced contractions in the PV and LA.** (A) Representative recording of LA contractions at a stimulation frequency of 0.1 Hz under control conditions (*left panel*), in the presence of ATX-II (15 nM) (*middle panel*) and in the presence of ATX-II and ORM-10103 (20 µM) (*right panel*). Graphs show PV (n=6) and LA (n=4) contractions induced by ATX-II at (B) 0.1 Hz electrical stimulation and (C) no electrical stimulation (no stim.) in the presence of ATX-II alone (15 nM) and after addition of ORM-10103 (10 µM or 20 µM). All data are presented as mean ± s.e.m. * indicates P<0.05 for ATX-II *vs.* ORM-10103 treatment.

Table 4.5. **The effect of 20 μM of ORM-10103 on the action potentials evoked by 1 Hz electrical stimulation**

	PV (n=3)		LA (n=3)	
	Control	ORM-10103 (20 μM)	Control	ORM-10103 (20 μM)
Peak (mV)	84.1 ± 3.4	84.1 ± 2.0	84.7 ± 7.7	86.4 ± 6.4
Rise Time (ms)	0.7 ± 0.1	0.7 ± 0.1	1.2 ± 0.1	1.0 ± 0.2
dV/dt (mV/ms)	144.9 ± 5.9	155.0 ± 0.8	127.0 ± 25.9	134.2 ± 18.6
APD_{50} (ms)	6.6 ± 0.7	6.8 ± 0.9	7.0 ± 1.0	10.2 ± 2.5
APD_{90} (ms)	28.2 ± 2.9	28.8 ± 4.6	29.8 ± 3.5	30.1 ± 4.2
Membrane Potential (mV)	-74.7 ± 2.6	-75.5 ± 3.7	-78.1 ± 4.8	-77.9 ± 4.4

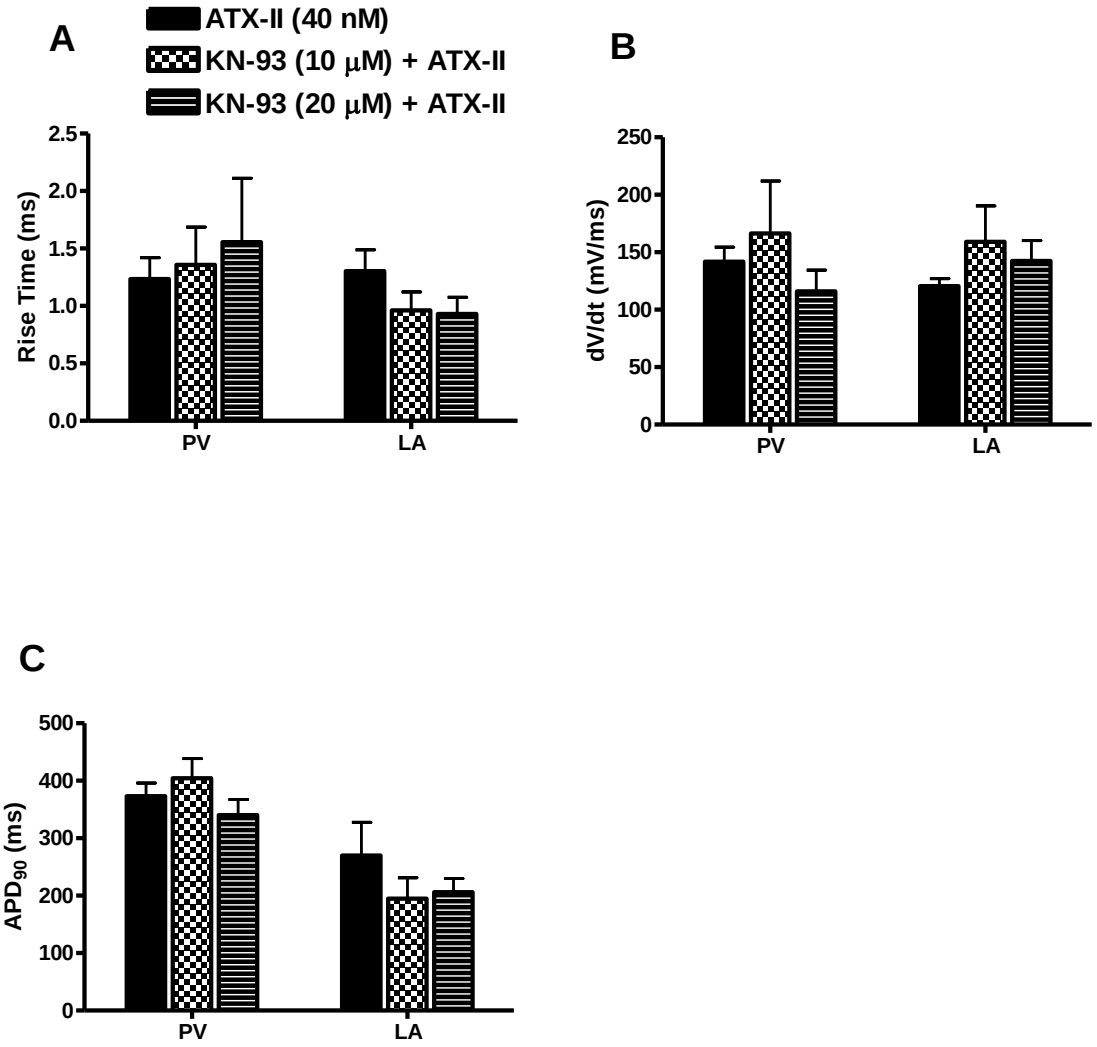

Figure 4.11. **The effect of ORM-1013 on ATX-II induced changes in action potential characteristics of the PV and LA.** Action potential rise time (A); dV/dt_{max} (B); and APD_{90} (C) elicited by electrical stimulation at 1 Hz, in the presence of 40 nM ATX-II (PV, n=11/4; LA, n=6/3) and ATX-II (40 nM) in the presence of 10 μM ORM-10103 (PV, n=9/4; LA, n=8/3) or 20 μM of ORM-10103 (PV, n=8/4; LA, n=8/3 rats). All data are presented as mean ± s.e.m.

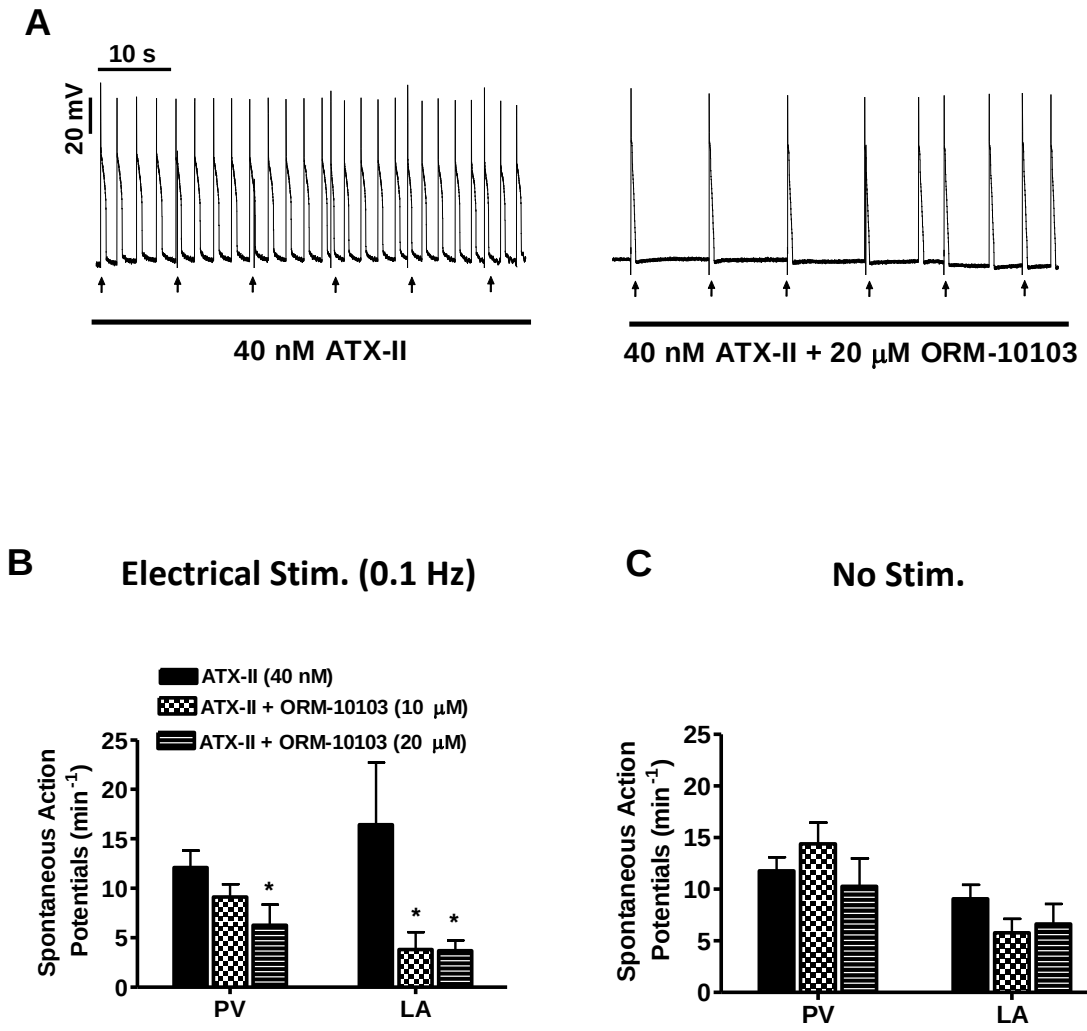

Figure 4.12 **The effect of ORM-10103 on ATX-II induced arrhythmogenic activity.** (A) Representative recordings of the PV in the presence of ATX-II (40 nM) (*left panel*) and after treatment with ORM-10103 (20 μM) (*right panel*). (B) The rate of ATX-II induced spontaneous action potentials in the presence of 40 nM ATX-II (PV, n=10/4; LA, n=12/4) and after treatment with 10 μM ORM-10103 (PV, n=8/4; LA, n=10/4) and then 20 μM ORM-10103 (PV, n=8/4; LA, n=10/4). (C) Summary data in the absence of electrical stimulation (no stim.), of the rate of spontaneous action potentials per minute in the presence of 40 nM ATX-II (PV, n=13/4; LA, n=13/4) and after treatment with 10 μM ORM-10103 (PV, n=8/4; LA, n=8/4) and 20 μM ORM-10103 (PV, n=8/4; LA, n=8/4). All data are presented as mean ± s.e.m. * indicates $P<0.05$ ATX-II treatment *vs.* ORM-10103 treatment. Arrows represent the electrical stimulus.

Table 4.6 **The effect of ORM-10103 on ATX-II induced EADs in PV and LA tissues**

	PV cells with EADs (%)			LA cells with EADs (%)		
	ATX-II (40 nM)	ATX-II + ORM (10 µM)	ATX-II + ORM (20 µM)	ATX-II (40 nM)	ATX-II + ORM (10 µM)	ATX + ORM (20 µM)
0.1 Hz	53 ± 14 (n=10/4)	25 ± 25 (n=8/4)	33 ± 19 (n=8/4)	81 ± 19 (n=10/4)	42 ± 21 (n=10/4)	50 ± 14 (n=10/4)
No Stim	42 ± 30 (n=13/4)	44 ± 29 (n=8/4)	22 ± 22 (n=8/4)	81 ± 19 (n=13/4)	50 ± 29 (n=8/4)	42 ± 30 (n=8/4)

The *n* number is reported as: the number of recordings/number of rats.

4.4 Discussion

4.4.1 The effect electrical stimulation rate on ATX-II induced spontaneous contractions

Treatment with ATX-II (15 nM) induced contractions in the absence of electrical stimulation as well as at electrical stimulation frequencies up to 0.3 Hz in PV tissues and up to 1 Hz in LA tissues. Therefore highlighting the ability of ATX-II to induce arrhythmogenic activity in the rat PV and the LA. Previous studies in mouse and guinea pig isolated atrial cardiomyocytes demonstrated that ATX-II directly increased the I_{NaL} (Song *et al.*, 2008; Fischer *et al.*, 2015). Wolkowicz *et al.* (2014) showed that the ATX-II induced increase in the I_{NaL} could initiate spontaneous contractions in rat LA preparations, which were attenuated by inhibition of the I_{NaL} with ranolazine. Therefore in the current study, the spontaneous contractions observed in the PV and LA tissues may be attributed to an ATX-II mediated increase in $I_{NaL.}$ This could lead to Na^+ dependent Ca^{2+} accumulation in the cytosol (Sossalla *et al.*, 2008), which is associated with contractile dysfunction in cardiomyocytes (Undrovinas *et al.*, 2010). The spontaneous contractions displayed a rate dependent relationship with the electrical stimulation frequency in both tissues, as the extra contractions were abolished at higher (> 1 Hz) electrical stimulation frequencies. This is in agreement with Wolkowicz *et al.* (2014), who reported that spontaneous contractions were abolished at frequencies above 1 Hz in the rat LA. The abolition of the ATX-II induced spontaneous contractions at higher electrical stimulation frequencies in both tissues is also thought to suggest the ATX-II arrhythmogenic activity is attributed to the I_{NaL}. Guo *et al.* (2011) demonstrated the electrical stimulation rate dependence of the I_{NaL}, as a reduction in I_{NaL} density was recorded at more rapid electrical stimulation frequencies. At faster electrical stimulation rates, Na^+ channels become increasingly inactivated and so the reduction of the I_{NaL} at these more rapid electrical stimulation frequencies is attributed to the channels slow inactivation and recovery kinetics (Guo et al., 2011). In addition, since the Na^+ channel kinetics were similar between the PV and LA (as previously shown in Section 3.3.3), the suppression of ATX-II extra contractions by a lower electrical stimulation frequency in the PV in comparison to the LA could suggest an increased sensitivity of the LA to ATX-II, compared to the PV. A recent study revealed rabbit

LA cardiomyocytes exhibited an enhanced sensitivity to ATX-II and ranolazine in comparison to left ventricular cardiomyocytes as the EC_{50} of ATX-II was lower in atrial cardiomyocytes in comparison to ventricular cardiomyocytes (Luo *et al.*, 2014). Furthermore, ranolazine decreased I_{NaL} more in atrial than ventricular cardiomyocytes (Luo *et al.*, 2014). This was thought to be attributed to a larger I_{NaL} current density in the LA cardiomyocytes (Luo *et al.*, 2014).

In contrast, Malécot *et al.* (2014) reported the absence of I_{NaL} in rat PV and LA cardiomyocytes. Although, during their whole cell patch clamp studies they observed a small current typical of I_{NaL}, this was not blocked by the I_{NaL} inhibitor, ranolazine. However, the external solution only contained 30 mM NaCl, which may not provide sufficient Na^+ influx to observe the I_{NaL}. Other groups tend to use a more physiological external NaCl concentration of around 140 mM, to allow measurement of I_{NaL} in cardiomyocytes (Maltsev *et al.*, 1998, 2007; Undrovinas *et al.*, 2006, 2010; Luo *et al.*, 2014).

In the current study, treatment with ATX-II did not alter the shape or time course of the contractions, as the spontaneous contraction upstroke and duration in both tissues was similar to those of the electrically evoked contractions under control conditions. Similar results were also recorded in guinea pig papillary muscles (Ravens, 1976).

4.4.2 The effect of ATX-II on the action potential characteristics of the PV and LA

The presence of the lower ATX-II concentration (15 nM), altered the rise time, rate of rise and APD_{90} of electrically evoked action potentials in the PV, but only affected the APD_{90} in the LA. However, increasing the ATX-II concentration to 40 nM altered the characteristics of the electrically evoked action potentials in both the PV and LA. This effect of ATX-II is presumably due to an increase in $I_{NaL,}$ since previous studies in LA cardiomyocytes have shown that ATX-II enhances I_{NaL} (Song *et al.*, 2008, 2009). The ATX-II mediated increase in rise time and decrease in the rate of rise in both tissues shown in the current study, was also previously reported by Ravens, (1976) in guinea pig ventricular papillary muscles. The prolongation of

the APD_{90} and increase in the ERP recorded in both PV and LA tissues after treatment with ATX-II is also in agreement with similar studies on guinea-pig isolated atrial cardiomyocytes (Song *et al*., 2008) and rabbit PV preparations (Lu *et al*., 2012; Chen *et al*., 2014). A balance of inward and outward currents usually determines the APD (Carmeliet and Mubagwa, 1998), and ATX-II is thought to shift the balance of currents in favour of inward currents, which prolongs the APD (Antzelevitch, 2004). An increase in APD is a well-known characteristic of an enhanced I_{NaL} (Kiyosue and Arita, 1989; Liu *et al.*, 1992; Song *et al.*, 2004, 2008), further supporting the assumption in this study that the ATX-II induced effects in the PV and LA are mediated by an increase in $I_{NaL.}$ In addition, the prolonged APD_{90} was more pronounced at the lower electrical stimulation frequency of 0.1 Hz, compared to 1 Hz, in both tissues (Appendix, Figure 6.12). This is likely due to the ATX-II induced increase in I_{NaL}, since I_{NaL} is thought to be greater at lower frequencies (Zygmunt *et al.*, 2001; Grandi *et al*., 2007; Guo *et al*., 2011). Although AF is usually associated with an abbreviated APD, a prolonged APD is also associated with this arrhythmia (Benito *et al.*, 2008; Zellerhoff *et al.*, 2009). Several gain of function SCN5A mutations, which are common to LQTS, are associated with increased I_{NaL}, prolonged APD and a high incidence of AF (Benito *et al*., 2008; Zellerhoff *et al.*, 2009).

4.4.3 The contribution of TTX-sensitive sodium channels to ATX-II mediated activity

In the present study, inhibition of TTX-sensitive Na^+ channels with TTX (100 nM) did not alter the spontaneous contractions in either the PV or LA tissue. This suggests that blockade of TTX-sensitive channels alone is not sufficient to reduce ATX-II induced arrhythmogenesis. However, the higher concentration of TTX (10 µM) suppressed the ATX-II induced spontaneous contractions in both tissues. In previous studies inhibition of TTX-sensitive and TTX-resistant Na^+ channels with micromolar concentrations of TTX decreased I_{NaL} in human ventricular cardiomyocytes as well as decreasing the I_{NaL} enhanced by ATX-II (Isenberg and Ravens, 1984; Maltsev *et al.*, 1998). Moreover, micromolar concentrations of TTX also suppressed ATX-II induced EADs and DADs in ventricular cardiomyocytes

(Maltsev *et al*., 1998; Song *et al*., 2008; Sag *et al*., 2014) and attenuated the ATX-II induced prolongation of the APD (Ravens, 1976; Studenik *et al*., 2001). Thus, suggesting that inhibition of both TTX-resistant and TTX-sensitive Na^+ channels is needed to reduce ATX-II induced arrhythmogenic activity. The Na^+ dependence of I_{NaL} induced arrhythmias has also been shown in rat and rabbit PV as well as rat and guinea pig atrial preparations as ATX-II induced activity was suppressed by ranolazine (Song *et al.*, 2008; Lu *et al.*, 2012; Wolkowicz *et al.*, 2014).

The ability of 100 nM TTX to slightly attenuate the ATX-II mediated prolongation of the APD_{90} in the PV suggests that there could be a small TTX-sensitive Na^+ channel contribution to this effect in PV cardiomyocytes. This is in agreement with Nishio *et al.* (1991) who observed a reduction in the ATX-II induced prolongation of the $APD_{90,}$ by inhibition of the TTX-sensitive Na^+ channels in guinea pig papillary preparations.

4.4.4 Treatment with ATX-II induces spontaneous action potentials and EADs in PV and LA tissues

Increasing the ATX-II concentration to 40 nM resulted in arrhythmogenic activity in the form of spontaneous action potentials and EADs in both PV and LA tissues. Previous studies on the rabbit PV and guinea pig atrium also reported the appearance of EADs and spontaneous action potentials in the presence of ATX-II, which was inhibited by ranolazine (Song *et al.*, 2008; Lu *et al.*, 2012; Chen *et al.*, 2014). Therefore the spontaneous action potentials and EADs were likely due to an increase in the I_{NaL}, which could lead to ectopic activity in the PV. Song *et al.* (2008) reported that the ATX-II induced action potentials were thought to stem from DADs and EADs, in line with an accumulation of intracellular Ca^{2+}, secondary to an enhanced I_{NaL}. The ATX-II induced DADs and triggered activity were attributed to an increase in the I_{ti}, which is associated with Ca^{2+} overload (Song *et al.*, 2008), whereas the ATX-II induced EADs are thought to be due to the prolonged APD (Song *et al.*, 2008).

4.4.5 The effect of KN-93 on ATX-II induced arrhythmogenic activity in PV and LA tissues

The suppression of ATX-II induced spontaneous contractions by pre-incubation of the PV or LA with the CaMKII inhibitor, KN-93, suggests the involvement of CaMKII in this arrhythmogenic activity. These results support the findings of Wolkowicz *et al*. (2014) in which KN-93 also inhibited spontaneous contractions induced by ATX-II in the rat LA. In the present study, the requirement for CaMKII activity in ATX-II mediated arrhythmogenesis in PV and LA tissues was further demonstrated by the finding that KN-93 attenuated the rate of spontaneous action potentials and the appearance of EADs. This is in agreement with previous investigations in mouse ventricular cardiomyocytes where inhibition of CaMKII by AIP reduced ATX-II dependent DADs (Sag *et al*., 2014). Since ATX-II is thought to increase I_{NaL}, then CaMKII activation may play a role in I_{NaL} mediated arrhythmogenic activity in PV and LA tissues. Furthermore, inhibition of CaMKII also prevented isoproterenol or phenylephrine induced EADs and DADs in rabbit PV preparations (Lo *et al.*, 2007). Sag *et al.* (2014) reported that treatment of mouse ventricular cardiomyocytes with ATX-II increased the activation of CaMKII, which was reversed by ranolazine. Therefore it is likely the ATX-II mediated increase in I_{NaL} in PV and LA tissues resulted in an increase in CaMKII activity.

In the present study, CaMKII inhibition also attenuated the ATX-II induced APD_{90} prolongation in both the PV and LA. Since prolongation of the APD promotes EADs in cardiac tissue (January and Riddle, 1989; Zeng and Rudy, 1995), the suppression of EADs could be attributed to the reduction in APD_{90}. This is consistent with an earlier study in rabbit isolated ventricular cardiomyocytes, which reported that the ability of the non-specific I_{NaL} activator H_2O_2 to prolong the APD and induce EADs was attenuated by the presence of KN-93 (Xie *et al.*, 2009).

Though KN-93 is thought of as a relatively selective blocker for CaMKII, previous studies have demonstrated non-specific effects on other ion channels. Specifically KN-93 at a concentration above 1μM was shown to inhibit several voltage gated K^+ channels in heterologous cell lines (Rezazadeh *et al.*, 2006). In addition, Gao *et al.*

(2006) reported that in a neuroblastoma cell line transfected with $Ca_v1.3$, 10 µM KN-93 suppressed the L-type Ca^{2+} current. As enhanced L-type Ca^{2+} current can contribute to the generation of EADs (January and Riddle, 1989), the KN-93 suppression of EADs could be partly due to decrease in L-type Ca^{2+} current. However, the highest concentration of KN-93 had no effect on action potential parameters in this study, including the APD_{50} which has previously been shown to be reduced by L-type Ca^{2+} channel blockers (Mitchell *et al.*, 1984; Schouten and Keurs, 1985). The lack of effect of KN-93 on action potential characteristics highlights that CaMKII does not play a key role in action potential characteristics of the PV and LA under control conditions. This is in line with previous work in which KN-93 had no effect on the APD of rabbit PV (Lo *et al.*, 2007) or ventricular cardiomyocytes (Anderson *et al.*, 1998). The inactivate derivative of KN-93, KN-92, which lacks kinase activity but inhibits a number of similar ion channels in comparison to KN-93 (Anderson et al., 1998; Chelu et al., 2009; Xie et al., 2009; Wolkowicz et al., 2014) could be used in future to establish if the anti-arrhythmic effect observed in the presence of KN-93 is due to the inhibition of CaMKII or non-specific effects on ion channels.

Although these results suggest that CaMKII activity contributes to ATX-II mediated arrhythmogenesis in the PV and LA, further work is needed in order to fully elucidate its arrhythmogenic action. An upregulation in CaMKII activity can affect Na^+ channel gating, resulting in increased I_{NaL} and accumulation of intracellular Na^+ in ventricular cardiomyocytes (Wagner *et al.*, 2006, 2011). The increase in intracellular Na^+ can lead to Na^+ dependent Ca^{2+} overload, which has been shown to enhance CaMKII phosphorylation (Sag *et al.*, 2014). This could in turn lead to a positive feedback loop of CaMKII activation and intracellular Na^+ accumulation, promoting arrhythmogenesis (Sag *et al.*, 2014). A simplistic representation of this positive feedback loop is shown in Figure 4.13. In addition, the increase in CaMKII activity could also promote phosphorylation of the ryanodine receptor, leading to Ca^{2+} release from the sarcoplasmic reticulum (Neef *et al.*, 2010; Fischer *et al.*, 2015). Neef *et al.* (2010) reported an increase in phosphorylation of the ryanodine receptor type 2 at the CaMKII specific Ser 2814 site, in line with an increase in CaMKII

expression and CaMKII activity in cardiomyocytes from the right atrial appendage of human AF patients. This CaMKII mediated hyperphosphorylation of the ryanodine receptor is thought to be responsible for the arrhythmogenic sarcoplasmic reticulum Ca^{2+} leak and increased diastolic Ca^{2+} in the atrial cardiomyocytes from AF patients (Neef *et al.*, 2010). In mouse ventricular cardiomyocytes, exposure to ATX-II resulted in an increased diastolic sarcoplasmic reticulum Ca^{2+} loss, despite an unaltered sarcoplasmic reticulum content, which resulted in DADs (Sag *et al.*, 2014). A decrease in the intracellular Na^{+} concentration by TTX and ranolazine or block of CaMKII reduced the sarcoplasmic Ca^{2+} loss and suppressed the DADs, further demonstrating the role of an increased intracellular Na^{+} concentration and CaMKII activity in sarcoplasmic Ca^{2+} loss (Sag *et al*., 2014). Activation of CaMKII may also phosphorylate I_{CaL}, slowing I_{CaL} inactivation, which would prolong the APD and lead to EADs (Qi *et al.*, 2009).

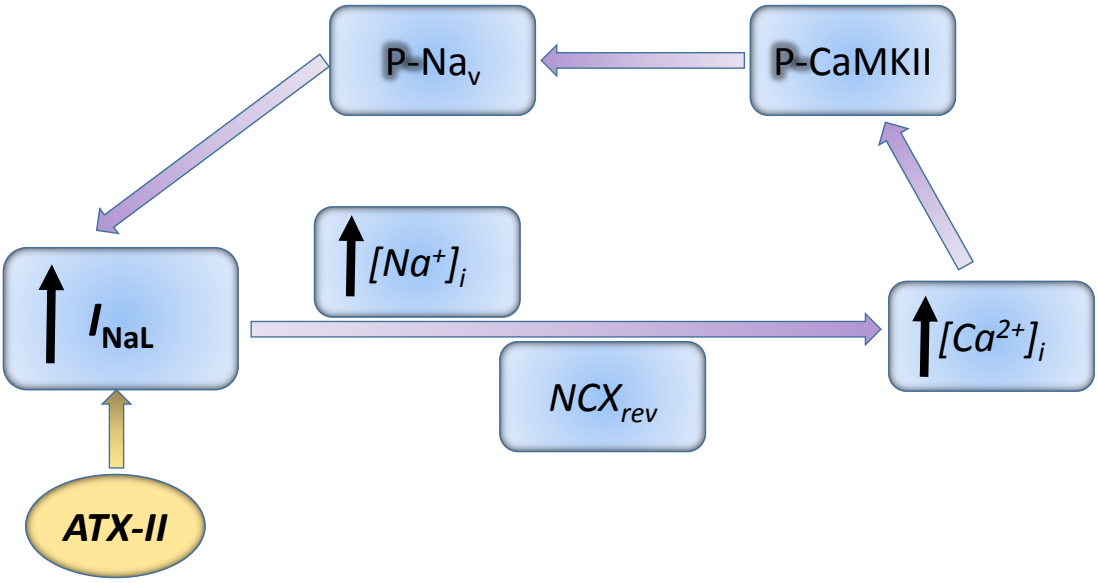

Figure 4.13. **Simplistic representation of the ATX-II induced positive feedback loop.** The presence of ATX-II increases the I_{NaL}, leading to accumulation of intracellular Na^+ and activation of reverse mode NCX. This resultant increase in intracellular Ca^{2+} can activate CaMKII, which phosphorylates Na^+ channels, subsequently increasing the I_{NaL}.

4.4.6 The effect of ORM-10103 on ATX-II induced arrhythmogenesis in PV and LA tissues

The suppression of ATX-II induced spontaneous contractions and spontaneous action potentials by ORM-10103, when the tissue was electrically stimulated at 0.1 Hz, suggests that the NCX contributes to ATX-II mediated arrhythmogenic activity in the PV and the LA. In ventricular cardiomyocytes, it has been shown that arrhythmogenic activity could be triggered by a Ca^{2+} induced increase in forward mode NCX, generating the I_{ti} (Tweedie *et al.*, 2000; Fujiwara *et al.*, 2008) or increased reverse mode NCX to remove excess intracellular Na^{+}, leading to Ca^{2+} overload (Faber and Rudy, 2000; Sossalla *et al.*, 2008; Undrovinas *et al*., 2010). Treatment with ORM-10103 reduced the ATX-II induced increase in intracellular Ca^{2+} in dog ventricular cardiomyocytes, and the activity was thought to be primarily due to the reverse mode of the NCX (Nagy *et al.*, 2014). This could suggest that ORM-10103 may exert its antiarrhythmogenic action by reducing the Na^{+} induced Ca^{2+} overload. Whether this is also the case in PV and LA cardiomyocytes awaits further study.

Inhibition of NCX by ORM-10103 did not suppress EADs in either of the tissues, suggesting that ATX-II induced EADs in the PV and LA are not dependent on forward or reverse mode NCX. Song *et al*. (2008) showed that the less selective NCX blocker KB-R7943 also failed to inhibit ATX-II induced EADs in guinea pig atrial cardiomyocytes. Furthermore, they reported that the ATX-II induced EADs were not inhibited by the sarcoplasmic reticulum Ca^{2+} release inhibitor ryanodine, or the Ca^{2+} chelators EGTA and BAPTA suggesting that the EADs are unlikely to be due to forward mode NCX following Ca^{2+} release from the sarcoplasmic reticulum (Song *et al*., 2008). Previous studies have demonstrated that the ATX-II induced EADs in LA cardiomyocytes were suppressed by TTX (at μM concentrations) or ranolazine and so they are reliant on Na^{+} influx (Song *et al.*, 2008). In the current study ORM-10103 did not suppress the ATX-II induced prolongation of APD_{90}. Since EADs occur when the APD is prolonged (January and Riddle, 1989; Clancy *et*

al., 2003), the lack of effect of ORM-10103 on the ATX-II induced APD prolongation could also explain the lack of EAD inhibition by ORM-10103. This is in agreement with a previous study which reported that selective NCX inhibition did not reduce ATX-II induced APD prolongation in dog papillary muscles and Purkinje fibres (Nagy *et al*., 2014).

The lack of effect of the NCX inhibitor, ORM-10103, on the action potential characteristics of the PV and LA is also consistent with Nagy *et al*. (2014) who reported a lack of effect of ORM-10103 on electrically evoked action potentials from dog papillary muscle and Purkinje fibre preparations. They hypothesised that the lack of effect of NCX inhibition on the action potential is due to compensation by other repolarising currents as a consequence of the strong repolarisation reserve in cardiomyocytes (Roden, 1998; Biliczki et al., 2002). The failure of ORM-10103 (20 µM) to alter the action potential characteristics suggests that this inhibitor may not exhibit non-specific effects on a number of ion channels. Although previous work by Jost *et al.* (2013) showed that ORM-10103 at the lower concentration of 10 µM had no effect on $I_{CaL,}$ the Na^+/K^+ pump or the main K^+ currents, with the exception of a small reduction in I_{Kr}, it is currently unknown if the higher concentration of 20 µM ORM-10103 effects these ion currents.

4.4.7 Summary

In summary, the results show that the presence of ATX-II leads to arrhythmogenic spontaneous contractions, action potentials and EADs in both PV and LA tissues, which may be due to an ATX-II induced increase in I_{NaL}. Therefore an increase in I_{NaL} could be an underlying mechanism in ectopic activity generated in PV or LA preparations which can lead to AF. Enhanced I_{NaL} also leads to a prolonged APD_{90} in both tissues, which generates EADs. The TTX-sensitive Na^+ channels may contribute to I_{NaL} in the PV, although block of the TTX-sensitive channels alone was not sufficient to suppress I_{NaL} mediated arrhythmogenic activity. Lastly, CaMKII and NCX activation contributes to ATX-II mediated arrhythmogenic activity in PV and LA tissues, although EADs are not dependent on the NCX.

Chapter 5

General Discussion

5.1 General Discussion

5.1.1 Characteristics of the I_{Na} in the PV and LA

Characterisation of the electrophysiological properties of the rat PV and LA revealed that there was no obvious difference in the action potential characteristics of the cardiomyocytes in either tissue. This similarity in the action potentials is consistent with previous studies in rat tissues (Miyauchi *et al.*, 2004, 2005). Since the action potential peak amplitude, rise time, rate of rise, and ERP are primarily governed by the properties of the Na^+ channels, this suggests that the Na^+ channel properties are also similar in both tissues. This was supported by subsequent studies on isolated cardiomyocytes from the PV and LA, where no significant difference in the I_{Na} density, or the activation and inactivation characteristics of the I_{Na} was found.

5.1.2 The TTX-sensitive I_{Na} in the PV and LA

Although there was no significant difference in the total I_{Na} in PV and LA cardiomyocytes, the lack of a TTX-sensitive I_{Na} in LA cardiomyocytes, suggests that there may be a difference in the expression of Na^+ channel isoforms in the two tissues. It is not yet clear whether this could be attributed to the absence of $Na_v1.1$ mRNA in the LA, since in the current study $Na_v1.1$ mRNA was absent in LA tissue. Although the immunocytochemistry studies with the $Na_v1.1$ antibody appeared to detect this subunit in the LA, western blotting is required to confirm the specificity of this antibody for $Na_v1.1$.

As established in the present study, the TTX-sensitive Na^+ channel isoforms are not significantly involved in initiating the action potential in the PV or LA. However, it has been hypothesised that the more depolarised activation properties of the TTX-sensitive Na^+ channels may aid in preserving normal cardiac excitation in disease conditions, where the myocardium is likely to be more depolarised (Huang *et al.*, 2001; Protas *et al.*, 2009; Anyukhovsky *et al.*, 2011). For example, rat and mouse ventricular cardiomyocytes transfected with $Na_v1.4$ displayed a greater ability to preserve the action potential dV/dt_{max} under depolarised conditions (high K^+ concentration), compared to cardiomyocytes without the transfection (Protas *et al.*, 2009; Anyukhovsky *et al.*, 2011). This is not a property of the main cardiac Na^+

channel, as overexpression of $Na_v1.5$ did not provide the same enhanced ability to preserve the action potential dV/dt_{max} in depolarised conditions (Protas et al., 2009). A number of studies have observed an increase in the mRNA expression of TTX-sensitive Na^+ channels in ventricular tissue from animal models with disease conditions associated with AF. Upregulation of $Na_v1.1$ mRNA was reported in ventricular preparations from rat and dog myocardial infarction and heart failure models (Huang *et al.*, 2001; Xi *et al.*, 2009; Mishra *et al.*, 2014). In addition, an increased expression of $Na_v1.6$ was observed in ventricular cardiomyocytes from the rat heart failure model (Xi *et al.*, 2009). Thus, it is reasonable to hypothesise that TTX-sensitive Na^+ channels could also aid in preserving the dV/dt_{max} in depolarised conditions in the PV and LA. Future work could determine whether the TTX-sensitive Na^+ channel subunits are also upregulated in the PV and LA from animal models with pathologies that may predispose to AF and where the cardiomyocytes can be depolarised, such as heart failure (Chang *et al.*, 2011).

The small reduction in contraction of the PV and LA observed after block of the TTX-sensitive Na^+ channels, suggests that they may play a minor role in excitation contraction coupling. However, there is an uncertainty to the involvement of TTX-sensitive channels in the decrease in contraction amplitude in the LA, since there was no evidence of the TTX-sensitive I_{Na} in the LA cardiomyocytes. It is possible that block of the TTX-sensitive channels in neurons by TTX, thereby preventing neurotransmitter release, contributed to the observed decrease in contractility. Therefore, further work is needed to give clearer insight into the role of TTX-sensitive Na^+ channels in excitation-contraction coupling in the PV and LA. Previous studies in rat ventricular cardiomyocytes have also shown that inhibition of TTX-sensitive Na^+ channels increased the Ca^{2+} transient latency (Lines *et al.*, 2006), reduced sarcoplasmic reticulum Ca^{2+} release, and decreased the Ca^{2+} transient amplitude in rabbit ventricular cardiomyocytes (Torres *et al.*, 2010). This has led to the hypothesis that TTX-sensitive Na^+ channels can modulate sarcoplasmic reticulum Ca^{2+} release as they also reside in couplons. The Na^+ accumulation could activate reverse mode of the NCX, thereby priming the dyadic cleft with Ca^{2+}. This, in turn, could increase the probability of the ryanodine receptor opening, following

the influx of Ca^{2+} via the L-type Ca^{2+} channels (Torres *et al.*, 2010). Whether a similar mechanism exits in the PV and LA awaits further study.

5.2.1 ATX-II induced arrhythmogenic activity

Treatment with ATX-II initiated arrhythmogenic activity in the PV and LA in the form of spontaneous contractions, spontaneous action potentials, and EADs. This toxin is a well-established enhancer of I_{NaL} and has been shown to directly increase I_{NaL} in isolated atrial and ventricular cardiomyocytes, resulting in EADs, DADs and triggered activity (Isenberg and Ravens, 1984; Song *et al.*, 2004, 2009; Fischer *et al.*, 2015). Although there have been no studies examining the direct effect of ATX-II on the I_{NaL} in PV cardiomyocytes; previous studies have shown that ATX-II resulted in arrhythmogenic activity in the rabbit PV, which was suppressed by the I_{NaL} inhibitor ranolazine (Lu *et al.*, 2012; Chen *et al.*, 2014). Thus, it could be hypothesised that the induction of spontaneous activity and EADs in the PV and LA in the present study is due to an ATX-II mediated increase in $I_{NaL.}$

5.2.2 The contribution of Na^+ channels to ATX-II induced arrhythmogenic activity

The ATX-II induced APD_{90} prolongation was partially reversed by 100 nM TTX in the PV, suggesting that the TTX-sensitive Na^+ channels could contribute to the I_{NaL}. The TTX-sensitive channels also contribute to the I_{NaL} in dog ventricular cardiomyocytes (Biet *et al.*, 2012; Mishra *et al.*, 2014). In contrast, inhibition of TTX-sensitive Na^+ channels had no effect on the ATX-II induced prolongation of the APD_{90} in the LA. Since there was no evidence of a TTX-sensitive Na^+ current in the LA cardiomyocytes, this may explain why 100 nM TTX had no effect on the ATX-II induced prolongation of the APD_{90} in the LA.

Although TTX-sensitive Na^+ channel inhibition partially reversed the ATX-II induced APD_{90} prolongation, 100 nM TTX did not suppress the ATX-II induced spontaneous contractions in the PV. This suggests that TTX-sensitive Na^+ channels do not play a major role in the ATX-II induced arrhythmogenic activity. Inhibition of both TTX-sensitive and TTX-resistant I_{Na} (with 10 μM TTX) was needed to

significantly reduce the ATX-II induced spontaneous contractions in both tissues. This is in agreement with earlier studies in atrial and ventricular cardiomyocytes, which reported that micromolar concentrations of TTX were required to suppress the ATX-II induced arrhythmogenic activity in atrial and ventricular cardiomyocytes (Maltsev *et al*., 1998; Song *et al*., 2008; Sag *et al.*, 2014). Whether the suppression of the ATX-II induced spontaneous contractions by 10 µM TTX is due to block of the main cardiac Na^+ channel $Na_v1.5$, or if the other TTX-resistant Na^+ channel isoforms such as $Na_v1.8$ or $Na_v1.9$ also contribute to the I_{NaL} in PV and LA cardiomyocytes remains unknown. Although there is a lack of specific inhibitors for $Na_v1.9$, a number of studies reported A-803467 as a selective $Na_v1.8$ channel blocker (Jarvis *et al.*, 2007; Yang *et al.*, 2012). Treatment of mouse and rabbit ventricular cardiomyocytes with A-803467 decreased the I_{NaL} and suppressed ATX-II induced EADs (Yang *et al.*, 2012). Since no mRNA was detected for $Na_v1.8$ in the rat PV or LA, the inhibitor was not tested in the present study.

5.2.3 The contribution of CaMKII and NCX to ATX-II induced arrhythmogenic activity

The CaMKII inhibitor, KN-93 suppressed the ATX-II induced spontaneous activity and EADs, as well as attenuated the prolongation of the APD_{90} in both tissues. This suggests that CaMKII is somehow linked to the ATX-II induced arrhythmogenic activity in the rat PV and LA. However, the mechanism by which this occurs in the PV and LA remains to be elucidated. In ventricular cardiomyocytes, a positive feedback loop is thought to exist between CaMKII activation and the ATX-II mediated increase in I_{NaL}. Yoon *et al.* (2009) reported that CaMKII was constitutively active in rat ventricular cardiomyocytes, and regulates Na^+ channel function. Further studies in mouse and rabbit ventricular cardiomyocytes revealed that overexpression of CaMKII alters the Na^+ channel gating, resulting in an increased I_{NaL} and intracellular Na^+ accumulation (Wagner *et al.*, 2006, 2011). This could lead to Na^+ induced Ca^{2+} overload, which has been reported to enhance CaMKII activation (Sag *et al*., 2014). In addition, in mouse ventricular cardiomyocytes, an ATX-II induced increase in the I_{NaL} was shown to increase the activation of CaMKII (Wagner *et al.*, 2006, 2011; Sag *et al.*, 2014). This positive

feedback loop could promote arrhythmogenic activity in the PV and LA and so should be explored further. Hence, the effect of CaMKII inhibition on the I_{NaL} itself in PV and LA cardiomyocytes should be determined. An increase in the I_{NaL} has been found in a heart failure model (Valdivia *et al.*, 2005; Maltsev *et al.*, 2007; Xi *et al.*, 2009; Chang *et al.*, 2011), which can lead to DADs and spontaneous action potentials in the PV (Chang *et al.*, 2011). Whether CaMKII is also upregulated in the PV and LA of this model, remains to be determined and the model could be used to gain further insight into the positive feedback loop involving CaMKII and the I_{NaL}. The ability of CaMKII inhibition to decrease the heart failure induced increase in I_{NaL} as well as suppress any arrhythmogenic contractions and action potentials present in the PV and LA could also be examined.

Treatment with the NCX inhibitor, ORM-10103 also suppressed spontaneous contractions and action potentials in both the PV and LA, suggesting that the NCX is involved in ATX-II mediated arrhythmogenic activity. Previously, the presence of ATX-II has been shown to activate forward as well as reverse mode NCX in ventricular cardiomyocytes (Faber and Rudy, 2000; Tweedie *et al.*, 2000; Fujiwara *et al.*, 2008; Sossalla *et al.*, 2008; Undrovinas *et al.*, 2010), and recently Nagy *et al.* (2014) reported that the NCX blockers ORM-10103 and SEA-0400 most likely exerted their antiarrhythmic effect by inhibiting the reverse mode of the NCX. They established, in dog ventricular cardiomyocytes, that ATX-II increased the I_{NaL} as well as increased the Ca^{2+} transient amplitude, indicating the Na^{+} influx may have promoted reverse NCX activity resulting in Ca^{2+} overload. This Na^{+} induced Ca^{2+} overload was prevented by pre-treatment with ORM-10103 or SEA-0400 and suppressed by either NCX inhibitor following ATX-II treatment, which is indicative of a reverse NCX block (Nagy *et al.*, 2014).

5.2.4 Other sources of Ca^{2+} in ATX-II induced arrhythmogenic activity

Although this thesis demonstrated the importance of CaMKII and the NCX in ATX-II induced arrhythmogenic activity in the PV and LA, the mechanism of ATX-II induced arrhythmogenic activity in these tissues could be explored further. Song *et al.* (2008) established that the ATX-II mediated arrhythmogenic activity in LA

cardiomyocytes was suppressed by verapamil and ryanodine, suggesting that Ca^{2+} entry via the L-type Ca^{2+} channels and Ca^{2+} release from the sarcoplasmic reticulum is essential for this type of activity. However, as reported by Wolkowicz *et al.* (2014), alternative sources of Ca^{2+} also contribute to the ATX-II induced arrhythmogenic activity in rat LA tissues. They found that the ATX-II induced spontaneous extra contractions were suppressed by LOE-908, an inhibitor of voltage independent, arachidonate regulated, Ca^{2+} channels, suggesting that complex Ca^{2+} dependent signalling may be involved in the ATX-II induced arrhythmia. Their study also reported that inhibitors of the voltage-independent Ca^{2+} release Orai channels, ML-7 and SKF-96365, suppressed ATX-II induced triggered activity and EADs (Wolkowicz *et al.*, 2014).

As well as CaMKII other kinases, such as protein kinase A (PKA), and protein kinase C (PKC) may also be involved in ATX-II induced arrhythmic activity (Ma *et al.*, 2012; Fischer *et al.*, 2015; Wu *et al.*, 2015). For instance, PKC, which is activated by an increase in the local Ca^{2+} concentration (Nishizuka, 1992), can also phosphorylate Na^{+} channels, resulting in an increase in the I_{NaL} (Qu *et al.*, 1996; Murray *et al.*, 1997; Ward and Giles, 1997). Furthermore, in rabbit ventricular cardiomyocytes, the I_{NaL} which was enhanced by an increased Ca^{2+} concentration in the intracellular solution, or treatment with ouabain, was suppressed by the presence of the PKC inhibitor bisindolylmaleimide (BIM) (Ma *et al.*, 2012; Wu *et al.*, 2015). This suggests a potential role for PKC in I_{NaL} induced arrhythmogenic activity. However, whether inhibition of PKC could suppress spontaneous contractions, spontaneous action potentials and EADs induced by ATX-II remains to be elucidated. This could provide further insight into the mechanism of ATX-II induced arrhythmogenic activity in the PV and LA.

5.3 Clinical relevance

Although AF is primarily associated with a reduced APD, which is a consequence of electrical remodelling (Wijffels *et al.*, 1995), increasing evidence has also linked AF to an increase in the APD, which can be associated with an enhanced I_{NaL} (Song *et al.*, 2008, 2009). For example, in a number of cases, AF has been linked to long QT

syndrome (LQTS), which is associated with a prolonged APD (Johnson *et al.*, 2008; Zellerhoff *et al.*, 2009). The prevalence of LQTS has been shown to be a result of gain of function SCN5A mutations, which leads to an increase in I_{NaL} (Benito *et al.*, 2008; Blana *et al.*, 2010; Lemoine *et al.*, 2011). Furthermore, a number of small clinical trials have demonstrated the involvement of I_{NaL} in AF (Murdock *et al.*, 2008, 2009; Miles *et al.*, 2011; De Ferrari *et al.*, 2015). The I_{NaL} inhibitor, ranolazine prevented post-operative AF, suppressed paroxysmal AF and reduced AF recurrence after cardioversion (Murdock *et al.*, 2008, 2009; Miles *et al.*, 2011; De Ferrari *et al.*, 2015). Although, ranolazine is highly selective for I_{NaL}, it should also be taken into account that ranolazine also exhibits minor effects on other currents (Antzelevitch *et al.*, 2004).

Whether suppression of CaMKII activation would be viable as an antiarrhythmic strategy in clinical AF requires further work. Inhibition of CaMKII suppressed arrhythmogenic sarcoplasmic reticulum Ca^{2+} leak in atrial cardiomyocytes isolated from chronic AF patients (Neef *et al.*, 2010; Fischer *et al.*, 2015). However, CaMKII is involved in a number of other physiological processes and so systemic inhibition of CaMKII may produce a number of unwanted side effects such as impaired memory or reduced fertility (Marín-Briggiler *et al.*, 2005; Backs *et al.*, 2010; Halt *et al.*, 2012). In order to tackle this issue, future work could focus on the effect of inhibiting downstream/upstream targets in the CaMKII pathway as well as localised CaMKII inhibition in cardiomyocytes, to determine if its inhibition could be clinically relevant (Duan, 2015). Whether this localised inhibition could be achieved by inhibiting specific CaMKII isoforms and splice variants, which are common to cardiomyocytes remains to be elucidated.

5.4 Summary

To summarise, this study has shown that there was no significant difference in the action potential characteristics between the PV and LA. The I_{Na} characteristics were also similar in the PV compared to the LA. However, a detailed examination of the TTX-sensitive I_{Na} revealed that it contributed 20% to the total I_{Na} in PV cardiomyocytes, with the current activated at more depolarised potentials compared

to the TTX-resistant I_{Na}. In contrast, there was no evidence of a TTX-sensitive I_{Na} in the LA cardiomyocytes. Further investigation revealed that TTX-sensitive Na^+ channels do not significantly contribute to the action potential characteristics.

Examination of the arrhythmogenic properties of the PV and LA revealed the I_{NaL} enhancer ATX-II could induce spontaneous contractions, action potentials and EADs in both tissues. Further investigation revealed the complex mechanism underlying ATX-II induced arrhythmogenic activity is reliant on the Na^+ channels as well as CaMKII and NCX activity. Thus, the excitability of cells from both the PV and LA is influenced by both the direct and indirect action of Na^+ influx through the action of ATX-II.

Chapter 6

Appendix

Table 6.1. **Cardiomyocyte isolation solutions**

	Isolation Solutions (mM)			
	Isolation solution 1	**Isolation solution 2**	**Isolation solution 3**	**Isolation solution 4**
NaCl	140	120	140	120
KCl	4.2	5.4	5.4	5.4
KH_2PO_4	1.2	-	-	-
$MgCl_2$	1.5	5	1	3.5
HEPES	10	10	5	20
EGTA	0.1	-	-	-
NaH_2PO_4	-	-	-	0.52
Creatine	-	-	-	10
Taurine	-	20	-	20
Glucose	-	20	10	11.1
pH	7.4 NaOH	6.9 or 7.4 NaOH	7.4 NaOH	7.4 NaOH

Figure 6.1 **Multiple sequence alignment of SCN1A DNA**. The alignment of the extracted DNA from the rat PV against the predicted SCN1A ($Na_v1.1$) 519 bp amplicon. The matching nucleotides in the DNA sequence are highlighted in black. The forward primer used in the detection is underlined.

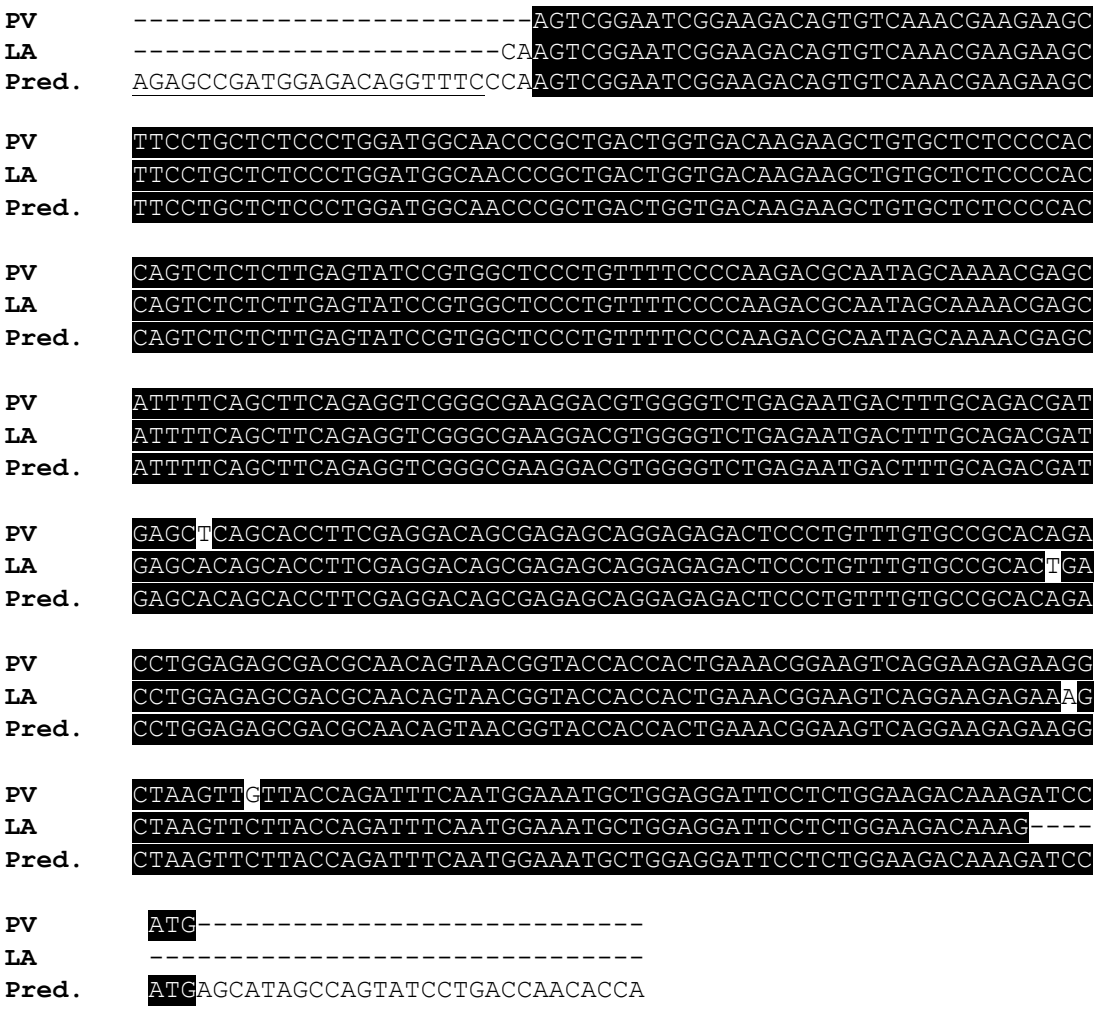

Figure 6.2 **Multiple sequence alignment of SCN3A DNA**. The alignment of the extracted DNA from the rat PV and LA against the predicted SCN3A ($Na_v1.3$) 451 bp amplicon. The matching nucleotides in the DNA sequence are highlighted in black. The forward primer used in the detection is underlined.

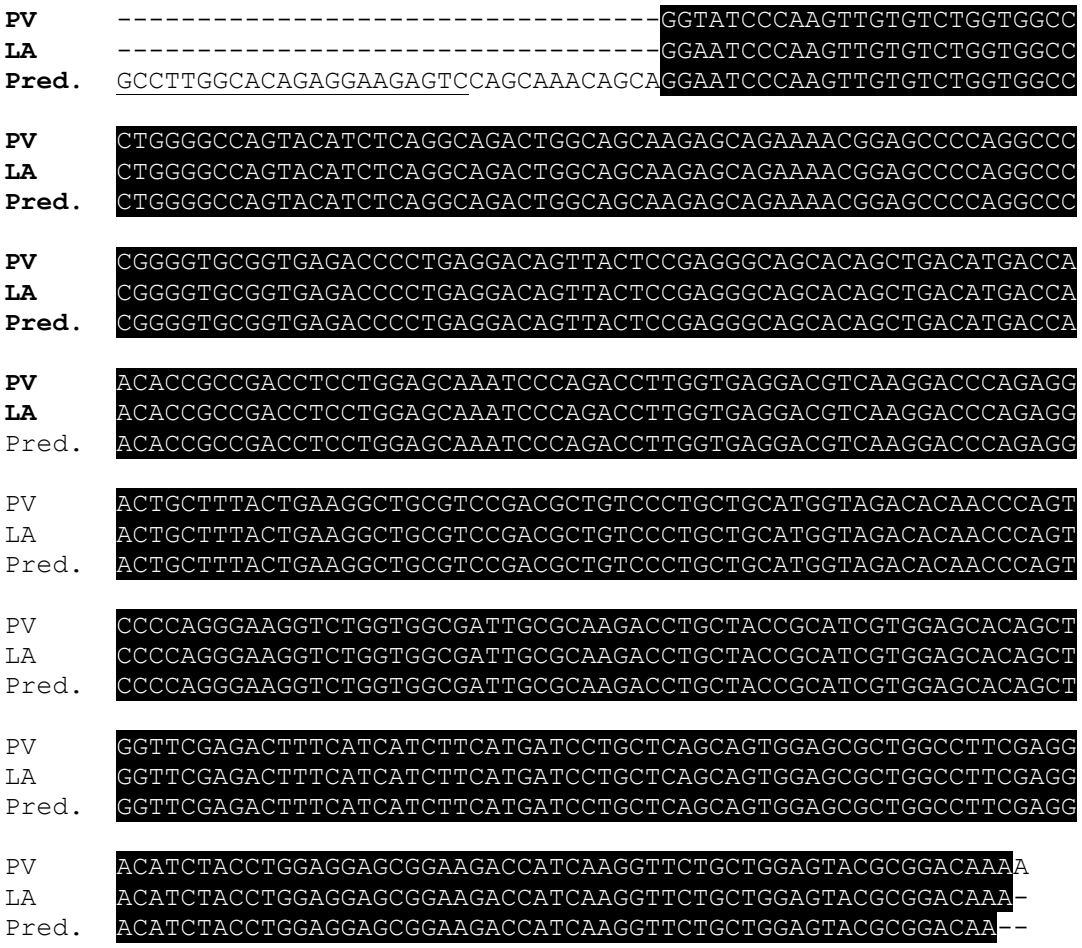

Figure 6.3 **Multiple sequence alignment of SCN5A DNA (band 1)**. The alignment of the extracted DNA from the rat PV and LA against the predicted SCN5A ($Na_v1.5$) 532 bp amplicon from band 1. The matching nucleotides in the DNA sequence are highlighted in black. The forward primer used in the detection is underlined.

Figure 6.4 **Multiple sequence alignment of SCN5A DNA (band 3)**. The alignment of the extracted DNA from the rat PV and LA against the predicted SCN5A ($Na_v1.5$) splice variant 372 bp amplicon. The matching nucleotides in the DNA sequence are highlighted in black. The forward primer used in the detection is underlined.

```
PV      ----------------------CCCGAGGTAGTGTATGGGATGACCCTCAAAATCCTGT

LA      ----------------------CCCGAGCTAGTGTATGGGATGACCCTCAAAATCCTGT
Pred.   GCTGCGTGGAGGTGGATTCTGAGACCGAGGCAGTGTATGGGATGACCTTCAAAATCCTGT

PV      GTATCTCCTGTAAGCGTCGTAGTGAGACCACCGCCGAGACCTTCACGGAGTGGACCTTCC
LA      GTATCTCCTGTAAGCGTCGTAGTGAGACCACCGCCGAGACCTTCACGGAGTGGACCTTCC
Pred.   GTATCTCCTGTAAGCGTCGTAGTGAGACCACCGCCGAGACCTTCACGGAGTGGACCTTCC

PV      GCCAGAAGGGCACAGAGGAATTTGTCAAGATCCTACGCTATGAGAATGAGGTGCTGCAGC
LA      GCCAGAAGGGCACAGAGGAATTTGTCAAGATCCTACGCTATGAGAATGAGGTGCTGCAGC
Pred.   GCCAGAAGGGCACAGAGGAATTTGTCAAGATCCTACGCTATGAGAATGAGGTGCTGCAGC

PV      TGGAGGAAGATGAGCGCTTTGAGGGCCGTGTGGTGTGGAACGGTAGTCGGGGCACCAAGG
LA      TGGAGGAAGATGAGCGCTTTGAGGGCCGTGTGGTGTGGAACGGTAGTCGGGGCACCAAGG
Pred.   TGGAGGAAGATGAGCGCTTTGAGGGCCGTGTGGTGTGGAACGGTAGTCGGGGCACCAAGG

PV      ACCTGCAGGACCTGTCCATCTTCATCACCAATGTCACCTACAACCACTCTGGCGACTACG
LA      ACCTGCAGGACCTGTCCATCTTCATCACCAATGTCACCTACAACCACTCTGGCGACTACG
Pred.   ACCTGCAGGACCTGTCCATCTTCATCACCAATGTCACCTACAACCACTCTGGCGACTACG

PV      AATGTCACGTCTACCGTCTCCTCTTCTTTGATAATTACGAGCACAACACCAGCGTCGTCA
LA      AATGTCACGTCTACCGTCTCCTCTTCTTTGATAATTACGAGCACAACACCAGCGTCGTCA
Pred.   AATGTCACGTCTACCGTCTCCTCTTCTTTGATAATTACGAGCACAACACCAGCGTCGTCA

PV      AGAAGATCCACCTGGAGGTGGTGGACAAGGCCAACAGAGATATGGCATCCATCGTGTCAG
LA      AGAAGATCCACCTGGAGGTGGTGGACAAGGCCAACAGAGATATGGCATCCATCGTGTCAG
Pred.   AGAAGATCCACCTGGAGGTGGTGGACAAGGCCAACAGAGATATGGCATCCATCGTGTCAG

PV      AGATCATGATGTACGTGCTCATTGTGGTGTTAACCATATGGCTCGTGGCGGAGATGGTGT
LA      AGATCATGATGTACGTGCTCATTGTGGTGTTAACCATATGGCTCGTGGCGGAGATGGTGT
Pred.   AGATCATGATGTACGTGCTCATTGTGGTGTTAACCATATGGCTCGTGGCGGAGATGGTGT

PV      ACTGCTACAAGAAGATTGCTGCTGCCACGGAAGCTGCTGCACAAGAGAATGCCT------
LA      ACTGCTACAAGAAGATTGCTGCTGCCACGGAAGCTGCTGCACAAGAGAA----------
Pred.   ACTGCTACAAGAAGATTGCTGCTGCCACGGAAGCTGCTGCACAAGAGAATGCCTCGGAAT

PV      ----------------------
LA      ----------------------
Pred.   ACCTGGCCATTACTTCCGAGA
```

Figure 6.5 **Multiple sequence alignment of SCNB1 DNA**. The alignment of the extracted DNA from the rat PV and LA against the predicted SCNB1 (β1) 561 bp amplicon. The matching nucleotides in the DNA sequence are highlighted in black. The forward primer used in the detection is underlined.

```
PV      ----------------------------CCTGCCTTCAGCCTCACGGGGCTCAGTCTGTT
LA      ------------------------TCGCCCTGCCTTCAGCCTCACGGGGCTCAGTCTGTT
Pred.   AATGCACAGGGATGCCTGGCTACCTCGCCCTGCCTTCAGCCTCACGGGGCTCAGTCTGTT

PV      TTTCTCTTTGGTGCCCTCGGGGCGGAGCATGGAAGTCACAGTCCCCACCACTCTTAGTGT
LA      TTTCTCTTTGGTGCCCTCGGGGCGGAGCATGGAAGTCACAGTCCCCACCACTCTTAGTGT
Pred.   TTTCTCTTTGGTGCCCTCGGGGCGGAGCATGGAAGTCACAGTCCCCACCACTCTTAGTGT

PV      CCTCAACGGGTCTGATACCCGCCTGCCCTGTACCTTCAACTCCTGCTATACCGTGAACCA
LA      CCTCAACGGGTCTGATACCCGCCTGCCCTGTACCTTCAACTCCTGCTATACCGTGAACCA
Pred.   CCTCAACGGGTCTGATACCCGCCTGCCCTGTACCTTCAACTCCTGCTATACCGTGAACCA

PV      CAAGCAGTTCTCTCTGAACTGGACTTACCAGGAGTGTAGCAATTGCTCAGAGGAGATGTT
LA      CAAGCAGTTCTCTCTGAACTGGACTTACCAGGAGTGTAGCAATTGCTCAGAGGAGATGTT
Pred.   CAAGCAGTTCTCTCTGAACTGGACTTACCAGGAGTGTAGCAATTGCTCAGAGGAGATGTT

PV      CCTCCAGTTCCGAATGAAGATCATCAACCTGAAGCTGGAGCGGTTTGGAGACCGCGTAGA
LA      CCTCCAGTTCCGAATGAAGATCATCAACCTGAAGCTGGAGCGGTTTGGAGACCGCGTAGA
Pred.   CCTCCAGTTCCGAATGAAGATCATCAACCTGAAGCTGGAGCGGTTTGGAGACCGCGTAGA

PV      GTTCTCGGGGAACCCCAGTAAGTACGACGTGTCAGTGACTCTAAAGAACGTGCAGCTAGA
LA      GTTCTCGGGGAACCCCAGTAAGTACGACGTGTCAGTGACTCTAAAGAACGTGCAGCTAGA
Pred.   GTTCTCGGGGAACCCCAGTAAGTACGACGTGTCAGTGACTCTAAAGAACGTGCAGCTAGA

PV      AGACGAAGGCATTTACAACTGCTACATCACCAACCCTCCAGACCGCAACCGTGGCCATGG
LA      AGACGAAGGCATTTACAACTGCTACATCACCAACCCTCCAGACCGCCACCGTGGCCATGG
Pred.   AGACGAAGGCATTTACAACTGCTACATCACCAACCCTCCAGACCGCCACCGTGGCCATGG

PV      CAAGATCTACCTGCAGGTCCTTCTAGAAGTGCCCCC------------------------
LA      CAAGATCTACCTGCAGGTCCTTCTAGAAGTGCCCCCAGAGCGG----------------
Pred.   CAAGATCTACCTGCAGGTCCTTCTAGAAGTGCCCCCAGAGCGGGACTCCACGGTGGCAGT

PV      --------------------
LA      --------------------
Pred.   CATCGTGGGTGCCTCAGTGG
```

Figure 6.6 **Multiple sequence alignment of SCNB2 DNA**. The alignment of the extracted DNA from the rat PV and LA against the predicted SCNB2 (β2) 500 bp amplicon. The matching nucleotides in the DNA sequence are highlighted in black. The forward primer used in the detection is underlined.

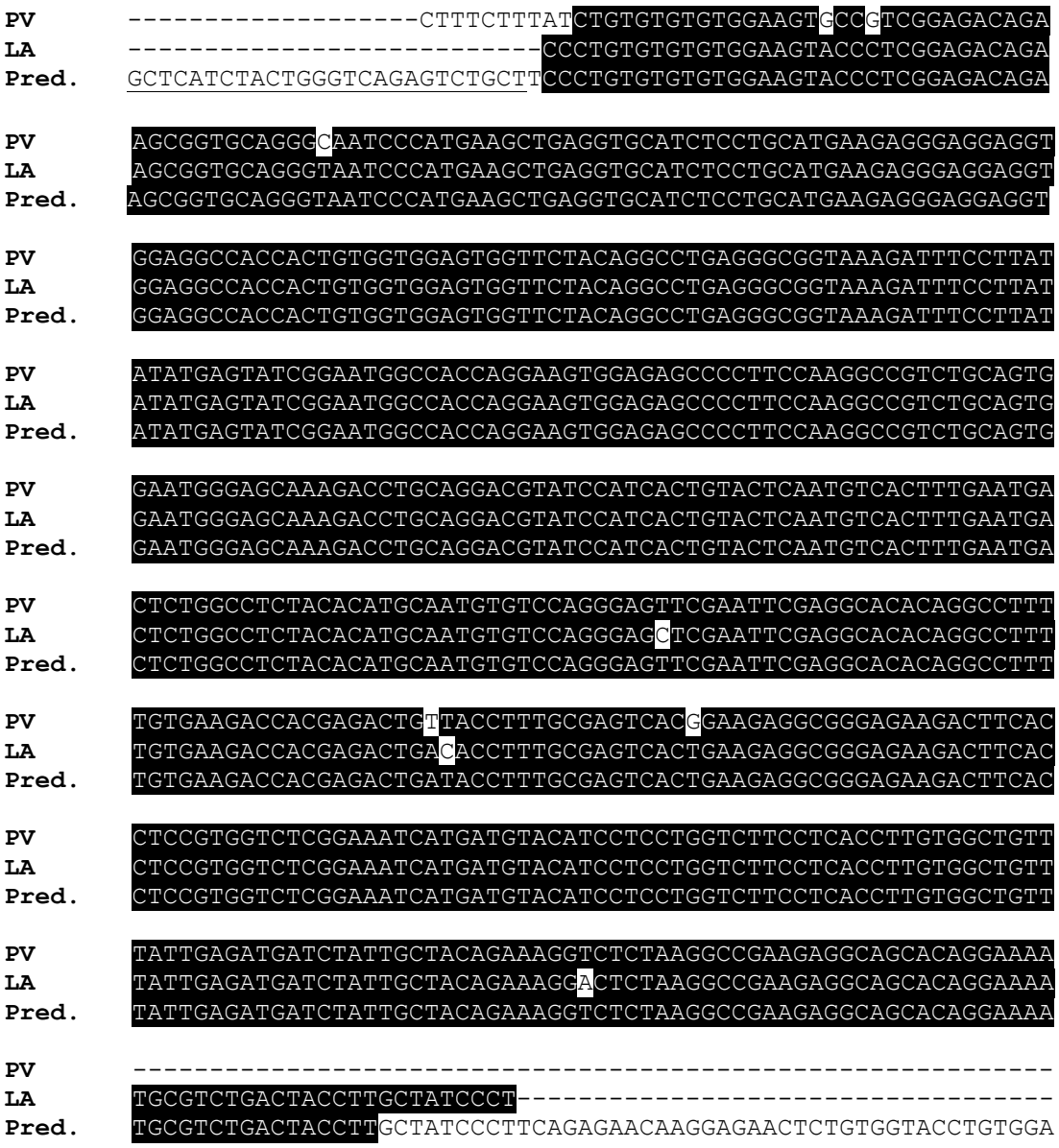

Figure 6.7 **Multiple sequence alignment of SCNB3 DNA**. The alignment of the extracted DNA from the rat PV and LA against the predicted SCNB3 (β3) 601 bp amplicon. The matching nucleotides in the DNA sequence are highlighted in black. The forward primer used in the detection is underlined.

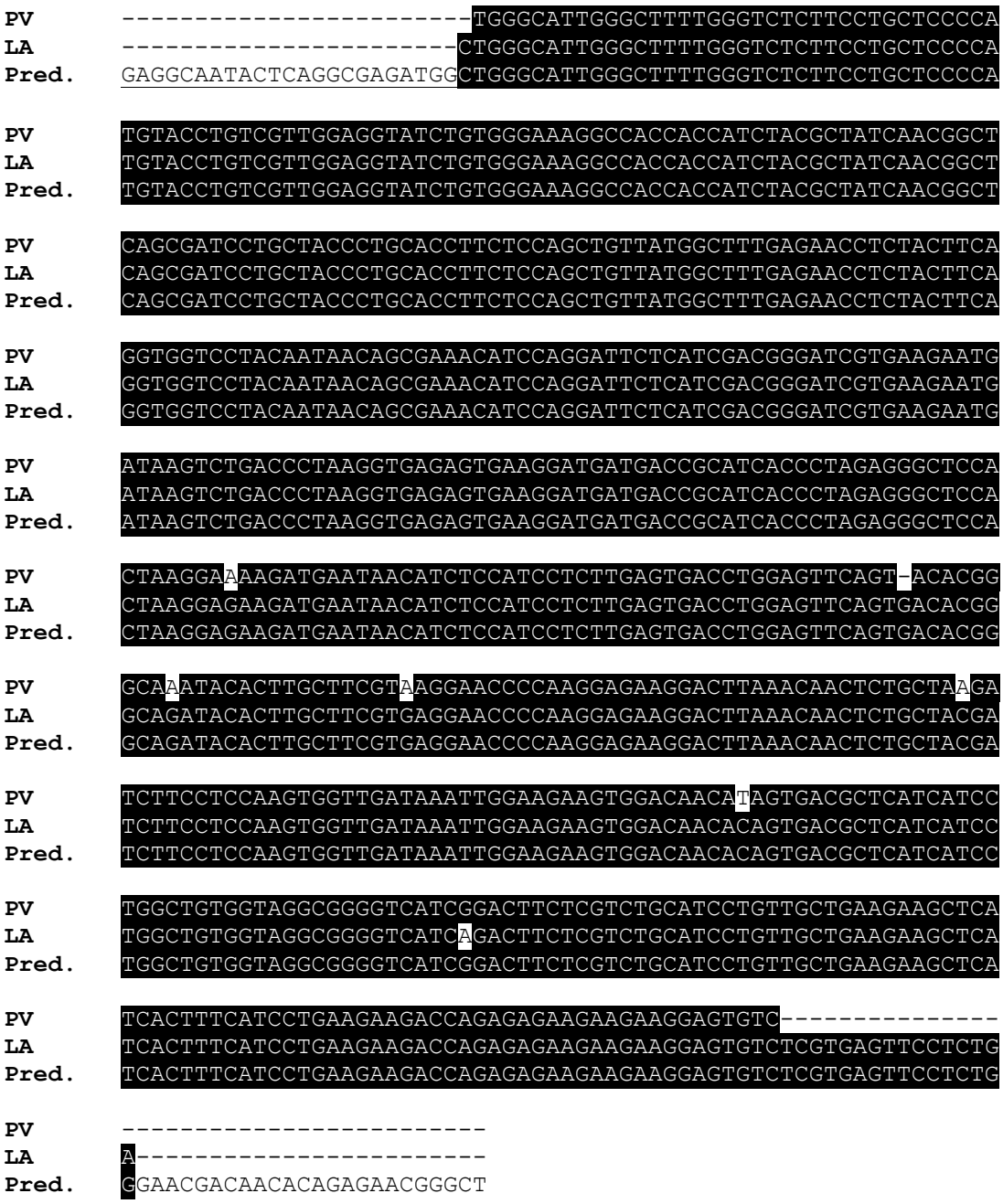

Figure 6.8 **Multiple sequence alignment of SCNB4 DNA**. The alignment of the extracted DNA from the rat PV and LA against the predicted SCNB4 (β4) 625 bp amplicon. The matching nucleotides in the DNA sequence are highlighted in black. The forward primer used in the detection is underlined.

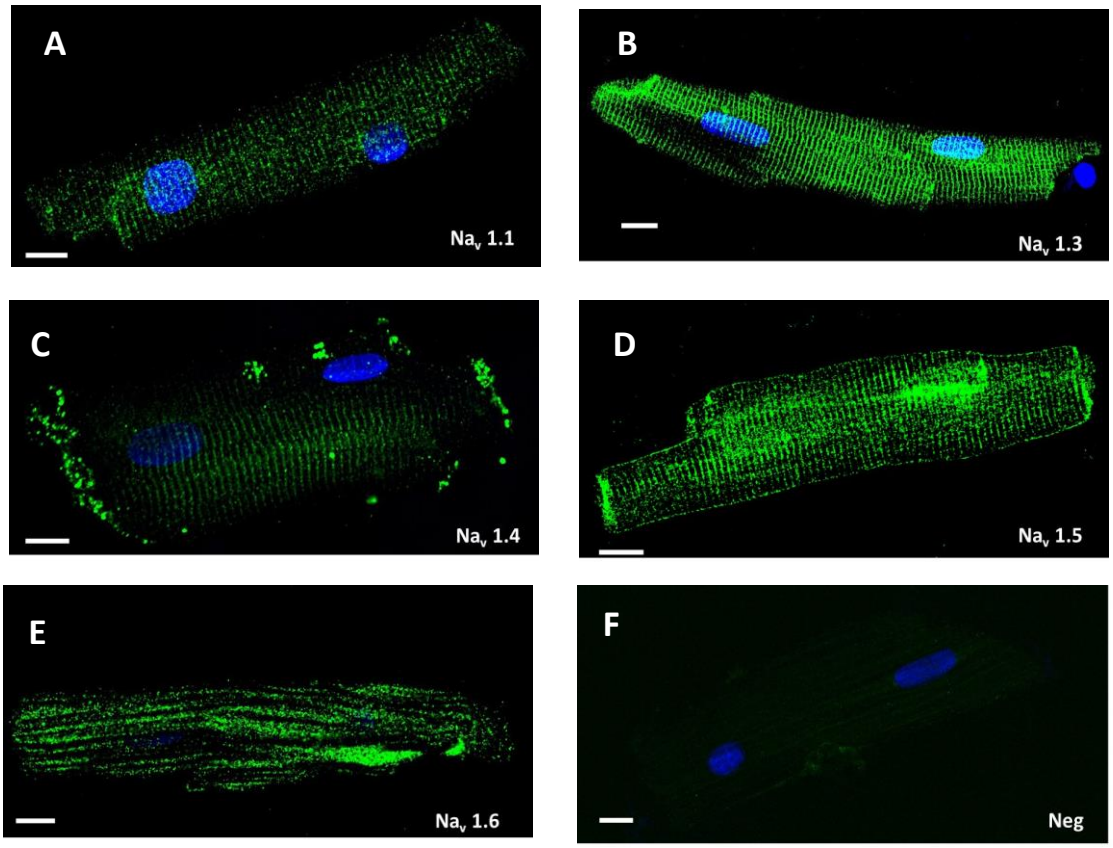

Figure 6.9 **Immunostaining of Na^+ channel α-subunits in rat ventricular cardiomyocytes.** Rat ventricular cardiomyocytes were isolated using the Langendorff method and labelled with a (A) $Na_v1.1$; (B) $Na_v1.3$; (C) $Na_v1.4$; (D) $Na_v1.5$; (E) $Na_v1.6$ primary antibodies and an Alexa 488 secondary antibody (green). (F) Negative control in which the primary antibody was omitted are also shown. DAPI staining of the nucleus is shown in blue. For these images, the plane of focus was within the cell. Scale bars are 10 µm. This was repeated using cells from three separate rats

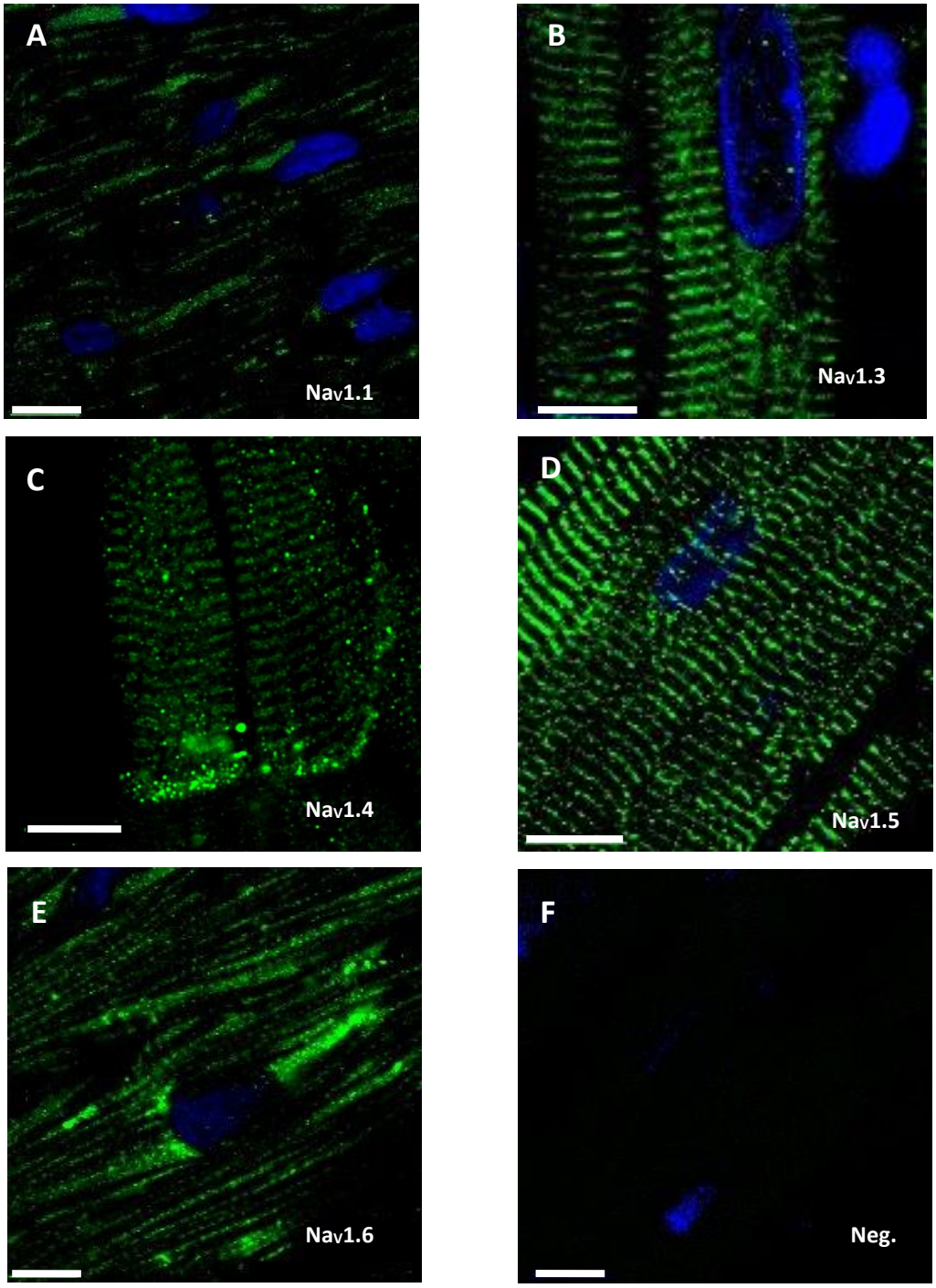

Figure 6.10 **Immunostaining of Na^+ channel α-subunits in human ventricular tissue.** Human ventricular tissue sections were labelled with (A) $Na_v1.1$; (B) $Na_v1.3$; (C) $Na_v1.4$; (D) $Na_v1.5$ and (E) $Na_v1.6$ antibodies and Alexa 488 secondary antibody (green). (F) Negative controls in which the primary antibody was omitted. DAPI staining of the nucleus is shown in blue. Scale bars are 10 μm. Staining was carried out in tissue from two patients.

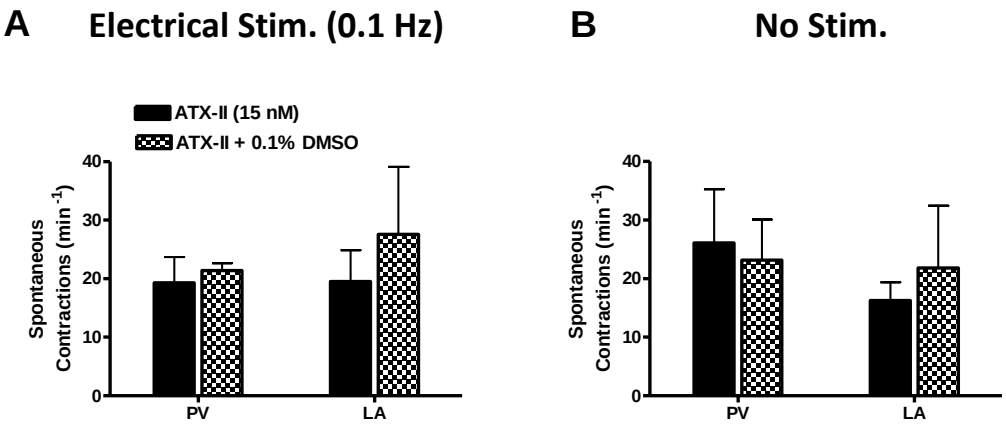

Figure 6.11 **Effect of 0.1% DMSO on ATX-II induced contractions in the PV and LA**. Graphs show PV (n=3) and LA (n=3) contractions induced by ATX-II at (B) 0.1 Hz electrical stimulation and (C) no electrical stimulation (no stim.) in the presence of ATX-II alone (15 nM) and after addition of 0.1% DMSO. All data are presented as mean ± s.e.m.

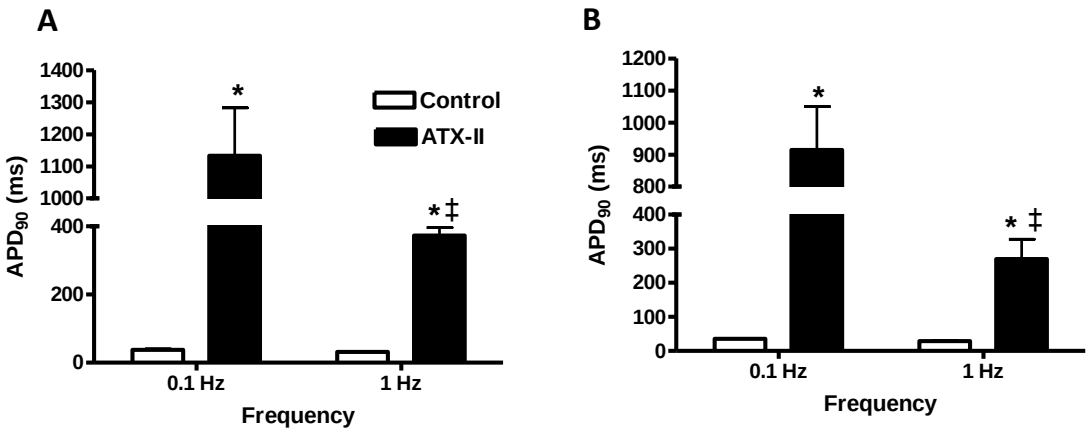

Figure 6.12 **The effect of ATX-II (40 nM) on the APD_{90} of the PV and LA at electrical stimulation frequencies of 0.1 Hz and 1 Hz**. The APD_{90} in PV (A) and LA (B) preparations was recorded under control conditions, when the tissue was electrically stimulated at 0.1 Hz (PV n=9/4, LA n=9/4) and at 1 Hz (PV n=10/4, LA n=9/4). This was repeated in the presence of 40 nM ATX-II at 0.1 Hz (PV n=10/4, LA n=12/4) and 1 Hz (PV n=18/4, LA n=18/4) electrical stimulation. All data are presented as mean ± s.e.m. * indicates $P<0.05$ for control *vs.* ATX-II treatment. ‡ indicates $P<0.05$ for 0.1 Hz *vs.* 1 Hz.

Chapter 7 – References

Abriel, H. (2010). Cardiac sodium channel $Na_v1.5$ and interacting proteins: Physiology and pathophysiology. J. Mol. Cell. Cardiol. *48*: 2–11.

Ahmed, C.M., Ware, D.H., Lee, S.C., Patten, C.D., Ferrer-Montiel, A.V., Schinder, A.F., *et al*. (1992). Primary structure, chromosomal localization, and functional expression of a voltage-gated sodium channel from human brain. Proc. Natl. Acad. Sci. U. S. A. *89*: 8220–8224.

Aiba, T., Hesketh, G.G., Liu, T., Carlisle, R., Villa-Abrille, M.C., O'Rourke, B., *et al*. (2010). Na^+ channel regulation by Ca^{2+}-calmodulin and Ca^{2+}-calmodulin-dependent protein kinase II in guinea-pig ventricular myocytes. Cardiovasc. Res. *85*: 454–463.

Aidonidis, I., Doulas, K., Hatziefthimiou, A., Tagarakis, G., Simopoulos, V., Rizos, I., *et al*. (2013). Ranolazine-induced postrepolarization refractoriness suppresses induction of atrial flutter and fibrillation in anesthetized rabbits. J. Cardiovasc. Pharmacol. Ther. *18*: 94–101.

Akalin, F., Tirtir, A., and Yilmaz, Y. (2003). Increased QT dispersion in epileptic children. Acta Paediatr. Oslo Nor. 1992 *92*: 916–920.

Akopian, A.N., Sivilotti, L., and Wood, J.N. (1996). A tetrodotoxin-resistant voltage-gated sodium channel expressed by sensory neurons. Nature *379*: 257–262.

Allessie, M.A., Bonke, F.I., and Schopman, F.J. (1976). Circus movement in rabbit atrial muscle as a mechanism of tachycardia. II. The role of nonuniform recovery of excitability in the occurrence of unidirectional block, as studied with multiple microelectrodes. Circ. Res. *39*: 168–177.

Allessie, M.A., Bonke, F.I., and Schopman, F.J. (1977). Circus movement in rabbit atrial muscle as a mechanism of tachycardia. III. The 'leading circle' concept: a new model of circus movement in cardiac tissue without the involvement of an anatomical obstacle. Circ. Res. *41*: 9–18.

Allessie, M.A., Boyden, P.A., Camm, A.J., Kléber, A.G., Lab, M.J., Legato, M.J., *et al*. (2001). Pathophysiology and prevention of atrial fibrillation. Circulation *103*: 769–777.

Alsen, C., Béress, L., Fischer, K., Proppe, D., Reinberg, T., and Sattler, R.W. (1976). The action of a toxin from the sea anemone Anemonia sulcata upon Mammalian heart muscles. Naunyn. Schmiedebergs Arch. Pharmacol. *295*: 55–62.

Alsen, C., Peters, T., and Scheufler, E. (1982). Studies on the mechanism of the positive inotropic effect of ATX II (Anemonia sulcata) on isolated guinea pig atria. J. Cardiovasc. Pharmacol. *4*: 63–69.

Anderson, M.E., Braun, A.P., Wu, Y., Lu, T., Wu, Y., Schulman, H., *et al*. (1998). KN-93, an inhibitor of multifunctional Ca^{2+}/calmodulin-dependent protein kinase, decreases early afterdepolarizations in rabbit heart. J. Pharmacol. Exp. Ther. *287*: 996–1006.

Antzelevitch, C. (2004). Cellular basis and mechanism underlying normal and abnormal myocardial repolarization and arrhythmogenesis. Ann. Med. *36*: 5–14.

Antzelevitch, C., Belardinelli, L., Zygmunt, A.C., Burashnikov, A., Di Diego, J.M., Fish, J.M., *et al*. (2004). Electrophysiological effects of ranolazine, a novel antianginal agent with antiarrhythmic properties. Circulation *110*: 904–910.

Anyukhovsky, E.P., Sosunov, E.A., Kryukova, Y.N., Prestia, K., Ozgen, N., Rivaud, M., *et al*. (2011). Expression of skeletal muscle sodium channel $Na_v1.4$ or connexin32 prevents reperfusion arrhythmias in murine heart. Cardiovasc. Res. *89*: 41–50.

Armour, J.A., Murphy, D.A., Yuan, B.X., Macdonald, S., and Hopkins, D.A. (1997). Gross and microscopic anatomy of the human intrinsic cardiac nervous system. Anat. Rec. *247*: 289–298.

Arora, R., Ulphani, J.S., Villuendas, R., Ng, J., Harvey, L., Thordson, S., *et al*. (2008). Neural substrate for atrial fibrillation: implications for targeted parasympathetic blockade in the posterior left atrium. Am. J. Physiol. Heart Circ. Physiol. *294*: H134–144.

Arora, R., Verheule, S., Scott, L., Navarrete, A., Katari, V., Wilson, E., *et al.* (2003). Arrhythmogenic substrate of the pulmonary veins assessed by high-resolution optical mapping. Circulation *107*: 1816–1821.

Aslanidi, O.V., Colman, M.A., Varela, M., Zhao, J., Smaill, B.H., Hancox, J.C., *et al.* (2013). Heterogeneous and anisotropic integrative model of pulmonary veins: computational study of arrhythmogenic substrate for atrial fibrillation. Interface Focus *3*: 20120069.

Auld, V.J., Goldin, A.L., Krafte, D.S., Catterall, W.A., Lester, H.A., Davidson, N., *et al*. (1990). A neutral amino acid change in segment IIS4 dramatically alters the gating properties of the voltage-dependent sodium channel. Proc. Natl. Acad. Sci. *87*: 323–327.

Baba, S., Dun, W., Hirose, M., and Boyden, P.A. (2006). Sodium current function in adult and aged canine atrial cells. Am. J. Physiol. - Heart Circ. Physiol. *291*: H756–H761.

Backs, J., Stein, P., Backs, T., Duncan, F.E., Grueter, C.E., McAnally, J., *et al.* (2010). The γ isoform of CaM kinase II controls mouse egg activation by regulating cell cycle resumption. Proc. Natl. Acad. Sci. *107*: 81–86.

Baruscotti, M., Barbuti, A., and Bucchi, A. (2010). The cardiac pacemaker current. J. Mol. Cell. Cardiol. *48*: 55–64.

Benito, B., Brugada, R., Perich, R.M., Lizotte, E., Cinca, J., Mont, L., *et al.* (2008). A mutation in the sodium channel is responsible for the association of long QT syndrome and familial atrial fibrillation. Heart Rhythm Off. J. Heart Rhythm Soc. *5*: 1434–1440.

Bennett, M.A., and Pentecost, B.L. (1970). The pattern of onset and spontaneous cessation of atrial fibrillation in man. Circulation *41*: 981–988.

Bennett, P.B., Yazawa, K., Makita, N., and George, A.L. (1995). Molecular mechanism for an inherited cardiac arrhythmia. Nature *376*: 683–685.

Bers, D.M., and Despa, S. (2009). Na^+ transport in cardiac myocytes; Implications for excitation-contraction coupling. IUBMB Life *61*: 215–221.

Bertaglia, E., Stabile, G., Senatore, G., Pratola, C., Verlato, R., Lowe, M., *et al*. (2014). Documentation of pulmonary vein isolation improves long term efficacy of persistent atrial fibrillation catheter ablation. Int. J. Cardiol. *171*: 174–178.

Biet, M., Barajas-Martínez, H., Ton, A.-T., Delabre, J.-F., Morin, N., and Dumaine, R. (2012). About half of the late sodium current in cardiac myocytes from dog ventricle is due to non-cardiac-type Na^+ channels. J. Mol. Cell. Cardiol. *53*: 593–598.

Birinyi, P., Acsai, K., Bányász, T., Tóth, A., Horváth, B., Virág, L., *et al*. (2005). Effects of SEA0400 and KB-R7943 on Na^+ /Ca^{2+} exchange current and L-type Ca^{2+} current in canine ventricular cardiomyocytes. Naunyn. Schmiedebergs Arch. Pharmacol. *372*: 63–70.

Bishop, J.E. (1998). Regulation of cardiovascular collagen deposition by mechanical forces. Mol. Med. Today *4*: 69–75.

Blana, A., Kaese, S., Fortmüller, L., Laakmann, S., Damke, D., Bragt, K. van, *et al*. (2010). Knock-in gain-of-function sodium channel mutation prolongs atrial action potentials and alters atrial vulnerability. Heart Rhythm Off. J. Heart Rhythm Soc. *7*: 1862–1869.

Blatter, L.A., Hüser, J., and Ríos, E. (1997). Sarcoplasmic reticulum Ca^{2+} release flux underlying Ca^{2+} sparks in cardiac muscle. Proc. Natl. Acad. Sci. U. S. A. *94*: 4176–4181.

Blechschmidt, S., Haufe, V., Benndorf, K., and Zimmer, T. (2008). Voltage-gated Na^+ channel transcript patterns in the mammalian heart are species-dependent. Prog. Biophys. Mol. Biol. *98*: 309–318.

Bleeker, W.K., Mackaay, A.J., Masson-Pévet, M., Bouman, L.N., and Becker, A.E. (1980). Functional and morphological organization of the rabbit sinus node. Circ. Res. *46*: 11–22.

Boldt, A., Wetzel, U., Lauschke, J., Weigl, J., Gummert, J., Hindricks, G., *et al*. (2004). Fibrosis in left atrial tissue of patients with atrial fibrillation with and without underlying mitral valve disease. Heart Br. Card. Soc. *90*: 400–405.

Bond, R.C., Choisy, S.C.M., Bryant, S.M., Hancox, J.C., and James, A.F. (2014). Inhibition of a TREK-like K^+ channel current by noradrenaline requires both β1- and β2-adrenoceptors in rat atrial myocytes. Cardiovasc. Res. cvu192.

Bosch, R.F., Scherer, C.R., Rüb, N., Wöhrl, S., Steinmeyer, K., Haase, H., *et al.* (2003). Molecular mechanisms of early electrical remodeling: transcriptional downregulation of ion channel subunits reduces $I_{Ca,L}$ and I_{to} in rapid atrial pacing in rabbits. J. Am. Coll. Cardiol. *41*: 858–869.

Bosch, R.F., Zeng, X., Grammer, J.B., Popovic, K., Mewis, C., and Kühlkamp, V. (1999). Ionic mechanisms of electrical remodelling in human atrial fibrillation. Cardiovasc. Res. *44*: 121–131.

Boutjdir, M., and Sherif, N. el- (1991). Pharmacological evaluation of early afterdepolarisations induced by sea anemone toxin (ATXII) in dog heart. Cardiovasc. Res. *25*: 815–819.

Brackenbury, W.J., and Isom, L.L. (2011). Na Channel β Subunits: Overachievers of the Ion Channel Family. Front. Pharmacol. *2*: 53.

Brette, F., and Orchard, C.H. (2006). No apparent requirement for neuronal sodium channels in excitation-contraction coupling in rat ventricular myocytes. Circ. Res. *98*: 667–674.

Bronquard, C., Maupoil, V., Arbeille, B., Fetissof, F., Findlay, I., Cosnay, P., *et al.* (2007). Contractile and relaxant properties of rat-isolated pulmonary veins related to localization and histology. Fundam. Clin. Pharmacol. *21*: 55–65.

Brugada, J., Gürsoy, S., Brugada, P., Atié, J., Guiraudon, G., and Andries, E. (1993). Cibenzoline transforms random re-entry into ordered re-entry in the atria. Eur. Heart J. *14*: 267–272.

Brugada, P., and Wellens, H.J. (1984). The role of triggered activity in clinical ventricular arrhythmias. Pacing Clin. Electrophysiol. PACE *7*: 260–271.

Brunton, T., and Fayrer, J. (1876). Note on the independent pulsation of the pulmonery veins and vena cava. Proc R Soc Lond *25*: 174–176.

Buchanan, J.W., Saito, T., and Gettes, L.S. (1985). The effects of antiarrhythmic drugs, stimulation frequency, and potassium-induced resting membrane potential changes on conduction velocity and dV/dt_{max} in guinea pig myocardium. Circ. Res. *56*: 696–703.

Burashnikov, A., and Antzelevitch, C. (2003). Reinduction of atrial fibrillation immediately after termination of the arrhythmia is mediated by late phase 3 early afterdepolarization-induced triggered activity. Circulation *107*: 2355–2360.

Burashnikov, A., Di Diego, J.M., Sicouri, S., Ferreiro, M., Carlsson, L., and Antzelevitch, C. (2008). Atrial-selective effects of chronic amiodarone in the management of atrial fibrillation. Heart Rhythm Off. J. Heart Rhythm Soc. *5*: 1735–1742.

Burashnikov, A., Di Diego, J.M., Zygmunt, A.C., Belardinelli, L., and Antzelevitch, C. (2007). Atrium-selective sodium channel block as a strategy for suppression of

atrial fibrillation: differences in sodium channel inactivation between atria and ventricles and the role of ranolazine. Circulation *116*: 1449–1457.

Calkins, H., Brugada, J., Packer, D.L., Cappato, R., Chen, S.-A., Crijns, H.J.G., *et al.* (2007). HRS/EHRA/ECAS expert consensus statement on catheter and surgical ablation of atrial fibrillation: recommendations for personnel, policy, procedures and follow-up. Eur. Eur. Pacing Arrhythm. Card. Electrophysiol. J. Work. Groups Card. Pacing Arrhythm. Card. Cell. Electrophysiol. Eur. Soc. Cardiol. *9*: 335–379.

Camm, A.J., Kirchhof, P., Lip, G.Y.H., Schotten, U., Savelieva, I., Ernst, S., *et al.* (2010). Guidelines for the management of atrial fibrillation: the Task Force for the Management of Atrial Fibrillation of the European Society of Cardiology (ESC). Eur. Eur. Pacing Arrhythm. Card. Electrophysiol. J. Work. Groups Card. Pacing Arrhythm. Card. Cell. Electrophysiol. Eur. Soc. Cardiol. *12*: 1360–1420.

Cannell, M.B., Cheng, H., and Lederer, W.J. (1995). The control of calcium release in heart muscle. Science *268*: 1045–1049.

Cappola, A.R., Fried, L.P., Arnold, A.M., Danese, M.D., Kuller, L.H., Burke, G.L., *et al*. (2006). Thyroid status, cardiovascular risk, and mortality in older adults. JAMA *295*: 1033–1041.

Carmeliet, E., and Mubagwa, K. (1998). Antiarrhythmic drugs and cardiac ion channels: mechanisms of action. Prog. Biophys. Mol. Biol. *70*: 1–72.

Cech, S. (1969). Adrenergic innervation of blood vessels in the lung of some mammals. Acta Anat. (Basel) *74*: 169–182.

Chambers, J.C., Zhao, J., Terracciano, C.M.N., Bezzina, C.R., Zhang, W., Kaba, R., *et al*. (2010). Genetic variation in SCN10A influences cardiac conduction. Nat. Genet. *42*: 149–152.

Chang, S.-H., Chen, Y.-C., Chiang, S.-J., Higa, S., Cheng, C.-C., Chen, Y.-J., *et al.* (2008). Increased Ca^{2+} sparks and sarcoplasmic reticulum Ca^{2+} stores potentially determine the spontaneous activity of pulmonary vein cardiomyocytes. Life Sci. *83*: 284–292.

Chang, S.-L., Chen, Y.-C., Chen, Y.-J., Wangcharoen, W., Lee, S.-H., Lin, C.-I., *et al.* (2007). Mechanoelectrical feedback regulates the arrhythmogenic activity of pulmonary veins. Heart Br. Card. Soc. *93*: 82–88.

Chang, S.-L., Chen, Y.-C., Yeh, Y.-H., Lin, Y.-K., Wu, T.-J., Lin, C.-I., *et al.* (2011). Heart failure enhanced pulmonary vein arrhythmogenesis and dysregulated sodium and calcium homeostasis with increased calcium sparks. J. Cardiovasc. Electrophysiol. *22*: 1378–1386.

Cha, T.-J., Ehrlich, J.R., Zhang, L., Chartier, D., Leung, T.K., and Nattel, S. (2005). Atrial tachycardia remodeling of pulmonary vein cardiomyocytes: comparison with left atrium and potential relation to arrhythmogenesis. Circulation *111*: 728–735.

Chelu, M.G., Sarma, S., Sood, S., Wang, S., Oort, R.J. van, Skapura, D.G., *et al.* (2009). Calmodulin kinase II-mediated sarcoplasmic reticulum Ca^{2+} leak promotes atrial fibrillation in mice. J. Clin. Invest. *119*: 1940–1951.

Cheng, H., Lederer, W.J., and Cannell, M.B. (1993). Calcium sparks: elementary events underlying excitation-contraction coupling in heart muscle. Science *262*: 740–744.

Cheng, Z., Powley, T.L., Schwaber, J.S., and Doyle III, F.J. (1997). Vagal afferent innervation of the atria of the rat heart reconstructed with confocal microscopy. J. Comp. Neurol. *381*: 1–17.

Chen, L., Zhang, W., Fang, C., Jiang, S., Shu, C., Cheng, H., *et al.* (2011). Polymorphism H558R in the human cardiac sodium channel SCN5A gene is associated with atrial fibrillation. J. Int. Med. Res. *39*: 1908–1916.

Chen, P.-S., Chou, C.-C., Tan, A.Y., Zhou, S., Fishbein, M.C., Hwang, C., *et al.* (2006a). The mechanisms of atrial fibrillation. J. Cardiovasc. Electrophysiol. *17 Suppl 3*: S2–7.

Chen, S.-A., Hsieh, M.-H., Tai, C.-T., Tsai, C.-F., Prakash, V.S., Yu, W.-C., *et al.* (1999). Initiation of atrial fibrillation by ectopic beats originating from the pulmonary veins electrophysiological characteristics, pharmacological responses, and effects of radiofrequency ablation. Circulation *100*: 1879–1886.

Chen, Y.-C., Chen, S.-A., Chen, Y.-J., Chang, M.-S., Chan, P., and Lin, C.-I. (2002a). Effects of thyroid hormone on the arrhythmogenic activity of pulmonary vein cardiomyocytes. J. Am. Coll. Cardiol. *39*: 366–372.

Chen, Y.-C., Chen, S.-A., Chen, Y.-J., Tai, C.-T., Chan, P., and Lin, C.-I. (2004). T-Type calcium current in electrical activity of cardiomyocytes isolated from rabbit pulmonary vein. J. Cardiovasc. Electrophysiol. *15*: 567–571.

Chen, Y.-C., Lu, Y.-Y., Cheng, C.-C., Lin, Y.-K., Chen, S.-A., and Chen, Y.-J. (2014). Sinoatrial node electrical activity modulates pulmonary vein arrhythmogenesis. Int. J. Cardiol. *173*: 447–452.

Chen, Y.-C., Pan, N.-H., Cheng, C.-C., Higa, S., Chen, Y.-J., and Chen, S.-A. (2009). Heterogeneous expression of potassium currents and pacemaker currents potentially regulates arrhythmogenesis of pulmonary vein cardiomyocytes. J. Cardiovasc. Electrophysiol. *20*: 1039–1045.

Chen, Y.J., Chen, S.A., Chang, M.S., and Lin, C.I. (2000). Arrhythmogenic activity of cardiac muscle in pulmonary veins of the dog: implication for the genesis of atrial fibrillation. Cardiovasc. Res. *48*: 265–273.

Chen, Y.-J., Chen, S.-A., Chen, Y.-C., Yeh, H.-I., Chang, M.-S., and Lin, C.-I. (2002b). Electrophysiology of single cardiomyocytes isolated from rabbit pulmonary veins: implication in initiation of focal atrial fibrillation. Basic Res. Cardiol. *97*: 26–34.

Chen, Y.J., Chen, S.A., Chen, Y.C., Yeh, H.I., Chan, P., Chang, M.S., *et al.* (2001). Effects of rapid atrial pacing on the arrhythmogenic activity of single cardiomyocytes from pulmonary veins: implication in initiation of atrial fibrillation. Circulation *104*: 2849–2854.

Chen, Y.-J., Chen, Y.-C., Tai, C.-T., Yeh, H.-I., Lin, C.-I., and Chen, S.-A. (2006b). Angiotensin II and angiotensin II receptor blocker modulate the arrhythmogenic activity of pulmonary veins. Br. J. Pharmacol. *147*: 12–22.

Cheung, D.W. (1981). Electrical activity of the pulmonary vein and its interaction with the right atrium in the guinea-pig. J. Physiol. *314*: 445–456.

Chou, C.-C., Nihei, M., Zhou, S., Tan, A., Kawase, A., Macias, E.S., *et al*. (2005). Intracellular calcium dynamics and anisotropic reentry in isolated canine pulmonary veins and left atrium. Circulation *111*: 2889–2897.

Christidis, D., Kalogerakis, D., Chan, T.Y., Mauri, D., Alexiou, G., and Terzoudi, A. (2006). Is primidone the drug of choice for epileptic patients with QT-prolongation? A comprehensive analysis of literature. Seizure *15*: 64–66.

Clancy, C.E., Tateyama, M., Liu, H., Wehrens, X.H.T., and Kass, R.S. (2003). Non-equilibrium gating in cardiac Na^+ channels: an original mechanism of arrhythmia. Circulation *107*: 2233–2237.

Clerc, L. (1976). Directional differences of impulse spread in trabecular muscle from mammalian heart. J. Physiol. *255*: 335–346.

Cohen, C.J., Bean, B.P., and Tsien, R.W. (1984). Maximal upstroke velocity as an index of available sodium conductance. Comparison of maximal upstroke velocity and voltage clamp measurements of sodium current in rabbit Purkinje fibers. Circ. Res. *54*: 636–651.

Cohen, S.A. (1996). Immunocytochemical localization of rH1 sodium channel in adult rat heart atria and ventricle. Presence in terminal intercalated disks. Circulation *94*: 3083–3086.

Colatsky, T.J. (1980). Voltage clamp measurements of sodium channel properties in rabbit cardiac Purkinje fibres. J. Physiol. *305*: 215–234.

Colman, M.A., Aslanidi, O.V., Kharche, S., Boyett, M.R., Garratt, C., Hancox, J.C., *et al*. (2013). Pro-arrhythmogenic effects of atrial fibrillation-induced electrical remodelling: insights from the three-dimensional virtual human atria. J. Physiol. *591*: 4249–4272.

Comtois, P., Kneller, J., and Nattel, S. (2005). Of circles and spirals: bridging the gap between the leading circle and spiral wave concepts of cardiac reentry. Eur. Eur. Pacing Arrhythm. Card. Electrophysiol. J. Work. Groups Card. Pacing Arrhythm. Card. Cell. Electrophysiol. Eur. Soc. Cardiol. *7 Suppl 2*: 10–20.

Coutu, P., Chartier, D., and Nattel, S. (2006). Comparison of Ca^{2+}-handling properties of canine pulmonary vein and left atrial cardiomyocytes. Am. J. Physiol. Heart Circ. Physiol. *291*: H2290–2300.

Cox, J.L., Boineau, J.P., Schuessler, R.B., Jaquiss, R.D., and Lappas, D.G. (1995a). Modification of the maze procedure for atrial flutter and atrial fibrillation. I. Rationale and surgical results. J. Thorac. Cardiovasc. Surg. *110*: 473–484.

Cox, J.L., Jaquiss, R.D., Schuessler, R.B., and Boineau, J.P. (1995b). Modification of the maze procedure for atrial flutter and atrial fibrillation. II. Surgical technique of the maze III procedure. J. Thorac. Cardiovasc. Surg. *110*: 485–495.

Darbar, D., Kannankeril, P.J., Donahue, B.S., Kucera, G., Stubblefield, T., Haines, J.L., *et al.* (2008). Cardiac sodium channel (SCN5A) variants associated with atrial fibrillation. Circulation *117*: 1927–1935.

Davidenko, J.M., Pertsov, A.V., Salomonsz, R., Baxter, W., and Jalife, J. (1992). Stationary and drifting spiral waves of excitation in isolated cardiac muscle. Nature *355*: 349–351.

De Ferrari, G.M., Maier, L.S., Mont, L., Schwartz, P.J., Simonis, G., Leschke, M., *et al.* (2015). Ranolazine in the treatment of atrial fibrillation: Results of the dose-ranging RAFFAELLO (Ranolazine in Atrial Fibrillation Following An ELectricaL CardiOversion) study. Heart Rhythm *12*: 872–878.

Dhar Malhotra, J., Chen, C., Rivolta, I., Abriel, H., Malhotra, R., Mattei, L.N., *et al.* (2001). Characterization of sodium channel α- and β-subunits in rat and mouse cardiac myocytes. Circulation *103*: 1303–1310.

Dibb, K.M., Clarke, J.D., Horn, M.A., Richards, M.A., Graham, H.K., Eisner, D.A., *et al.* (2009). Characterization of an Extensive Transverse Tubular Network in Sheep Atrial Myocytes and its Depletion in Heart Failure. Circ. Heart Fail. *2*: 482–489.

Dib-Hajj, S.D., Tyrrell, L., Black, J.A., and Waxman, S.G. (1998). NaN, a novel voltage-gated Na^+ channel, is expressed preferentially in peripheral sensory neurons and down-regulated after axotomy. Proc. Natl. Acad. Sci. U. S. A. *95*: 8963–8968.

DiFrancesco, D. (1991). The contribution of the 'pacemaker' current (I_f) to generation of spontaneous activity in rabbit sino-atrial node myocytes. J. Physiol. *434*: 23–40.

Ding, H.-Y., Yang, X.-C., Liu, X.-L., Liu, T.-F., and Bao, R.-F. (2006). Characteristics of the action potentials and the underlying ionic mechanisms in the cardiomyocytes from rabbit pulmonary vein sleeves. Sheng Li Xue Bao *58*: 129–135.

Dobrev, D., and Nattel, S. (2010). New antiarrhythmic drugs for treatment of atrial fibrillation. Lancet *375*: 1212–1223.

Dobrev, D., Wettwer, E., Kortner, A., Knaut, M., Schüler, S., and Ravens, U. (2002). Human inward rectifier potassium channels in chronic and postoperative atrial fibrillation. Cardiovasc. Res. *54*: 397–404.

Doisne, N., Maupoil, V., Cosnay, P., and Findlay, I. (2009). Catecholaminergic automatic activity in the rat pulmonary vein: electrophysiological differences between cardiac muscle in the left atrium and pulmonary vein. Am. J. Physiol. Heart Circ. Physiol. *297*: H102–108.

Doyle, D.D., Guo, Y., Lustig, S.L., Satin, J., Rogart, R.B., and Fozzard, H.A. (1993). Divalent cation competition with [3H]saxitoxin binding to tetrodotoxin-resistant and -sensitive sodium channels. A two-site structural model of ion/toxin interaction. J. Gen. Physiol. *101*: 153–182.

Draper, M.H., and Weidmann, S. (1951). Cardiac resting and action potentials recorded with an intracellular electrode. J. Physiol. *115*: 74–94.

Duan, D.D. (2015). Calm down when the heart is stressed: Inhibiting calmodulin-dependent protein kinase II for antiarrhythmias. Trends Cardiovasc. Med. *25*: 398–400.

Duan, D., Fermini, B., and Nattel, S. (1993). Potassium channel blocking properties of propafenone in rabbit atrial myocytes. J. Pharmacol. Exp. Ther. *264*: 1113–1123.

Dudley, S.C., Hoch, N.E., McCann, L.A., Honeycutt, C., Diamandopoulos, L., Fukai, T., *et al*. (2005). Atrial fibrillation increases production of superoxide by the left atrium and left atrial appendage: role of the NADPH and xanthine oxidases. Circulation *112*: 1266–1273.

Duff, H.J., Offord, J., West, J., and Catterall, W.A. (1992). Class I and IV antiarrhythmic drugs and cytosolic calcium regulate mRNA encoding the sodium channel α-subunit in rat cardiac muscle. Mol. Pharmacol. *42*: 570–574.

Dzau, V.J. (1993). Tissue renin-angiotensin system in myocardial hypertrophy and failure. Arch. Intern. Med. *153*: 937–942.

Dzhura, I., Wu, Y., Colbran, R.J., Balser, J.R., and Anderson, M.E. (2000). Calmodulin kinase determines calcium-dependent facilitation of L-type calcium channels. Nat. Cell Biol. *2*: 173–177.

Ednie, A.R., Horton, K.-K., Wu, J., and Bennett, E.S. (2013). Expression of the sialyltransferase, ST3Gal4, impacts cardiac voltage-gated sodium channel activity, refractory period and ventricular conduction. J. Mol. Cell. Cardiol. *59*: 117–127.

Egorov, Y.V., Kuz'min, V.S., Glukhov, A.V., and Rosenshtraukh, L.V. (2015). Electrophysiological characteristics, rhythm, disturbances and conduction discontinuities under autonomic stimulation in the rat pulmonary vein myocardium. J. Cardiovasc. Electrophysiol.

Ehrlich, J.R., Biliczki, P., Hohnloser, S.H., and Nattel, S. (2008). Atrial-selective approaches for the treatment of atrial fibrillation. J. Am. Coll. Cardiol. *51*: 787–792.

Ehrlich, J.R., Cha, T.-J., Zhang, L., Chartier, D., Melnyk, P., Hohnloser, S.H., *et al.* (2003). Cellular electrophysiology of canine pulmonary vein cardiomyocytes: action potential and ionic current properties. J. Physiol. *551*: 801–813.

Ehrlich, J.R., Zicha, S., Coutu, P., Hébert, T.E., and Nattel, S. (2005). Atrial fibrillation-associated minK38G/S polymorphism modulates delayed rectifier current and membrane localization. Cardiovasc. Res. *67*: 520–528.

Escande, D., Coulombe, A., Faivre, J.F., Deroubaix, E., and Coraboeuf, E. (1987). Two types of transient outward currents in adult human atrial cells. Am. J. Physiol. - Heart Circ. Physiol. *252*: H142–H148.

Faber, G.M., and Rudy, Y. (2000). Action potential and contractility changes in $[Na^+](i)$ overloaded cardiac myocytes: a simulation study. Biophys. J. *78*: 2392–2404.

Fabiato, A., and Fabiato, F. (1971). The two components of the human atrial action potential. Circ. Res. *29*: 296–305.

Fabiato, A., and Fabiato, F. (1978). Calcium-induced release of calcium from the sarcoplasmic reticulum of skinned cells from adult human, dog, cat, rabbit, rat, and frog hearts and from fetal and new-born rat ventricles*. Ann. N. Y. Acad. Sci. *307*: 491–522.

Facer, P., Punjabi, P.P., Abrari, A., Kaba, R.A., Severs, N.J., Chambers, J., *et al.* (2011). Localisation of SCN10A gene product $Na_v1.8$ and novel pain-related ion channels in human heart. Int. Heart. J. *52*: 146–152.

Firouzi, M., Ramanna, H., Kok, B., Jongsma, H.J., Koeleman, B.P.C., Doevendans, P.A., *et al.* (2004). Association of human connexin40 gene polymorphisms with atrial vulnerability as a risk factor for idiopathic atrial fibrillation. Circ. Res. *95*: e29–33.

Fischer, T.H., Herting, J., Mason, F.E., Hartmann, N., Watanabe, S., Nikolaev, V.O., *et al.* (2015). Late I_{Na} increases diastolic SR-Ca^{2+}-leak in atrial myocardium by activating PKA and CaMKII. Cardiovasc. Res. *107*: 184–196.

Fisher, A.W. (1965). The intrinsic innervation of the pulmonary vessels. Acta Anat. (Basel) *60*: 481–496.

Forfar, J.C., Miller, H.C., and Toft, A.D. (1979). Occult thyrotoxicosis: A correctable cause of 'idiopathic' atrial fibrillation. Am. J. Cardiol. *44*: 9–12.

Franzini-Armstrong, C., Protasi, F., and Ramesh, V. (1999). Shape, size, and distribution of Ca^{2+} release units and couplons in skeletal and cardiac muscles. Biophys. J. *77*: 1528–1539.

Fujiki, A., Nagasawa, H., Sakabe, M., Sakurai, K., Nishida, K., Mizumaki, K., *et al.* (2001). Spectral characteristics of human atrial fibrillation waves of the right atrial free wall with respect to the duration of atrial fibrillation and effect of class I antiarrhythmic drugs. Jpn. Circ. J. *65*: 1047–1051.

Fujiwara, K., Tanaka, H., Mani, H., Nakagami, T., and Takamatsu, T. (2008). Burst emergence of intracellular Ca^{2+} waves evokes arrhythmogenic oscillatory depolarization via the Na^{+}-Ca^{2+} exchanger: simultaneous confocal recording of membrane potential and intracellular Ca^{2+} in the heart. Circ. Res. *103*: 509–518.

Fukuda, K., Watanabe, J., Yagi, T., Wakayama, Y., Nakano, M., Kondo, M., *et al.* (2011). A sodium channel blocker, pilsicainide, produces atrial post-repolarization refractoriness through the reduction of sodium channel availability. Tohoku J. Exp. Med. *225*: 35–42.

Fuster, V., Rydén, L.E., Cannom, D.S., Crijns, H.J., Curtis, A.B., Ellenbogen, K.A., *et al*. (2006). ACC/AHA/ESC 2006 guidelines for the management of patients with atrial fibrillation-executive summary: a report of the American College of Cardiology/American Heart Association Task Force on Practice Guidelines and the European Society of Cardiology Committee for Practice Guidelines (Writing Committee to Revise the 2001 Guidelines for the Management of Patients with Atrial Fibrillation). Eur. Heart J. *27*: 1979–2030.

Gaborit, N., Le Bouter, S., Szuts, V., Varro, A., Escande, D., Nattel, S., *et al*. (2007). Regional and tissue specific transcript signatures of ion channel genes in the non-diseased human heart. J. Physiol. *582*: 675–693.

Gaspo, R., Bosch, R.F., Talajic, M., and Nattel, S. (1997). Functional mechanisms underlying tachycardia-induced sustained atrial fibrillation in a chronic dog model. Circulation *96*: 4027–4035.

Gellens, M.E., George, A.L., Chen, L.Q., Chahine, M., Horn, R., Barchi, R.L., *et al.* (1992). Primary structure and functional expression of the human cardiac tetrodotoxin-insensitive voltage-dependent sodium channel. Proc. Natl. Acad. Sci. U. S. A. *89*: 554–558.

Gherghiceanu, M., Hinescu, M.E., Andrei, F., Mandache, E., Macarie, C.E., Faussone-Pellegrini, M.-S., *et al*. (2008). Interstitial Cajal-like cells (ICLC) in myocardial sleeves of human pulmonary veins. J. Cell. Mol. Med. *12*: 1777–1781.

Giles, W.R., and Imaizumi, Y. (1988). Comparison of potassium currents in rabbit atrial and ventricular cells. J. Physiol. *405*: 123–145.

Gintant, G.A., Datyner, N.B., and Cohen, I.S. (1984). Slow inactivation of a tetrodotoxin-sensitive current in canine cardiac Purkinje fibers. Biophys. J. *45*: 509–512.

Goette, A., Arndt, M., Röcken, C., Spiess, A., Staack, T., Geller, J.C., *et al.* (2000). Regulation of angiotensin II receptor subtypes during Atrial Fibrillation in humans. Circulation *101*: 2678–2681.

Grandi, E., Puglisi, J.L., Wagner, S., Maier, L.S., Severi, S., and Bers, D.M. (2007). Simulation of Ca-calmodulin-dependent protein kinase II on rabbit ventricular myocyte ion currents and action potentials. Biophys. J. *93*: 3835–3847.

Greiser, M., Neuberger, H.-R., Harks, E., El-Armouche, A., Boknik, P., Haan, S. de, *et al.* (2009). Distinct contractile and molecular differences between two goat models of atrial dysfunction: AV block-induced atrial dilatation and atrial fibrillation. J. Mol. Cell. Cardiol. *46*: 385–394.

Guo, D., Lian, J., Liu, T., Cox, R., Margulies, K.B., Kowey, P.R., *et al*. (2011). Contribution of late sodium current (I_{NaL}) to rate adaptation of ventricular repolarization and reverse use-dependence of QT-prolonging agents. Heart Rhythm Off. J. Heart Rhythm Soc. *8*: 762–769.

Guo, D., Young, L., Wu, Y., Belardinelli, L., Kowey, P.R., and Yan, G.-X. (2010). Increased late sodium current in left atrial myocytes of rabbits with left ventricular hypertrophy: its role in the genesis of atrial arrhythmias. Am. J. Physiol. Heart Circ. Physiol. *298*: H1375–1381.

Guy, H.R., and Seetharamulu, P. (1986). Molecular model of the action potential sodium channel. Proc. Natl. Acad. Sci. U. S. A. *83*: 508–512.

Haïssaguerre, M., Jaïs, P., Shah, D.C., Takahashi, A., Hocini, M., Quiniou, G., *et al.* (1998). Spontaneous initiation of atrial fibrillation by ectopic beats originating in the pulmonary veins. N. Engl. J. Med. *339*: 659–666.

Hakim, P., Brice, N., Thresher, R., Lawrence, J., Zhang, Y., Jackson, A.P., *et al.* (2010a). SCN3b knockout mice exhibit abnormal sino-atrial and cardiac conduction properties. Acta Physiol. Oxf. Engl. *198*: 47–59.

Hakim, P., Gurung, I.S., Pedersen, T.H., Thresher, R., Brice, N., Lawrence, J., *et al.* (2008). SCN3b knockout mice exhibit abnormal ventricular electrophysiological properties. Prog. Biophys. Mol. Biol. *98*: 251–266.

Hakim, P., Thresher, R., Grace, A.A., and Huang, C.L.-H. (2010b). Effects of flecainide and quinidine on action potential and ventricular arrhythmogenic properties in Scn3b knockout mice. Clin. Exp. Pharmacol. Physiol. *37*: 782–789.

Halt, A.R., Dallapiazza, R.F., Zhou, Y., Stein, I.S., Qian, H., Juntti, S., *et al.* (2012). CaMKII binding to GluN2B is critical during memory consolidation. EMBO J. *31*: 1203–1216.

Hamabe, A., Okuyama, Y., Miyauchi, Y., Zhou, S., Pak, H.-N., Karagueuzian, H.S., *et al.* (2003). Correlation between anatomy and electrical activation in canine pulmonary veins. Circulation *107*: 1550–1555.

Hanafy, D.A., Chen, Y.-C., Chang, S.-L., Lu, Y.-Y., Lin, Y.-K., Kao, Y.-H., *et al.* (2013). Different effects of dronedarone and amiodarone on pulmonary vein electrophysiology, mechanical properties and H2O2-induced arrhythmogenicity. Eur. J. Pharmacol. *702*: 103–108.

Hashizume, H., Tango, M., and Ushiki, T. (1998). Three-dimensional cytoarchitecture of rat pulmonary venous walls: a light and scanning electron microscopic study. Anat. Embryol. (Berl.) *198*: 473–480.

Hassink, R.J., Aretz, H.T., Ruskin, J., and Keane, D. (2003). Morphology of atrial myocardium in human pulmonary veins: a postmortem analysis in patients with and without atrial fibrillation. J. Am. Coll. Cardiol. *42*: 1108–1114.

Haufe, V., Camacho, J.A., Dumaine, R., Günther, B., Bollensdorff, C., Banchet, G.S. von, *et al*. (2005a). Expression pattern of neuronal and skeletal muscle voltage-gated Na^+ channels in the developing mouse heart. J. Physiol. *564*: 683–696.

Haufe, V., Cordeiro, J.M., Zimmer, T., Wu, Y.S., Schiccitano, S., Benndorf, K., *et al*. (2005b). Contribution of neuronal sodium channels to the cardiac fast sodium current I_{Na} is greater in dog heart Purkinje fibers than in ventricles. Cardiovasc. Res. *65*: 117–127.

Hayashi, H., Fujiki, A., Tani, M., Usui, M., and Inoue, H. (1998). Different effects of class IC and III antiarrhythmic drugs on vagotonic atrial fibrillation in the canine heart. J. Cardiovasc. Pharmacol. *31*: 101–107.

Heinemann, S.H., Terlau, H., Stühmer, W., Imoto, K., and Numa, S. (1992). Calcium channel characteristics conferred on the sodium channel by single mutations. Nature *356*: 441–443.

He, X., Wang, H., Shen, Y., Zhong, Q., Fang, S., Peng, W., *et al*. (2012). Cardiomyocyte progenitors in a canine pulmonary vein model of persistent atrial fibrillation. J. Cardiol. *60*: 242–247.

Hirose, M., Ohkubo, Y., Takano, M., Hamazaki, M., Sekido, T., and Yamada, M. (2007a). Mechanisms of the Preventive Effect of Pilsicainide on Atrial Fibrillation Originating From the Pulmonary Vein. Circ. J. *71*: 1805–1814.

Hirose, M., Ohkubo, Y., Takano, M., Hamazaki, M., Sekido, T., and Yamada, M. (2007b). Mechanisms of the preventive effect of pilsicainide on atrial fibrillation originating from the pulmonary vein. Circ. J. Off. J. Jpn. Circ. Soc. *71*: 1805–1814.

Hocini, M., Ho, S.Y., Kawara, T., Linnenbank, A.C., Potse, M., Shah, D., *et al*. (2002). Electrical conduction in canine pulmonary veins: electrophysiological and anatomic correlation. Circulation *105*: 2442–2448.

Hodgkin, A.L., and Huxley, A.F. (1952a). A quantitative description of membrane current and its application to conduction and excitation in nerve. J. Physiol. *117*: 500–544.

Hodgkin, A.L., and Huxley, A.F. (1952b). The dual effect of membrane potential on sodium conductance in the giant axon of Loligo. J. Physiol. *116*: 497–506.

Hoey, A., Harrison, S.M., Boyett, M.R., and Ravens, U. (1994). Effects of the Anemonia sulcata toxin (ATX II) on intracellular sodium and contractility in rat and guinea-pig myocardium. Pharmacol. Toxicol. *75*: 356–365.

Hoff, M.J.B. van den, Kruithof, B.P.T., and Moorman, A.F.M. (2004). Making more heart muscle. BioEssays News Rev. Mol. Cell. Dev. Biol. *26*: 248–261.

Holm, H., Gudbjartsson, D.F., Arnar, D.O., Thorleifsson, G., Thorgeirsson, G., Stefansdottir, H., *et al.* (2010). Several common variants modulate heart rate, PR interval and QRS duration. Nat. Genet. *42*: 117–122.

Hondeghem, L.M., and Katzung, B.G. (1984). Antiarrhythmic agents: the modulated receptor mechanism of action of sodium and calcium channel-blocking drugs. Annu. Rev. Pharmacol. Toxicol. *24*: 387–423.

Honjo, H., Boyett, M.R., Kodama, I., and Toyama, J. (1996). Correlation between electrical activity and the size of rabbit sino-atrial node cells. J. Physiol. *496*: 795–808.

Honjo, H., Boyett, M.R., Niwa, R., Inada, S., Yamamoto, M., Mitsui, K., *et al.* (2003). Pacing-induced spontaneous activity in myocardial sleeves of pulmonary veins after treatment with ryanodine. Circulation *107*: 1937–1943.

Hoppe, U.C., Jansen, E., Südkamp, M., and Beuckelmann, D.J. (1998). Hyperpolarization-activated inward current in ventricular myocytes from normal and failing human hearts. Circulation *97*: 55–65.

Horvath, B., Banyasz, T., Jian, Z., Hegyi, B., Kistamas, K., Nanasi, P.P., *et al.* (2013). Dynamics of the late Na^+ current during cardiac action potential and its contribution to afterdepolarizations. J. Mol. Cell. Cardiol. *64*: 59–68.

Hosoyamada, Y., Ichimura, K., Koizumi, K., and Sakai, T. (2010). Structural organization of pulmonary veins in the rat lung, with special emphasis on the musculature consisting of cardiac and smooth muscles. Anat. Sci. Int. *85*: 152–159.

Ho, S.Y., Cabrera, J.A., Tran, V.H., Farré, J., Anderson, R.H., and Sánchez-Quintana, D. (2001). Architecture of the pulmonary veins: relevance to radiofrequency ablation. Heart Br. Card. Soc. *86*: 265–270.

Hoyer, K., Song, Y., Wang, D., Phan, D., Balschi, J., Ingwall, J.S., *et al.* (2011). Reducing the late sodium current improves cardiac function during sodium pump inhibition by ouabain. J. Pharmacol. Exp. Ther. *337*: 513–523.

Huang, B., El-Sherif, T., Gidh-Jain, M., Qin, D., and El-Sherif, N. (2001). Alterations of sodium channel kinetics and gene expression in the postinfarction remodeled myocardium. J. Cardiovasc. Electrophysiol. *12*: 218–225.

Hwang, C., Karagueuzian, H.S., and Chen, P.S. (1999). Idiopathic paroxysmal atrial fibrillation induced by a focal discharge mechanism in the left superior pulmonary vein: possible roles of the ligament of Marshall. J. Cardiovasc. Electrophysiol. *10*: 636–648.

Ikeda, T., Uchida, T., Hough, D., Lee, J.J., Fishbein, M.C., Mandel, W.J., *et al.* (1996). Mechanism of spontaneous termination of functional reentry in isolated canine right atrium. Evidence for the presence of an excitable but nonexcited core. Circulation *94*: 1962–1973.

Irons, G.V., and Orgain, E.S. (1966). Digitalis-induced arrhythmias and their management. Prog. Cardiovasc. Dis. *8*: 539–569.

Isenberg, G., and Klockner, U. (1982). Calcium tolerant ventricular myocytes prepared by preincubation in a 'KB medium'. Pflüg. Arch. Eur. J. Physiol. *395*: 6–18.

Isenberg, G., and Ravens, U. (1984). The effects of the Anemonia sulcata toxin (ATX II) on membrane currents of isolated mammalian myocytes. J. Physiol. *357*: 127–149.

Ishibashi, K., Inoue, D., Sakai, R., Inoue, M., Shirayama, T., Asayama, J., *et al.* (1995). Effects of disopyramide on the atrial fibrillation threshold in the human atrium. Int. J. Cardiol. *52*: 177–184.

Isom, L.L., De Jongh, K.S., Patton, D.E., Reber, B.F., Offord, J., Charbonneau, H., *et al*. (1992). Primary structure and functional expression of the β1 subunit of the rat brain sodium channel. Science *256*: 839–842.

Iwasaki, Y., Nishida, K., Kato, T., and Nattel, S. (2011). Atrial fibrillation pathophysiology: implications for management. Circulation *124*: 2264–2274.

Jaïs, P., Hocini, M., Macle, L., Choi, K.-J., Deisenhofer, I., Weerasooriya, R., *et al.* (2002). Distinctive electrophysiological properties of pulmonary veins in patients with atrial fibrillation. Circulation *106*: 2479–2485.

Jakob, H., and Nawrath, H. (1988). Tetrodotoxin slightly shortens action potential duration in ventricular but not in atrial heart muscle. Experientia *44*: 16–17.

James, T.N., Sherf, L., Fine, G., and Morales, A.R. (1966). Comparative ultrastructure of the sinus node in man and dog. Circulation *34*: 139–163.

January, C.T., and Riddle, J.M. (1989). Early afterdepolarizations: mechanism of induction and block. A role for L-type Ca^{2+} current. Circ. Res. *64*: 977–990.

Jarvis, M.F., Honore, P., Shieh, C.-C., Chapman, M., Joshi, S., Zhang, X.-F., *et al.* (2007). A-803467, a potent and selective $Na_v1.8$ sodium channel blocker, attenuates neuropathic and inflammatory pain in the rat. Proc. Natl. Acad. Sci. U. S. A. *104*: 8520–8525.

Johnson, J.N., Tester, D.J., Perry, J., Salisbury, B.A., Reed, C.R., and Ackerman, M.J. (2008). Prevalence of early-onset atrial fibrillation in congenital long QT syndrome. Heart Rhythm Off. J. Heart Rhythm Soc. *5*: 704–709.

Johnson, P.N., Freedberg, A.S., and Marshall, J.M. (1973). Action of thyroid hormone on the transmembrane potentials from sinoatrial node cells and atrial muscle cells in isolated atria of rabbits. Cardiology *58*: 273–289.

Jones, S.A., Yamamoto, M., Tellez, J.O., Billeter, R., Boyett, M.R., Honjo, H., *et al.* (2008). Distinguishing properties of cells from the myocardial sleeves of the pulmonary veins: a comparison of normal and abnormal pacemakers. Circ. Arrhythm. Electrophysiol. *1*: 39–48.

Jones, W.K., Sánchez, A., and Robbins, J. (1994). Murine pulmonary myocardium: developmental analysis of cardiac gene expression. Dev. Dyn. Off. Publ. Am. Assoc. Anat. *200*: 117–128.

Joshi, S.K., Mikusa, J.P., Hernandez, G., Baker, S., Shieh, C.-C., Neelands, T., *et al.* (2006). Involvement of the TTX-resistant sodium channel Na_v 1.8 in inflammatory and neuropathic, but not post-operative, pain states. Pain *123*: 75–82.

Jost, N., Nagy, N., Corici, C., Kohajda, Z., Horváth, A., Acsai, K., *et al*. (2013). ORM-10103, a novel specific inhibitor of the Na^+/Ca^{2+} exchanger, decreases early and delayed afterdepolarizations in the canine heart. Br. J. Pharmacol. *170*: 768–778.

Ju, Y.K., Saint, D.A., and Gage, P.W. (1992). Effects of lignocaine and quinidine on the persistent sodium current in rat ventricular myocytes. Br. J. Pharmacol. *107*: 311–316.

Kandel, E., Schwartz, J., and Jessell, T. (2000). Principles of Neural Science (McGraw-Hill).

Kanki, H., Mitamura, H., Takatsuki, S., Sueyoshi, K., Shinagawa, K., Sato, T., *et al*. (1998). Postrepolarization refractoriness as a potential anti–atrial fibrillation mechanism of pilsicainide, a pure sodium channel blocker with slow recovery kinetics. Cardiovasc. Drugs Ther. *12*: 475–482.

Kass, R.S., Lederer, W.J., Tsien, R.W., and Weingart, R. (1978). Role of calcium ions in transient inward currents and aftercontractions induced by strophanthidin in cardiac Purkinje fibres. J. Physiol. *281*: 187–208.

Kaufmann, S.G., Westenbroek, R.E., Maass, A.H., Lange, V., Renner, A., Wischmeyer, E., *et al*. (2013). Distribution and function of sodium channel subtypes in human atrial myocardium. J. Mol. Cell. Cardiol. *61*: 133–141.

Kayano, T., Noda, M., Flockerzi, V., Takahashi, H., and Numa, S. (1988). Primary structure of rat brain sodium channel III deduced from the cDNA sequence. FEBS Lett. *228*: 187–194.

Kazen-Gillespie, K.A., Ragsdale, D.S., D'Andrea, M.R., Mattei, L.N., Rogers, K.E., and Isom, L.L. (2000). Cloning, localization, and functional expression of sodium channel β1A subunits. J. Biol. Chem. *275*: 1079–1088.

Kholová, I., and Kautzner, J. (2003). Anatomic characteristics of extensions of atrial myocardium into the pulmonary veins in subjects with and without atrial fibrillation. Pacing Clin. Electrophysiol. PACE *26*: 1348–1355.

Kim, D. (1993). Mechanism of rapid desensitization of muscarinic K^+ current in adult rat and guinea pig atrial cells. Circ. Res. *73*: 89–97.

Kirchhof, P., Engelen, M., Franz, M.R., Ribbing, M., Wasmer, K., Breithardt, G., *et al*. (2005). Electrophysiological effects of flecainide and sotalol in the human atrium during persistent atrial fibrillation. Basic Res. Cardiol. *100*: 112–121.

Kiyosue, T., and Arita, M. (1989). Late sodium current and its contribution to action potential configuration in guinea pig ventricular myocytes. Circ. Res. *64*: 389–397.

Kontis, K.J., Rounaghi, A., and Goldin, A.L. (1997). Sodium Channel Activation Gating Is Affected by Substitutions of Voltage Sensor Positive Charges in All Four Domains. J. Gen. Physiol. *110*: 391–401.

Kostin, S., Klein, G., Szalay, Z., Hein, S., Bauer, E.P., and Schaper, J. (2002). Structural correlate of atrial fibrillation in human patients. Cardiovasc. Res. *54*: 361–379.

Koumi, S., Arentzen, C.E., Backer, C.L., and Wasserstrom, J.A. (1994). Alterations in muscarinic K^+ channel response to acetylcholine and to G protein-mediated activation in atrial myocytes isolated from failing human hearts. Circulation *90*: 2213–2224.

Koumi, S., Backer, C.L., and Arentzen, C.E. (1995). Characterization of inwardly rectifying K^+ channel in human cardiac myocytes. Alterations in channel behavior in myocytes isolated from patients with idiopathic dilated cardiomyopathy. Circulation *92*: 164–174.

Kracklauer, M.P., Feng, H.-Z., Jiang, W., Lin, J.L.-C., Lin, J.J.-C., and Jin, J.-P. (2013). Discontinuous thoracic venous cardiomyocytes and heart exhibit synchronized developmental switch of troponin isoforms. FEBS J. *280*: 880–891.

Kramer, A.W., and Marks, L.S. (1965). The occurrence of cardiac muscle in the pulmonary veins of Rodenita. J. Morphol. *117*: 135–149.

Kumagai, K., Ogawa, M., Noguchi, H., Yasuda, T., Nakashima, H., and Saku, K. (2004a). Electrophysiologic properties of pulmonary veins assessed using a multielectrode basket catheter. J. Am. Coll. Cardiol. *43*: 2281–2289.

Kumagai, K., Tojo, H., Noguchi, H., Yasuda, T., Ogawa, M., Nakashima, H., *et al.* (2004b). Effects of the Na^+ channel blocker pilsicainide on the electrophysiologic

properties of pulmonary veins in patients with atrial fibrillation. J. Cardiovasc. Electrophysiol. *15*: 1396–1401.

Laitinen-Forsblom, P.J., Mäkynen, P., Mäkynen, H., Yli-Mäyry, S., Virtanen, V., Kontula, K., *et al*. (2006). SCN5A mutation associated with cardiac conduction defect and atrial arrhythmias. J. Cardiovasc. Electrophysiol. *17*: 480–485.

Lei, M., Jones, S.A., Liu, J., Lancaster, M.K., Fung, S.S.-M., Dobrzynski, H., *et al.* (2004). Requirement of neuronal- and cardiac-type sodium channels for murine sinoatrial node pacemaking. J. Physiol. *559*: 835–848.

Lemoine, M.D., Duverger, J.E., Naud, P., Chartier, D., Qi, X.Y., Comtois, P., *et al.* (2011). Arrhythmogenic left atrial cellular electrophysiology in a murine genetic long QT syndrome model. Cardiovasc. Res. *92*: 67–74.

Lenaerts, I., Bito, V., Heinzel, F.R., Driesen, R.B., Holemans, P., D'hooge, J., *et al.* (2009). Ultrastructural and Functional Remodeling of the Coupling Between Ca2+ Influx and Sarcoplasmic Reticulum Ca2+ Release in Right Atrial Myocytes From Experimental Persistent Atrial Fibrillation. Circ. Res. *105*: 876–885.

Levin, M.D., Lu, M.M., Petrenko, N.B., Hawkins, B.J., Gupta, T.H., Lang, D., *et al*. (2009). Melanocyte-like cells in the heart and pulmonary veins contribute to atrial arrhythmia triggers. J. Clin. Invest. *119*: 3420–3436.

Li, D., Fareh, S., Leung, T.K., and Nattel, S. (1999). Promotion of Atrial Fibrillation by Heart Failure in Dogs Atrial Remodeling of a Different Sort. Circulation *100*: 87–95.

Li, D., Melnyk, P., Feng, J., Wang, Z., Petrecca, K., Shrier, A., *et al*. (2000). Effects of experimental heart failure on atrial cellular and ionic electrophysiology. Circulation *101*: 2631–2638.

Li, D., Shinagawa, K., Pang, L., Leung, T.K., Cardin, S., Wang, Z., *et al.* (2001). Effects of angiotensin-converting enzyme inhibition on the development of the atrial fibrillation substrate in dogs with ventricular tachypacing-induced congestive heart failure. Circulation *104*: 2608–2614.

Li, G.-R., Lau, C.-P., and Shrier, A. (2002). Heterogeneity of sodium current in atrial vs epicardial ventricular myocytes of adult guinea pig hearts. J. Mol. Cell. Cardiol. *34*: 1185–1194.

Li, G.R., and Nattel, S. (1997). Properties of human atrial I_{Ca} at physiological temperatures and relevance to action potential. Am. J. Physiol. - Heart Circ. Physiol. *272*: H227–H235.

Li, J.-Y., Wang, H.-J., Xu, B., Wang, X.-P., Fu, Y.-C., Chen, M.-Y., *et al*. (2012). Hyperpolarization activated cation current (I_f) in cardiac myocytes from pulmonary vein sleeves in the canine with atrial fibrillation. J. Geriatr. Cardiol. JGC *9*: 366–374.

Lim, P.B., Malcolme-Lawes, L.C., Stuber, T., Wright, I., Francis, D.P., Davies, D.W., *et al*. (2011). Intrinsic cardiac autonomic stimulation induces pulmonary vein ectopy and triggers atrial fibrillation in humans. J. Cardiovasc. Electrophysiol. *22*: 638–646.

Lines, G.T., Sande, J.B., Louch, W.E., Mørk, H.K., Grøttum, P., and Sejersted, O.M. (2006). Contribution of the Na^+/Ca^{2+} exchanger to rapid Ca^{2+} release in cardiomyocytes. Biophys. J. *91*: 779–792.

Lin, Y.-K., Chen, Y.-C., Cheng, C.-C., Lin, F.Y., Chen, S.A., and Chen, Y.J. (2011). Interactions of aging and hydrogen peroxide on pulmonary vein electrical activity: implications in the pathophysiology of atrial fibrillation. Acta Cardiol Sin *27*: 109–14.

Lin, Y.-K., Lin, F.-Z., Chen, Y.-C., Cheng, C.-C., Lin, C.-I., Chen, Y.-J., *et al.* (2010). Oxidative stress on pulmonary vein and left atrium arrhythmogenesis. Circ. J. Off. J. Jpn. Circ. Soc. *74*: 1547–1556.

Li, Q., Huang, H., Liu, G., Lam, K., Rutberg, J., Green, M.S., *et al.* (2009). Gain-of-function mutation of $Na_v1.5$ in atrial fibrillation enhances cellular excitability and lowers the threshold for action potential firing. Biochem. Biophys. Res. Commun. *380*: 132–137.

Li, R.-G., Wang, Q., Xu, Y.-J., Zhang, M., Qu, X.-K., Liu, X., *et al*. (2013). Mutations of the SCN4B-encoded sodium channel β4 subunit in familial atrial fibrillation. Int. J. Mol. Med. *32*: 144–150.

Liu, J., Huang, C., Jiang, H., Bao, M., Cao, F., and Wang, T. (2005). Characteristics of hyperpolarization-activated inward current in rabbit pulmonary vein muscle sleeve cells. Chin. Med. J. (Engl.) *118*: 2014–2019.

Liu, Y.M., DeFelice, L.J., and Mazzanti, M. (1992). Na channels that remain open throughout the cardiac action potential plateau. Biophys. J. *63*: 654–662.

Li, Y.-D., Hong, Y.-F., Zhang, Y., Zhou, X.-H., Ji, Y.-T., Li, H.-L., *et al.* (2014). Association between reversal in the expression of hyperpolarization-activated cyclic nucleotide-gated (HCN) channel and age-related atrial fibrillation. Med. Sci. Monit. Int. Med. J. Exp. Clin. Res. *20*: 2292–2297.

Logantha, S.J.R.J., Cruickshank, S.F., Rowan, E.G., and Drummond, R.M. (2010). Spontaneous and electrically evoked Ca^{2+} transients in cardiomyocytes of the rat pulmonary vein. Cell Calcium *48*: 150–160.

Lo, L.-W., Chen, Y.-C., Chen, Y.-J., Wongcharoen, W., Lin, C.-I., and Chen, S.-A. (2007). Calmodulin kinase II inhibition prevents arrhythmic activity induced by α and β adrenergic agonists in rabbit pulmonary veins. Eur. J. Pharmacol. *571*: 197–208.

Lopez-Santiago, L.F., Meadows, L.S., Ernst, S.J., Chen, C., Malhotra, J.D., McEwen, D.P., *et al*. (2007). Sodium channel SCN1b null mice exhibit prolonged QT and RR intervals. J. Mol. Cell. Cardiol. *43*: 636–647.

Lu, C.M., Han, J., Rado, T.A., and Brown, G.B. (1992). Differential expression of two sodium channel subtypes in human brain. FEBS Lett. *303*: 53–58.

Ludatscher, R.M. (1968). Fine structure of the muscular wall of rat pulmonary veins. J. Anat. *103*: 345–357.

Luk, H.-N., Lin, C., Wei, J., and Chang, C.-L. (1988). Depressant effects of isoflurane and halothane on isolated human atrial fibers. J. Am. Soc. Anesthesiol. *69*: 667–676.

Luk, H.-N., Lo, C.-P., Tien, H.-C., Lee, D., Chen, Z.-L., Wang, F., *et al*. (2008). Mechanical characterization of rabbit pulmonary vein sleeves in in vitro intact ring preparation. J. Chin. Med. Assoc. JCMA *71*: 610–618.

Luo, A., Ma, J., Song, Y., Qian, C., Wu, Y., Zhang, P., *et al*. (2014). Larger late sodium current density as well as greater sensitivities to ATX II and ranolazine in rabbit left atrial than left ventricular myocytes. Am. J. Physiol. - Heart Circ. Physiol. *306*: H455–H461.

Luo, M.H., Li, Y.S., and Yang, K.P. (2007). Fibrosis of collagen I and remodelling of connexin 43 in atrial myocardium of patients with atrial fibrillation. Cardiology *107*: 248–253.

Lu, Y.-Y., Cheng, C.-C., Chen, Y.-C., Chen, S.-A., and Chen, Y.-J. (2012). ATX-II-induced pulmonary vein arrhythmogenesis related to atrial fibrillation and long QT syndrome. Eur. J. Clin. Invest. *42*: 823–831.

Mackenzie, L., Roderick, H.L., Berridge, M.J., Conway, S.J., and Bootman, M.D. (2004). The spatial pattern of atrial cardiomyocyte calcium signalling modulates contraction. J. Cell Sci. *117*: 6327–6337.

MacLeod, D.P., and Hunter, E.G. (1967). The pharmacology of the cardiac muscle of the great veins of the rat. Can. J. Physiol. Pharmacol. *45*: 463–473.

Maier, L.S., Zhang, T., Chen, L., DeSantiago, J., Brown, J.H., and Bers, D.M. (2003). Transgenic CaMKIIdeltaC overexpression uniquely alters cardiac myocyte Ca^{2+} handling: reduced SR Ca^{2+} load and activated SR Ca^{2+} release. Circ. Res. *92*: 904–911.

Maier, S.K.G., Westenbroek, R.E., McCormick, K.A., Curtis, R., Scheuer, T., and Catterall, W.A. (2004). Distinct subcellular localization of different sodium channel α and β subunits in single ventricular myocytes from mouse heart. Circulation *109*: 1421–1427.

Maier, S.K.G., Westenbroek, R.E., Schenkman, K.A., Feigl, E.O., Scheuer, T., and Catterall, W.A. (2002). An unexpected role for brain-type sodium channels in

coupling of cell surface depolarization to contraction in the heart. Proc. Natl. Acad. Sci. U. S. A. *99*: 4073–4078.

Ma, J., Luo, A., Wu, L., Wan, W., Zhang, P., Ren, Z., *et al*. (2012). Calmodulin kinase II and protein kinase C mediate the effect of increased intracellular calcium to augment late sodium current in rabbit ventricular myocytes. Am. J. Physiol. Cell Physiol. *302*: C1141–1151.

Makielski, J.C., Limberis, J.T., Chang, S.Y., Fan, Z., and Kyle, J.W. (1996). Coexpression of β1 with cardiac sodium channel α subunits in oocytes decreases lidocaine block. Mol. Pharmacol. *49*: 30–39.

Makielski, J.C., Sheets, M.F., Hanck, D.A., January, C.T., and Fozzard, H.A. (1987). Sodium current in voltage clamped internally perfused canine cardiac Purkinje cells. Biophys. J. *52*: 1–11.

Makiyama, T., Akao, M., Shizuta, S., Doi, T., Nishiyama, K., Oka, Y., *et al.* (2008). A novel SCN5A gain-of-function mutation M1875T associated with familial atrial fibrillation. J. Am. Coll. Cardiol. *52*: 1326–1334.

Malécot, C.O., Bredeloux, P., Findlay, I., and Maupoil, V. (2014). A TTX-Sensitive Resting Na^+ Permeability Contributes to the Catecholaminergic Automatic Activity in Rat Pulmonary Vein. J. Cardiovasc. Electrophysiol.

Malécot, C.O., Bredeloux, P., Findlay, I., and Maupoil, V. (2015). A TTX-sensitive resting Na^+ permeability contributes to the catecholaminergic automatic activity in rat pulmonary vein. J. Cardiovasc. Electrophysiol. *26*: 311–319.

Maltsev, V.A., Kyle, J.W., Mishra, S., and Undrovinas, A. (2008). Molecular identity of the late sodium current in adult dog cardiomyocytes identified by $Na_v1.5$ antisense inhibition. Am. J. Physiol. - Heart Circ. Physiol. *295*: H667–H676.

Maltsev, V.A., Kyle, J.W., and Undrovinas, A. (2009). Late Na^+ current produced by human cardiac Na^+ channel isoform $Na_v1.5$ is modulated by its β1 subunit. J. Physiol. Sci. JPS *59*: 217–225.

Maltsev, V.A., Sabbah, H.N., Higgins, R.S., Silverman, N., Lesch, M., and Undrovinas, A.I. (1998). Novel, ultraslow inactivating sodium current in human ventricular cardiomyocytes. Circulation *98*: 2545–2552.

Maltsev, V.A., Silverman, N., Sabbah, H.N., and Undrovinas., A.I. (2007). Chronic heart failure slows late sodium current in human and canine ventricular myocytes: implications for repolarization variability. Eur. J. Heart Fail. *9*: 219–227.

Maltsev, V.A., and Undrovinas, A.I. (1997). Cytoskeleton modulates coupling between availability and activation of cardiac sodium channel. Am. J. Physiol. *273*: H1832–1840.

Marín-Briggiler, C.I., Jha, K.N., Chertihin, O., Buffone, M.G., Herr, J.C., Vazquez-Levin, M.H., *et al*. (2005). Evidence of the presence of calcium/calmodulin-

dependent protein kinase IV in human sperm and its involvement in motility regulation. J. Cell Sci. *118*: 2013–2022.

Marionneau, C., Couette, B., Liu, J., Li, H., Mangoni, M.E., Nargeot, J., *et al.* (2005). Specific pattern of ionic channel gene expression associated with pacemaker activity in the mouse heart. J. Physiol. *562*: 223–234.

Masani, F. (1986). Node-like cells in the myocardial layer of the pulmonary vein of rats: an ultrastructural study. J. Anat. *145*: 133–142.

Maupoil, V., Bronquard, C., Freslon, J.-L., Cosnay, P., and Findlay, I. (2007). Ectopic activity in the rat pulmonary vein can arise from simultaneous activation of α1- and β1-adrenoceptors. Br. J. Pharmacol. *150*: 899–905.

McLean, M.R., Bursztyn Goldberg, P., and Roberts, J. (1983). An ultrastructural study of the effects of age on sympathetic innervation and atrial tissue in the rat. J. Mol. Cell. Cardiol. *15*: 75–92.

Melby, S.J., Schuessler, R.B., and Damiano, R.J. (2013). Ablation technology for the surgical treatment of atrial fibrillation. ASAIO J. Am. Soc. Artif. Intern. Organs 1992 *59*: 461–468.

Melnyk, P., Ehrlich, J.R., Pourrier, M., Villeneuve, L., Cha, T.-J., and Nattel, S. (2005). Comparison of ion channel distribution and expression in cardiomyocytes of canine pulmonary veins versus left atrium. Cardiovasc. Res. *65*: 104–116.

Michelakis, E.D., Weir, E.K., Wu, X., Nsair, A., Waite, R., Hashimoto, K., *et al.* (2001). Potassium channels regulate tone in rat pulmonary veins. Am. J. Physiol. - Lung Cell. Mol. Physiol. *280*: L1138–L1147.

Mihm, M.J., Yu, F., Carnes, C.A., Reiser, P.J., McCarthy, P.M., Van Wagoner, D.R., *et al.* (2001). Impaired myofibrillar energetics and oxidative injury during human atrial fibrillation. Circulation *104*: 174–180.

Milberg, P., Pott, C., Fink, M., Frommeyer, G., Matsuda, T., Baba, A., *et al.* (2008). Inhibition of the Na^+/Ca^{2+} exchanger suppresses torsades de pointes in an intact heart model of long QT syndrome-2 and long QT syndrome-3. Heart Rhythm Off. J. Heart Rhythm Soc. *5*: 1444–1452.

Miles, R.H., Passman, R., and Murdock, D.K. (2011). Comparison of effectiveness and safety of ranolazine versus amiodarone for preventing atrial fibrillation after coronary artery bypass grafting. Am. J. Cardiol. *108*: 673–676.

Millino, C., Sarinella, F., Tiveron, C., Villa, A., Sartore, S., and Ausoni, S. (2000). Cardiac and smooth muscle cell contribution to the formation of the murine pulmonary veins. Dev. Dyn. Off. Publ. Am. Assoc. Anat. *218*: 414–425.

Mishra, S., Reznikov, V., Maltsev, V.A., Undrovinas, N.A., Sabbah, H.N., and Undrovinas, A. (2014). Contribution of sodium channel neuronal isoform $Na_v1.1$ to late sodium current in ventricular myocytes from failing hearts. J. Physiol.

Mitchell, M.R., Powell, T., Terrar, D.A., and Twist, V.W. (1984). Strontium, nifedipine and 4-aminopyridine modify the time course of the action potential in cells from rat ventricular muscle. Br. J. Pharmacol. *81*: 551–556.

Miyasaka, Y., Barnes, M.E., Gersh, B.J., Cha, S.S., Bailey, K.R., Abhayaratna, W.P., *et al*. (2006). Secular trends in incidence of atrial fibrillation in Olmsted County, Minnesota, 1980 to 2000, and implications on the projections for future prevalence. Circulation *114*: 119–125.

Miyauchi, Y., Fishbein, M.C., and Karagueuzian, H.S. (2004). Electrical current-induced atrial and pulmonary vein action potential duration shortening and repetitive activity. Am. J. Physiol. Heart Circ. Physiol. *287*: H178–186.

Miyauchi, Y., Hayashi, H., Miyauchi, M., Okuyama, Y., Mandel, W.J., Chen, P.-S., *et al.* (2005). Heterogeneous pulmonary vein myocardial cell repolarization implications for reentry and triggered activity. Heart Rhythm Off. J. Heart Rhythm Soc. *2*: 1339–1345.

Moe, G.K. (1962). On the multiple wavelet hypothesis of atrial fibrillation. Arch Int Pharmacodyn Ther *140*: 183.

Moe, G.K., and Abildskov, J.A. (1959). Atrial fibrillation as a self-sustaining arrhythmia independent of focal discharge. Am. Heart J. *58*: 59–70.

Mokadam, N.A., McCarthy, P.M., Gillinov, A.M., Ryan, W.H., Moon, M.R., Mack, M.J., *et a*l. (2004). A prospective multicenter trial of bipolar radiofrequency ablation for atrial fibrillation: early results. Ann. Thorac. Surg. *78*: 1665–1670.

Mommersteeg, M.T.M., Brown, N.A., Prall, O.W.J., Gier-de Vries, C. de, Harvey, R.P., Moorman, A.F.M., *et al.* (2007). Pitx2c and Nkx2-5 are required for the formation and identity of the pulmonary myocardium. Circ. Res. *101*: 902–909.

Morel, E., Meyronet, D., Thivolet-Bejuy, F., and Chevalier, P. (2008). Identification and distribution of interstitial Cajal cells in human pulmonary veins. Heart Rhythm *5*: 1063–1067.

Morotti, S., Edwards, A.G., McCulloch, A.D., Bers, D.M., and Grandi, E. (2014). A novel computational model of mouse myocyte electrophysiology to assess the synergy between Na^+ loading and CaMKII. J. Physiol. *592*: 1181–1197.

Moubarak, J.B., Rozwadowski, J.V., Strzalka, C.T., Buck, W.R., Tan, W.S., Kish, G.F., *et al.* (2000). Pulmonary veins-left atrial junction: anatomic and histological study. Pacing Clin. Electrophysiol. *23*: 1836–1838.

Mueller-Hoecker, J., Beitinger, F., Fernandez, B., Bahlmann, O., Assmann, G., Troidl, C., *et al.* (2008). Of rodents and humans: a light microscopic and ultrastructural study on cardiomyocytes in pulmonary veins. Int. J. Med. Sci. *5*: 152–158.

Muir, A.R. (1967). The effects of divalent cations on the ultrastructure of the perfused rat heart. J. Anat. *101*: 239–261.

Murdock, D.K., Kersten, M., Kaliebe, J., and Larrain, G. (2009). The Use Of Oral Ranolazine To Convert New Or Paroxysmal Atrial Fibrillation: A Review Of Experience With Implications For Possible 'Pill In The Pocket' Approach To Atrial Fibrillation. Indian Pacing Electrophysiol. J. *9*: 260–267.

Murdock, D.K., Overton, N., Kersten, M., Kaliebe, J., and Devecchi, F. (2008). The effect of ranolazine on maintaining sinus rhythm in patients with resistant atrial fibrillation. Indian Pacing Electrophysiol. J. *8*: 175–181.

Murphy, N.F., Simpson, C.R., Jhund, P.S., Stewart, S., Kirkpatrick, M., Chalmers, J., *et al*. (2007). A national survey of the prevalence, incidence, primary care burden and treatment of atrial fibrillation in Scotland. Heart Br. Card. Soc. *93*: 606–612.

Murray, K.T., Hu, N., Daw, J.R., Shin, H.-G., Watson, M.T., Mashburn, A.B., *et al.* (1997). Functional effects of protein kinase C activation on the human cardiac Na^+ channel. Circ. Res. *80*: 370–376.

Nagy, N., Kormos, A., Kohajda, Z., Szebeni, Á., Szepesi, J., Pollesello, P., *et al.* (2014). Selective Na^+ /Ca^{2+} exchanger inhibition prevents Ca^{2+} overload-induced triggered arrhythmias. Br. J. Pharmacol. *171*: 5665–5681.

Namekata, I., Tsuneoka, Y., Takahara, A., Shimada, H., Sugimoto, T., Takeda, K., *et al*. (2009). Involvement of the Na^+/Ca^{2+} exchanger in the automaticity of guinea-pig pulmonary vein myocardium as revealed by SEA0400. J. Pharmacol. Sci. *110*: 111–116.

Nánási, P.P., Varró, A., Bryant, S.H., and Lathrop, D.A. (1994). Effects of veratrine on ion currents in single rabbit cardiomyocytes. Gen. Pharmacol. Vasc. Syst. *25*: 1667–1672.

Nao, T., Ohkusa, T., Hisamatsu, Y., Inoue, N., Matsumoto, T., Yamada, J., *et al.* (2003). Comparison of expression of connexin in right atrial myocardium in patients with chronic atrial fibrillation versus those in sinus rhythm. Am. J. Cardiol. *91*: 678–683.

Nathan, H., and Eliakim, M. (1966). The junction between the left atrium and the pulmonary veins. An anatomic study of human hearts. Circulation *34*: 412–422.

Nattel, S. (2002). New ideas about atrial fibrillation 50 years on. Nature *415*: 219–226.

Neef, S., Dybkova, N., Sossalla, S., Ort, K.R., Fluschnik, N., Neumann, K., *et al.* (2010). CaMKII-dependent diastolic SR Ca^{2+} leak and elevated diastolic Ca^{2+} levels in right atrial myocardium of patients with atrial fibrillation. Circ. Res. *106*: 1134–1144.

Ng, J., Villuendas, R., Cokic, I., Schliamser, J.E., Gordon, D., Koduri, H., *et al.* (2011). Autonomic remodeling in the left atrium and pulmonary veins in heart failure: creation of a dynamic substrate for atrial fibrillation. Circ. Arrhythm. Electrophysiol. *4*: 388–396.

Nguyen, B.L., Fishbein, M.C., Chen, L.S., Chen, P.-S., and Masroor, S. (2009). Histopathological substrate for chronic atrial fibrillation in humans. Heart Rhythm Off. J. Heart Rhythm Soc. *6*: 454–460.

Nguyen Dinh Cat, A., and Touyz, R.M. (2011). A new look at the renin–angiotensin system—Focusing on the vascular system. Peptides *32*: 2141–2150.

Nishio, M., Ohmura, T., Kigoshi, S., and Muramatsu, I. (1991). Supersensitivity to tetrodotoxin and lignocaine of sea anemone toxin II-treated sodium channel in guinea-pig ventricular muscle. Br. J. Pharmacol. *104*: 504–508.

Nishizuka, Y. (1992). Intracellular signaling by hydrolysis of phospholipids and activation of protein kinase C. Science *258*: 607–614.

Noda, M., Shimizu, S., Tanabe, T., Takai, T., Kayano, T., Ikeda, T., *et al*. (1984). Primary structure of Electrophorus electricus sodium channel deduced from cDNA sequence. Nature *312*: 121–127.

Noujaim, S.F., Kaur, K., Milstein, M., Jones, J.M., Furspan, P., Jiang, D., *et a*l. (2012). A null mutation of the neuronal sodium channel $Na_v1.6$ disrupts action potential propagation and excitation-contraction coupling in the mouse heart. FASEB J. *26*: 63–72.

Oakes, R.S., Badger, T.J., Kholmovski, E.G., Akoum, N., Burgon, N.S., Fish, E.N., *et al*. (2009). Detection and quantification of left atrial structural remodelling with delayed-enhancement magnetic resonance imaging in patients with atrial fibrillation. Circulation *119*: 1758–1767.

Okamoto, Y., Kawamura, K., Nakamura, Y., and Ono, K. (2014). Pathological impact of hyperpolarization-activated chloride current peculiar to rat pulmonary vein cardiomyocytes. J. Mol. Cell. Cardiol. *66*: 53–62.

Okamoto, Y., Takano, M., Ohba, T., and Ono, K. (2012). Arrhythmogenic coupling between the Na^+ -Ca^{2+} exchanger and inositol 1,4,5-triphosphate receptor in rat pulmonary vein cardiomyocytes. J. Mol. Cell. Cardiol. *52*: 988–997.

Olesen, M.S., Jespersen, T., Nielsen, J.B., Liang, B., Møller, D.V., Hedley, P., *et al.* (2011). Mutations in sodium channel β-subunit SCN3B are associated with early-onset lone atrial fibrillation. Cardiovasc. Res. *89*: 786–793.

Paes de Almeida, O., Bohm, C.M., Paula Carvalho, M. de, and Paes de Carvalho, A. (1975). The cardiac muscle in the pulmonary vein of the rat: a morphological and electrophysiological study. J. Morphol. *145*: 409–433.

Papadatos, G.A., Wallerstein, P.M.R., Head, C.E.G., Ratcliff, R., Brady, P.A., Benndorf, K., *et al.* (2002). Slowed conduction and ventricular tachycardia after targeted disruption of the cardiac sodium channel gene Scn5a. Proc. Natl. Acad. Sci. *99*: 6210–6215.

Patlak, J.B., and Ortiz, M. (1985). Slow currents through single sodium channels of the adult rat heart. J. Gen. Physiol. *86*: 89–104.

Patterson, E., Jackman, W.M., Beckman, K.J., Lazzara, R., Lockwood, D., Scherlag, B.J., *et al.* (2007). Spontaneous pulmonary vein firing in man: relationship to tachycardia-pause early afterdepolarizations and triggered arrhythmia in canine pulmonary veins in vitro. J. Cardiovasc. Electrophysiol. *18*: 1067–1075.

Patterson, E., Po, S.S., Scherlag, B.J., and Lazzara, R. (2005). Triggered firing in pulmonary veins initiated by in vitro autonomic nerve stimulation. Heart Rhythm Off. J. Heart Rhythm Soc. *2*: 624–631.

Pauza, D.H., Skripka, V., Pauziene, N., and Stropus, R. (2000). Morphology, distribution, and variability of the epicardiac neural ganglionated subplexuses in the human heart. Anat. Rec. *259*: 353–382.

Payandeh, J., Scheuer, T., Zheng, N., and Catterall, W.A. (2011). The crystal structure of a voltage-gated sodium channel. Nature *475*: 353–358.

Peach, M.J. (1977). Renin-angiotensin system: biochemistry and mechanisms of action. Physiol. Rev. *57*: 313–370.

Pérez-García, M.T., Chiamvimonvat, N., Marban, E., and Tomaselli, G.F. (1996). Structure of the sodium channel pore revealed by serial cysteine mutagenesis. Proc. Natl. Acad. Sci. *93*: 300–304.

Pérez-García, M.T., Chiamvimonvat, N., Ranjan, R., Balser, J.R., Tomaselli, G.F., and Marban, E. (1997). Mechanisms of sodium/calcium selectivity in sodium channels probed by cysteine mutagenesis and sulfhydryl modification. Biophys. J. *72*: 989–996.

Perez-Lugones, A., McMahon, J.T., Ratliff, N.B., Saliba, W.I., Schweikert, R.A., Marrouche, N.F., *et al*. (2003). Evidence of specialized conduction cells in human pulmonary veins of patients with atrial fibrillation. J. Cardiovasc. Electrophysiol. *14*: 803–809.

Pertsov, A.M., Davidenko, J.M., Salomonsz, R., Baxter, W.T., and Jalife, J. (1993). Spiral waves of excitation underlie reentrant activity in isolated cardiac muscle. Circ. Res. *72*: 631–650.

Pfeufer, A., Noord, C. van, Marciante, K.D., Arking, D.E., Larson, M.G., Smith, A.V., *et al*. (2010). Genome-wide association study of PR interval. Nat. Genet. *42*: 153–159.

Plummer, N.W., Galt, J., Jones, J.M., Burgess, D.L., Sprunger, L.K., Kohrman, D.C., *et al*. (1998). Exon organization, coding sequence, physical mapping, and polymorphic intragenic markers for the human neuronal sodium channel gene SCN8A. Genomics *54*: 287–296.

Po, S.S., Li, Y., Tang, D., Liu, H., Geng, N., Jackman, W.M., *et al.* (2005). Rapid and stable re-entry within the pulmonary vein as a mechanism initiating paroxysmal atrial fibrillation. J. Am. Coll. Cardiol. *45*: 1871–1877.

Poulet, C., Wettwer, E., Grunnet, M., Jespersen, T., Fabritz, L., Matschke, K., *et al.* (2015). Late sodium current in human atrial cardiomyocytes from patients in sinus rhythm and atrial fibrillation. PLoS ONE *10*: e0131432.

Prasad, S.M., Maniar, H.S., Camillo, C.J., Schuessler, R.B., Boineau, J.P., Sundt, T.M., *et al*. (2003). The Cox maze III procedure for atrial fibrillation: long-term efficacy in patients undergoing lone versus concomitant procedures. J. Thorac. Cardiovasc. Surg. *126*: 1822–1828.

Protas, L., Dun, W., Jia, Z., Lu, J., Bucchi, A., Kumari, S., *et al.* (2009). Expression of skeletal but not cardiac Na^+ channel isoform preserves normal conduction in a depolarized cardiac syncytium. Cardiovasc. Res. *81*: 528–535.

Qin, N., D'Andrea, M.R., Lubin, M.-L., Shafaee, N., Codd, E.E., and Correa, A.M. (2003). Molecular cloning and functional expression of the human sodium channel β1B subunit, a novel splicing variant of the β1 subunit. Eur. J. Biochem. FEBS *270*: 4762–4770.

Qi, X., Yeh, Y.-H., Chartier, D., Xiao, L., Tsuji, Y., Brundel, B.J.J.M., *et al*. (2009). The calcium/calmodulin/kinase system and arrhythmogenic afterdepolarizations in bradycardia-related acquired long-QT syndrome. Circ. Arrhythm. Electrophysiol. *2*: 295–304.

Qi, X.Y., Yeh, Y.-H., Xiao, L., Burstein, B., Maguy, A., Chartier, D., *et al.* (2008). Cellular signalling underlying atrial tachycardia remodelling of L-type calcium current. Circ. Res. *103*: 845–854.

Qu, Y., Rogers, J.C., Tanada, T.N., Catterall, W.A., and Scheuer, T. (1996). Phosphorylation of S1505 in the cardiac Na+ channel inactivation gate is required for modulation by protein kinase C. J. Gen. Physiol. *108*: 375–379.

Rabert, D.K., Koch, B.D., Ilnicka, M., Obernolte, R.A., Naylor, S.L., Herman, R.C., *et al*. (1998). A tetrodotoxin-resistant voltage-gated sodium channel from human dorsal root ganglia, hPN3/SCN10A. Pain *78*: 107–114.

Radwański, P.B., Brunello, L., Veeraraghavan, R., Ho, H.-T., Lou, Q., Makara, M.A., *et al.* (2015). Neuronal Na^+ channel blockade suppresses arrhythmogenic diastolic Ca^{2+} release. Cardiovasc. Res. *106*: 143–152.

Ravens, U. (1976). Electromechanical studies of an Anemonia sulcata toxin in mammalian cardiac muscle. Naunyn. Schmiedebergs Arch. Pharmacol. *296*: 73–78.

Reed, J.K., and Raftery, M.A. (1976). Properties of the tetrodotoxin binding component in plasma membranes isolated from Electrophorus electricus. Biochemistry (Mosc.) *15*: 944–953.

Remme, C.A. (2013). Cardiac sodium channelopathy associated with SCN5A mutations: electrophysiological, molecular and genetic aspects. J. Physiol. *591*: 4099–4116.

Remme, C.A., and Wilde, A.A.M. (2014). Targeting sodium channels in cardiac arrhythmia. Curr. Opin. Pharmacol. *15*: 53–60.

Renaud, J.F., Kazazoglou, T., Lombet, A., Chicheportiche, R., Jaimovich, E., Romey, G., *et al.* (1983). The Na^+ channel in mammalian cardiac cells. Two kinds of tetrodotoxin receptors in rat heart membranes. J. Biol. Chem. *258*: 8799–8805.

Rensma, P.L., Allessie, M.A., Lammers, W.J., Bonke, F.I., and Schalij, M.J. (1988). Length of excitation wave and susceptibility to reentrant atrial arrhythmias in normal conscious dogs. Circ. Res. *62*: 395–410.

Rezazadeh, S., Claydon, T.W., and Fedida, D. (2006). KN-93 (2-[N-(2-hydroxyethyl)]-N-(4-methoxybenzenesulfonyl)]amino-N-(4-chlorocinnamyl)-N-methylbenzylamine), a calcium/calmodulin-dependent protein kinase II inhibitor, is a direct extracellular blocker of voltage-gated potassium channels. J. Pharmacol. Exp. Ther. *317*: 292–299.

Richards, M.A., Clarke, J.D., Saravanan, P., Voigt, N., Dobrev, D., Eisner, D.A., *et al.* (2011). Transverse tubules are a common feature in large mammalian atrial myocytes including human. Am. J. Physiol. - Heart Circ. Physiol. *301*: H1996–H2005.

Rietdorf, K., Bootman, M.D., and Sanderson, M.J. (2014). Spontaneous, pro-arrhythmic calcium signals disrupt electrical pacing in mouse pulmonary vein sleeve cells. PloS One *9*: e88649.

Roberts, D.E., Hersh, L.T., and Scher, A.M. (1979). Influence of cardiac fiber orientation on wavefront voltage, conduction velocity, and tissue resistivity in the dog. Circ. Res. *44*: 701–712.

Röcken, C., Peters, B., Juenemann, G., Saeger, W., Klein, H.U., Huth, C., *et al.* (2002). Atrial amyloidosis: an arrhythmogenic substrate for persistent atrial fibrillation. Circulation *106*: 2091–2097.

Rook, M.B., Evers, M.M., Vos, M.A., and Bierhuizen, M.F.A. (2012). Biology of cardiac sodium channel $Na_v1.5$ expression. Cardiovasc. Res. *93*: 12–23.

Rostock, T., Steven, D., Lutomsky, B., Servatius, H., Drewitz, I., Klemm, H., *et al.* (2008). Atrial fibrillation begets atrial fibrillation in the pulmonary veins on the impact of atrial fibrillation on the electrophysiological properties of the pulmonary veins in humans. J. Am. Coll. Cardiol. *51*: 2153–2160.

Roux, N., Havet, E., and Mertl, P. (2004). The myocardial sleeves of the pulmonary veins: potential implications for atrial fibrillation. Surg. Radiol. Anat. SRA *26*: 285–289.

Sag, C.M., Mallwitz, A., Wagner, S., Hartmann, N., Schotola, H., Fischer, T.H., *et al*. (2014). Enhanced late I_{Na} induces proarrhythmogenic SR Ca leak in a CaMKII-dependent manner. J. Mol. Cell. Cardiol. *76*: 94–105.

Saito, T., Waki, K., and Becker, A.E. (2000). Left atrial myocardial extension onto pulmonary veins in humans: anatomic observations relevant for atrial arrhythmias. J. Cardiovasc. Electrophysiol. *11*: 888–894.

Sakakibara, Y., Wasserstrom, J.A., Furukawa, T., Jia, H., Arentzen, C.E., Hartz, R.S., *et al.* (1992). Characterization of the sodium current in single human atrial myocytes. Circ. Res. *71*: 535–546.

Sanders, K.M. (1996). A case for interstitial cells of Cajal as pacemakers and mediators of neurotransmission in the gastrointestinal tract. Gastroenterology *111*: 492–515.

Sandoval, E., Castella, M., and Pomar, J.-L. (2011). Current state of the surgical treatment of atrial fibrillation. Cardiol. Res. Pract. *2011*: 746054.

Sanfilippo, A.J., Abascal, V.M., Sheehan, M., Oertel, L.B., Harrigan, P., Hughes, R.A., *et al.* (1990). Atrial enlargement as a consequence of atrial fibrillation. A prospective echocardiographic study. Circulation *82*: 792–797.

Sangameswaran, L., Delgado, S.G., Fish, L.M., Koch, B.D., Jakeman, L.B., Stewart, G.R., *et al.* (1996). Structure and function of a novel voltage-gated, tetrodotoxin-resistant sodium channel specific to sensory neurons. J. Biol. Chem. *271*: 5953–5956.

Sano, T., Takayama, N., and Shimamoto, T. (1959). Directional difference of conduction velocity in the cardiac ventricular syncytium studied by microelectrodes. Circ. Res. *7*: 262–267.

Satin, J., Kyle, J.W., Chen, M., Bell, P., Cribbs, L.L., Fozzard, H.A., *et al.* (1992). A mutant of TTX-resistant cardiac sodium channels with TTX-sensitive properties. Science *256*: 1202–1205.

Sato, C., Sato, M., Iwasaki, A., Doi, T., and Engel, A. (1998). The sodium channel has four domains surrounding a central pore. J. Struct. Biol. *121*: 314–325.

Savio Galimberti, E., Vanoye, C.G., Yang, T., Atack, T.C., Muhammad, R., Roden, D.M., *et al.* (2012). SCN10A rare variants associated with atrial fibrillation and slow ventricular rates reveal increased late sodium current. Heart Rhythm *9*: 1911.

Savio-Galimberti, E., Weeke, P., Muhammad, R., Blair, M., Ansari, S., Short, L., *et al.* (2014). SCN10A/$Na_v1.8$ modulation of peak and late sodium currents in patients with early onset atrial fibrillation. Cardiovasc. Res. *104*: 355–363.

Schaller, K.L., Krzemien, D.M., Yarowsky, P.J., Krueger, B.K., and Caldwell, J.H. (1995). A novel, abundant sodium channel expressed in neurons and glia. J. Neurosci. Off. J. Soc. Neurosci. *15*: 3231–3242.

Schauerte, P., Scherlag, B.J., Patterson, E., Scherlag, M.A., Matsudaria, K., Nakagawa, H., *et al*. (2001). Focal atrial fibrillation: experimental evidence for a pathophysiologic role of the autonomic nervous system. J. Cardiovasc. Electrophysiol. *12*: 592–599.

Scherf, D., Romano, F.J., and Terranova, R. (1948). Experimental studies on auricular flutter and auricular fibrillation. Am. Heart J. *36*: 241–251.

Schotten, U., Greiser, M., Benke, D., Buerkel, K., Ehrenteidt, B., Stellbrink, C., *et al*. (2002). Atrial fibrillation-induced atrial contractile dysfunction: a tachycardiomyopathy of a different sort. Cardiovasc. Res. *53*: 192–201.

Schouten, V.J., and Keurs, H.E. ter (1985). The slow repolarization phase of the action potential in rat heart. J. Physiol. *360*: 13–25.

Scicluna, B.P., Remme, C.A., Verkerk, A.O., Amin, A.S., Tanck, M.W., Beekman, L., *et al*. (2008). Abstract 1504: Scn4b Is A Genetic Modifier Of Cardiac Conduction Disease In Mice. Circulation *118*: S_339.

Scirica, B.M., Belardinelli, L., Chaitman, B.R., Waks, J.W., Volo, S., Karwatowska-Prokopczuk, E., *et al*. (2015). Effect of ranolazine on atrial fibrillation in patients with non-ST elevation acute coronary syndromes: observations from the MERLIN-TIMI 36 trial. Europace *17*: 32–37.

Shah, A.N., Mittal, S., Sichrovsky, T.C., Cotiga, D., Arshad, A., Maleki, K., *et al*. (2008). Long-term outcome following successful pulmonary vein isolation: pattern and prediction of very late recurrence. J. Cardiovasc. Electrophysiol. *19*: 661–667.

Sicouri, S., Belardinelli, L., and Antzelevitch, C. (2013). Antiarrhythmic effects of the highly selective late sodium channel current blocker GS-458967. Heart Rhythm Off. J. Heart Rhythm Soc. *10*: 1036–1043.

Sicouri, S., Belardinelli, L., Carlsson, L., and Antzelevitch, C. (2009). Potent antiarrhythmic effects of chronic amiodarone in canine pulmonary vein sleeve preparations. J. Cardiovasc. Electrophysiol. *20*: 803–810.

Sicouri, S., Cordeiro, J.M., Talarico, M., and Antzelevitch, C. (2011). Antiarrhythmic effects of losartan and enalapril in canine pulmonary vein sleeve preparations. J. Cardiovasc. Electrophysiol. *22*: 698–705.

Sicouri, S., Glass, A., Belardinelli, L., and Antzelevitch, C. (2008). Antiarrhythmic effects of ranolazine in canine pulmonary vein sleeve preparations. Heart Rhythm Off. J. Heart Rhythm Soc. *5*: 1019–1026.

Sicouri, S., Pourrier, M., Gibson, J.K., Lynch, J.J., and Antzelevitch, C. (2012). Comparison of electrophysiological and antiarrhythmic effects of vernakalant,

ranolazine, and sotalol in canine pulmonary vein sleeve preparations. Heart Rhythm Off. J. Heart Rhythm Soc. *9*: 422–429.

Sills, M.N., Xu, Y.C., Baracchini, E., Goodman, R.H., Cooperman, S.S., Mandel, G., *et al.* (1989). Expression of diverse Na^+ channel messenger RNAs in rat myocardium. Evidence for a cardiac-specific Na^+ channel. J. Clin. Invest. *84*: 331–336.

Sivilotti, L., Okuse, K., Akopian, A.N., Moss, S., and Wood, J.N. (1997). A single serine residue confers tetrodotoxin insensitivity on the rat sensory-neuron-specific sodium channel SNS. FEBS Lett. *409*: 49–52.

Slawsky, M.T., and Castle, N.A. (1994). K^+ channel blocking actions of flecainide compared with those of propafenone and quinidine in adult rat ventricular myocytes. J. Pharmacol. Exp. Ther. *269*: 66–74.

Smith, M.R., Smith, R.D., Plummer, N.W., Meisler, M.H., and Goldin, A.L. (1998). Functional analysis of the mouse SCN8A sodium channel. J. Neurosci. Off. J. Soc. Neurosci. *18*: 6093–6102.

Song, Y., Shryock, J.C., and Belardinelli, L. (2008). An increase of late sodium current induces delayed afterdepolarizations and sustained triggered activity in atrial myocytes. Am. J. Physiol. Heart Circ. Physiol. *294*: H2031–2039.

Song, Y., Shryock, J.C., and Belardinelli, L. (2009). A slowly inactivating sodium current contributes to spontaneous diastolic depolarization of atrial myocytes. Am. J. Physiol. Heart Circ. Physiol. *297*: H1254–1262.

Song, Y., Shryock, J.C., Wu, L., and Belardinelli, L. (2004). Antagonism by ranolazine of the pro-arrhythmic effects of increasing late I_{Na} in guinea pig ventricular myocytes. J. Cardiovasc. Pharmacol. *44*: 192–199.

Sossalla, S., Kallmeyer, B., Wagner, S., Mazur, M., Maurer, U., Toischer, K., *et al.* (2010). Altered Na^+ currents in atrial fibrillation effects of ranolazine on arrhythmias and contractility in human atrial myocardium. J. Am. Coll. Cardiol. *55*: 2330–2342.

Sossalla, S., Wagner, S., Rasenack, E.C.L., Ruff, H., Weber, S.L., Schöndube, F.A., *et al.* (2008). Ranolazine improves diastolic dysfunction in isolated myocardium from failing human hearts; role of late sodium current and intracellular ion accumulation. J. Mol. Cell. Cardiol. *45*: 32–43.

Sotoodehnia, N., Isaacs, A., Bakker, P.I.W. de, Dörr, M., Newton-Cheh, C., Nolte, I.M., *et al.* (2010). Common variants in 22 loci are associated with QRS duration and cardiac ventricular conduction. Nat. Genet. *42*: 1068–1076.

Spach, M.S., Heidlage, J.F., Dolber, P.C., and Barr, R.C. (2000). Electrophysiological effects of remodeling cardiac gap junctions and cell size: experimental and model studies of normal cardiac growth. Circ. Res. *86*: 302–311.

Starmer, C.F., Grant, A.O., and Strauss, H.C. (1984). Mechanisms of use-dependent block of sodium channels in excitable membranes by local anesthetics. Biophys. J. *46*: 15–27.

Steiner, I., Hájková, P., Kvasnicka, J., and Kholová, I. (2006). Myocardial sleeves of pulmonary veins and atrial fibrillation: a postmortem histopathological study of 100 subjects. Virchows Arch. Int. J. Pathol. *449*: 88–95.

Stillitano, F., Lonardo, G., Zicha, S., Varro, A., Cerbai, E., Mugelli, A., *et al*. (2008). Molecular basis of funny current (I_f) in normal and failing human heart. J. Mol. Cell. Cardiol. *45*: 289–299.

Studenik, C.R., Zhou, Z., and January, C.T. (2001). Differences in action potential and early afterdepolarization properties in LQT2 and LQT3 models of long QT syndrome. Br. J. Pharmacol. *132*: 85–92.

Stühmer, W., Conti, F., Suzuki, H., Wang, X.D., Noda, M., Yahagi, N., *et al.* (1989). Structural parts involved in activation and inactivation of the sodium channel. Nature *339*: 597–603.

Suenari, K., Cheng, C.-C., Chen, Y.-C., Lin, Y.-K., Nakano, Y., Kihara, Y., *et al*. (2012). Effects of ivabradine on the pulmonary vein electrical activity and modulation of pacemaker currents and calcium homeostasis. J. Cardiovasc. Electrophysiol. *23*: 200–206.

Sugawara, T., Mazaki-Miyazaki, E., Ito, M., Nagafuji, H., Fukuma, G., Mitsudome, A., et al. (2001a). $Na_v1.1$ mutations cause febrile seizures associated with afebrile partial seizures. Neurology *57*: 703–705.

Sugawara, T., Tsurubuchi, Y., Agarwala, K.L., Ito, M., Fukuma, G., Mazaki-Miyazaki, E., *et al.* (2001b). A missense mutation of the Na^+ channel α-II subunit gene $Na_v1.2$ in a patient with febrile and afebrile seizures causes channel dysfunction. Proc. Natl. Acad. Sci. U. S. A. *98*: 6384–6389.

Sun, Q., Tang, M., Pu, J., and Zhang, S. (2008). Pulmonary venous structural remodelling in a canine model of chronic atrial dilation due to mitral regurgitation. Can. J. Cardiol. *24*: 305–308.

Swynghedauw, B. (1999). Molecular mechanisms of myocardial remodelling. Physiol. Rev. *79*: 215–262.

Tagawa, M., Higuchi, K., Chinushi, M., Washizuka, T., Ushiki, T., Ishihara, N., *et al*. (2001). Myocardium extending from the left atrium onto the pulmonary veins: a comparison between subjects with and without atrial fibrillation. Pacing Clin. Electrophysiol. PACE *24*: 1459–1463.

Takahara, A., Sugimoto, T., Kitamura, T., Takeda, K., Tsuneoka, Y., Namekata, I., *et al.* (2011). Electrophysiological and pharmacological characteristics of triggered activity elicited in guinea-pig pulmonary vein myocardium. J. Pharmacol. Sci. *115*: 176–181.

Takahara, A., Takeda, K., Tsuneoka, Y., Hagiwara, M., Namekata, I., and Tanaka, H. (2012). Electrophysiological effects of the class Ic antiarrhythmic drug pilsicainide on the guinea-pig pulmonary vein myocardium. J. Pharmacol. Sci. *118*: 506–511.

Takahashi, Y., Iesaka, Y., Takahashi, A., Goya, M., Kobayashi, K., Fujiwara, H., *et al.* (2003). Reentrant tachycardia in pulmonary veins of patients with paroxysmal atrial fibrillation. J. Cardiovasc. Electrophysiol. *14*: 927–932.

Tanaka, H., Nishimaru, K., Aikawa, T., Hirayama, W., Tanaka, Y., and Shigenobu, K. (2002). Effect of SEA0400, a novel inhibitor of sodium-calcium exchanger, on myocardial ionic currents. Br. J. Pharmacol. *135*: 1096–1100.

Tanaka, H., Shimada, H., Namekata, I., Kawanishi, T., Iida-Tanaka, N., and Shigenobu, K. (2007). Involvement of the Na^+/Ca^{2+} exchanger in ouabain-induced inotropy and arrhythmogenesis in guinea-pig myocardium as revealed by SEA0400. J. Pharmacol. Sci. *103*: 241–246.

Tan, A.Y., Li, H., Wachsmann-Hogiu, S., Chen, L.S., Chen, P.-S., and Fishbein, M.C. (2006). Autonomic innervation and segmental muscular disconnections at the human pulmonary vein-atrial junction: implications for catheter ablation of atrial-pulmonary vein junction. J. Am. Coll. Cardiol. *48*: 132–143.

Tan, A.Y., Zhou, S., Jung, B.C., Ogawa, M., Chen, L.S., Fishbein, M.C., *et al.* (2008). Ectopic atrial arrhythmias arising from canine thoracic veins during in vivo stellate ganglia stimulation. Am. J. Physiol. Heart Circ. Physiol. *295*: H691–698.

Tan, H.L., Kupershmidt, S., Zhang, R., Stepanovic, S., Roden, D.M., Wilde, A.A.M., *et al.* (2002). A calcium sensor in the sodium channel modulates cardiac excitability. Nature *415*: 442–447.

Tate, S., Benn, S., Hick, C., Trezise, D., John, V., Mannion, R.J., *et al.* (1998). Two sodium channels contribute to the TTX-R sodium current in primary sensory neurons. Nat. Neurosci. *1*: 653–655.

Tessier, S., Karczewski, P., Krause, E.G., Pansard, Y., Acar, C., Lang-Lazdunski, M., *et al.* (1999). Regulation of the transient outward K^+ current by Ca^{2+}/calmodulin-dependent protein kinases II in human atrial myocytes. Circ. Res. *85*: 810–819.

Toda, N. (1969). Effects of calcium, sodium and potassium ions on contractility of isolated atria and their responses to noradrenaline. Br. J. Pharmacol. *36*: 350–367.

Toledo-Aral, J.J., Moss, B.L., He, Z.J., Koszowski, A.G., Whisenand, T., Levinson, S.R., *et al.* (1997). Identification of PN1, a predominant voltage-dependent sodium channel expressed principally in peripheral neurons. Proc. Natl. Acad. Sci. U. S. A. *94*: 1527–1532.

Torres, N.S., Larbig, R., Rock, A., Goldhaber, J.I., and Bridge, J.H.B. (2010). Na^+ currents are required for efficient excitation–contraction coupling in rabbit

ventricular myocytes: a possible contribution of neuronal Na^+ channels. J. Physiol. *588*: 4249–4260.

Tremblay, C., Berret, E., Henry, M., Nehmé, B., Nadeau, L., and Mouginot, D. (2011). Neuronal sodium leak channel is responsible for the detection of sodium in the rat median preoptic nucleus. J. Neurophysiol. *105*: 650–660.

Trimmer, J.S., Cooperman, S.S., Tomiko, S.A., Zhou, J.Y., Crean, S.M., Boyle, M.B., *et al.* (1989). Primary structure and functional expression of a mammalian skeletal muscle sodium channel. Neuron *3*: 33–49.

Tsai, C.F., Tai, C.T., Hsieh, M.H., Lin, W.S., Yu, W.C., Ueng, K.C., *et al.* (2000). Initiation of atrial fibrillation by ectopic beats originating from the superior vena cava: electrophysiological characteristics and results of radiofrequency ablation. Circulation *102*: 67–74.

Tsao, H.-M., Weerateerangkul, P., Chen, Y.-C., Kao, Y.-H., Lin, Y.-K., Huang, J.-H., *et al*. (2012). Amyloid peptide regulates calcium homoeostasis and arrhythmogenesis in pulmonary vein cardiomyocytes. Eur. J. Clin. Invest. *42*: 589–598.

Tsuneoka, Y., Kobayashi, Y., Honda, Y., Namekata, I., and Tanaka, H. (2012). Electrical activity of the mouse pulmonary vein myocardium. J. Pharmacol. Sci. *119*: 287–292.

Tweedie, D., Harding, S.E., and MacLeod, K.T. (2000). Sarcoplasmic reticulum Ca content, sarcolemmal Ca^{2+} influx and the genesis of arrhythmias in isolated guinea-pig cardiomyocytes. J. Mol. Cell. Cardiol. *32*: 261–272.

Undrovinas, A.I., Belardinelli, L., Undrovinas, N.A., and Sabbah, H.N. (2006). Ranolazine improves abnormal repolarization and contraction in left ventricular myocytes of dogs with heart failure by inhibiting late sodium current. J. Cardiovasc. Electrophysiol. *17 Suppl 1*: S169–S177.

Undrovinas, N.A., Maltsev, V.A., Belardinelli, L., Sabbah, H.N., and Undrovinas, A. (2010). Late sodium current contributes to diastolic cell Ca^{2+} accumulation in chronic heart failure. J. Physiol. Sci. JPS *60*: 245–257.

Vaitkevicius, R., Saburkina, I., Zaliunas, R., Pauziene, N., Vaitkeviciene, I., Schauerte, P., *et al*. (2008). Innervation of pulmonary veins: morphologic pattern and pathways of nerves in the human foetus. Ann. Anat. Anat. Anz. Off. Organ Anat. Ges. *190*: 158–166.

Valdivia, C.R., Chu, W.W., Pu, J., Foell, J.D., Haworth, R.A., Wolff, M.R., *et al.* (2005). Increased late sodium current in myocytes from a canine heart failure model and from failing human heart. J. Mol. Cell. Cardiol. *38*: 475–483.

VELDEN, H.M. w. van der, KEMPEN, M.J. a. van, Wijefels, M.C. e. ., ZIJVERDEN, M. van, Groenewegen, W.A., Allessie, M.A., *et al*. (1998). Altered

Pattern of Connexin40 Distribution in Persistent Atrial Fibrillation in the Goat. J. Cardiovasc. Electrophysiol. *9*: 596–607.

Verheule, S., Tuyls, E., Gharaviri, A., Hulsmans, S., Hunnik, A. van, Kuiper, M., *et al.* (2013). Loss of continuity in the thin epicardial layer because of endomysial fibrosis increases the complexity of atrial fibrillatory conduction. Circ. Arrhythm. Electrophysiol. *6*: 202–211.

Verheule, S., Wilson, E.E., Arora, R., Engle, S.K., Scott, L.R., and Olgin, J.E. (2002). Tissue structure and connexin expression of canine pulmonary veins. Cardiovasc. Res. *55*: 727–738.

Verkerk, A.O., Remme, C.A., Schumacher, C.A., Scicluna, B.P., Wolswinkel, R., Jonge, B. de, *et al.* (2012). Functional $Na_v1.8$ channels in intracardiac neurons: the link between SCN10A and cardiac electrophysiology. Circ. Res. *111*: 333–343.

Vest, J.A., Wehrens, X.H.T., Reiken, S.R., Lehnart, S.E., Dobrev, D., Chandra, P., *et al.* (2005). Defective cardiac ryanodine receptor regulation during atrial fibrillation. Circulation *111*: 2025–2032.

Voigt, N., Li, N., Wang, Q., Wang, W., Trafford, A.W., Abu-Taha, I., *et al.* (2012). Enhanced sarcoplasmic reticulum Ca^{2+} leak and increased Na^{+}-Ca^{2+} exchanger function underlie delayed afterdepolarizations in patients with chronic atrial fibrillation. Circulation *125*: 2059–2070.

Wagner, S., Dybkova, N., Rasenack, E.C.L., Jacobshagen, C., Fabritz, L., Kirchhof, P., *et al.* (2006). Ca^{2+}/calmodulin-dependent protein kinase II regulates cardiac Na^{+} channels. J. Clin. Invest. *116*: 3127–3138.

Wagner, S., Ruff, H.M., Weber, S.L., Bellmann, S., Sowa, T., Schulte, T., *et al.* (2011). Reactive oxygen species-activated Ca/calmodulin kinase IIδ is required for late I_{Na} augmentation leading to cellular Na^{+} and Ca^{2+} overload. Circ. Res. *108*: 555–565.

Wagoner, D.R.V., Pond, A.L., McCarthy, P.M., Trimmer, J.S., and Nerbonne, J.M. (1997). Outward K^{+} current densities and $K_v1.5$ expression are reduced in chronic human atrial fibrillation. Circ. Res. *80*: 772–781.

Wakili, R., Yeh, Y.-H., Yan Qi, X., Greiser, M., Chartier, D., Nishida, K., *et al.* (2010). Multiple potential molecular contributors to atrial hypocontractility caused by atrial tachycardia remodeling in dogs. Circ. Arrhythm. Electrophysiol. *3*: 530–541.

Wang, P., Yang, Q., Wu, X., Yang, Y., Shi, L., Wang, C., *et al.* (2010). Functional dominant-negative mutation of sodium channel subunit gene SCN3B associated with atrial fibrillation in a Chinese GeneID population. Biochem. Biophys. Res. Commun. *398*: 98–104.

Wang, Q., Shen, J., Splawski, I., Atkinson, D., Li, Z., Robinson, J.L., *et al*. (1995). SCN5A mutations associated with an inherited cardiac arrhythmia, long QT syndrome. Cell *80*: 805–811.

Wang, T., Chiang, C., Sheu, J., Tsou, C., Chang, H., and Luk, H. (2003). Homogenous distribution of fast response action potentials in canine pulmonary vein sleeves: a contradictory report. Int. J. Cardiol. *89*: 187–195.

Wang, Z., Fermini, B., and Nattel, S. (1993). Delayed rectifier outward current and repolarization in human atrial myocytes. Circ. Res. *73*: 276–285.

Wang, Z., Fermini, B., and Nattel, S. (1994). Rapid and slow components of delayed rectifier current in human atrial myocytes. Cardiovasc. Res. *28*: 1540–1546.

Wang, Z., Pagé, P., and Nattel, S. (1992). Mechanism of flecainide's antiarrhythmic action in experimental atrial fibrillation. Circ. Res. *71*: 271–287.

Ward, C.A., and Giles, W.R. (1997). Ionic mechanism of the effects of hydrogen peroxide in rat ventricular myocytes. J. Physiol. *500*: 631–642.

Watanabe, E., Fujikawa, A., Matsunaga, H., Yasoshima, Y., Sako, N., Yamamoto, T., *et al*. (2000). Na_v2/NaG channel is involved in control of salt-intake behavior in the CNS. J. Neurosci. Off. J. Soc. Neurosci. *20*: 7743–7751.

Watanabe, H., Darbar, D., Kaiser, D.W., Jiramongkolchai, K., Chopra, S., Donahue, B.S., *et al*. (2009). Mutations in sodium channel β1- and β2-subunits associated with atrial fibrillation. Circ. Arrhythm. Electrophysiol. *2*: 268–275.

Watanabe, H., Koopmann, T.T., Le Scouarnec, S., Yang, T., Ingram, C.R., Schott, J.-J., *et al*. (2008). Sodium channel β1 subunit mutations associated with Brugada syndrome and cardiac conduction disease in humans. J. Clin. Invest. *118*: 2260–2268.

Watano, T., Harada, Y., Harada, K., and Nishimura, N. (1999). Effect of Na^+/Ca^{2+} exchange inhibitor, KB-R7943 on ouabain-induced arrhythmias in guinea-pigs. Br. J. Pharmacol. *127*: 1846–1850.

Westenbroek, R.E., Bischoff, S., Fu, Y., Maier, S.K.G., Catterall, W.A., and Scheuer, T. (2013). Localization of sodium channel subtypes in mouse ventricular myocytes using quantitative immunocytochemistry. J. Mol. Cell. Cardiol. *64*: 69–78.

Wettwer, E., Hála, O., Christ, T., Heubach, J.F., Dobrev, D., Knaut, M., *et al*. (2004). Role of I_{Kur} in controlling action potential shape and contractility in the human atrium influence of chronic atrial fibrillation. Circulation *110*: 2299–2306.

White, M.M., Chen, L.Q., Kleinfield, R., Kallen, R.G., and Barchi, R.L. (1991). SkM2, a Na^+ channel cDNA clone from denervated skeletal muscle, encodes a tetrodotoxin-insensitive Na+ channel. Mol. Pharmacol. *39*: 604–608.

Wijffels, M.C., Kirchhof, C.J., Dorland, R., and Allessie, M.A. (1995). Atrial fibrillation begets atrial fibrillation. A study in awake chronically instrumented goats. Circulation *92*: 1954–1968.

Wilke, T., Groth, A., Mueller, S., Pfannkuche, M., Verheyen, F., Linder, R., *et al.* (2013). Incidence and prevalence of atrial fibrillation: an analysis based on 8.3 million patients. Eur. Eur. Pacing Arrhythm. Card. Electrophysiol. J. Work. Groups Card. Pacing Arrhythm. Card. Cell. Electrophysiol. Eur. Soc. Cardiol. *15*: 486–493.

Winegrad, S., and Shanes, A.M. (1962). Calcium flux and contractility in guinea pig atria. J. Gen. Physiol. *45*: 371–394.

Wit, A.L., and Cranefield, P.F. (1976). Triggered activity in cardiac muscle fibers of the simian mitral valve. Circ. Res. *38*: 85–98.

Witcher, D.R., Kovacs, R.J., Schulman, H., Cefali, D.C., and Jones, L.R. (1991). Unique phosphorylation site on the cardiac ryanodine receptor regulates calcium channel activity. J. Biol. Chem. *266*: 11144–11152.

Woeber, K.A. (1992). Thyrotoxicosis and the heart. N. Engl. J. Med. *327*: 94–98.

Wolf, P.A., Dawber, T.R., Thomas, H.E., and Kannel, W.B. (1978). Epidemiologic assessment of chronic atrial fibrillation and risk of stroke: the Framingham study. Neurology *28*: 973–977.

Wolkowicz, P., Umeda, P.K., Sharifov, O.F., White, C.R., Huang, J., Mahtani, H., *et al.* (2014). Inhibitors of arachidonate-regulated calcium channel signaling suppress triggered activity induced by the late sodium current. Eur. J. Pharmacol. *724*: 92–101.

Wongcharoen, W., Chen, Y.-C., Chen, Y.-J., Chang, C.-M., Yeh, H.-I., Lin, C.-I., *et al.* (2006). Effects of a Na^+/Ca^{2+} exchanger inhibitor on pulmonary vein electrical activity and ouabain-induced arrhythmogenicity. Cardiovasc. Res. *70*: 497–508.

Workman, A.J., Kane, K.A., and Rankin, A.C. (2001). The contribution of ionic currents to changes in refractoriness of human atrial myocytes associated with chronic atrial fibrillation. Cardiovasc. Res. *52*: 226–235.

Wu, Y., Wang, L., Ma, J., Song, Y., Zhang, P., Luo, A., *et al.* (2015). Protein kinase C and Ca^{2+}–calmodulin-dependent protein kinase II mediate the enlarged reverse I_{NCX} induced by ouabain-increased late sodium current in rabbit ventricular myocytes. Exp. Physiol. *100*: 399–409.

Xie, L.-H., Chen, F., Karagueuzian, H.S., and Weiss, J.N. (2009). Oxidative-stress-induced afterdepolarizations and calmodulin kinase II signaling. Circ. Res. *104*: 79–86.

Xi, Y., Wu, G., Yang, L., Han, K., Du, Y., Wang, T., *et al.* (2009). Increased late sodium currents are related to transcription of neuronal isoforms in a pressure-overload model. Eur. J. Heart Fail. *11*: 749–757.

Xu, J., Cui, G., Esmailian, F., Plunkett, M., Marelli, D., Ardehali, A., *et al*. (2004). Atrial extracellular matrix remodelling and the maintenance of atrial fibrillation. Circulation *109*: 363–368.

Xu, X.P., and Best, P.M. (1990). Increase in T-type calcium current in atrial myocytes from adult rats with growth hormone-secreting tumors. Proc. Natl. Acad. Sci. *87*: 4655–4659.

Xu, Y., Sharma, D., Li, G., and Liu, Y. (2013). Atrial remodeling: new pathophysiological mechanism of atrial fibrillation. Med. Hypotheses *80*: 53–56.

Yagi, T., Pu, J., Chandra, P., Hara, M., Danilo, P., Rosen, M.R., *et al*. (2002). Density and function of inward currents in right atrial cells from chronically fibrillating canine atria. Cardiovasc. Res. *54*: 405–415.

Yamamoto, M., Dobrzynski, H., Tellez, J., Niwa, R., Billeter, R., Honjo, H., *et a*l. (2006). Extended atrial conduction system characterised by the expression of the HCN4 channel and connexin45. Cardiovasc. Res. *72*: 271–281.

Yang, T., Atack, T.C., Stroud, D.M., Zhang, W., Hall, L., and Roden, D.M. (2012). Blocking SCN10A channels in heart reduces late sodium current and is antiarrhythmic. Circ. Res. *111*: 322–332.

Yao, L., Fan, P., Jiang, Z., Viatchenko-Karpinski, S., Wu, Y., Kornyeyev, D., *et al.* (2011). $Na_v1.5$-dependent persistent Na^+ influx activates CaMKII in rat ventricular myocytes and N1325S mice. Am. J. Physiol. Cell Physiol. *301*: C577–586.

Yasuda, T., Kumagai, K., Ogawa, M., Nakashima, H., Zhang, B., Miura, S., *et al.* (2010). Comparison of the effects of Na^+ and K^+ channel blockers on the electrophysiological properties of the pulmonary veins in patients with atrial fibrillation. J. Arrhythmia *26*: 259–266.

Yeager, M., and Gilula, N.B. (1992). Membrane topology and quaternary structure of cardiac gap junction ion channels. J. Mol. Biol. *223*: 929–948.

Yoon, J.-Y., Ho, W.-K., Kim, S.-T., and Cho, H. (2009). Constitutive CaMKII activity regulates Na^+ channel in rat ventricular myocytes. J. Mol. Cell. Cardiol. *47*: 475–484.

Yue, L., Feng, J., Li, G.R., and Nattel, S. (1996). Characterization of an ultrarapid delayed rectifier potassium channel involved in canine atrial repolarization. J. Physiol. *496*: 647–662.

Yue, L., Feng, J.L., Wang, Z., and Nattel, S. (2000). Effects of ambasilide, quinidine, flecainide and verapamil on ultra-rapid delayed rectifier potassium currents in canine atrial myocytes. Cardiovasc. Res. *46*: 151–161.

Yue, L., Melnyk, P., Gaspo, R., Wang, Z., and Nattel, S. (1999). Molecular mechanisms underlying ionic remodelling in a dog model of atrial fibrillation. Circ. Res. *84*: 776–784.

Yu, F.H., Westenbroek, R.E., Silos-Santiago, I., McCormick, K.A., Lawson, D., Ge, P., *et al*. (2003). Sodium channel β4, a new disulfide-linked auxiliary subunit with similarity to β2. J. Neurosci. Off. J. Soc. Neurosci. *23*: 7577–7585.

Zarzoso, M., Rysevaite, K., Milstein, M.L., Calvo, C.J., Kean, A.C., Atienza, F., *et al.* (2013). Nerves projecting from the intrinsic cardiac ganglia of the pulmonary veins modulate sinoatrial node pacemaker function. Cardiovasc. Res. *99*: 566–575.

Zellerhoff, S., Pistulli, R., Mönnig, G., Hinterseer, M., Beckmann, B.-M., Köbe, J., *et al.* (2009). Atrial arrhythmias in long-QT syndrome under daily life conditions: a nested case control study. J. Cardiovasc. Electrophysiol. *20*: 401–407.

Zeng, J., and Rudy, Y. (1995). Early afterdepolarizations in cardiac myocytes: mechanism and rate dependence. Biophys. J. *68*: 949–964.

Zhang, H., Garratt, C.J., Zhu, J., and Holden, A.V. (2005). Role of up-regulation of I_{K1} in action potential shortening associated with atrial fibrillation in humans. Cardiovasc. Res. *66*: 493–502.

Zimmermann, M., and Kalusche, D. (2001). Fluctuation in autonomic tone is a major determinant of sustained atrial arrhythmias in patients with focal ectopy originating from the pulmonary veins. J. Cardiovasc. Electrophysiol. *12*: 285–291.

Zimmer, T., Bollensdorff, C., Haufe, V., Birch-Hirschfeld, E., and Benndorf, K. (2002). Mouse heart Na^+ channels: primary structure and function of two isoforms and alternatively spliced variants. Am. J. Physiol. Heart Circ. Physiol. *282*: H1007–1017.

Zou, R., Kneller, J., Leon, L.J., and Nattel, S. (2005). Substrate size as a determinant of fibrillatory activity maintenance in a mathematical model of canine atrium. Am. J. Physiol. Heart Circ. Physiol. *289*: H1002–1012.

Zygmunt, A.C., Eddlestone, G.T., Thomas, G.P., Nesterenko, V.V., and Antzelevitch, C. (2001). Larger late sodium conductance in M cells contributes to electrical heterogeneity in canine ventricle. Am. J. Physiol. Heart Circ. Physiol. *281*: H689–697.

Zygmunt, A.C., Nesterenko, V.V., Rajamani, S., Hu, D., Barajas-Martinez, H., Belardinelli, L., *et al*. (2011). Mechanisms of atrial-selective block of Na^+ channels by ranolazine: I. Experimental analysis of the use-dependent block. Am. J. Physiol. Heart Circ. Physiol. *301*: H1606–1614.